

Assessing the formation and preservation of organic signatures in extreme environments

in the context of the ExoMars 2020 rover mission

Dissertation

zur Erlangung des mathematisch-naturwissenschaftlichen Doktorgrades

„Doctor rerum naturalium“

der Georg-August-Universität Göttingen

im Promotionsprogramm Geowissenschaften

der Georg-August University School of Science (GAUSS)

vorgelegt von

Manuel Reinhardt

aus Coburg

Göttingen, 2019

Betreuungsausschuss:

Prof. Dr. Volker Thiel

Georg-August-Universität Göttingen, Geowissenschaftliches Zentrum, Abteilung Geobiologie

PD Dr. Walter Goetz

Max-Planck-Institut für Sonnensystemforschung, Göttingen

Mitglieder der Prüfungskommission:

Referent: Prof. Dr. Volker Thiel

Georg-August-Universität Göttingen, Geowissenschaftliches Zentrum, Abteilung Geobiologie

1. Korreferent: PD Dr. Walter Goetz

Max-Planck-Institut für Sonnensystemforschung, Göttingen

2. Korreferent: Prof. Dr. Lorenz Schwark

Christian-Albrechts-Universität zu Kiel, Institut für Geowissenschaften, Abteilung Organische Geochemie

Weitere Mitglieder der Prüfungskommission:

Prof. Dr. Gernot Arp

Georg-August-Universität Göttingen, Geowissenschaftliches Zentrum, Abteilung Geobiologie

Dr. Martin Blumenberg

Bundesanstalt für Geowissenschaften und Rohstoffe, Hannover

Dr. Fred Goesmann

Max-Planck-Institut für Sonnensystemforschung, Göttingen

Prof. Dr. Joachim Reitner

Georg-August-Universität Göttingen, Geowissenschaftliches Zentrum, Abteilung Geobiologie

Tag der mündlichen Prüfung: 17.05.2019

In memory of my grandmother, Leni Reinhardt, the most optimistic and supportive person in my life.

Contents

Acknowledgements	ix
Preface	xi
Abstract	xiii
Zusammenfassung	xv
1 Introduction	1
1.1 ExoMars 2020 and the search for traces of life on Mars	1
1.2 Life as we know it.....	2
1.3 Emergence of life on the early Earth and habitability of Mars	2
1.3.1 Emergence of life on the early Earth.....	2
1.3.2 Mars, also a habitable planet?	3
1.4 Molecular biosignatures and their preservational fate	4
1.5 Thesis objectives and study approaches.....	6
References	7
2 Organic signatures in Pleistocene cherts from Lake Magadi (Kenya), analogs for early Earth hydrothermal deposits.....	13
2.1 Introduction	14
2.2 Materials and Methods.....	15
2.2.1 Sample material, petrographic and bulk geochemical analyses.....	15
2.2.2 Organic-geochemical preparation.....	15
2.2.3 Catalytic hydrolysis (HyPy)	15
2.2.4 Gas chromatography–mass spectrometry (GC–MS)	16
2.2.5 Gas chromatography–combustion–isotope ratio mass spectrometry (GC–C–IRMS)	16
2.2.6 Raman spectroscopy	16
2.3 Results	16
2.3.1 Petrography, bulk-geochemistry and Raman spectroscopy	16
2.3.2 Bitumen	18
2.3.2.1 Functionalized lipids	18
2.3.2.2 Aliphatic hydrocarbons	22
2.3.2.3 Polycyclic aromatic hydrocarbons (PAHs)	23
2.3.3 Kerogen (high temperature HyPy step, up to 520 °C).....	23
2.3.3.1 Aliphatic hydrocarbons	23
2.3.3.2 PAHs	24
2.4 Discussion.....	25

2.4.1 Thermal maturity and syngeneity of the organic matter	25
2.4.2 Geobiology of the Lake Magadi during chert deposition	26
2.4.2.1 Prokaryotes.....	26
2.4.2.2 Eukaryotes.....	26
2.4.2.3 Hydrothermal impact on organic matter	28
2.4.3 Organic signatures from the Magadi cherts: implications for the Archean	29
2.5 Conclusions	29
Acknowledgements.....	30
References	30
3 Ideas and perspectives: hydrothermally driven redistribution and sequestration of early Archean biomass—the “hydrothermal pump hypothesis”	37
3.1 Introduction	38
3.2 Material and methods	38
3.2.1 Sample preparation.....	38
3.2.2 Petrography and Raman spectroscopy.....	38
3.2.3 Raman-derived H/C data	39
3.2.4 Molecular analysis of the Dresser kerogen.....	39
3.2.5 Molecular analysis of pre-extracted cyanobacterial biomass (<i>Anabaena cylindrica</i>)	41
3.2.6 Fischer–Tropsch-type synthesis of organic matter under hydrothermal conditions	41
3.2.7 Gas chromatography–mass spectrometry	41
3.2.8 Polyaromatic hydrocarbon ratios.....	41
3.2.9 Total organic carbon (TOC) and $\delta^{13}\text{C}$ analyses (TOC and compound specific)	41
3.3 Results	42
3.4 Discussion.....	44
3.4.1 Maturity of the Dresser kerogen.....	44
3.4.2 Syngeneity of the Dresser kerogen-derived compounds	44
3.4.3 Origin of the Dresser kerogen: hydrothermal vs. biological origin	46
3.4.4 The “hydrothermal pump hypothesis”.....	46
3.5 Conclusions	48
Acknowledgements.....	48
References	48
4 The taphonomic fate of isorenieratene in Lower Jurassic shales—controlled by iron?.....	55
4.1 Introduction	56
4.2 Material and methods	56
4.2.1 Geological setting and sample material.....	56
4.2.2 Petrography and bulk analyses	57

4.2.3 Organic geochemical preparation	57
4.2.3.1 Bitumen	57
4.2.3.2 Kerogen	58
4.2.4 Catalytic hydrolysis (HyPy, open system)	58
4.2.5 Hydrous pyrolysis in gold capsules (closed system)	58
4.2.6 Gas chromatography–mass spectrometry (GC–MS)	58
4.2.7 Compound-specific stable carbon isotope ($\delta^{13}\text{C}_{\text{V-PDB}}$) analysis	59
4.3 Results	59
4.3.1 Petrographic observations and bulk geochemical data	59
4.3.2 Biomarkers from bitumens and kerogens	60
4.3.2.1 Aliphatic hydrocarbons	60
4.3.2.2 Aromatic hydrocarbons	61
4.3.2.3 Compound-specific stable carbon isotopes	62
4.4 Discussion	64
4.4.1 Syngeneity and maturity of the organic matter	64
4.4.2 Bächental kerogens—archives for isorenieratene derivatives?	65
4.4.3 Implications for the diagenetic fate of isorenieratene	66
4.4.4 A competition for sulfur: Iron vs. organics	67
4.4.5 The fate of isorenieratene in the Bächental basin: Controlled by iron?	67
4.5 Conclusions	67
Acknowledgments	68
References	68
5 Testing MOMA flight-like pyrolysis GC–MS on analog samples from Earth (iron-rich shale and opaline chert)—implications for MOMA pyrolysis during the ExoMars 2020 rover mission	73
5.1 Introduction	74
5.2 Material and methods	75
5.2.1 Sample material	75
5.2.2 MOMA flight-like pyrolysis GC–MS	75
5.2.3 GC–MS configuration	75
5.3 Results	76
5.3.1 Iron-rich shale (Bäch-1383)	76
5.3.2 Opaline chert (LM-1693)	76
5.3.3 Hydrocarbon standards (<i>n</i> -octadecane and phytane)	78
5.4 Discussion	79
5.4.1 Intact biomarkers in MOMA FAS pyrolysates	79
5.4.2 Secondary pyrolysis products	81

5.4.3 Pyrolysis products from macromolecules	83
5.4.4 Effects of mineral matrix on the pyrolysis outcome	83
5.4.5 Implications for MOMA pyrolysis GC–MS on Mars.....	84
5.5 Conclusions	84
Acknowledgements.....	85
References	85
6 Assessing the formation and preservation of organic signatures on Oxia Planum	91
6.1 Origin of organic matter on Oxia Planum.....	91
6.1.1 Abiogenic processes	91
6.1.2 Biology	91
6.1.3 Discrimination between biogenic and abiogenic organic matter	92
6.2 Preservation of organic matter on Oxia Planum	92
References	93
7 Summary, conclusions and outlook	97
7.1 Summary and conclusions	97
7.2 Outlook	98
References	99
Appendices	101
Appendix A	103
Appendix B	111
Appendix C	123
Appendix D	135
Curriculum Vitae.....	141

Acknowledgements

“It’s one of those things where you have to break through [...]”

Carson Palmer

This thesis work would not have been possible without the contribution and help of many great people that deserve to be credited here.

First of all, I would like to thank my supervisors Volker Thiel and Walter Goetz for giving me the opportunity to start in this project, for all the freedom you have given me, for the numerous scientific discussions, for any mental support and for being fantastic colleagues to work with. I cannot imagine a better guidance through the three years of scientific and personal development in the course of this thesis.

Next, a huge thanks to my good old friend Jan-Peter Duda and my office mate Christine Heim for your unlimited support, including the millions of questions you answered, mental support in hard times, scientific input, proofreading, coffee, kanel crispbread and just being good friends.

I would furthermore like to thank my thesis committee members Gernot Arp, Martin Blumenberg, Fred Goesmann, Lorenz Schwark, and Joachim Reitner for agreeing to evaluate this work. Gernot, Martin, Fred and Joachim are additionally thanked for their technical and scientific support.

Everyday life would have been much harder without Lilli, Wolfgang, Dario, Birgit, Helge, Max, Lia, Nils, Moe, Valentin, Meike, Jonas, my brothers Marcel and Julian, and especially my nephew Hannes.

Further people that contributed to this work are Cornelia Conradt, Jens Dyckmans, Dorothea Hause-Reitner, Conny and Gerhard Hundertmark, Volker Karius, Lothar Laake, Tobias Licha, the MOMA Science Team, Christian Ostertag-Henning, Andreas Reimer, Olaf Roders, Nadine Schäfer, Burkhard Schmidt, Sonja Schuh, Johanna Wagner-Farssi, Wiebke Warner and Klaus Wemmer. Thank you very much.

Finally, special thanks to my parents Sibylle and Uwe Reinhardt. Without your faith and permanent motivation I would have never made it to this point.

This work was financially supported by the International Max Planck Research School for Solar System Science at the University of Göttingen.

Preface

This is a cumulative thesis that includes four individual scientific studies in the form of published articles and manuscripts in preparation (chapters 2–5). The thesis furthermore contains an introduction (chapter 1) and a synthesis focusing on the implications of the general results for (i) organic matter formation and preservation in a hypothetical paleoenvironment at the ExoMars 2020 landing site Oxia Planum, and (ii) the operation of the Mars Organic Molecule Analyzer on Mars (chapter 6). A summary-, conclusions- and outlook-chapter (chapter 7) completes the thesis.

The following published articles and manuscripts in preparation form the main part of this thesis (§ = corresponding author):

Reinhardt, M.§, Goetz, W., Duda, J.-P., Heim, C., Reitner, J., & Thiel, V. (2019). Organic signatures in Pleistocene cherts from Lake Magadi (Kenya), analogs for early Earth hydrothermal deposits. *Biogeosciences Discuss.*, accepted with minor revisions for publication in *Biogeosciences*. <https://doi.org/10.5194/bg-2018-513> (chapter 2)

Own contribution: Design of the study, petrographic analyses, organic geochemical sample preparation and analyses (GC–MS, GC–C–IRMS), HyPy experiments, Raman spectroscopy, μ -XRF, data evaluation of all analyses, and writing of the manuscript

Duda, J.-P.§, Thiel, V., Bauersachs, T., Mißbach, H., Reinhardt, M., Schäfer, N., Van Kranendonk, M. J., & Reitner, J. (2018). Ideas and perspectives: hydrothermally driven redistribution and sequestration of early Archaean biomass – the “hydrothermal pump hypothesis”, *Biogeosciences*, 15, 1535–1548. <https://doi.org/10.5194/bg-15-1535-2018>, 2018 (chapter 3)

Own contribution: HyPy experiments, data evaluation (GC–MS on HyPy products, GC–C–IRMS on HyPy products), proofreading of the manuscript

Reinhardt, M.§, Duda, J.-P., Blumenberg, M., Ostertag-Henning, C., Reitner, J., Heim, C., & Thiel, V. (2018). The taphonomic fate of isorenieratene in Lower Jurassic shales—controlled by iron?, *Geobiology*, 16, 237–251. <https://doi.org/10.1111/gbi.12284> (chapter 4)

Own contribution: Design of the study, petrographic analyses, organic geochemical sample preparation and analyses (GC–MS, GC–C–IRMS), HyPy experiments, data evaluation of all analyses, and writing of the manuscript

Reinhardt, M.§, Goetz, W., & Thiel, V. (manuscript in preparation). Testing MOMA flight-like pyrolysis GC–MS on analog samples from Earth (iron-rich shale and opaline chert)—implications for MOMA pyrolysis during the ExoMars 2020 rover mission, to be submitted to *Astrobiology*. (chapter 5)

Own contribution: Design of the study, MOMA FAS experiments, data evaluation, and writing of the manuscript

Individual contributions were adapted to the overall style of this thesis.

Abstract

The search for extraterrestrial life is one of the greatest scientific quests of our time. The ESA/Roscosmos ExoMars 2020 rover mission seeks to find evidence for past or modern life on Mars by investigating (sub-)surface sediments at Oxia Planum for molecular biosignatures. To accomplish this goal, the rover is equipped with a variety of extremely sensitive analytical instruments that allow for the identification and characterization of organic matter (e.g., a Raman spectrometer and the Mars Organic Molecule Analyzer, MOMA). A drill allows to obtain samples from up to 2 m depths. The validation and interpretation of any data on potential organic matter produced during this mission, however, requires a sound understanding on possible accumulation and preservation pathways of organic matter at Oxia Planum. This is non-trivial to accomplish, as organic matter on Mars has been exposed to a variety of degradative processes over billions of years through the planet's history (e.g., radiative and oxidative destruction, thermal alteration by volcanism and impacts). This thesis aims at facilitating the validation and interpretation of potential organic signatures, including specific molecules indicative for biology that might be detected during the ESA/Roscosmos ExoMars 2020 rover mission. More specifically, the thesis provides a detailed picture of organic signature formation and preservation in Oxia Planum-relevant analog environments on Earth (hydrothermal, anoxic iron-rich). The main objectives of this thesis are (i) the assessment of organic sources (abiotic vs. biological), (ii) the discrimination of unambiguous molecular biosignatures, and (iii) the evaluation of organic matter preservation pathways (bitumen vs. kerogen) in the analog environments. These studies are complemented by systematic tests on the detectability of molecular biosignatures in the analyzed materials with MOMA flight-like pyrolysis gas chromatography–mass spectrometry (GC–MS).

The first study focusses on organic matter contained in modern hydrothermal cherts from the Pleistocene Lake Magadi (Kenya). The bitumens were dominated by immature archaeal and bacterial “biolipids” (e.g., glycerol mono- and diethers), as well as mature “geolipids” like hopanes, *n*-alkanes and polycyclic aromatic hydrocarbons (PAHs). Several independent molecular maturity indices from bitumens suggested that parts of the organic matter has been hydrothermally altered. Maturity parameters were also inconsistent for the kerogens, probably reflecting the synsedimentary introduction of pre-altered macromolecules into the depositional environment. However, despite *in-situ* hydrothermal alteration (particularly defunctionalization) specific molecular fingerprints, such as archaeal isoprenoids, were still incorporated into kerogen. These findings demonstrate that lipid biomarkers may survive syndepositional hydrothermal alteration by rapid sequestration into macromolecular networks (i.e., proto-kerogen and kerogen). This is of great relevance for the preservation of molecular biosignatures on Mars, as such networks are thought to efficiently shield bound compounds against degradative processes like radiation, oxidation and thermal maturation.

The second study centers on the analysis of kerogen enclosed in an Archean hydrothermal chert vein (ca. 3.5 Ga, Dresser Formation, Pilbara Craton, Western Australia). While the material experienced lower greenschist metamorphism (ca. 300 °C), the HyPy kerogen pyrolysate still yielded *n*-alkanes (up to *n*-C₂₂) that showed a distinct distribution pattern (sharp decrease in abundance > *n*-C₁₈). A similar chain-length preference was also detected in HyPy pyrolysates of modern bacterial biomass (*Anabaena cylindrica*), but never in abiotic organic products obtained via Fischer–Tropsch-type synthesis. These findings suggest that the *n*-alkanes yielded from the Dresser kerogen derive from a biological source. At the same time, the study shows that kerogen can facilitate a preservation of molecular biosignatures over billions of years, even if the organic matter has been subjected to degradative processes such as biodegradation and thermal maturation. It therefore appears possible that the ExoMars 2020 rover may detect biosignatures from the early history of the planet in Noachian–Hesperian (ca. 3.9–3.0 Ga) sediments on Oxia Planum.

The third study focusses on the preservation of aromatic carotenoids (pigments from anoxygenic phototrophs) in iron- and sulfur-rich shales from Lower Jurassic anoxic environments (Bächental oil shale, Posidonia Shale). The preservation of organic molecules in such settings is commonly aided by the formation of macromolecules, like kerogen, through early diagenetic sulfurization. Despite high sulfur contents (up to 4.6 wt.%), however, the samples contained only low amounts of sulfurized compounds. Furthermore, aromatic carotenoid biomarkers, including cyclized derivatives, were almost completely found in the bitumens rather than the corresponding kerogens. The results suggest that sulfur crosslinking was probably inhibited by (i) fast defunctionalization of the carotenoid molecules due to cyclization processes and (ii) hydrogenation and/or buffering of sulfide by excess of reduced iron (pyrite formation). This is highly relevant for the ExoMars2020 rover mission as Oxia Planum

contains iron-rich sediments (Fe/Mg-smectite clays). It may therefore be possible that crosslinking of organic molecules, and thus the formation of macromolecules, has been suppressed at this site, decreasing their preservation potential over large geological time scales.

In the fourth study, one hydrothermal chert (Lake Magadi, Kenya, first study) and one iron-rich shale (Bächental, Austria, third study) were analyzed via MOMA flight-like pyrolysis GC–MS to assess pyrolytic effects on organic signatures. The pyrolysis outcome was mainly driven by the type of organic matter rather than differences in mineral composition (iron-rich smectite vs. opaline silica). Hydrocarbon biomarkers like phytane and arylisoprenoids stayed intact during stepwise pyrolysis (300 °C, 500 °C, 700 °C). Additionally, however, artificial products (e.g., PAHs) were formed during pyrolysis, especially in the 500 °C and 700 °C runs. The pyrolysates from these temperature steps were additionally blurred through carryover effects (i.e., by compounds from previous runs). These findings demonstrate that only the combined application of all techniques available on MOMA (including LDI–MS and derivatization/thermochemolysis GC–MS) will allow for a thorough characterization and interpretation of organic matter.

In summary, the results presented in this thesis set important benchmarks for the validation and accurate interpretation of potential data obtained during the ESA/Roscosmos ExoMars 2020 rover mission. At the same time, the studies highlight important limitations and possibilities of the planned analyses. For instance, *in-situ* hydrothermal defunctionalization and iron-buffering may have hindered the formation of protective macromolecules in potential iron-rich hydrothermal environments at Oxia Planum during Noachian-Hesperian times. This would decrease the preservation potential, as macromolecules effectively shield incorporated compounds against destructive processes like UV-radiation, oxidation by perchlorates, volcanism and impacts. On the other hand, the formation of kerogen-like structures may have not completely been inhibited, and the preservation of organic molecules may have additionally been facilitated by further parameters such as mineral matrix effects and high sedimentation rates. Regardless of these issues, it will clearly require the full set of MOMA’s analytical payload to validate and interpret any potential organic signature on Oxia Planum. Perspectively, a more detailed knowledge on the formation and preservation of organic (bio-)signatures will be essential for the realization of future missions aiming at the detection of organic signatures on planetary bodies beyond Earth.

Zusammenfassung

Die Suche nach außerirdischem Leben ist eines der bedeutendsten Forschungsthemen moderner Wissenschaft. Dieser Fragestellung widmet sich die ESA/Roscosmos ExoMars 2020 Rover Mission, mit besonderem Ziel Spuren von vergangenem oder noch existentem Leben in Form von molekularen Biosignaturen in über- und unterirdischen Sedimenten der Oxia Planum Region (Mars) nachzuweisen. Für diese Aufgabe besitzt der Rover eine Vielzahl von hochempfindlichen Analysegeräten, welche die Identifizierung und Charakterisierung von organischem Material erlauben (z.B. ein Raman Spektrometer und den Mars Organic Molecule Analyzer, MOMA). Eine Bohrvorrichtung macht es außerdem möglich an Proben aus bis zu zwei Metern Tiefe zu gelangen. Die Überprüfung und Interpretation jeglicher potenzieller Organik-Befunde benötigt jedoch fundierte Erkenntnisse über mögliche Akkumulation und Erhaltung organischen Materials in der Oxia Planum Region. Dies ist entscheidend, da organisches Material auf dem Mars über Milliarden von Jahren verschiedensten zerstörerischen Abbauprozessen ausgesetzt war und immer noch ist (UV-Strahlung und Oxidation, thermische Degradation durch Vulkanismus und Impaktereignisse). Diese Arbeit hat deshalb zum Ziel, die Überprüfung und Interpretation möglicher Daten organischer Signaturen (molekulare Biosignaturen eingeschlossen), welche im Zuge der ESA/Roscosmos ExoMars 2020 Rover Mission generiert werden, zu unterstützen. Die Arbeit soll dementsprechend ein detailliertes Bild der Entstehung und Erhaltung von organischen Signaturen in Oxia Planum-relevanten Analogmilieus (hydrothermal, anoxisch eisenreich) darstellen. Die Hauptziele der Arbeit sind (i) die Einschätzung der Herkunft des organischen Materials (abiogen oder biogen), (ii) die Abgrenzung eindeutiger molekularer Biosignaturen und (iii) die Bewertung der Erhaltung des organischen Materials (Bitumen oder Kerogen) in den Analogmilieus. Die Analogstudien sollen durch systematische Tests, welche die Detektierbarkeit molekularer Biosignaturen mit MOMA Pyrolyse-Gaschromatographie–Massenspektrometrie (GC–MS; flugäquivalentes System) untersuchen, komplementiert werden.

Die erste Studie befasst sich mit organischem Material aus hydrothermalen Cherts des Pleistozänen Lake Magadi (Kenia). Die Bitumina wiesen überwiegend immature „Biolipide“ von Archaeen und Bakterien auf (z.B. Glycerolmonoether und –diether) sowie mature „Geolipide“, wie Hopane, *n*-Alkane und polyzyklische aromatische Kohlenwasserstoffe (PAKs). Diverse unabhängige molekulare Maturitätsindikatoren der Bitumina deuteten darauf hin, dass Teile organischen Materials bereits hydrothermal alteriert wurden. Maturitätsindikatoren des Kerogens wiesen ebenfalls Heterogenitäten auf, was auf einen synsedimentären Eintrag bereits degradierteter Makromoleküle in das Ablagerungsmilieu hindeuten könnte. Trotz der hydrothermalen In-situ-Alteration (vor allem Defunktionalisierung) wurden bestimmte molekulare Biosignaturen, wie zum Beispiel Isoprenoide von Archaeen, in das Kerogen eingebaut. Diese Ergebnisse deuten deshalb darauf hin, dass Lipidbiomarker synsedimentäre hydrothermale Alterationsprozesse durch rasche Bindung in makromolekulare Netzwerke (wie Protokerogen und Kerogen) überdauern können. Diese Erkenntnis ist äußerst wichtig für die Einschätzung der Erhaltung molekularer Biosignaturen auf dem Mars, da die genannten Netzwerke womöglich inkorporierte Moleküle gegen degradative Prozesse, wie UV-Strahlung, Oxidation und thermische Maturierung, abschirmen.

In der zweiten Studie wurde Kerogen aus einem hydrothermalen Chertgang aus dem Archaikum (ca. 3.5 Ga, Dresser Formation, Pilbara Kraton, Westaustralien) analysiert. Obwohl das Material bereits grünschieferfaziell überprägt wurde (bis zu 300 °C), lieferten die Kerogenpyrolysate (HyPy) dennoch *n*-Alkane (bis *n*-C₂₂), welche ein besonderes Verteilungsmuster aufwiesen (deutlicher Konzentrationseinbruch > *n*-C₁₈). Eine ähnliche Kettenlängenverteilung wurde in Pyrolysaten (HyPy) rezenter bakterieller Biomasse (*Anabaena cylindrica*) entdeckt, jedoch niemals in abiotischer Organik, die durch Fischer–Tropsch-Synthese generiert wurde. Diese Ergebnisse lassen den Schluss zu, dass die *n*-Alkane aus Kerogen der Dresser Formation biologischen Ursprungs sein könnten. Gleichzeitig verdeutlicht die Studie, dass Kerogen die Erhaltung molekularer Biosignaturen über Milliarden von Jahren begünstigt, selbst wenn das organische Material degradativen Prozessen, wie Biodegradation und thermischer Maturierung, ausgesetzt war. In diesem Sinne scheint es durchaus möglich, dass der ExoMars 2020 Rover Biosignaturen der Frühgeschichte des Mars (Noachische bis Hesperische Periode; ca. 3.9–3.0 Ga) in Sedimenten der Oxia Planum Region nachweisen könnte.

In der dritten Studie wurde die Erhaltung aromatischer Carotinoide (Pigmente in anoxygenen Phototrophen) in eisen- und schwefelreichen Tonsteinen aus unterjurassischen anoxischen Milieus (Bächental Ölschiefer, Posidonienschiefer) untersucht. In solchen Milieus wird die Erhaltung organischer Moleküle normalerweise durch

die Bildung von Makromolekülen, wie Kerogen, durch Schwefelungsprozesse begünstigt. Trotz hoher Schwefelgehalte (bis zu 4.6 gew.%) enthielten die Proben jedoch nur geringe Mengen an geschwefelten Molekülen. Des Weiteren traten Biomarker aromatischer Carotinoide, deren zyklisierte Derivate eingeschlossen, nahezu ausschließlich in den Bitumina auf, jedoch kaum in den entsprechenden Kerogenen. Diese Ergebnisse lassen vermuten, dass die Vernetzung über Schwefelbindungen höchstwahrscheinlich unterdrückt wurde, was durch (i) schnelle Defunktionalisierung der Carotinoide aufgrund von Zyklisierung und (ii) Hydrierung und/oder das Abpuffern von Sulfid durch einen Überschuss an reduziertem Eisen (Pyritfällung) bedingt sein kann. Ein solcher Mechanismus könnte hoch relevant für die ExoMars 2020 Rover Mission werden, da die Sedimente der Oxia Planum Region wahrscheinlich eisenreich sind (Fe/Mg-Smektit). Dadurch könnte die Vernetzung von organischen Molekülen, und dementsprechend die Bildung von Makromolekülen, unterdrückt werden, was das Erhaltungspotential organischer Moleküle über lange geologische Zeiträume gravierend verringert.

In der vierten Studie wurden je ein hydrothermaler Chert (Lake Magadi, Kenia; erste Studie) und ein eisenreicher Tonstein (Bächental, Österreich; dritte Studie) mit fluganaloger MOMA Pyrolyse-GC-MS analysiert, um pyrolytische Effekte auf die organischen Signaturen einschätzen zu können. Die Pyrolyseergebnisse wurden hauptsächlich von der Art des organischen Materials bestimmt, kaum jedoch von mineralogischen Unterschieden der Proben (eisenreicher Smektit oder opalartiges Silikat). Kohlenwasserstoffbiomarker wie Phytan und Arylisoprenoide blieben während der schrittweisen Pyrolyse (300 °C, 500 °C, 700 °C) intakt. Zusätzlich wurden jedoch speziell in den 500 °C und 700 °C Schritten künstliche Pyrolyseprodukte (z.B. PAKs) erzeugt. Des Weiteren wurden die Pyrolysate dieser Temperaturbereiche von Verschleppungseffekten beeinflusst (d.h., durch organische Verbindungen aus vorherigen Läufen). Diese Ergebnisse zeigen, dass es notwendig sein wird, alle Analysetechniken von MOMA (LDI-MS und Derivatisierung/Thermochemolyse-GC-MS eingeschlossen) zu kombinieren, um eine genaue Charakterisierung und Interpretation organischen Materials vornehmen zu können. Summa summarum schaffen die Ergebnisse dieser Doktorarbeit wichtige Bezugspunkte für die Bestätigung und genaue Interpretation potenzieller ExoMars 2020-Daten. Gleichzeitig heben die Studien wichtige Einschränkungen, aber auch Optionen der geplanten Analysen hervor. Zum Beispiel könnten hydrothermale In-situ-Defunktionalisierung und Puffereffekte durch reduziertes Eisen die Bildung von schützenden Makromolekülen in den potenziell eisenreichen hydrothermalen Milieus der Oxia Planum Region während der Noachischen bis Hesperischen Periode erschwert haben. Solche Prozesse würden das Erhaltungspotenzial von Organik deutlich verringern, da Makromoleküle inkorporierte Verbindungen wirksam vor destruktiven Prozessen, wie UV-Strahlung, Oxidation durch Perchlorate, und thermischer Alteration durch Vulkanismus und Impakte schützt. Allerdings könnte die Bildung kerogen-artiger Netzwerke nicht gänzlich eingeschränkt gewesen sein. Die Erhaltung von organischen Molekülen könnte nämlich durch weitere Parameter, wie Mineralmatrixeffekte und hohe Sedimentationsraten begünstigt worden sein. Nichtsdestotrotz wird es notwendig sein, die komplette Analysetechnik MOMAs anzuwenden, um mögliche organische Signaturen der Oxia Planum Region zu bestätigen und zu interpretieren. Perspektivisch gesehen wird ein detaillierteres Wissen über die Bildung und Erhaltung von organischen (Bio-)Signaturen die Umsetzung zukünftiger Missionen, die nach organischen Signaturen auf anderen Himmelskörpern suchen, deutlich erleichtern.

1 Introduction

1.1 ExoMars 2020 and the search for traces of life on Mars

The search for traces of life on Mars already started in the late 1970s with Viking Lander 1, followed by Viking Lander 2 and Phoenix (see Goetz et al., 2016 and references therein for an overview). In 2020 the ESA/Roscosmos ExoMars rover will be launched to further assess the existence of past or extant life on the Red Planet. The rover's Pasteur payload instruments, including a subsurface drill, cameras, infrared spectrometers, radar, a neutron detector, a Raman laser and the Mars Organic Molecule Analyzer (MOMA; Goesmann et al., 2017), provide an outstanding analytical set-up to identify potential morphological and especially chemical biosignatures in Martian (sub-)surface materials (Vago et al., 2017). MOMA will be the key instrument onboard that rover, capable of detecting organic (bio-)molecules via pyrolysis and derivatization/thermochemolysis gas chromatography–mass spectrometry (GC–MS), as well as laser desorption/ionization–mass spectrometry (LDI–MS; Li et al., 2017).

The mission is heading for Oxia Planum, a clay-rich basin on Chryse Planitia near the Martian dichotomy boarder (between 16° and 19° N, –23° and –28° E; Quantin et al., 2016; see Fig. 1.1). Orbital imaging spectrometry (Observatoire pour la Minéralogie, l'Eau, les Glaces et l'Activité (OMEGA); Bibring et al., 2004b; Compact Reconnaissance Imaging Spectrometer for Mars (CRISM); Murchie et al., 2007) indicates the widespread presence of Late to Middle Noachian Fe/Mg phyllosilicates (crater count age of ca. 3.9 Ga), probably Fe-Mg-rich smectite clays, as well as the localized occurrence of Al-rich phyllosilicates and opaline silica (Carter et al., 2016; Quantin et al., 2016). The clay-rich units are partly covered by fluvio-deltaic deposits (probably Hesperian age; see timeline in Fig. 1.1). Together, all these observations imply the presence of water in that area during Noachian-Hesperian times (Quantin et al., 2016). In some parts, the early Martian sediments are overlain by a dark unit, interpreted as lava cover (Amazonian age, ca. 2.6 Ga). However, the Noachian-Hesperian sediments at Oxia Planum were exposed since the last 100 Ma due to aeolian erosion (Carter et al., 2016; Quantin et al., 2016), opening up a juvenile window into previously cryptic strata. A protection from destructive radiation at the surface of Mars for long geological time-scales after deposition may have aided the preservation of organic matter in the old sediments and underlines the suitability of Oxia Planum as destination for the ExoMars 2020 rover to search for organic traces of life.

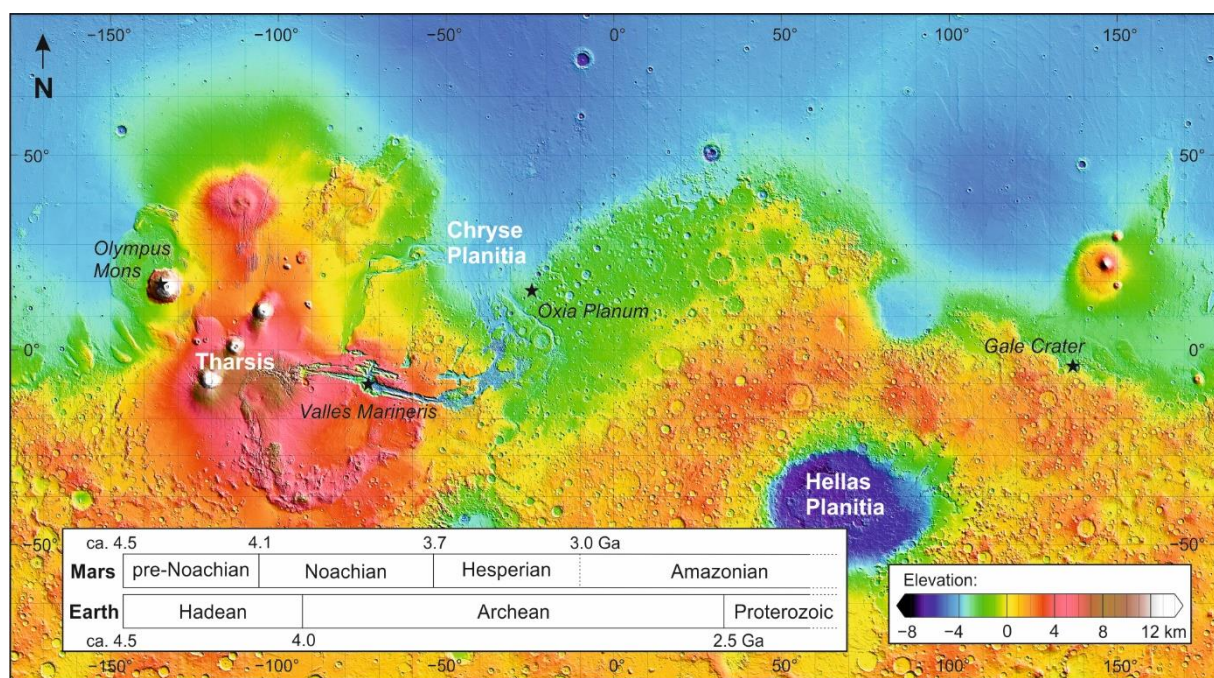


Fig. 1.1: Topography of Mars (elevation is color-coded; modified after NASA GSFC (2000), original image: https://marsweb.nas.nasa.gov/globalData/images/fullscale/MOLA_mercat.jpg). Locations mentioned in this thesis are marked by an asterisk, important areas by white lettering. Oxia Planum, the designated ExoMars 2020 landing site, is located

at the south-eastern edge of Chryse Planitia, near the Martian dichotomy border between the northern lowlands and southern highlands. Note the timeline comparing the early history of Earth and Mars (bottom left).

1.2 Life as we know it

According to de Duve (2011, p. 620) life is simply “*an obligatory manifestation of matter*”, implying that it may arise in numerous environments of our universe. To search for life outside of Earth, it is, however, necessary to determine what will be accepted as life. Many attempts were made in providing a proper definition, e.g., describing life as “*a self-sustained chemical system capable of undergoing Darwinian evolution*” (Joyce, 1995) or “*any autonomous system with open-ended evolutionary capacities*” (Ruiz-Mirazo et al., 2004, p. 330). The complexity of life is best expressed by summarizing its properties and requirements:

Life, as we know it from Earth, is (i) a self-organizing system, (ii) carbon-based, (iii) in disequilibrium with its surroundings, (iv) able to transform energy, (v) able to maintain low entropy, and (vi) able to replicate itself (see Schulze-Makuch & Irwin, 2004; Clarke, 2014; Westall & Brack, 2018 and references therein).

It therefore requires e.g., (i) physical or chemical energy and a carbon source (beside C, important building blocks are H, N, O, P, S, as well as transition metals like Fe, Ni, Mn, Cu), (ii) liquid water, (iii) temperatures that allow chemical bonding (ca. -20 to 120 °C), (iv) chemical disequilibrium, and (v) cellular isolation (e.g., Chaplin, 2001; Benner et al., 2004; Follmann & Brownson, 2009; Clarke, 2014; Westall & Brack, 2018).

These requirements are essential to prospect for potential habitable environments outside of Earth. The terms “habitable” or “habitability” (from Latin: *habitare* = *to live*), are widely used in the field of Astrobiology. A “habitable environment” basically describes any location “*capable of supporting the activity of at least one known organism*” (Cockell, 2014, p. 182; Cockell et al., 2016, p. 2), but does not imply the existence of life in that specific location at the moment. Beyond Earth, life may thrive in “extreme environments” (extreme, as compared to the overall environmental conditions of modern Earth). By definition “extreme environments”, include physical extremes, e.g., regarding temperature, radiation or pressure, and also geochemical extremes, e.g., regarding availability of water and oxygen, salinity, pH, or redox potential (Rothschild & Mancinelli, 2001).

1.3 Emergence of life on the early Earth and habitability of Mars

1.3.1 Emergence of life on the early Earth

Present-day Earth is the habitat for numerous life forms that developed over billions of years from a so far unknown precursor (“Last Universal Common Ancestor”, LUCA; e.g., Forterre & Philippe, 1999; Penny & Poole, 1999; Koonin, 2003; see Fig. 1.2). The exact timing and environmental conditions for the origin of life have been debated over decades (Urey, 1952; Oparin, 1957; Oró et al., 1990; Bada et al., 1994; Whittet, 1996). In its initial stage, proto-Earth was a hostile environment, and was probably completely molten (“magma ocean”) until first crustal fragments solidified around 4.4 Ga (Matsui & Abe, 1986; Zahnle et al., 2007; Valley et al., 2014; Kamber, 2015; Hadean, see timeline in Fig. 1.1). The hot proto-Earth, however, was probably strongly dynamic and crustal material was constantly overturned (Zahnle et al., 2007; Griffin et al., 2014; Kamber, 2015). The first atmosphere and ocean probably formed through degassing and condensation after a giant impact (Matsui & Abe, 1986; Zahnle, 2006; Elkins-Tanton, 2011). Impacts strongly influenced the early Earth by delivering volatiles and organic matter to the planet (e.g., Chyba, 1990; Botta & Bada, 2002; Zahnle et al., 2007; Marty et al., 2016). However, beside few zircons (~ 4.37 Ga; Valley et al., 2014), nothing is preserved from these early time periods. The oldest rocks on Earth are dated around 4.0 Ga (Acasta Gneiss Complex, Canada; Bowring & Williams, 1999; Mojzsis et al., 2014), while first evidences of organic matter are preserved as graphite in 3.8 Ga old metasediments (Isua Supracrustal Belt, Greenland; Ueno et al., 2002; van Zuilen et al., 2003, 2005). Rocks of this region may also contain the earliest fingerprints of life (~ 3.7 Ga) expressed by isotopic signatures, stromatolites and element enrichments in carbonaceous inclusions (Schidlowski et al., 1979; Nutman et al., 2016; Hassenkam et al., 2017), but these signatures are questioned. Stromatolites and organic biosignatures then frequently appear in ca. 3.4–3.5 Ga old cherts and carbonates from the Barberton Greenstone Belt, South Africa, and the Pilbara Craton, Western Australia (e.g., [chapter 3](#); Walter et al., 1980; Byerly et al., 1986; Marshall et al., 2007; Van Kranendonk et al., 2008; Duda et al., 2016, 2018; Hickman-Lewis et al., 2018). Early habitats for life may have included hydrothermal marine environments (e.g., Allwood et al., 2006; Duda et al., 2018; Hickman-Lewis et al., 2018) and terrestrial hot springs (Djokic et al., 2017).

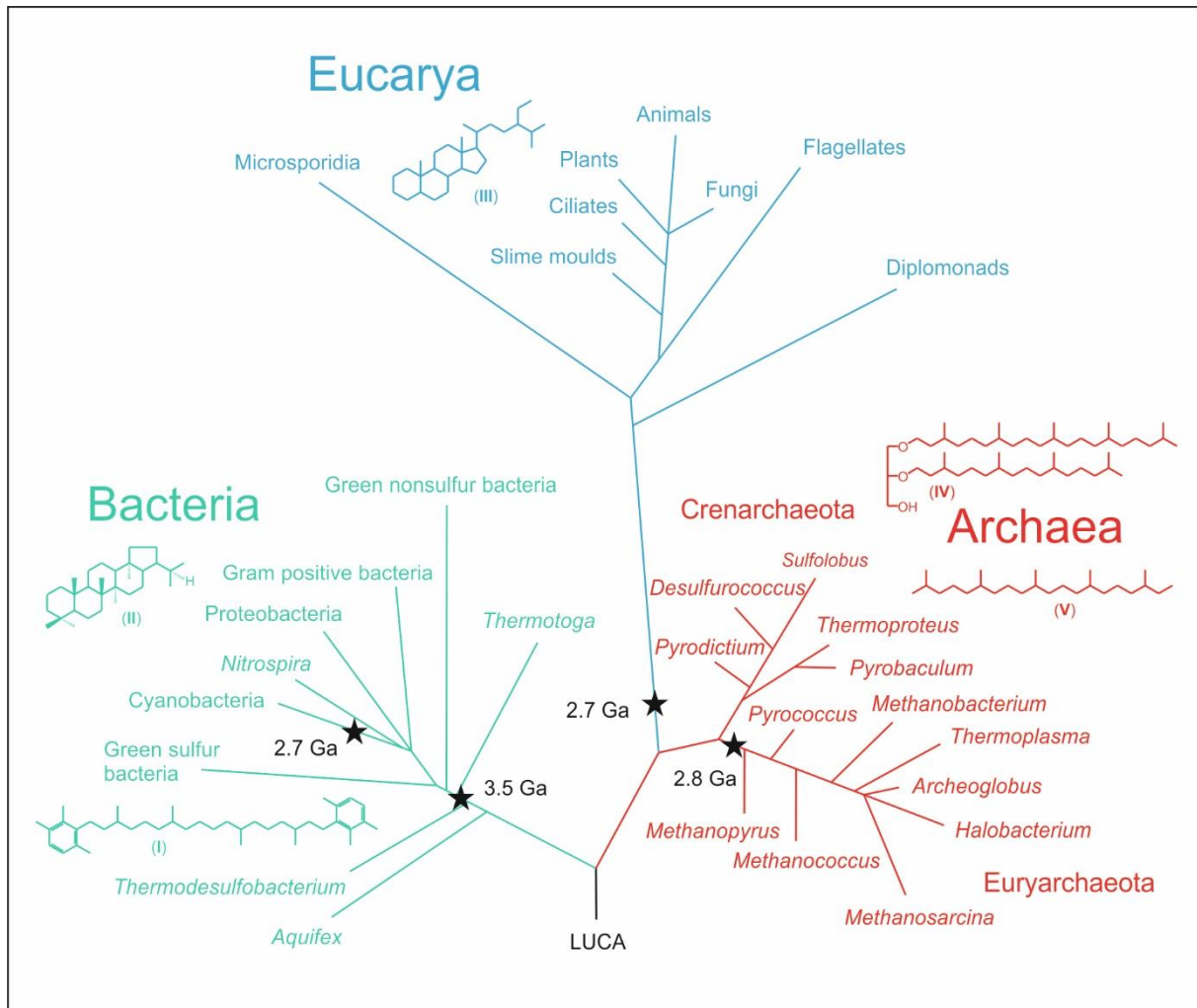


Fig. 1.2: Phylogenetic tree of life (modified after Brocks & Summons, 2005), including characteristic biomarkers of the three domains of life (I = isorenieratane, II = C₃₁ hopane 22 R, III = stigmastane, IV = archaeol, V = 2,6,10,14,18-pentamethylsane). Important branching points of life in the early history of Earth are marked by an asterisk (minimum ages; see Brocks & Summons, 2005 and references therein). LUCA = Last Universal Common Ancestor.

1.3.2 Mars, also a habitable planet?

In its beginnings, Mars and Earth may have taken a similar path. Due to the smaller size of Mars and its distance to the Sun, cooling and differentiation into core, mantle and crust likely happened faster than on Earth (Lee & Halliday, 1997; Blichert-Toft et al., 1999; Kleine et al., 2002; Carr & Head III, 2010 and references therein). An atmosphere may have developed via degassing during initial cooling, and further temperature decrease may have led to water condensation, forming an early ocean (Elkins-Tanton, 2011). Impact rates were high in the pre-Noachian/Noachian period, causing the formation of large basins like Hellas Planitia (probably between 4.1–3.8 Ga; Frey, 2006; Carr & Head III, 2010; see Fig. 1.1 for location) and the northern lowlands (formation of the Martian dichotomy probably through a massive impact; Frey, 2006; Andrews-Hanna et al., 2008; Carr & Head III, 2010; see Fig. 1.1 for location). These impact events may also have supplied volatiles and organic matter to Mars (see Anders & Owen, 1977; Botta & Bada, 2002; Marty et al., 2016). In addition to impacts, extensive volcanism was shaping the surface of the planet, probably starting in the Noachian (especially at Tharsis and Olympus Mons; see Williams et al., 2008; Carr & Head III, 2010; Xiao et al., 2012; Isherwood et al., 2013; see Fig. 1.1 for location). Volcanic activity likely also led to the formation of structural features, like faults and grabens, and potentially initiated the formation of Valles Marineris (e.g., Plescia & Saunders, 1982; Kronberg et al., 2007; Andrews-Hanna, 2012; see Fig. 1.1 for location). Plate tectonics, as known from Earth, likely did not establish (van Thienen et al., 2004). In the presence of liquid water, both, volcanism and impacts may have provided thermal energy for the formation of hydrothermal systems (Farmer, 1996; Osinski et al., 2013). Such settings are considered as potential habitats for early life on Mars (e.g., Schulte et al., 2006; Westall et al., 2015; Vago et al., 2017). If life ever evolved on Mars, it more likely happened during its early history (pre-Noachian/Noachian-Hesperian), when liquid water

and essential volatiles (C, H, N, O, P, S, and organic molecules that allow prebiotic chemistry) were available, and environmental conditions were more or less stable in time and space (Cockell et al., 2014 and references therein; Westall et al., 2013, 2015; Vago et al., 2017). While liquid water is probably not present at the surface of modern Mars, water ice was found at the poles and in the subsurface (e.g., Bibring et al., 2004a; Christensen, 2006; Bandfield, 2007). Water ice reaches a liquid-like behavior under the influence of UV-radiation (Tachibana et al., 2017), fostering the production of organic molecules that are relevant for biosynthesis (Dworkin et al., 2002). Destructive radiation is strong on the surface of modern Mars, but may rapidly diminish with depth (e.g., Mancinelli & Klovstad, 2000; Moores et al., 2007). Life may therefore survive in secure subsurface environments (see Cockell, 2014 and references therein). Certainly, the assessment of Martian habitability will be a great challenge for current and future missions to Mars (like ExoMars 2020).

1.4 Molecular biosignatures and their preservational fate

Life may leave specific traits in the rock record, including (i) morphological (e.g., body fossils or stromatolites), (ii) isotopic (e.g., fractionation of the carbon isotope pool), and (iii) molecular biosignatures, like organic biomarkers (e.g., Walter, 1976; Simoneit et al., 1998; Cady et al., 2003; Peters et al., 2005; Summons et al., 2008; Westall & Cavalazzi et al., 2011). A molecular biosignature or biomarker, as used in this thesis, is any organic molecule or molecular pattern that can be unambiguously linked to a biological precursor (e.g., specific structure or stable carbon isotope signature; cf., Peters et al., 2005 and references therein; Summons et al., 2008). Typical molecular biosignatures for life on Earth are summarized in Tab. 1.1.

Tab. 1.1: Typical molecular biosignatures for modern and ancient life on Earth and possible detectability with MOMA (modified after Simoneit et al., 1998)

Organic compound class	Main biological source	Potential MOMA technique for detection
<i>Molecular biosignatures for modern life, unstable over geological time-scales</i>		
Amino acids and peptides	Non-specific	Derivatization* GC–MS
Nucleotides and bases	Non-specific	Derivatization* GC–MS
Polysaccharides/sugars	Mainly flora	Pyrolysis and derivatization* GC–MS, LDI–MS?
Unsaturated lipids	Non-specific	Pyrolysis and derivatization* GC–MS
<i>Molecular biosignatures for ancient life, more stable over geological time-scales</i>		
Pigments (e.g., aromatic carotenoids)	Microbial (or flora)	Pyrolysis GC–MS, LDI–MS
Isoprenoids	Photosynthetic life, Archaea	Pyrolysis GC–MS
Diterpenoids	Flora (or microbial)	Pyrolysis GC–MS?, LDI–MS?
Triterpenoids (e.g., hopanes)	Bacteria (or flora)	LDI–MS?
Steroids	Eucarya	LDI–MS?
Biopolymers	Microbial (or flora)	Pyrolysis GC–MS, LDI–MS
Chain-length-preferences of aliphatic hydrocarbons	Non-specific	Pyrolysis GC–MS

*Including thermochemolysis

Organic matter, however, can also originate from abiotic processes, i.e., from synthesis in protoplanetary disks (e.g., Anders et al., 1973; Ciesla & Stanford, 2012), synthesis during impacts (Chyba & Sagan, 1992; Steele et al., 2016), Fischer–Tropsch-type synthesis (McCollom et al., 1999a, Rushdi & Simoneit, 2001; Mißbach et al., 2018),

and electrochemical fluid-mineral reactions (Steele et al., 2018). The sound interpretation of molecular biosignatures may therefore be hampered. Typical compounds that possess both, a biological and abiotic source include alkanes, alkanolic acids, and alkanols, as well as polycyclic aromatic hydrocarbons (PAHs; Eglinton & Hamilton, 1967; McCollom et al., 1999a, b; Rushdi & Simoneit, 2001; Sephton et al., 2004, 2005; Mißbach et al., 2018). In such cases, molecular distribution patterns or chain-length-preferences may be used as a biosignature, as biology only synthesizes a small subset of compounds of all chemical possibilities (see Summons et al., 2008). In contrast, abiotic synthesis produces patterns with gradually decreasing abundances with increasing carbon number (cf., McCollom et al., 1999a; Rushdi & Simoneit, 2001; Mißbach et al., 2018).

To trace life through deep time, molecular biosignatures need to be preserved in the rock record. Hydrocarbons are commonly more stable over geological time scales than functionalized moieties (see Tab. 1.1; Simoneit et al., 1998). Problematically, only a minor fraction of the organic matter produced in the biosphere is transported into sediments, while the major part is directly recycled (e.g., Tissot & Welte, 1984; Schwarzbauer & Jovančićević, 2015). Free functionalized moieties may either condensate to macromolecules like fulvic and humic acids or defunctionalize (e.g., through biodegradation) into “free molecular fossils” that gather in the bitumen (see Fig. 1.3; cf., Tissot & Welte, 1984; Schwarzbauer & Jovančićević, 2015).

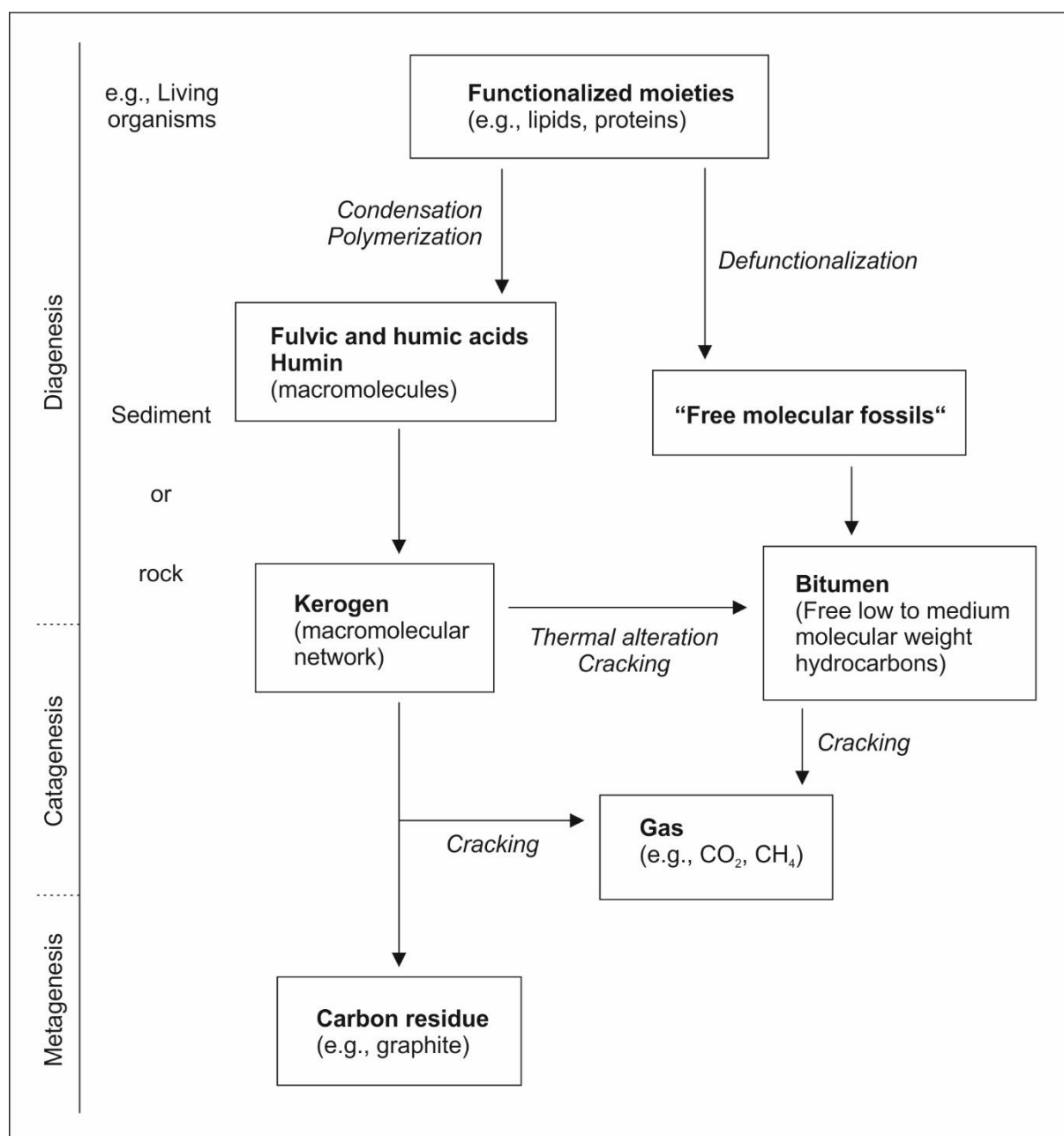


Fig. 1.3: Organic matter transformation as it occurs on Earth (simplified after Tissot & Welte, 1984). Organic biosignatures from living organisms can either be preserved in macromolecules, like kerogen, or as “free molecular fossils” in bitumen,

depending on early diagenetic processes. If condensation and polymerization outcompete defunctionalization, molecular biosignatures are incorporated into macromolecular networks, and vice versa.

During diagenesis, macromolecules may further grow to form large networks (i.e., kerogen; Fig. 1.3). On Earth an important process that strongly promotes molecular crosslinking especially in anoxic environments, is sulfurization (e.g., Sinninghe Damsté & de Leeuw, 1990; Hartgers et al., 1994; Wakeham et al., 1995). Such a preservation path may aid the long-term survival of molecular biosignatures, as the complex kerogen structure may effectively protect enclosed molecules from mild degradation (cf., Brocks et al., 2003; Marshall et al., 2007; Love et al., 2008; Eigenbrode et al., 2018). The formation of macromolecular networks may therefore be an essential requirement to preserve organic molecules over long geological time-scales on Mars (see McDonald et al., 1998; Eigenbrode et al., 2018). Otherwise, volcanism, impacts, intense radiation and oxidants like perchlorates may have rapidly led to destruction of organic moieties in Martian sediments (e.g., Hecht et al., 2009; Pavlov et al., 2012; Hassler et al., 2014; Westall et al., 2015).

1.5 Thesis objectives and study approaches

The successful detection of organic (bio-)signatures by the ExoMars 2020 rover, especially by MOMA, will strongly depend on (i) the fate of organic matter on Oxia Planum, including its formation, accumulation and preservation over long geological time-scales (see Fig. 1.3) and (ii) technical limitations of the analytical set-up onboard that rover. This thesis is aimed at providing a solid groundwork for the interpretation and validation of expected MOMA data by investigating organic signatures in extreme analog environments (hydrothermal and anoxic iron-rich) and by assessing analytical limitations of MOMA pyrolysis GC–MS. Specific questions that were addressed, include:

- (i) What is the origin of the organic matter in the specific analog materials (abiotic vs. biological)?
- (ii) Are unambiguous molecular biosignatures preserved?
- (iii) How are the molecular biosignatures preserved (bitumen vs. kerogen)?
- (iv) Which organic compounds can be detected with MOMA flight-like pyrolysis GC–MS?

The following studies, structured as individual chapters, were conducted to tackle these questions in the context of the ExoMars 2020 rover mission:

Organic matter on early Mars may have been influenced by hydrothermal alteration, as volcanic activity was strong and liquid water was probably available (see section 1.3.2). [Chapter 2](#) (Reinhardt et al., 2019) addresses the formation, alteration and preservation of organic matter in modern hydrothermal cherts from the Pleistocene Lake Magadi (Kenya). Petrographic and organic geochemical techniques (e.g., microscopy, Raman spectroscopy, GC–MS and catalytic hydropyrolysis (HyPy)) were combined to receive a detailed picture of organic matter characteristics on molecular and macroscopic levels. Furthermore, molecular biosignatures in bitumens and kerogens were investigated, aiming at understanding the preservational fate of biomolecules in hydrothermal environments.

The ExoMars 2020 target materials on Oxia Planum are Noachian sediments (ca. 3.9 Ga). Potential molecular biosignatures from these times, however, would have been subjected to degradative processes (volcanism, impacts, intensive UV-radiation, oxidants like perchlorates) and may have been intermixed with abiogenic organic matter. The study in [chapter 3](#) (Duda et al., 2018) focusses on molecular biosignatures from Earth’s early history. Kerogen and its HyPy products from a hydrothermal vein chert (ca. 3.5 Ga; Dresser Formation, Pilbara Craton, Western Australia) were investigated with Raman spectroscopy and GC–MS. To assess the origin of the organic matter (biogenic vs. abiogenic), the HyPy pyrolysis products were compared to those obtained from modern bacterial biomass (*Anabaena cylindrica*) and abiogenic organic matter generated through Fischer–Tropsch-type synthesis. Clay mineral assemblages on Oxia Planum (mainly Fe/Mg phyllosilicates; see section 1.1) imply a Noachian–Hesperian paleoenvironment characterized by liquid water and reduced iron. [Chapter 4](#) (Reinhardt et al., 2018) includes a study that investigated the preservation of aromatic carotenoids (pigments from anoxygenic phototrophs) in iron- and sulfur-rich shales from two Lower Jurassic anoxic settings (Bächental oil shale, Austria; Posidonia Shale, Germany). The appearance of aromatic carotenoid biomarkers in bitumens and kerogens (see Fig. 1.3) was compared and discussed in the context of the depositional environment (iron-rich, anoxic).

Chapter 5 (Reinhardt et al., to be submitted) tackles the limitations of MOMA pyrolysis GC–MS. Organic matter from an opaline chert (pre-characterized in [chapter 2](#), Reinhardt et al., 2019) and an iron-rich shale (pre-characterized in [chapter 4](#), Reinhardt et al., 2018) was pyrolysed in a MOMA flight-analog device. The study focused on pyrolytic effects that may hinder the identification of molecular biosignatures. Test-runs on two hydrocarbon standards (*n*-octadecane and phytane) were conducted to assess the stability of hydrocarbons under MOMA pyrolysis conditions.

Finally, in [chapter 6](#) the implications of these studies are discussed in the context of a hypothetical Noachian-Hesperian paleoenvironment at Oxia Planum (based on the geological information available from this site).

References

- Allwood, A. C., Walter, M. R., & Marshall, C. P. (2006). Raman spectroscopy reveals thermal palaeoenvironments of c. 3.5 billion-year-old organic matter. *Vib. Spectrosc.*, *41*, 190–197. <https://doi.org/10.1016/j.vibspec.2006.02.006>
- Anders, E., & Owen, T. (Mars and Earth: Origin and Abundance of Volatiles). 1977. *Science*, *198*, 453–465. <https://doi.org/10.1126/science.198.4316.453>
- Anders, E., Hayatsu, R., & Studier, M. H. (1973). Organic Compounds in Meteorites. *Science*, *182*, 781–790. <https://doi.org/10.1126/science.182.4114.781>
- Andrews-Hanna, J. C. (2012). The formation of Valles Marineris: 3. Trough formation through super-isostasy, stress, sedimentation, and subsidence. *J. Geophys. Res.*, *117*. <https://doi.org/10.1029/2012JE004059>
- Andrews-Hanna, J. C., Zuber, M. T., & Banerdt, W. B. (2008). The Borealis basin and the origin of the martian crustal dichotomy. *Nature*, 1212–1215. <https://doi.org/10.1038/nature07011>
- Bada, J. L., Bigham, C., & Miller, S. L. (1994). Impact melting of frozen oceans on the early Earth: Implications for the origin of life. *PNAS*, *91*, 1248–1250. <https://doi.org/10.1073/pnas.91.4.1248>
- Bandfield, J. L. (2007). High-resolution subsurface water-ice distributions on Mars. *Nature*, *447*, 64–67. <https://doi.org/10.1038/nature05781>
- Benner, S. A., Ricardo, A., & Carrigan, M., A. (2004). Is there a common chemical model for life in the universe? *Curr. Opin. Chem. Biol.*, *8*, 672–689. <https://doi.org/10.1016/j.cbpa.2004.10.003>
- Bibring, J.-P., Langevin, Y., Poulet, F., Gendrin, A., Gondet, B., Berthé, M., Soufflot, A., Drossart, P., Combes, M., Bellucci, G., Moroz, V., Mangold, N., Schmitt, B., & the OMEGA team (2004a). Perennial water ice identified in the south polar cap of Mars. *Nature*, *428*, 627–630. <https://doi.org/10.1038/nature02461>
- Bibring, J.-P., Soufflot, A., Berthé, M., Langevin, Y., Gondet, B., Drossart, P., Bouyé, M., Combes, M., Puget, P., Semery, A., Bellucci, G., Formisano, V., Moroz, V., Kottsov, V., & the OMEGA Co-1 team (2004b). OMEGA: Observatoire pour la Minéralogie, l'Eau, les Glaces et l'Activité. In A. Wilson (Ed.), *Mars Express: the scientific payload* (pp. 37–49). Noordwijk, Netherlands: ESA Publications.
- Blichert-Toft, J., Gleason, J., D., Télouk, P., & Albarède, F. (1999). The Lu–Hf isotope geochemistry of shergottites and the evolution of the Martian mantle–crust system. *Earth Planet. Sci. Lett.*, *173*, 25–39. [https://doi.org/10.1016/S0012-821X\(99\)00222-8](https://doi.org/10.1016/S0012-821X(99)00222-8)
- Botta, O., & Bada, J. L. (2002). Extraterrestrial Organic Compounds in Meteorites. *Surv. Geophys.*, *23*, 411–467. <https://doi.org/10.1023/A:1020139302770>
- Bowring, S. A., & Williams, I. S. (1999). Priscoan (4.00–4.03 Ga) orthogneisses from northwestern Canada. *Contrib. Mineral. Petrol.*, *134*, 3–16. <https://doi.org/10.1007/s004100050465>
- Brocks, J. J., & Summons, R. E. (2005). Sedimentary Hydrocarbons, Biomarkers for Early Life. In W. H. Schlesinger, H. D. Holland & K. K. Turekian (Eds.), *Treatise on Geochemistry, Vol. 8 Biogeochemistry* (pp. 702). Oxford: Elsevier.
- Brocks, J. J., Love, G. D., Snape, C. E., Logan, G. A., Summons, R. E., & Buick, R. (2003). Release of bound aromatic hydrocarbons from late Archean and Mesoproterozoic kerogens via hydrolysis. *Geochim. Cosmochim. Acta*, *67*, 1521–1530. [https://doi.org/10.1016/S0016-7037\(02\)01302-9](https://doi.org/10.1016/S0016-7037(02)01302-9)
- Byerly, G. R., Lower, D. R., & Walsh, M. M. (1986). Stromatolites from the 3,300–3,500-Myr Swaziland Supergroup, Barberton Mountain Land, South Africa. *Nature*, *319*, 489–491. <https://doi.org/10.1038/319489a0>
- Cady, S. L., Farmer, J. D., Grotzinger, J. P., Schopf, W., & Steele, A. (2003). Morphological Biosignatures and the Search for Life on Mars. *Astrobiology*, *3*, 351–368. <https://doi.org/10.1089/153110703769016442>
- Carr, M. H., & Head III, J. W. (2010). Geologic history of Mars. *Earth Planet. Sci. Lett.*, *294*, 185–203. <https://doi.org/10.1016/j.epsl.2009.06.042>

- Carter, J., Quantin, C., Tholot, P., Loizeau, D., Ody, A., & Lozach, L. (2016). Oxia Planum: A Clay-Laden Landing Site Proposed for the ExoMars Rover Mission: Aqueous Mineralogy and Alteration Scenarios. Paper presented at the 47th Lunar and Planetary Science Conference, The Woodlands, Texas.
- Ciesla, F. J., & Sandford, S. A. (2012). Organic Synthesis via Irradiation and Warming of Ice Grains in the Solar Nebula. *Science*, *336*, 452–454. <https://doi.org/10.1126/science.1217291>
- Chaplin, M. F. (2008). Water: its importance to life. *Biochem. Mol. Biol. Educ.*, *29*, 54–59. <https://doi.org/10.1111/j.1539-3429.2001.tb00070.x>
- Christensen, P. R. (2006). Water at the Poles and in Permafrost Regions of Mars. *Elements*, *2*, 151–155. <https://doi.org/10.2113/gselements.2.3.151>
- Chyba, C. F. (1990). Impact delivery and erosion of planetary oceans in the early inner Solar System. *Nature*, *343*, 129–133. <https://doi.org/10.1038/343129a0>
- Chyba, C. F., & Sagan, C. (1992). Endogenous production, exogenous delivery and impact-shock synthesis of organic molecules: an inventory for the origins of life. *Nature*, *355*, 125–132. <https://doi.org/10.1038/355125a0>
- Clarke, A. (2014). The thermal limits to life on Earth. *Int. J. Astrobiol.*, *13*, 141–154. <https://doi.org/10.1017/S1473550413000438>
- Cockell, C. S. (2014). Trajectories of Martian Habitability. *Astrobiology*, *14*, 182–203. <https://doi.org/10.1089/ast.2013.1106>
- Cockell, C. S., Bush, T., Bryce, C., Direito, S., Fox-Powell, M., Harrison, J. P., Lammer, H., Landenmark, H., Martin-Torres, J., Nocholson, N., Noack, L., O'Malley-James, J., Payler, S. J., Rushby, A., Samuels, T., Schwendner, P., Wadsworth, J., & Zorzano, M. P. (2016). Habitability: A Review. *Astrobiology*, *16*, 1–29. <https://doi.org/10.1089/ast.2015.1295>
- Djokic, T., Van Kranendonk, M. J., Campbell, K. A., Walter, M. R., & Ward, C. R. (2017). Earliest signs of life on land preserved in ca. 3.5 Ga hot spring deposits. *Nat. Commun.*, *8*, e15263. <https://doi.org/10.1038/ncomms15263>
- Duda, J.-P., Van Kranendonk, M. J., Thiel, V., Ionescu, D., Strauss, H., Schäfer, N., & Reitner, J. (2016). A Rare Glimpse of Paleoarchean Life: Geobiology of an Exceptionally Preserved Microbial Mat Facies from the 3.4 Ga Strelley Pool Formation, Western Australia. *PLoS ONE*, *11*, e0147629. <https://doi.org/10.1371/journal.pone.0147629>
- Duda, J.-P., Thiel, V., Bauersachs, T., Mißbach, H., Reinhardt, M., Schäfer, N., Van Kranendonk, M. J., & Reitner, J. (2018). Ideas and perspectives: hydrothermally driven redistribution and sequestration of early Archaean biomass – the “hydrothermal pump hypothesis”. *Biogeosciences*, *15*, 1535–1548. <https://doi.org/10.5194/bg-15-1535-2018>
- de Duve, C. (2011). Life as a cosmic imperative? *Phil. Trans. R. Soc. A*, *369*, 620–623. <https://doi.org/10.1098/rsta.2010.0312>
- Dworkin, J. P., Stanford, S. A., Bernstein, M. P., & Allamandola, L. J. (2002). *The Laboratory Production of Complex Organic Molecules in Simulated Interstellar Ices*.
- Eglinton, G., & Hamilton, R. J. (1967). Leaf Epicuticular Waxes. *Science*, *156*, 1322–1335. <https://doi.org/10.1126/science.156.3780.1322>
- Eigenbrode, J. L., Summons, R. E., Steele, A., Freissinet, C., Millan, M., Navarro-González, R., Sutter, B., McAdam, A. C., Franz, H. B., Glavin, D. P., Archer Jr, P. D., Mahaffy, P. R., Conrad, P. G., Hurowitz, J. A., Grotzinger, J. P., Gupta, S., Ming, D. W., Sumner, D. Y., Szopa, C., Malespin, C., Buch, A., & Coll, P. (2018). Organic matter preserved in 3-billion-year-old mudstones at Gale crater, Mars. *Science*, *360*, 1096–1101. <https://doi.org/10.1126/science.aas9185>
- Elkins-Tanton, L. T. (2011). Formation of early water oceans on rocky planets. *Astrophys. Space Sci.*, *332*, 359–364. <https://doi.org/10.1007/s10509-010-0535-3>
- Farmer, J. D. (1996). Hydrothermal systems on Mars: an assessment of present evidence. In G. R. Bock & J. A. Goode (Eds.), *Evolution of Hydrothermal Ecosystems on Earth (and Mars?)* (pp. 273–299). Chichester: Wiley.
- Frey, H. V. (2006). Impact constraints on, and a chronology for, major events in early Mars history. *J. Geophys. Res. Planets*, *111*, E08S91. <https://doi.org/10.1029/2005JE002449>
- Follmann, H., & Brownson, C. (2009). Darwin’s warm little pond revisited: from molecules to the origin of life. *Naturwissenschaften*, *96*, 1265–1292. <https://doi.org/10.1007/s00114-009-0602-1>
- Forterre, P., & Philippe, H. (1999). The Last Universal Common Ancestor (LUCA), Simple or Complex? *Biol. Bull.*, *196*, 373–377. <https://doi.org/10.2307/1542973>

- Goesmann, F., Brinckerhoff, W. B., Raulin, F., Goetz, W., Danell, R. M., Getty, S. A., Siljeström, S., Mißbach, H., Steininger, H., Arevalo Jr., R. D., Buch, A., Freissinet, C., Grubisic, A., Meierhenrich, U. J., Pinnick, V. T., Stalport, F., Szopa, C., Vago, J. L., Lindner, R., Schulte, M., Brucato, J. R., Glavin, D. P., Grand, N., Li, X., van Amerom, F. H. W., & the MOMA Science Team (2017). The Mars Organic Molecule Analyzer (MOMA) Instrument: Characterization of Organic Material in Martian Sediments. *Astrobiology*, *17*, 655–685. <https://doi.org/10.1089/ast.2016.1551>
- Goetz, W., Brinckerhoff, W. B., Arevalo Jr., R. D., Freissinet, C., Getty, S. A., Glavin, D. P., Siljeström, S., Buch, A., Stalport, F., Grubisic, A., Li, X., Pinnick, V. T., Danell, R. M., van Amerom, F. H. W., Goesmann, F., Steininger, H., Grand, N., Raulin, F., Szopa, C., Meierhenrich, U. J., Brucato, J. R., & the MOMA Science Team (2016). MOMA: the challenge to search for organics and biosignatures on Mars. *Int. J. Astrobiol.*, *15*, 239–250. <https://doi.org/10.1017/S1473550416000227>
- Griffin, W. L., Belousova, E. A., O'Neill, C., O'Reilly, S. Y., Malkovets, V., Pearson, N. J., Spetsius, S., & Wilde, S. A. (2014). The world turns over: Hadean–Archean crust–mantle evolution. *Lithos*, *189*, 2–15. <https://doi.org/10.1016/j.lithos.2013.08.018>
- Hartgers, W. A., Sinninghe Damsté, J. S., Requejo, A. G., Allan, J., Hayes, J. M., Ling, Y., Xie, T.-M., Primack, J., & de Leeuw, J. W. (1994). A molecular and carbon isotopic study towards the origin and diagenetic fate of diaromatic carotenoids. *Org. Geochem.*, *22*, 703–725. [https://doi.org/10.1016/0146-6380\(94\)90134-1](https://doi.org/10.1016/0146-6380(94)90134-1)
- Hassenkam, T., Andersson, M. P., Dalby, K. N., Mackenzie, D. M. A., & Rosing, M. T. (2017). Elements of Eoarchean life trapped in mineral inclusions. *Nature*, *548*, 78–81. <https://doi.org/10.1038/nature23261>
- Hassler, D. M., Zeitlin, C., Wimmer-Schweingruber, R. F., Ehresmann, B., Rafkin, S., Eigenbrode, J. L., Brinza, D. E., Weigle, G., Böttcher, S., Böhm, E., Burmeister, S., Guo, J., Köhler, J., Martin, C., Reitz, G., Cucinotta, F. A., Kim, M.-H., Grinspoon, D., Bullock, M. A., Posner, A., Gómez-Elvira, J., Vasvada, A., Grotzinger, J. P., & MSL Science Team (2014). Mars' Surface Radiation Environment Measured with the Mars Science Laboratory's Curiosity Rover. *Science*, *343*, 1244797. <https://doi.org/10.1126/science.1244797>
- Hecht, M. H., Kounaves, S. P., Quinn, R. C., West, S. J., Young, S. M. M., Ming, D. W., Catling, D. C., Clark, B. C., Boynton, W. V., Hoffman, J., DeFlores, L. P., Gospodinova, K., Kapit, J., & Smith, P. H. (2009). Detection of Perchlorate and the Soluble Chemistry of Martian Soil at the Phoenix Lander Site. *Science*, *325*, 64–67. <https://doi.org/10.1126/science.1172466>
- Hickman-Lewis, K., Cavalazzi, B., Foucher, F., & Westall, F. (2018). Most ancient evidence for life in the Barberton greenstone belt: Microbial mats and biofabrics of the ~3.47 Ga Middle Marker horizon. *Precambrian Res.*, *312*, 45–67. <https://doi.org/10.1016/j.precamres.2018.04.007>
- Isherwood, R. J., Jozwiak, L. M., Jansen, J. C., & Andrews-Hanna, J. C. (2013). The volcanic history of Olympus Mons from paleo-topography and flexural modeling. *Earth Planet. Sci. Lett.*, *363*, 88–96. <https://doi.org/10.1016/j.epsl.2012.12.020>
- Joyce, G. F. (1995). The RNA World: Life before DNA and Protein. In B. Zuckerman & M. H. Hart (Eds.), *Extraterrestrials: where are they?* (pp. 139–151). Cambridge: Cambridge University Press.
- Kamber, B. S. (2015). The evolving nature of terrestrial crust from the Hadean, through the Archaean, into the Proterozoic. *Precambrian Res.*, *258*, 48–82. <https://doi.org/10.1016/j.precamres.2014.12.007>
- Kleine, T., Münker, C., Mezger, K., & Palme, H. (2002). Rapid accretion and early core formation on asteroids and the terrestrial planets from Hf–W chronometry. *Nature*, *418*, 952–955. <https://doi.org/10.1038/nature00982>
- Koonin, E. V. (2003). Comparative genomics, minimal gene-sets and the last universal common ancestor. *Nat. Rev. Microbiol.*, *1*, 127–136. <https://doi.org/10.1038/nrmicro751>
- Kronberg, P., Hauber, E., Grott, M., Werner, S. C., Schäfer, T., Gwinner, K., Giese, B., P., M., & Neukum, G. (2007). Acheron Fossae, Mars: Tectonic rifting, volcanism, and implications for lithospheric thickness. *J. Geophys. Res.*, *112*. <https://doi.org/10.1029/2006JE002780>
- Lee, D.-C., & Halliday, A. N. (1997). Core formation on Mars and differentiated asteroids. *Nature*, *388*, 854–857. <https://doi.org/10.1038/42206>
- Li, X., Danell, R. M., Pinnick, V. T., Grubisic, A., van Amerom, F. H. W., Arevalo Jr., R. D., Getty, S. A., Brinckerhoff, W. B., Southard, A. E., Gonnsen, Z., D., & Adachi, T. (2017). Mars Organic Molecule Analyzer (MOMA) laser desorption/ionization source design and performance characterization. *Int. J. Mass Spectrom.*, *422*, 177–187. <https://doi.org/10.1016/j.ijms.2017.03.010>
- Love, G. D., Stalvies, C., Grosjean, E., Meredith, W., & Snape, C. E. (2008). Analysis of molecular biomarkers covalently bound within Neoproterozoic sedimentary kerogen. In P. H. Kelley & R. K. Bambach (Eds.), *From*

- Evolution to Geobiology: Research Questions Driving Paleontology at the Start of a New Century* (pp. 67–83). New Haven: Paleontological Society Papers.
- Mancinelli, R. L., & Klovstad, M. (2000). Martian soil and UV radiation: microbial viability assessment on spacecraft surfaces. *Planet. Space Sci.*, *48*, 1093–1097. [https://doi.org/10.1016/S0032-0633\(00\)00083-0](https://doi.org/10.1016/S0032-0633(00)00083-0)
- Marshall, C. P., Love, G. D., Snape, C. E., Hill, A. C., Allwood, A. C., Walter, M. R., Van Kranendonk, M. J., Bowden, S. A., Sylva, S. P., & Summons, R. E. (2007). Structural characterization of kerogen in 3.4 Ga Archaean cherts from the Pilbara Craton, Western Australia. *Precambrian Res.*, *155*, 1–23. <https://doi.org/10.1016/j.precamres.2006.12.014>
- Marty, B., Avice, G., Sano, Y., Altwegg, K., Balsiger, H., Hässig, M., Morbidelli, A., Mousis, O., Rubin, M. (2016). Origins of volatile elements (H, C, N, noble gases) on Earth and Mars in light of recent results from the ROSETTA cometary mission. *Earth Planet. Sci. Lett.*, *441*, 91–102. <https://doi.org/10.1016/j.epsl.2016.02.031>
- Matsui, T., & Abe, Y. (1986). Evolution of an impact-induced atmosphere and magma ocean on the accreting Earth. *Nature*, *319*, 303–305. <https://doi.org/10.1038/319303a0>
- McCollom, T. M., Ritter, G., & Simoneit, B. R. T. (1999a). Lipid Synthesis Under Hydrothermal Conditions by Fischer–Tropsch-Type Reactions. *Origins Life Evol. Biosphere*, *29*, 153–166. <https://doi.org/10.1023/A:1006592502746>
- McCollom, T. M., Simoneit, B. R. T., & Shock, E. L. (1999b). Hydrous Pyrolysis of Polycyclic Aromatic Hydrocarbons and Implications for the Origin of PAH in Hydrothermal Petroleum. *Energy Fuels*, *13*, 401–410. <https://doi.org/10.1021/ef980089i>
- McDonald, G. D., de Vanssay, E., & Buckley, J. R. (1998). Oxidation of Organic Macromolecules by Hydrogen Peroxide: Implications for Stability of Biomarkers on Mars. *Icarus*, *132*, 170–175. <https://doi.org/10.1006/icar.1998.5896>
- Mißbach, H., Schmidt, B. C., Duda, J.-P., Lünsdorf, N. K., Goetz, W., & Thiel, V. (2018). Assessing the diversity of lipids formed via Fischer–Tropsch-type reactions. *Org. Geochem.*, *119*, 110–121. <https://doi.org/10.1016/j.orggeochem.2018.02.012>
- Moody, 1976
- Mojzsis, S. J., Cates, N. L., Caro, G., Trail, D., Abramov, O., Guitreau, M., Blichert-Toft, J., Hopkins, M. D., Bleeker, W. (2014). Component geochronology in the polyphase ca. 3920 Ma Acasta Gneiss. *Geochim. Cosmochim. Acta*, *133*, 68–96. <https://doi.org/10.1016/j.gca.2014.02.019>
- Moore, J. E., Smith, P. H., Tanner, R., Schuerger, A. C., & Venkateswaran, K. J. (2007). The shielding effect of small-scale martian surface geometry on ultraviolet flux. *Icarus*, *192*, 417–433. <https://doi.org/10.1016/j.icarus.2007.07.003>
- Murchie, S., Arvidson, R., Bedini, P., Beisser, K., Bibring, J.-P., Bishop, J., Boldt, J., Cavender, P., Choo, T., Clancy, R. T., Darlington, E. H., Des Marais, D., Espiritu, R., Fort, D., Green, R., Guinness, E., Hayes, J., Hash, C., Heffernan, K., Hemmler, J., Heyler, G., Humm, D., Hutcheson, J., Izenberg, N., Lee, R., Lees, J., Lohr, D., Malaret, E., Martin, T., McGovern, J. A., McGuire, P., Morris, R., Mustard, J., Pelkey, S., Rhodes, E., Robinson, M., Roush, T., Schaefer, E., Seagrave, G., Seelos, F., Silvergate, P., Slavney, S., Smith, M., Shyong, W.-J., Strohbehn, K., Taylor, H., Thompson, P., Tossman, B., Wirzburger, M., & Wolff, M. (2007). Compact Reconnaissance Imaging Spectrometer for Mars (CRISM) on Mars Reconnaissance Orbiter (MRO). *J. Geophys. Res. Planets*, *112*. <https://doi.org/10.1029/2006JE002682>
- NASA GSFC (2000). https://marsoweb.nas.nasa.gov/globalData/images/fullscale/MOLA_mercat.jpg.
- Nutman, A. P., Bennett, V. C., Friend, C. R. L., Van Kranendonk, M. J., & Chivas, A. R. (2016). Rapid emergence of life shown by discovery of 3,700-million-year-old microbial structures. *Nature*, *537*, 535–538. <https://doi.org/10.1038/nature19355>
- Oparin, A. I. (1957). *Origin of Life on the Earth*. Edinburgh: Oliver and Boyd.
- Oró, J., Miller, S. L., & Lazcano, A. (1990). The origin and early evolution of life on Earth. *Annu. Rev. Earth Planet. Sci.*, *18*, 317–356.
- Osinski, G. R., Tornabene, L. L., Banerjee, N. R., Cockell, C. S., Flemming, R., Izawa, M. R. M., McCutcheon, J., Parnell, J., Preston, L. J., Pickersgill, A. E., Pontefract, A., Sapers, H. M., & Southam, G. (2013). Impact-generated hydrothermal systems on Earth and Mars. *Icarus*, *224*, 347–363. <https://doi.org/10.1016/j.icarus.2012.08.030>
- Pavlov, A. A., Vasilyev, G., Ostryakov, V. M., Pavlov, A. K., & Mahaffy, P. (2012). Degradation of the organic molecules in the shallow subsurface of Mars due to irradiation by cosmic rays. *Geophys. Res. Lett.*, *39*, L13202. <https://doi.org/10.1029/2012GL052166>

- Penny, D., & Poole, A. (1999). The nature of the last universal common ancestor. *Curr. Opin. Genet. Dev.*, 9, 672–677. [https://doi.org/10.1016/S0959-437X\(99\)00020-9](https://doi.org/10.1016/S0959-437X(99)00020-9)
- Peters, K. E., Walters, C. C., & Moldowan, J. M. (2005). *The biomarker guide: I. Biomarkers and isotopes in the environment and human history*, 2nd edn. Cambridge: Cambridge University Press.
- Plescia, J. B., & Saunders, R. S. (1982). Tectonic history of the Tharsis Region, Mars. *J. Geophys. Res. Solid Earth*, 87, 9775–9791. <https://doi.org/10.1029/JB087iB12p09775>
- Quantin, C., Carter, J., Thollot, P., Broyer, J., Lozach, L., Davis, J., Grindrod, P., Pajola, M., Baratti, E., Rossato, S., Allemand, P., Bultel, B., Leyrat, C., Fernando, J., & Ody, A. (2016). Oxia Planum, the landing site for ExoMars 2018. Paper presented at the 47th Lunar and Planetary Science Conference, The Woodlands, Texas.
- Reinhardt, M., Duda, J.-P., Blumenberg, M., Ostertag-Hennings, C., Reitner, J., Heim, C., & Thiel, V. (2018). The taphonomic fate of isorenieratene in Lower Jurassic shales—controlled by iron? *Geobiology*, 16, 237–251. <https://doi.org/10.1111/gbi.12284>
- Reinhardt, M., Goetz, W., Duda, J.-P., Heim, C., Reitner, J., & Thiel, V. (2019). Organic signatures in Pleistocene cherts from Lake Magadi (Kenya), analogs for early Earth hydrothermal deposits. *Biogeosci. Discuss.* <https://doi.org/10.5194/bg-2018-513>
- Reinhardt, M., Goetz, W., & Thiel, V.. *Testing MOMA flight-like pyrolysis GC–MS on analog samples from Earth (iron-rich shale and opaline chert)—implications for MOMA pyrolysis during the ExoMars 2020 rover mission.* (unpublished, to be submitted to *Astrobiology*)
- Rothschild, L. J., & Mancinelli, R. L. (2001). Life in extreme environments. *Nature*, 409, 1092–1101. <https://doi.org/10.1038/35059215>
- Ruiz-Mirazo, K., Peretó, J., & Moreno, A. (2004). A Universal Definition of Life: Autonomy and Open-Ended Evolution. *Origins Life Evol. Biosphere*, 34, 323–346. <https://doi.org/10.1023/B:ORIG.0000016440.53346.dc>
- Rushdi, A. I., & Simoneit, B. R. T. (2001). Lipid Formation by Aqueous Fischer–Tropsch-Type Synthesis over a Temperature Range of 100 to 400 °C. *Origins Life Evol. Biosphere*, 31, 103–118. <https://doi.org/10.1023/A:1006702503954>
- Schidlowski, M., Appel, P. W. U., Eichmann, R., & Junge, C. E. (1979). Carbon isotope geochemistry of the 3.7×10^9 -yr-old Isua sediments, West Greenland: implications for the Archaean carbon and oxygen cycles. *Geochim. Cosmochim. Acta*, 43, 189–199. [https://doi.org/10.1016/0016-7037\(79\)90238-2](https://doi.org/10.1016/0016-7037(79)90238-2)
- Schulte, M., Blake, D., Hoehler, T., & McCollom, T. M. (2006). Serpentinization and Its Implications for Life on the Early Earth and Mars. *Astrobiology*, 6, 364–376. <https://doi.org/10.1089/ast.2006.6.364>
- Schulze-Makuch, D., & Irwin, L. N. (2004). *Life in the Universe: Expectations and Constraints*. Cham: Springer.
- Schwarzbauer, J., & Jovančičević, B. (2015). *Fossil Matter in the Geosphere*. Dordrecht: Springer.
- Sephton, M. A., Love, G. D., Watson, J. S., Verchovsky, A. B., Wright, I. P., Snape, C. E., & Gilmour, I. (2004). Hydroxylation of insoluble carbonaceous matter in the Murchison meteorite: new insights into its macromolecular structure. *Geochim. Cosmochim. Acta*, 68, 1385–1393. <https://doi.org/10.1016/j.gca.2003.08.019>
- Sephton, M. A., Love, G. D., Meredith, W., Snape, C. E., Sun, C.-G., & Watson, J. S. (2005). Hydroxylation: A new technique for the analysis of macromolecular material in meteorites. *Planet. Space Sci.*, 53, 1280–1286. <https://doi.org/10.1016/j.pss.2005.06.008>
- Simoneit, B. R. T., Summons, R. E., & Jahnke, L. L. (1998). Biomarkers as Tracers for Life on Early Earth and Mars. *Origins Life Evol. Biosphere*, 28, 475–483. <https://doi.org/10.1023/A:1006508012904>
- Sinninghe Damsté, J. S., & de Leeuw, J. W. (1990). Analysis, structure and geochemical significance of organically-bound sulphur in the geosphere: State of the art and future research. *Org. Geochem.*, 16, 1077–1101. [https://doi.org/10.1016/0146-6380\(90\)90145-P](https://doi.org/10.1016/0146-6380(90)90145-P)
- Steele, A., McCubbin, F. M., & Fries, M. D. (2016). The provenance, formation, and implications of reduced carbon phases in Martian meteorites. *Meteorit. Planet. Sci.*, 51, 2203–2225. <https://doi.org/10.1111/maps.12670>
- Steele, A., Benning, L. G., Wirth, R., Siljeström, S., Fries, M. D., Hauri, E., Conrad, P. G., Rogers, K., Eigenbrode, J. L., Schreiber, A., Needham, A., Wang, J. H., McCubbin, F. M., Kiöcoyne, D., & Rodriguez Blanco, J. D. (2018). Organic synthesis on Mars by electrochemical reduction of CO₂. *Sci. Adv.*, 4, eaat5118. <https://doi.org/10.1126/sciadv.aat5118>
- Summons, R. E., Albrecht, P., McDonald, G. D., & Moldowan, J. M. (2008). Molecular Biosignatures. In O. Botta, J. L. Bada, J. Gomez-Elvira, E. Javaux, F. Selsis & R. E. Summons (Eds.), *Strategies of Life Detection* (pp. 133–159). Boston: Springer.

- Tachibana, S., Kouchi, A., Hama, T., Oba, Y., Piani, L., Sugawara, I., Endo, Y., Hidaka, H., Kimura, Y., Murata, K.-i., Yurimoto, H., & Watanabe, N. (2017). Liquid-like behavior of UV-irradiated interstellar ice analog at low temperatures. *Science*, 3, eaao2538. <https://doi.org/10.1126/sciadv.aao2538>
- van Thienen, P., Vlaar, N. J., & van den Berg, A. P. (2004). Plate tectonics on the terrestrial planets. *Phys. Earth Planet. Inter.*, 142, 61–74. <https://doi.org/10.1016/j.pepi.2003.12.008>
- Tissot, B. P., & Welte, D. H. (1984). *Petroleum formation and occurrence*, 2nd edn. Berlin: Springer. <https://doi.org/10.1007/978-3-642-87813-8>
- Ueno, Y., Yurimoto, H., Yoshioka, H., Komiya, T., & Maruyama, S. (2002). Ion microprobe analysis of graphite from ca. 3.8 Ga metasediments, Isua supracrustal belt, West Greenland: Relationship between metamorphism and carbon isotopic composition. *Geochim. Cosmochim. Acta*, 66, 1257–1268. [https://doi.org/10.1016/S0016-7037\(01\)00840-7](https://doi.org/10.1016/S0016-7037(01)00840-7)
- Urey, H. C. (1952). On the Early Chemical History of the Earth and the Origin of Life. *PNAS*, 38, 351–363.
- Vago, J. L., Westall, F., Pasteur Instrument Teams, Landing Site Selection Working Group, & Other Contributors (2017). Habitability on Early Mars and the Search for Biosignatures with the ExoMars Rover. *Astrobiology*, 17, 471–510. <https://doi.org/10.1089/ast.2016.1533>
- Valley, J. W., Cavosie, A. J., Ushikubo, T., Reinhard, D. A., Lawrence, D. F., Larson, J., Clifton, P. H., Kelly, T., F., Wilde, S., A., Moser, D. E., & Spicuzza, M. J. (2014). Hadean age for a post-magma-ocean zircon confirmed by atom-probe tomography. *Nat. Geosci.*, 7, 219–223. <https://doi.org/10.1038/ngeo2075>
- Van Kranendonk, M. J., Philippot, P., Lepot, K., Bodorkos, S., & Pirajno, F. (2008). Geological setting of Earth's oldest fossils in the ca. 3.5 Ga Dresser Formation, Pilbara Craton, Western Australia. *Precambrian Res.*, 167, 93–124. <https://doi.org/10.1016/j.precamres.2008.07.003>
- Wakeham, S. G., Sinninghe Damsté, J. S., Kohnen, M. E. L., & de Leeuw, J. W. (1995). Organic sulfur compounds formed during early diagenesis in Black Sea sediments. *Geochim. Cosmochim. Acta*, 59, 521–533. [https://doi.org/10.1016/0016-7037\(94\)00361-O](https://doi.org/10.1016/0016-7037(94)00361-O)
- Walter, M. R. (1976). *Stromatolites*. Amsterdam: Elsevier.
- Walter, M. R., Buick, R., & Dunlop, J. S. R. (1980). Stromatolites 3,400–3,500 Myr old from the North Pole area, Western Australia. *Nature*, 284, 443–445. <https://doi.org/10.1038/284443a0>
- Westall, F., & Brack, A. (2018). The Importance of Water for Life. *Space Sci. Rev.*, 214. <https://doi.org/10.1007/s11214-018-0476-7>
- Westall, F., & Cavalazzi, B. (2011). Biosignatures in Rocks. In J. Reitner & V. Thiel (Eds.), *Encyclopedia of Geobiology* (pp. 189–201). Dordrecht: Springer.
- Westall, F., Loizeau, D., Foucher, F., Bost, N., Bertrand, M., Vago, J. L., & Kminek, G. (2013). Habitability on Mars from a Microbial Point of View. *Astrobiology*, 13, 887–897. <https://doi.org/10.1089/ast.2013.1000>
- Westall, F., Foucher, F., Bost, N., Bertrand, M., Loizeau, D., Vago, J. L., Kminek, G., Gaboyer, F., Campbell, K. A., Bréhéret, J.-G., Gautret, P., & Cockell, C. S. (2015). Biosignatures on Mars: What, Where, and How? Implications for the Search for Martian Life. *Astrobiology*, 15, 998–1029. <https://doi.org/10.1089/ast.2015.1374>
- Whittet, D. C. B. (1996). Is Extraterrestrial Organic Matter Relevant to the Origin of Life on Earth? In D. C. B. Whittet (Ed.), *Planetary and Interstellar Processes Relevant to the Origins of Life* (pp. 249–262). Dordrecht: Springer.
- Williams, J.-P., Nimmo, F., Moore, W. B., & Paige, D. A. (2008). The formation of Tharsis on Mars: What the line-of-sight gravity is telling us. *J. Geophys. Res. Planets*, 113. <https://doi.org/10.1029/2007JE003050>
- Xiao, L., Huang, J., Christensen, P. R., Greeley, R., Williams, D. A., Zhao, J., & He, Q. (2012). Ancient volcanism and its implication for thermal evolution of Mars. *Earth Planet. Sci. Lett.*, 323–324, 9–18. <https://doi.org/10.1016/j.epsl.2012.01.027>
- Zahnle, K. (2006). Earth's Earliest Atmosphere. *Elements*, 2, 217–222. <https://doi.org/10.2113/gselements.2.4.217>
- Zahnle, K., Arndt, N., Cockell, C. S., Halliday, A. N., Nisbet, E., Selsis, F., & Sleep, N. H. (2007). Emergence of a Habitable Planet. *Space Sci. Rev.*, 129, 35–78. <https://doi.org/10.1007/s11214-007-9225-z>
- van Zuilen, M. A., Lepland, A., Teranes, J., Finarelli, J., Wahlen, M., & Arrhenius, G. (2003). Graphite and carbonates in the 3.8 Ga old Isua Supracrustal Belt, southern West Greenland. *Precambrian Res.*, 126, 331–348. [https://doi.org/10.1016/S0301-9268\(03\)00103-7](https://doi.org/10.1016/S0301-9268(03)00103-7)
- van Zuilen, M. A., Mathew, K., Wopenka, B., Lepland, A., Marti, K., & Arrhenius, G. (2005). Nitrogen and argon isotopic signatures in graphite from the 3.8-Ga-old Isua Supracrustal Belt, Southern West Greenland. *Geochim. Cosmochim. Acta*, 69, 1241–1252. <https://doi.org/10.1016/j.gca.2004.08.033>

2 Organic signatures in Pleistocene cherts from Lake Magadi (Kenya), analogs for early Earth hydrothermal deposits

Manuel Reinhardt, Walter Goetz, Jan-Peter Duda, Christine Heim, Joachim Reitner, & Volker Thiel

Biogeosciences Discussions (2019), accepted with minor revisions for publication in *Biogeosciences*

Organic matter in Archean hydrothermal cherts may provide an important archive for molecular traces of earliest life on Earth. The geobiological interpretation of this archive, however, requires a sound understanding of organic matter preservation and alteration in hydrothermal systems. Here we report on organic matter (including molecular biosignatures) enclosed in hydrothermally influenced cherts of the Pleistocene Lake Magadi (Kenya; High Magadi Beds and Green Beds)—important analogs for Archean cherts. The Magadi cherts contain low organic carbon (< 0.4 wt.%) that occurs in form of finely dispersed clots, layers, or encapsulated within microscopic carbonate rhombs. Both, extractable (bitumen) and non-extractable organic matter (kerogen) was analyzed. The bitumens contain immature “biolipids” like glycerol mono- and diethers (e.g., archaeol and extended archaeol), fatty acids and –alcohols indicative for, inter alia, thermophilic cyanobacteria, sulfate reducers, and haloarchaea. However, co-occurring “geolipids” such as n-alkanes, hopanes, and polycyclic aromatic hydrocarbons (PAHs) indicate that a fraction of the bitumen has been thermally altered to early or peak oil window maturity. This more mature fraction likely originated from defunctionalization of dissolved organic matter and/or hydrothermal petroleum formation at places of higher thermal flux. Like the bitumens, the kerogens also show variations in thermal maturities, which can partly be explained by admixture of thermally pre-altered macromolecules. However, findings of archaea-derived isoprenoid moieties in some of the kerogens indicate that a fast sequestration of microbial lipids into kerogen must have occurred while hydrothermal alteration was active. We posit that such early sequestration may enhance the survival of molecular biosignatures during in-situ hydrothermal (and post-depositional) alteration through deep time. Furthermore, the co-occurrence of organic matter with different thermal maturities in the Lake Magadi cherts suggests that similar findings in Archean hydrothermal deposits could partly reflect original environmental conditions, and not exclusively post-depositional overprint or contamination. Our results support the view that kerogen in Archean hydrothermal cherts may contain important information on early life. Our study also highlights the suitability of Lake Magadi as an analog system for hydrothermal chert environments on the Archean Earth.

2.1 Introduction

Organic matter trapped in Archean cherts is of utmost relevance for the reconstruction of earliest microbial processes on Earth, but its origin is only poorly constrained. Diagenesis and metamorphic processes have been obliterating the original organic matter over billions of years and complicate its interpretation. Many of the Archean cherts are associated with hydrothermal settings (e.g., Brasier et al., 2002; Duda et al., 2016, 2018; Djokic et al., 2017; Hickman-Lewis et al., 2018). In such environments, organic compounds may rapidly decompose due to elevated temperature and pressure conditions (Hawkes et al., 2015, 2016; Rossel et al., 2017) and may also be redistributed via hydrothermal cycling in the form of bitumen (e.g., Weston & Woolhouse, 1987; Clifton et al., 1990; Leif & Simoneit, 1995) or kerogen (Duda et al., 2018). The interpretation of organic signatures in Archean hydrothermal cherts therefore requires detailed knowledge on the preservation, alteration, and distribution pathways of organic matter in such environments. Some of these aspects can be studied in modern analogs.

Archean cherts generally originate from chemical precipitation or replacement processes of silica rather than biogenic precipitation by silicifying organisms (e.g., Sugitani et al., 2002; van den Boorn et al., 2007). Siliceous sediments associated with chemical precipitation are rare on the modern Earth, but can be found in some hot spring or shallow lacustrine environments. Important sites include the Taupo Volcanic Zone (New Zealand; Campbell et al., 2003), the Geysir hot spring area (Iceland; Jones et al., 2007; Jones & Renaut, 2010), the El Tatio geothermal field (Chile; Jones & Renaut, 1997; Nicolau et al., 2014) and the East African Rift system (Kenya; Renaut et al., 2002). Among the latter, the alkaline chert environment of Lake Magadi is of particular interest, as it represents an analog for Archean hydrothermal chert environments (Eugster & Jones, 1968; Pirajno & Van Kranendonk, 2005; Brenna, 2016).

Lake Magadi, the focus of this study, is located in the lowermost depression of the East African Rift Valley (south Kenya; ca. 1°54' S, 36°16' E). The geology of the surrounding hills is dominated by alkali trachyte (1.65 to 0.8 Ma; Baker, 1958, 1986). Cherts occur in three sedimentary units overlaying the trachytes, namely the Oloronga Beds (ca. 0.8 to 0.3 Ma; Fairhead et al., 1972; Behr & Röhricht, 2000), the Green Beds (*sensu* Behr and Röhricht 2000; Behr 2002; ca. 40 to 100 ka; Goetz & Hillaire-Marcel, 1992; Williamson et al., 1993) and the High Magadi Beds (9 to 25 ka; Williamson et al., 1993; Tichy & Seegers, 1999). Each of these units represents a different lake stage. Today, trona ($\text{Na}_3(\text{HCO}_3)(\text{CO}_3) \times \text{H}_2\text{O}$) is precipitating in large areas of the residual lake (Evaporite Series; Baker, 1958), and Lake Magadi is the type locality for cherts based on the sodium silicate mineral magadiite ($\text{NaSi}_7\text{O}_{13}(\text{OH})_3 \times 4(\text{H}_2\text{O})$; Eugster, 1967, 1969; Eugster & Jones, 1968; Hay, 1968).

Lake Magadi has strongly been influenced by changes in the local climate. Today the Magadi basin represents an evaporation pan with a closed hydrological cycle (i.e., no outflow) that is only recharged by ephemeral runoff and hydrothermal springs (ca. 28 to 86 °C at present; Eugster, 1970, 1986; Jones et al., 1977). During the Pleistocene, however, the water level has changed several times. The Oloronga Beds (not investigated in this study) were formed in a stratified freshwater lake (Roberts et al., 1993). The Green Beds, in contrast, were deposited in a highly dynamic, alkaline, shallow water environment, probably in periodically flooded hot spring mudflats (Behr & Röhricht, 2000). Lake levels may then have increased again during deposition of the High Magadi Beds (Behr & Röhricht, 2000), but the setting remained strongly evaporitic. However, chemical precipitation of silica gels, the precursor of most cherts at Lake Magadi, was likely induced by hydrothermal processes (Eugster & Jones, 1968), evaporation and microbial activity (Behr & Röhricht, 2000; Behr, 2002).

A variety of cherts from Lake Magadi and its surroundings contain microbial structures (Behr and Röhricht, 2000; Behr, 2002; Brenna, 2016). Especially the Green Bed cherts are associated with fingerprints of microbial activity such as stromatolites and silicified cyanobacteria cells (Behr & Röhricht, 2000). Organic matter archived in these cherts potentially encodes important information of geobiological value but has not been characterized so far.

Our study is focused on the origin, alteration and preservation of the organic matter in Pleistocene hydrothermal cherts from Lake Magadi, to support the interpretation of organic matter in early Earth hydrothermal deposits. For our analyses we used several complementary petrographic and organic-geochemical techniques, including (scanning electron) microscopy, Raman spectroscopy, catalytic hydrolysis (HyPy), gas chromatography–mass spectrometry (GC–MS) and gas chromatography–combustion–isotope ratio mass spectrometry (GC–C–IRMS). The combined application of petrographic and geochemical techniques is required to fully understand organic matter characteristics (e.g., appearance on macroscopic and molecular levels, identification of heterogeneities) in context of the depositional environment.

2.2 Materials and Methods

2.2.1 Sample material, petrographic and bulk geochemical analyses

Cherts from the Pleistocene High Magadi Beds (LM-1692–1695) and Green Beds (LM-1696–1699) were sampled from different surficial outcrops around the present Lake Magadi (extent area of the Pleistocene Lake Magadi; Röhricht, 1999). A recent siliceous sinter from Great Geysir, Iceland (IC-1700; 64°18'46'' N, 20°18'03'' W) was additionally analyzed as a reference.

Petrographic observation was performed on thin sections using a Zeiss SteREO Discovery.V8 stereomicroscope connected to an AxioCam MRc5 5-megapixel camera (transmitted and reflected light) and with a Leica DMLP microscope coupled to a Kappa Zelos-655C camera (polarized light). Chert fragments (sputtered with Au-Pd, 7.3 nm for 120 s) were furthermore investigated using a LEO 1530 Gemini scanning electron microscope (SEM) coupled with an Oxford INCA X-act energy dispersive X-ray spectrometer (EDX). Contents of organic carbon (C_{org}), inorganic carbon (C_{inorg}), sulfur and nitrogen were determined with a Hekatech Euro EA elemental analyzer and a Leco RC612 temperature programmable carbon analyzer. Element distributions were analyzed on sample slices using a Bruker M4 Tornado μ -XRF scanner equipped with a rhodium target X-ray tube at 50 kV and 200 μ A. Areas of ca. 50 mm² were mapped with scan resolution of 500 x 300 and using a spot size of 20 μ m.

2.2.2 Organic-geochemical preparation

All materials used for biomarker preparation were heated to 500 °C (3 hrs) and/or carefully rinsed with acetone. A blank (pre-combusted sea sand) was processed in parallel to track potential laboratory contamination. Outer surfaces (2–5 mm) of the chert samples were removed with a particularly cleaned rock saw, and the surfaces of the resulting inner blocks were carefully rinsed with dichloromethane (DCM). After grinding (Retsch MM 301 pebble mill), sample powders (50 g each) were ultrasonically extracted with 100 mL DCM/methanol (MeOH) (2/1, v/v), 100 mL DCM/MeOH (3/1, v/v) and 100 mL DCM (10 min, respectively). The total organic extract (TOE) was then desulfurized with reduced Cu. 10 % of each TOE was derivatized with trimethylchlorosilane (TMCS)/MeOH (1/9, v/v; heated for 1 h 30 min at 80 °C) and subsequently with *N,O*-bis(trimethylsilyl)trifluoroacetamide (BSTFA)/pyridine (3/2, v/v; heated for 1 h at 40 °C) to convert carboxyl groups into methyl esters, and hydroxyl groups into trimethylsilyl ethers. Another 50 % of each TOE was separated via column chromatography into a hydrocarbon (F1), alcohol/ketone (F2; including free lipids) and a polar fraction (F3). In brief, 7 g silica gel 60 were filled into a glass column (1.5 cm internal diameter), plugged with pre-extracted cotton wool and sand. The dried TOE was vapor-deposited onto ca. 0.5 g silica gel 60 and added to the column. F1 was eluted with 20 mL *n*-hexane/DCM (8/2, v/v), F2 with 30 mL DCM/ethyl acetate (9/1, v/v) and F3 with 100 mL DCM/MeOH (1/1, v/v) and 100 mL MeOH. F2 and F3 were derivatized with TMCS/MeOH (1/9, v/v; heated for 1 h 30 min at 80 °C) and with BSTFA/pyridine (3/2, v/v; heated for 1 h at 40 °C). The extraction residues were decalcified with HCl (37 %, 1 d, 20 °C) and desilicified with HF (48 %, 7 d, 20 °C). The remaining kerogens (i.e., the non-extractable portion of organic matter; Durand, 1980) from the Magadi cherts were used for catalytic hydrolysis (HyPy; 2.2.3; LM-1692–1693, LM-1695, LM-1697–1698) and Raman spectroscopy (2.2.6; LM-1692–1699). No kerogen could be isolated from IC-1700.

2.2.3 Catalytic hydrolysis (HyPy)

HyPy is an open-system pyrolysis technique for studying the molecular kerogen composition (Love et al., 1995). It involves the gentle release of kerogen-bound compounds through progressive heating under a high-pressure hydrogen atmosphere (150 bar) and in the presence of a sulfided molybdenum catalyst (ammonium dioxodithiomolybdate). HyPy has been demonstrated to be very sensitive and leaving the organic stereochemistry of released compounds largely intact (e.g., Love et al., 1995, 1997; Bishop et al., 1998; Meredith et al., 2014). Our experiments were conducted with a HyPy device from Strata Technology Ltd. (Nottingham, UK), following existing protocols (e.g., Brocks et al., 2003b; Marshall et al., 2007; Duda et al., 2018). In brief, between 1–10 mg of pre-extracted kerogen (3x ultrasonically extracted in DCM/MeOH (3/1, v/v)) was loaded with 10 wt.% of the catalyst and then pyrolyzed under a constant hydrogen flow of 6 L/min. HyPy was conducted following a two-step approach. The first step involved heating of the kerogens from ambient temperature to 250 °C (at 300 °C/min) and then to 330 °C (at 8 °C/min, held for 10 min). During this step, residual bitumens and compounds bound via unstable covalent bonds were released. In a second step, the remaining kerogens were heated from ambient temperature to 520 °C (at 8 °C/min), releasing solely covalently bound molecules. Pyrolysates from all steps were

collected in a silica gel trap cooled with dry ice (Meredith et al., 2004) and subsequently analyzed via GC–MS (2.2.4) and GC–C–IRMS (2.2.5). Blanks were run regularly to ensure constant experimental conditions and track potential contamination.

2.2.4 Gas chromatography–mass spectrometry (GC–MS)

Molecular fractions were analyzed using a Thermo Trace 1310 gas chromatograph (GC) coupled to a Thermo TSQ Quantum Ultra triple quadrupole mass spectrometer (MS). The GC was equipped with a fused silica capillary column (Phenomenex Zebron ZB-5MS, 30 m length, 250 μm internal diameter, 0.25 μm film thickness). Samples were injected with a Thermo TriPlus RSH autosampler into a splitless injector and transferred to the GC column at 320 $^{\circ}\text{C}$. The GC oven was heated under a constant He flow (1.5 mL/min) from 80 $^{\circ}\text{C}$ (held for 1 min) to 325 $^{\circ}\text{C}$ at 5 $^{\circ}\text{C}/\text{min}$ (held for 30 min). The MS source operated in electron ionization mode at 70 eV and 240 $^{\circ}\text{C}$. Organic compounds were analyzed in full scan mode (scan range 50–850 amu) and identified by comparison with published retention times and mass spectra.

2.2.5 Gas chromatography–combustion–isotope ratio mass spectrometry (GC–C–IRMS)

Compound-specific stable carbon isotope ratios ($\delta^{13}\text{C}_{\text{V-PDB}}$) were measured using a Thermo Scientific Trace GC coupled to a Delta Plus isotope ratio mass spectrometer (IRMS) via a combustion reactor (C). The GC was equipped with two serially linked silica capillary columns (Agilent DB-5 and DB-1, each with 30 m length, 250 μm internal diameter, 0.25 μm film thickness). The combustion reactor contained CuO, Ni and Pt, and was operated at 940 $^{\circ}\text{C}$. Fractions were injected into a splitless injector and transferred to the GC column at 290 $^{\circ}\text{C}$. The carrier gas was He with a flow rate of 1.2 mL/min. The temperature program started at 80 $^{\circ}\text{C}$, followed by heating to 325 $^{\circ}\text{C}$ at 5 $^{\circ}\text{C}/\text{min}$ (held for 60 min). Laboratory standards were analyzed to control the reproducibility of measuring conditions and CO_2 gas of known isotopic composition was used for calibration. $\delta^{13}\text{C}$ of the MeOH used for derivatization (methyl esters) and androstanol (underivatized, as well as TMS derivative) were measured to track isotopic changes through derivatization. The $\delta^{13}\text{C}$ values of derivatized compounds were then corrected according to Goñi & Eglinton (1996).

2.2.6 Raman spectroscopy

Raman spectroscopy was conducted on sample slices (thickness ca. 1 cm) and isolated kerogen flakes (see 2.2.2). At least 10 measurements were conducted per sample in order to evaluate internal variation and identify potential outliers. The measurements were performed with a WITEC alpha300 instrument. Spectra (scan range 100–4000 rel. cm^{-1}) were generated with a frequency-doubled continuous-wave Nd:YAG laser (532 nm, beam intensity of ca. 1 mW) over 10 s integration time by focusing through a 50x optical power objective. The reflected beam was dispersed by a 600 L/mm grating on its way into the detector (CCD, 248 pixels). The diameter of each measurement spot was ca. 0.7 μm . Calibration of the instrument (including stability over time) was routinely controlled by pure mineral phases (quartz, calcite, gypsum, beryl). The WITEC Control and Project FOUR 4.1 software was used to record and process all spectral data (smoothing, baseline correction, fitting). Choosing an appropriate Raman fitting method for organic carbon is not trivial as the established methods refer to specific temperature windows. In this study we applied a 6-Voigt-functions fit (after Schito et al., 2017) for low-temperature organic carbon and a 4-Voigt-functions fit (Beysac et al., 2002) for high-temperature organic carbon. Band nomenclature for the low-temperature organic carbon follows Rebelo et al. (2016), while the high-temperature organic carbon bands are named after Beysac et al. (2002). Peak temperatures (T_{max} ; averaged over all valid measurements on each sample) were inferred from (i) the vitrinite reflectance R_0 that in sum was calculated from the Raman band ratio RA2 for low-thermal-maturity spectra ($\text{RA2} = (\text{S} + \text{D1} + \text{D}) / (\text{Dr} + \text{G1} + \text{G})$; Schito et al., 2017; Barker & Pavlewicz, 1994) and (ii) the Raman band ratio R2 for high-thermal-maturity spectra ($\text{R2} = \text{D1} / (\text{G} + \text{D1} + \text{D2})$; Beysac et al., 2002).

2.3 Results

2.3.1 Petrography, bulk-geochemistry and Raman spectroscopy

Most of the Lake Magadi cherts studied reveal a dense silica matrix, except LM-1692 and LM-1693 which show microscopic pores of < 50 μm (Fig. 2.1a, d). The cherts exhibit brecciated (Fig. 2.1f), cloudy (Fig. 1g), and laminated (Fig. 2.1i–k) textures. Most of the textures resemble microbial mat fabrics and can contain distinct silicified microbial cells and filaments (Fig. 2.1e).

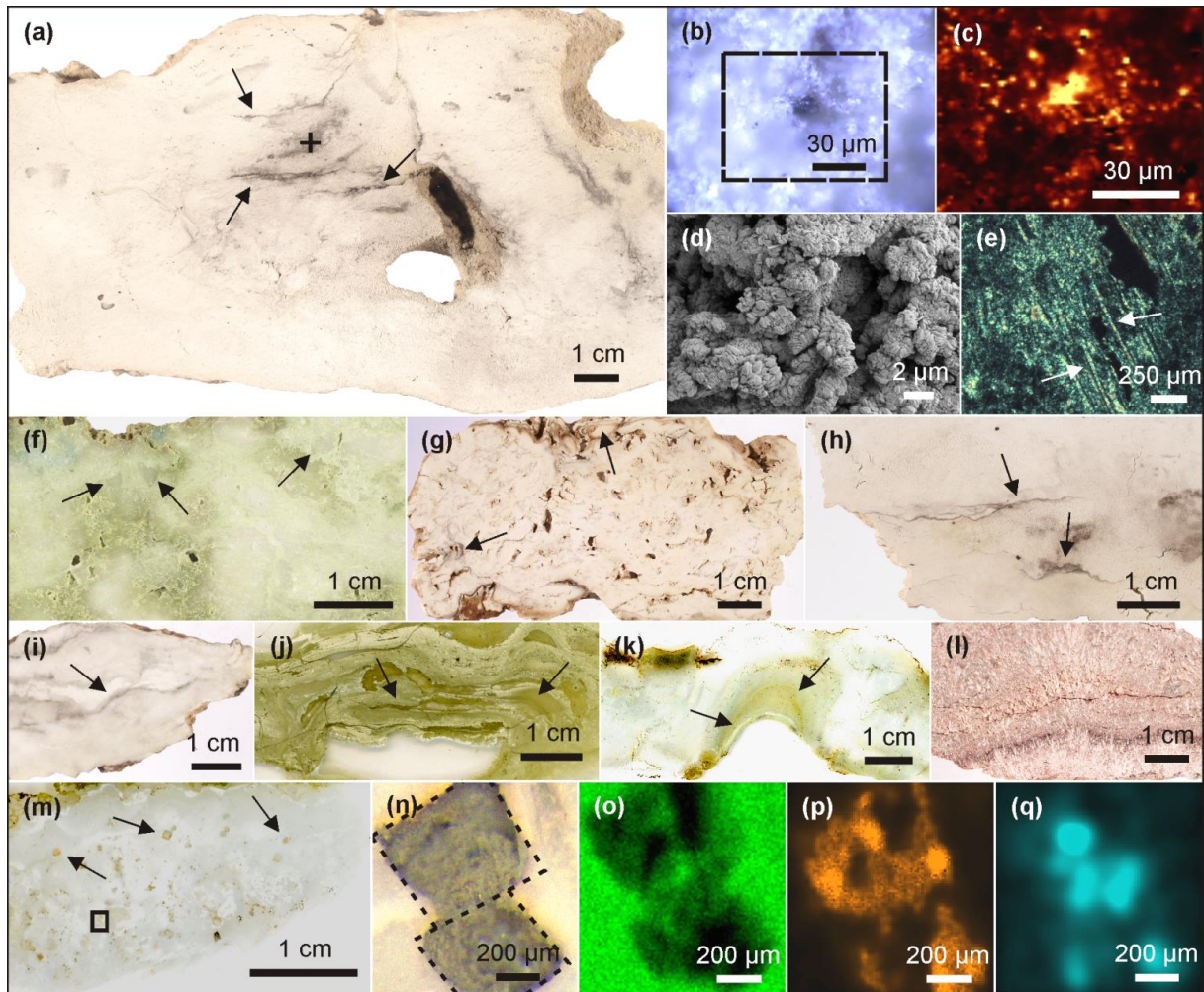


Fig. 2.1: Petrographic characteristics of Lake Magadi cherts. (a) Polished slice of LM-1692, revealing organic matter in the silica matrix (arrows). The cross marks the spot for Raman mapping (detailed in b–c). (b) Area of Raman mapping at $-2.5\ \mu\text{m}$ (dashed box, image scan 94×72 pixels). (c) Raman mapping result, yellow color indicates high abundances of organic matter. (d) SEM image from LM-1692, showing a porous matrix of microcrystalline quartz. (e) Silicified bacterial filaments from LM-1699 under polarized light (see arrows). (f) Brecciated texture (arrows) in LM-1699. (g) Cloudy microbial features (arrows) in LM-1694. (h) Layered organic matter (arrow) in LM-1693. (i–k) Laminated microbial mat patterns (arrows) preserved in LM-1695 (i), LM-1697 (j) and LM-1698 (k). (l) Silica sinter from Great Geysir, Iceland (IC-1700). (m) Carbonate rhombs (arrows) enclosed in the chert matrix of LM-1696. The box marks the area for μ -XRF scanning (n–q). (n) Close-up of boxed area showing carbonate rhombs under reflected light. (o–q) μ -XRF analyses of the same area showing silica (o), calcium (p), and sulfur (q) distributions (a brighter color indicates a higher concentration).

The samples show C_{org} values between 0.01 and 0.34 wt.% and CaCO_3 -contents of 0.05 to 4.47 wt% (Tab. 2.1). Total nitrogen (N) and sulfur (S) contents are generally low (< 0.02 – 0.05 wt.%, respectively; Tab. 2.1).

The organic matter occurs either layered (up to 0.5 mm; Fig. 2.1a, h), or finely dispersed in the form of small clots in the chert matrix ($< 20\ \mu\text{m}$; Fig. 2.1b–c). In some samples, organic matter is also associated with carbonate aggregates (Fig. 2.1m–q) and sulfur enrichments (Fig. 2.1q). The carbonate aggregates are up to 1 mm in size and partly have a rhombic shape (e.g., in LM-1696: Fig. 2.1m–q).

Raman spectra of isolated kerogen particles show a broad D-band centered at ca. $1354\ \text{cm}^{-1}$ and a G-band at ca. $1597\ \text{cm}^{-1}$ (Fig. 2.2). Vitrinite reflectance R_0 (calculated from RA2; Schito et al., 2017) generally ranges between 0.32 and 0.72 %, corresponding to maximum temperatures in the range of 40–110 °C (Tab. 2.2). Sample LM-1697 exhibited a second kerogen population with D- and G-bands centered at 1357 and 1577 cm^{-1} , respectively (Fig. 2.2), corresponding to a maximum temperature of ca. 440 °C (high-temperature, graphitic; Tab. 2.2, Fig. 2.2c; Beysac et al., 2002).

Tab. 2.1: Geochemical bulk data (C, N, S)

	C_{org}		C_{inorg}		calc. CaCO₃		N		S	
	wt. %	±	wt. %	±	wt. %	±	wt. %	±	wt. %	±
LM-1692	0.13	0.001					0.004	0.001	0.002	0.001
LM-1693	0.34	0.003	0.01	0.001	0.11	0.001	0.009	0.001	0.002	0.001
LM-1694	0.21	0.002	0.54	0.005	4.47	0.04	0.024	0.012	0.048	0.024
LM-1695	0.04	0.002	0.01	0.001	0.05	0.003	0.002	0.001	0.005	0.001
LM-1696	0.03	0.002	0.04	0.002	0.29	0.003	0.001	0.001	0.002	0.001
LM-1697	0.02	0.001	0.13	0.001	1.06	0.01	0.004	0.001	0.001	0.001
LM-1698	0.02	0.001	0.08	0.004	0.68	0.007	0.002	0.001	0.009	0.001
LM-1699	0.03	0.002	0.01	0.001	0.11	0.001	0.001	0.001	0.003	0.001
IC-1700	0.01	0.001					0.004	0.001	0.003	0.001

2.3.2 Bitumen

Figure 2.3 shows GC–MS chromatograms from bitumens of High Magadi Bed cherts (Fig. 2.3a–c), Green Bed cherts (Fig. 2.3d, e), and a recent siliceous sinter from Great Geysir in Iceland (Fig. 2.3f). The most noticeable compound classes in all samples are *n*-alkanes, *n*-alkanoic acids and *n*-alkan-1-ols (in decreasing abundance), plus glycerol diethers (Fig. 2.3a–c). GC-amenable aromatic compounds are low in abundance, but some polycyclic aromatic hydrocarbons (PAHs) were identified in all samples. One sample showed a pronounced unresolved complex mixture (UCM; LM-1697; Fig. 2.3d).

2.3.2.1 Functionalized lipids

Fatty acids (alkanoic and alkenoic acids)

n-Alkanoic acids typically range from C₁₂ to C₃₂ (Fig. 2.4a) and exhibit a clear even-over-odd-predominance, as expressed by OEP values $\ll 1$ (odd-to-even-predominance; Scalan & Smith, 1970; Tab. 2.3). The most abundant fatty acids are *n*-hexadecanoic acid (C_{16:0}) and *n*-octadecanoic acid (C_{18:0}). *n*-Alkenoic acids occur at low abundance and include C_{16:1}, C_{18:1} (tentatively identified as $\omega 9c/9t$) and C_{18:2}. Terminally methylated (*iso(i)*- and *anteiso(ai)*-) alkenoic acids are also present, including *i*-C_{15:0} and *i*-C_{17:0} (LM-1692–1694) plus *ai*-C_{14:0–17:0} and *ai*-C_{24:0–25:0} (LM-1692–1694). IC-1700 additionally shows *i*-C_{16:0}. Phytanic acid occurs in LM-1692–1695. The $\delta^{13}C$ signatures of the short- (C_{12–18}) and long-chain (C_{24–28}) alkenoic acids range from –22.4 to –29.6 ‰ in the Magadi cherts, and from –25.2 to –32.5 ‰ in IC-1700 (Tab. 2.4). The values do not differ much between short- and long-chain homologues ($\Delta < 2.4$ ‰), except for IC-1700 ($\Delta = 7.3$ ‰).

Alkanols and alkanones

n-Alkan-1-ols typically range from C₁₂ to C₃₂ (Fig. 2.4b). These compounds show a strong even-over-odd-predominance in all samples (OEP17 between 0.1 and 0.2, OEP29 between < 0.1 and 0.3; Tab. 2.3). Hexadecan-1-ol (C₁₆-OH) and octadecan-1-ol (C₁₈-OH) show highest abundances. In addition to the *n*-homologues, odd-numbered C_{15–25} *ai*-alkan-1-ols are present (see Fig. 2.4b). Short-chain (C₁₂ to C₁₈) *n*-alkan-1-ols from the Magadi cherts reveal mean $\delta^{13}C$ values between –29.4 and –35.9 ‰ (–27.7 ‰ in IC-1700). With increasing chain length, the homologues get more enriched in ¹³C (C_{24–28}, Δ up to 15.7 ‰ in LM-1694; Tab. 2.4).

n-Alkan-2-ols occur in diverse ranges (e.g., C₁₅ to C₃₁ in LM-1698; Fig. 2.5b). The distributions are unimodal (maximum at C₂₀) in LM-1692–1696, or bimodal (maxima at C₂₀ and C₃₁) in LM-1697–1699. In all samples, medium-chain *n*-alkan-2-ols (C_{18–24}) have no chain-length-predominance (OEP21 between 0.8 and 1.1; Tab. 2.3), while long-chain homologues (C_{25–31}) exhibit a clear odd-over-even-predominance (OEP29 between 1.9 and 5.9). IC-1700 shows a bimodal distribution with maxima at C₁₄ (minor) and C₂₀, and no chain-length-predominance.

n-Alkan-2-ones typically appear in the range of C₁₅ to C₃₁, but are virtually absent in LM-1699. Some samples show a unimodal distribution with no chain-length-preference (Fig. 2.5; Tab. 2.3), while most reveal a slight odd-over-even-predominance (OEP21 between 1.3 and 2.1). The isoprenoid ketone 6,10,14-trimethyl pentadecan-2-

one additionally occurs in every sample and is the most abundant alkan-2-one in LM-1692–1695 and IC-1700. Furthermore, *i*- and *ai*-alkan-2-ones appear in LM-1698 (C₁₈ to C₂₃; Fig. 2.5c).

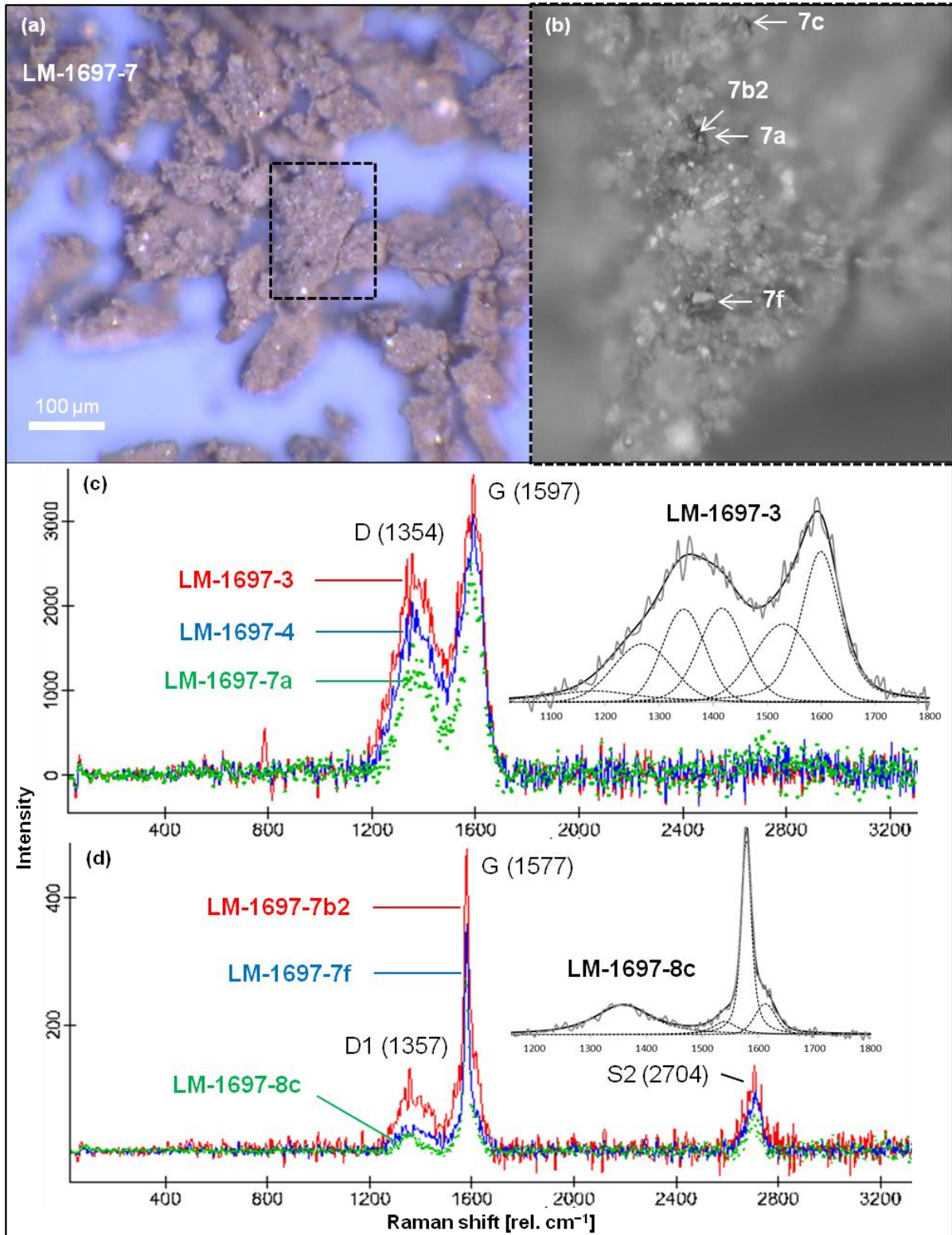


Fig. 2.2: Raman spectroscopy of kerogen isolated from Green Bed chert sample LM-1697. (a) Kerogen flakes under reflected light. (b) Detail from (a; dashed box) showing selected spots analyzed via Raman (arrows). (c, d) Raman spectra obtained from several spots on the kerogen flakes, including those denoted in (b); insets magnify the spectral range of ca. 1100–1800 rel. cm⁻¹ and show fits representative for kerogen populations (band order in c: S, D1, D, Dr, G1, G; Rebelo et al., 2016; band order in d: D1, D3, G, D2; Beyssac et al., 2002). Note the close spatial association of kerogen populations of low (immature; c) and high thermal maturity (graphitic; d) within the same sample.

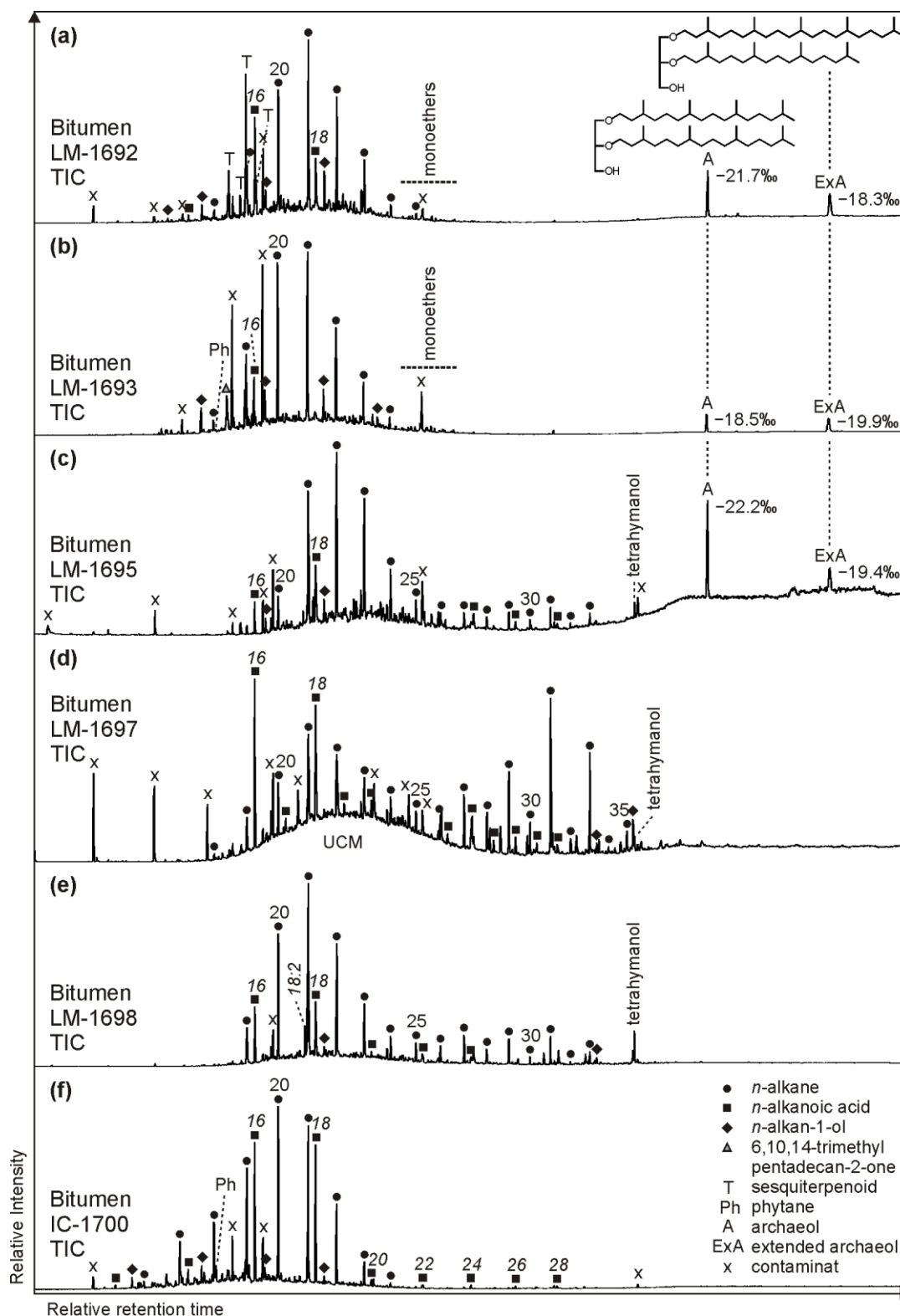


Fig. 2.3: Total ion chromatograms (TICs; 10–65 min) of the derivatized bitumens (alcohols were measured as trimethylsilyl ethers, carboxylic acids as methyl esters) from the High Magadi Bed cherts (a–c), the Green Bed cherts (d, e), and the Great Geysir silica sinter (f). Note pronounced *n*-alkanes showing a bell-shaped distribution in the medium-chain range (maxima at *n*-C₂₀, *n*-C₂₁ or *n*-C₂₂) in all chromatograms except LM-1697 (maximum at *n*-C₃₁). Other prominent compounds are hexa- and octadecanoic acid (all samples), tetrahymanol (LM-1695, LM-1697, LM-1698), glycerol monoethers (LM-1692–1693), and the glycerol diethers archaeol ($\delta^{13}\text{C}_{\text{V-PDB}}$ between -18.5 and -22.2 ‰) and extended archaeol ($\delta^{13}\text{C}_{\text{V-PDB}}$ between -18.3 and -19.9 ‰; LM-1692–1693 and LM-1695). Siloxanes and phthalates were identified as contaminants.

Other lipids

Glycerol monoethers (1-*O*-alkylglycerols) occur in all samples from Lake Magadi. Their highest diversity is observed in LM-1692–1694, including methyl-branched (*i*-C_{16:0}, 10Me-C_{16:0}, *i*-C_{17:0}, *ai*-C_{17:0}, Me-C_{17:0}, *i*-C_{18:0}), and straight (C_{15–18}) alkyl chains (see Fig. 2.4c). The most prominent monoether is 1-*O*-(10-methyl)-hexadecylglycerol (10Me-C_{16:0}). Furthermore, two glycerol diethers, namely di-*O*-phythanyl glycerol (archaeol; “A”, Fig. 2.3a–c) and *O*-phytanyl-*O*-sesterterpanylglycerol (extended archaeol; “ExA”, Fig. 2.3a–c) appear in LM-1692–1696 and LM-1699. Mono- and diethers show δ¹³C values between –10.9 and –22.2 ‰ (Tab. 2.4; Fig. 2.3a–c), with highest values in LM-1694 (–10.9 and –12.2 ‰, respectively).

Tab. 2.2: Environmental and maturity parameters from biomarker analysis (GC–MS) and Raman spectroscopy. The C₃₁ hopane S/(S+R) ratios (3rd column) are all in the range of 0.5 to 0.6 and therefore near saturation, implying that most organic compounds may have reached early-oil-window (vitrinite reflectance ≥ 0.6; Killops & Killops, 2005). These results are fully consistent with reflectances inferred from MPI-1 (5th and 6th column). Raman data (right-most two columns) have been acquired on few specific sample points and therefore reflect the heterogeneity of the sample rather than its bulk properties.

	C ₃₁								
	Pr/Ph ^a	Ph/ <i>n</i> -C ₁₈ ^b	S/(S+R) ^c	Phe/MP ^d	MPI-1 ^e	%R _c ^f	Flu/(Flu+Py) ^g	%R ₀ ^h	T _{max} [°C] ⁱ
<i>Bitumen</i>									
LM-1692	0.10	0.49	0.50	0.42	1.02	0.94	0.69		
LM-1693	0.18	0.36	0.58	0.62	0.63	0.66	0.66		
LM-1694	0.06	0.29	0.55	0.37	0.84	0.81	0.60		
LM-1695	0.37	0.39	0.49	0.61	0.69	0.70	0.48		
LM-1696	0.21	0.31	0.59	0.71	0.56	0.61	0.74		
LM-1697	0.25	0.37	0.61	0.95	0.48	0.56	0.79		
LM-1698	0.09	0.26	0.57	0.19	0.99	0.91	0.77		
LM-1699		0.29					0.61		
IC-1700	0.36	0.35		0.93	0.59	0.63	0.96		
<i>Kerogen</i>									
LM-1692		1.89		0.22	1.25	1.10	0.32	0.72	110
LM-1693		0.49		0.10	1.69	1.41	0.44	0.69	110
LM-1694								0.54	90
LM-1695	0.24	0.99		0.53	1.03	0.94	0.33	0.51	80
LM-1696								0.63	100
LM-1697				0.56	1.00	0.92	0.23	0.32	40
									440 ^j
LM-1698				0.72	0.89	0.85	0.32	0.35	50

^aPristane(Pr)/phytane(Ph) ratio

^bPhytane(Ph)/*n*-octadecane(*n*-C₁₈) ratio

^c17α, 21β(H)-C₃₁ hopane 22S/(S+R) ratio

^dPhenanthrene(Phe)/methylphenanthrene(MP) ratio

^eMethylphenanthrene index = 1.5 × (2-MP + 3-MP) / (Phe + 1-MP + 9-MP); Radke & Welte, 1983

^fComputed vitrinite reflectance = 0.7 × MPI-1 + 0.22 (Boreham et al., 1988), if Phe/MP < 1 (Brocks et al., 2003a)

^gFluoranthene(Flu)/(Flu + pyrene(Py)) ratio

^hVitrinite reflectance, calculated from Raman band ratio RA2 (Schito et al., 2017)

ⁱMean maximum temperature, calculated from R₀ (Barker & Pavlewicz, 1994)

^jMean maximum temperature, calculated from Raman band ratio R2 (Beysac et al., 2002)

Additionally, functionalized sesqui- and diterpenoids are always present and traces of C₃₁ or C₃₂ hopanoic acids are found in some samples. LM-1693 and LM-1695–1699 furthermore contain abundant tetrahymanol (δ¹³C

between -24.1 and -33.3 ‰). Sterols, particularly cholesterol and sitosterol, appear in small amounts in most samples.

2.3.2.2 Aliphatic hydrocarbons

n-Alkanes range from *n*-C₁₅ to *n*-C₃₃ and primarily show a unimodal distribution (maximum around *n*-C₂₁ and *n*-C₂₂; Figs. 2.3, 2.5a, A1) and no carbon chain-length-preference up to *n*-C₂₅ (OEP21 between 1.0 and 1.2; Tab. 2.3). However, an odd-over-even-preference is always observed for greater chain-lengths (OEP31 between 1.8 and 7.0; Tab. 2.3). Furthermore, *i*- and *ai*-alkanes are present (C₁₈ to C₂₅; Fig. 2.5a), following the distribution trend of the corresponding *n*-alkanes. Pristane (Pr) and phytane (Ph) are visible in all samples except LM-1699 (only Ph; Fig. A1). Pr/Ph ratios are below 0.37, while Ph/*n*-C₁₈ ratios range between 0.26 and 0.49 (Tab. 2.2). LM-1696 furthermore reveals 6-methylheptadecane (6Me-C₁₇; Fig. A1e). Medium-chain *n*-alkanes (C_{17–24}) show mean $\delta^{13}\text{C}$ values between -29.7 and -33.3 ‰ in the Lake Magadi cherts (-35.7 ‰ in IC-1700), while $\delta^{13}\text{C}$ values of higher homologues ($> \text{C}_{24}$) increase up to -26.2 ‰ (Δ between 1.9 and 7.2 ‰; Tab. 2.4).

The samples furthermore contain traces of 17 α ,21 β -hopanes (S+R isomers). The S/S+R isomer ratios of the C₃₁ pseudohomologues range between 0.49 and 0.61 (Tab. 2.2). Steranes are below detection limit.

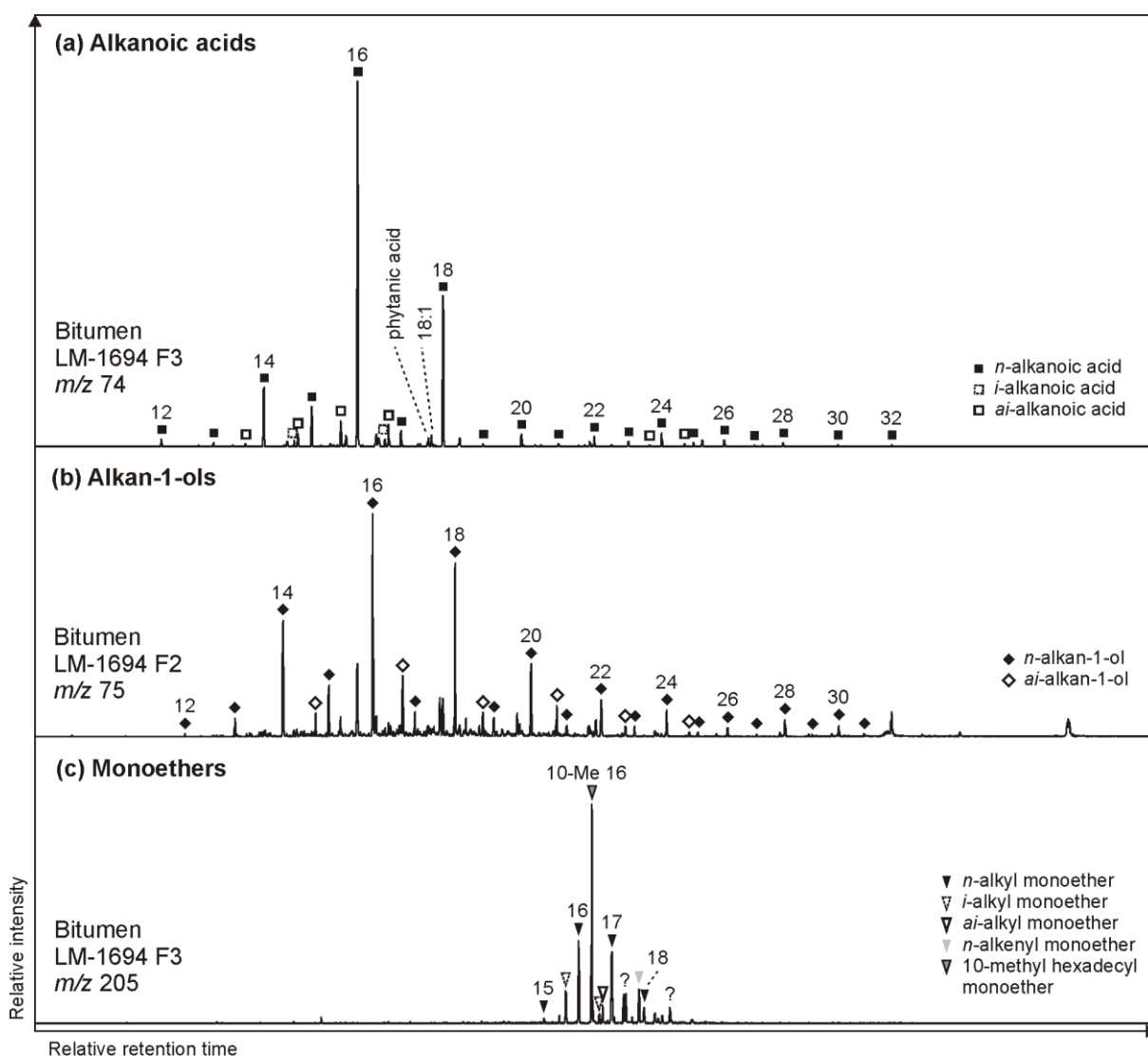


Fig. 2.4: Partial GC-MS ion chromatograms (10–60 min) of the derivatized alcohol/ketone (F2; alcohols were measured as trimethylsilyl ethers) and polar (F3; carboxylic acids were measured as methyl esters) fractions from bitumen of the High Magadi Bed chert LM-1694. Alkanoic acids (*m/z* 74; a) and alkan-1-ols (*m/z* 75; b) show a clear even-over-odd-predominance and dominances of linear C₁₆ and C₁₈ homologues. (c) Distribution of glycerol monoethers (*m/z* 205).

2.3.2.3 Polycyclic aromatic hydrocarbons (PAHs)

All samples contain low amounts of (monomethyl-) phenanthrenes, while anthracene is only observed in IC-1700. The methylphenanthrene indices (MPI-1, after Radke & Welte, 1983) vary between 0.48 and 1.02, resulting in calculated vitrinite reflectances (R_c , after Boreham et al., 1988) between 0.56 and 0.94 % (Tab. 2.2). Traces of dimethylphenanthrenes are detected in LM-1692–1698. Other PAHs observed are fluoranthene (Flu) and pyrene (Py) with Flu/(Flu+Py) ratios between 0.48 and 0.96 (Tab. 2.2).

Tab. 2.3: Odd-to-even-predominances (OEPs; Scalán & Smith, 1970) in bitumens and kerogens

	<i>Alkanoic acids</i>		<i>Alkan-1-ols</i>		<i>Alkan-2-ols</i>		<i>Alkan-2-ones</i>		<i>n-Alkanes</i>	
	OEP	OEP	OEP	OEP	OEP	OEP	OEP	OEP	OEP	OEP
	15	29	17	29	21	29	21	29	21	31
<i>Bitumen</i>										
LM-1692	0.2	0.3	0.1	<0.1	1.1		2.1		1.2	2.8
LM-1693	0.4	0.4	0.2	0.1	1.0	2.3	1.5		1.1	3.3
LM-1694	0.1	0.3	0.1	0.1	1.0	5.9	1.8		1.1	5.2
LM-1695	0.1	0.3	0.1	0.1	1.0		1.3		1.1	3.5
LM-1696	0.2	0.4	0.1	<0.1	1.0	2.2	1.3		1.1	2.3
LM-1697	0.2	0.5	0.2	0.3	0.9	1.9	1.1	1.2	1.0	6.5
LM-1698	0.1	0.5	0.2	0.2	1.0	1.9	1.1	1.5	1.0	7.0
LM-1699	0.2	0.4	0.1	0.1	0.8	4.5			1.0	4.0
IC-1700	0.1	0.2	0.2	<0.1	1.1		1.0		1.1	1.8
<i>Kerogen</i>										
LM-1692									1.0	0.9
LM-1693									1.0	0.7
LM-1695									1.0	0.7
LM-1697									1.0	0.8
LM-1698									1.0	0.7

$$\text{OEP}_n = (\text{C}_{n-2} + 6 \times \text{C}_n + \text{C}_{n+2}) / (4 \times \text{C}_{n-1} + 4 \times \text{C}_{n+1})^{(-1)^{(n+1)}}$$

2.3.3 Kerogen (high temperature HyPy step, up to 520 °C)

The high temperature HyPy pyrolysates (up to 520 °C; see 2.2.3) can be divided in two groups according to their compositions. LM-1692 and LM-1693 show a strong aromatic character (aliphatics/aromatics of 0.4 and 0.2, respectively), which is not observed in LM-1695 and LM-1697–1698 (aliphatic/aromatic of 1.1, 1.0 and 1.5, respectively). All pyrolyzed kerogens reveal varying distributions of *n*-alkanes (Fig. 2.6; see below).

2.3.3.1 Aliphatic hydrocarbons

Kerogen-bound *n*-alkanes exhibit maxima around *n*-C₁₈ (LM-1693, LM-1695, LM-1698), *n*-C₂₁ (LM-1692–1693, 1697) and *n*-C₃₂ (LM-1695, LM-1697–1698), and range from *n*-C₁₈ to *n*-C₃₆ (LM-1692–1693), *n*-C₁₄ to *n*-C₄₄ (LM-1695) or *n*-C₁₆ to *n*-C₄₆ (LM-1697–1698). No carbon chain-length-preference is visible up to *n*-C₂₆ (OEP₂₁ always 1.0, except for LM-1695; Tab. 2.3; Fig. 2.6c), but a slight even-over-odd-preference is observed for longer chains (OEP₃₁ between 0.7 and 0.9; Table 3). Moreover, all pyrolysates contain few *i*- and *ai*-alkanes (Fig. 2.6). Mean $\delta^{13}\text{C}$ values of medium-chain *n*-alkane moieties (C_{17–24}) range from –23.5 to –34.2 ‰, whereas long-chain *n*-alkanes (C_{25–40}) reveal values between –21.9 and –30.2 ‰ (Δ between 1.3 and 7.1 ‰; Tab. 2.4).

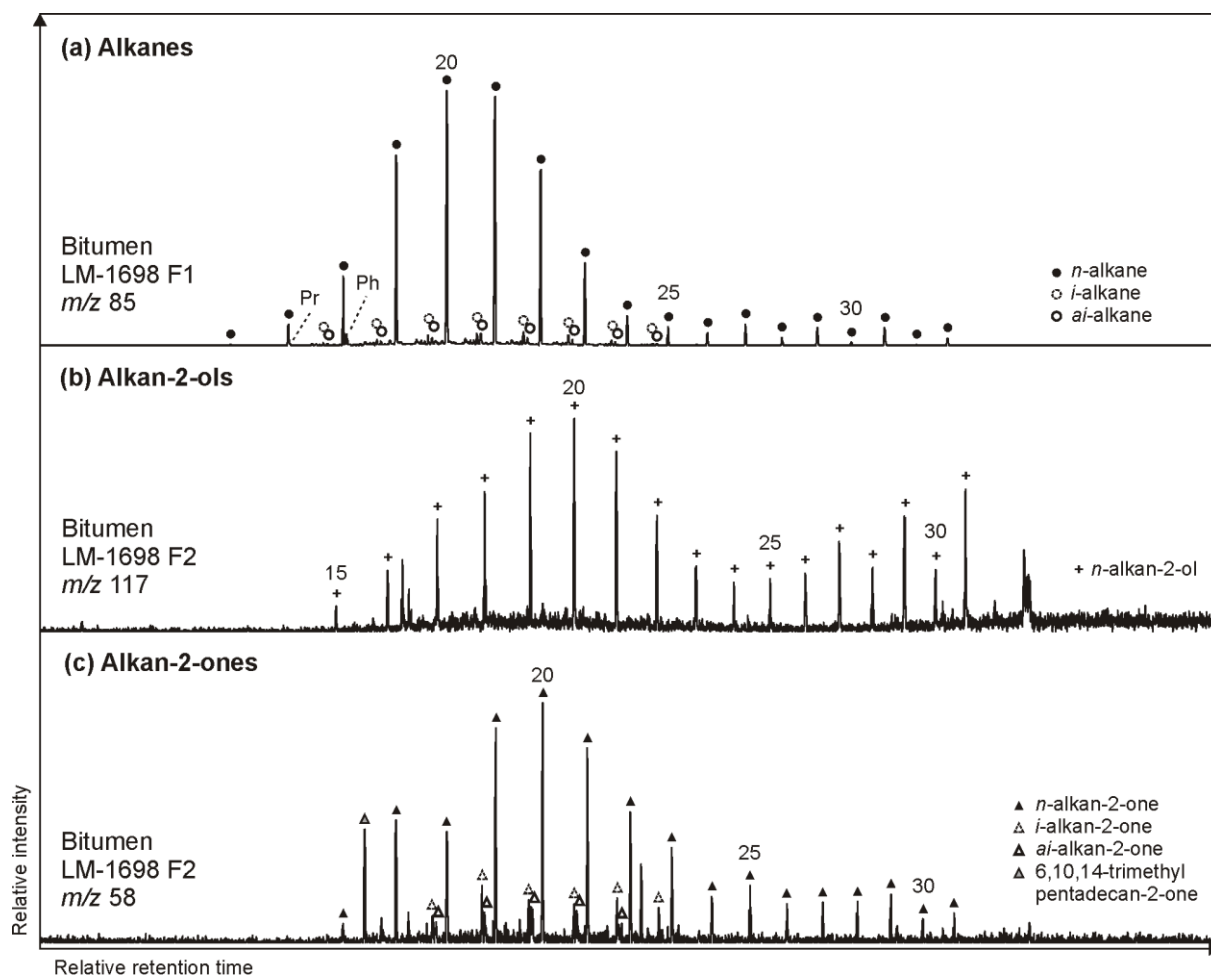


Fig. 2.5: Partial GC–MS ion chromatograms (10–55 min) of the hydrocarbon (F1) and derivatized alcohol/ketone fraction (F2; alcohols were measured as trimethylsilyl ethers) from bitumen of the Green Bed chert LM-1698. Medium-chain ($\sim C_{20}$) alkanes (m/z 85; a), alkan-2-ols (m/z 117; b) and alkan-2-ones (m/z 85; c) show similar distributions with no chain-length-predominance, while long-chain compounds reveal a clear odd-over-even-predominance particularly for alkanes and alkan-2-ols. Hydrothermal cracking of kerogen may produce alkanes that are then converted into alkan-2-ols and subsequently alkan-2-ones (Leif and Simoneit, 1995).

The regular acyclic isoprenoids phytane (Ph) and 2,6,10,14,18-pentamethylcosane (PMI_{reg} ; identified via mass spectrum; Fig. A2; Risatti et al., 1984; Greenwood & Summons, 2003) appear in LM-1692–1693 and LM-1695 ($Ph/n-C_{18}$ between 0.49 and 1.89). The regular acyclic isoprenoids farnesane (Far), norpristane (Nor) and pristane (Pr) are only present in LM-1695 ($Pr/Ph = 0.24$; Tab. 2.2), and biphytane occurs in LM-1693 and LM-1695 (Fig. 2.6b–c). The detection of phytane and PMI_{reg} in the kerogens of LM-1692–1693 and LM-1695 coincides with the appearance of archaeol and extended archaeol in the corresponding bitumens (Fig. 2.3a–c). $\delta^{13}C$ values of PMI_{reg} vary between -22.0 and -24.6 ‰, while phytane exhibits $\delta^{13}C$ values between -25.1 and -28.5 ‰ (Tab. 2.4; Fig. 2.6a–c).

2.3.3.2 PAHs

All kerogen pyrolysates contain (mono- and dimethylated) phenanthrenes, anthracene, plus various 4- and 5-ring PAHs. MPI-1 ranges from 0.89 to 1.69, corresponding to R_c values between 0.85 and 1.41 ‰ (Tab. 2.2). Fluoranthene (Flu) and pyrene (Py) with $Flu/(Flu+Py)$ ratios between 0.23 and 0.44 are also present. Methyl naphthalenes only occur in LM-1693 and LM-1695, while di- and trimethyl naphthalenes appear in LM-1693, LM-1695 and LM-1698.

Tab. 2.4: Mean $\delta^{13}\text{C}_{\text{V-PDB}}$ values in ‰ of key compound classes and selected biomarkers in bitumens and kerogens

	LM-1692	LM-1693	LM-1694	LM-1695	LM-1696	LM-1697	LM-1698	LM-1699	IC-1700
<i>Bitumen</i>									
Long-chain <i>n</i> -alkanoic acids (C _{24–28})	-25.2	-27.0	-26.3	-28.9	-22.4	-25.1	-27.4	-29.6	-32.5
Long-chain <i>n</i> -alkan-1-ols (C _{24–32})	-25.0	-32.3	-20.2	-29.1	-25.1	-23.7	-23.2	-24.0	-26.1
Long-chain <i>n</i> -alkanes (C _{25–33})				-30.9	-30.1	-31.5	-26.2	-26.5	
Short-chain <i>n</i> -alkanoic acids (C _{12–18})	-27.6	-26.5	-26.8	-28.9	-24.0	-25.8	-25.6	-27.0	-25.2
Short-chain <i>n</i> -alkan-1-ols (C _{12–18})	-33.5	-32.2	-35.9	-30.5	-32.6	-33.1	-29.4	-31.8	-27.7
Medium-chain <i>n</i> -alkanes (C _{17–24})	-32.1	-31.7	-31.7	-32.8	-32.6	-33.3	-33.3	-29.7	-35.7
Phytane	-33.3	-30.9	-30.0	-36.1	-34.7	-33.8	-35.3		-38.6
Archaeol	-21.7	-18.5	-12.2	-22.2	-14.8			-16.6	
Extended archaeol	-18.3	-19.9	-15.3	-19.4	-19.6				
Monoethers	-20.2	-20.2	-10.9	-18.6					
<i>Kerogen</i>									
Long-chain <i>n</i> -alkanes (C _{25–40})	-27.6	-30.2		-24.9		-21.9	-27.1		
Medium-chain <i>n</i> -alkanes (C _{17–24})	-30.5	-31.4		-28.3		-23.5	-34.2		
Phytane	-25.1	-26.8		-28.5					
PMI _{reg} ^a	-22.0	-24.0		-24.6					

^a2,6,10,14,18-pentamethylcosane (regular acyclic C₂₅ isoprenoid)

2.4 Discussion

2.4.1 Thermal maturity and syngeneity of the organic matter

The studied Lake Magadi cherts are of Pleistocene age and have not been buried. This is in good accordance with several molecular characteristics of the bitumens that suggest an immature nature of the organic matter. These features include the OEP29 of *n*-alkanoic acids (0.3–0.5) and *n*-alkan-1-ols (< 0.1–0.3), the OEP31 of *n*-alkanes (2.3–7.0), and the presence of intact functionalized lipids (e.g., archaeol, extended archaeol and monoethers). On the other hand, the OEP21 of medium-chain *n*-alkanes (1.0–1.2), Ph/*n*-C₁₈ ratios (≤ 0.49), MPI-1 ratios (0.48–1.02, mean 0.75), R_c values (0.56–0.94 %, mean 0.74 %) and C₃₁ S/(S+R) ratios (0.49–0.61, mean 0.56) are in line with early to peak oil window maturity (see ten Haven et al., 1987; Killips & Killips, 2005; Peters et al., 2005; Tab. 2.2). Hence, the bitumen preserved in the Magadi cherts consists of at least two fractions, a “fresh” immature portion co-occurring with a thermally mature component.

A similar maturity offset is also reflected in bulk- and molecular kerogen characteristics. A low thermal maturity is for instance indicated by low Raman-derived T_{max}-signatures in some samples (LM-1697 and LM-1698; ca. 40 and 50 °C; Fig. 2.2c; Tab. 2.2), and a slight even-over-odd preference of long-chain *n*-alkanes in all kerogen pyrolysates (OEP31 between 0.7 and 0.9; Tab. 2.3). At the same time, MPI-1 ratios (≤ 1.69), R_c values (≤ 1.41 %), the OEP21 of medium-chain *n*-alkanes (1.0 = no preference) indicate an elevated thermal maturity, which is in good accordance with Raman temperatures from the High Magadi Bed cherts and LM-1696 (T_{max} of up to 110 °C; Tab. 2.2). Some of the Raman spectra from the LM-1697 kerogen even evidence the presence of a high-temperature graphitic component (i.e., T_{max} ~440 °C; Fig. 2.2d, Tab. 2.2).

Such offsets between different thermal maturity parameters are typically related to an emplacement of organic material from another source (e.g., modern endoliths; e.g., Golubic et al., 1981; Hallmann et al., 2015). Most of the Lake Magadi cherts studied reveal a dense silica matrix, but a few samples (LM-1692, LM-1693) indeed show small pores that would allow for such emplacements. However, a recent emplacement is unlikely for the following reasons:

- (i) The analyzed samples did not show any viable microbial colonization (e.g., biofilms, or endolith borings).
- (ii) No carbonaceous microbial remains were discovered via SEM coupled to EDX and all detected microfossils are silicified (see Fig. 2.1e).
- (iii) Kerogens contain fingerprints of functionalized moieties in their corresponding bitumens (e.g., isoprenoids appear only in kerogens that show archaeol and extended archaeol in their corresponding bitumens; Figs. 2.3 and 2.6).
- (iv) The $\delta^{13}\text{C}$ values of long-chain *n*-alkanes from the Green Bed chert kerogens matches the $\delta^{13}\text{C}$ values of long-chain *n*-alkanoic acids from bitumens ($\Delta \leq 3 \text{‰}$), supporting their taphonomic relation.

Consequently, both, the rather immature and the thermally altered organic matter can be considered syngenetic to the Pleistocene cherts.

2.4.2 Geobiology of the Lake Magadi during chert deposition

2.4.2.1 Prokaryotes

Archaeol and extended archaeol appear in all High Magadi Bed and two Green Bed chert bitumens (LM-1696 and LM-1699), and their molecular fossils are important contributors to the corresponding kerogens. While archaeol is a common constituent of Euryarchaeal lipids (e.g., Koga, 1993; Pancost et al., 2011; Dawson et al., 2012; Villanueva et al., 2014), extended archaeol is restricted to alkaliphilic and non-alkaliphilic haloarchaea (e.g., De Rosa et al., 1982; Teixidor et al., 1993; Dawson et al., 2012) and, in traces, to some methanogens (e.g., Grant et al., 1985; Becker et al., 2016). Archaeol and extended archaeol were also found in various halophilic archaea from recent Lake Magadi (e.g., *Natronobacterium pharaonis*, *Natronobacterium magadii*, *Natronobacterium gregoryi*, *Natronococcus occultus*; Tindall et al., 1985) and haloarchaea are abundant in recent Lake Magadi hot spring communities (Kambura et al., 2016). It is therefore likely that these halophiles have contributed the archaeols to the Lake Magadi cherts.

Cyanobacterial contribution to primary production is directly evidenced by 6Me-C₁₇ in LM-1696 (Fig. A1e), which is typically produced by the nitrogen-fixing thermophile *Fischerella* (Coates et al., 2014). Bacterial activity in the chert environment is also indicated by the C₃₂-hopanoic acid in LM-1693 and LM-1694, an early degradation product of bacteriohopanepolyols (Farrimond et al., 2002). Further molecular traits of bacteria are C₁₅ and C₁₇ *i*-/*ai*-fatty acids (cf., Parkes & Taylor, 1983) and monounsaturated and saturated C₁₆ and C₁₈ fatty acids, although the latter can also derive from algae (e.g., Taipale et al., 2013, 2016) or higher plant polymers (Kolattukudy, 1980). The monoethers found in the High Magadi Bed chert bitumens occur in various bacteria, and are particularly prevalent in sulfate reducers (e.g., Yang et al., 2015; Vinçon-Laugier et al., 2016 and references therein). Given the hydrothermally influenced setting, the broad variety of these compounds in the Magadi cherts (C₁₅ to C₁₉ moieties) may be attributed to thermophiles. Indeed, *i*-C_{16:0}, C_{16:0} and *ai*-C_{17:0} monoethers are dominant in Thermodesulfobacteria (Langworthy et al., 1983; Hamilton-Brehm et al., 2013), while C_{18:1} and C_{18:0} monoethers were reported from Aquificales (Huber et al., 1992; Jahnke et al., 2001). The most abundant monoether in the Magadi cherts, 10Me-C_{16:0}, was recently detected in mesophilic heterotrophic Desulfobacterales, i.e. sulfate-reducing bacteria (Vinçon-Laugier et al., 2016).

All archaeal lipids in bitumens show an enrichment in ¹³C compared to the fatty acids (Δ up to +14.6 ‰ between archaeol and short-chain fatty acids in LM-1694). Such heavy values are known from CO₂-limited hypersaline environments (e.g., Schidlowski et al., 1984; Schouten et al., 2001) and may be amplified by high bioproductivity (e.g., de Marais et al., 1989; Schidlowski et al., 1994). Halobacteria, however, are heterotrophs and use an organic rather than an inorganic carbon source (e.g., Tindall, 1984; Dawson et al., 2012). If so, these organisms must have fed on an isotopically heavy, thus autochthonous pool of primary produced organic matter (cf., Birgel et al. 2014). This is also in good agreement with the fact that all monoethers are enriched in ¹³C compared to other lipids (Tab. 2.4) and underpins that the cherts formed in an evaporitic environment.

2.4.2.2 Eukaryotes

Tetrahymanol is typically produced by ciliates (Mallory et al., 1963; Harvey & McManus et al., 1991), but may also originate from few bacteria (e.g., Kleemann et al., 1990; Banta et al., 2015), ferns (Zander et al., 1969) and fungi (Kemp et al., 1984). It is furthermore associated with alkaline environments (e.g., ten Haven et al., 1989; Thiel et al., 1997), which is well in line with the evaporative setting of Lake Magadi.

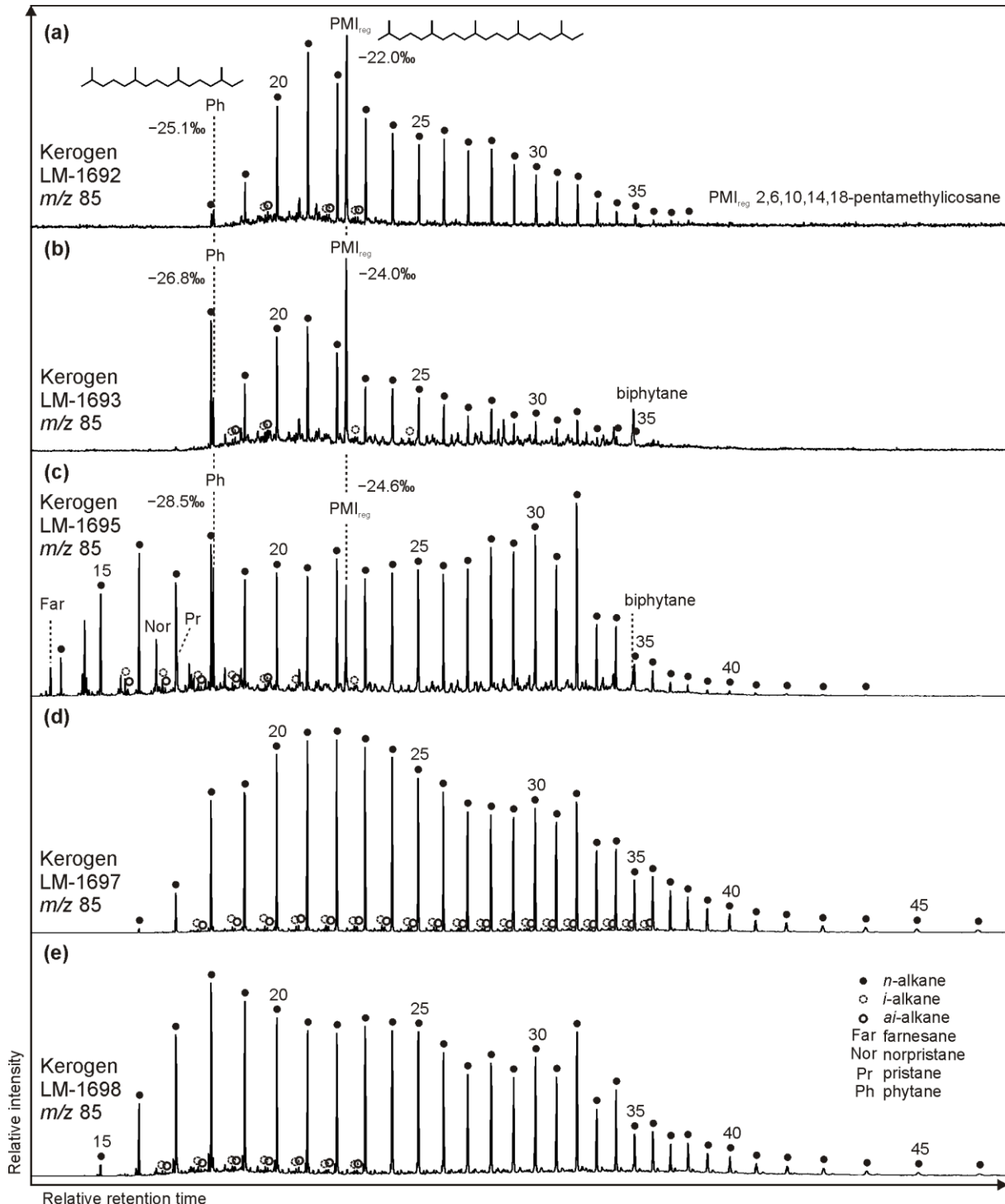


Fig. 2.6: Partial GC–MS ion chromatograms (m/z 85; 10–70 min) from kerogen HyPy pyrolysates (high temperature step, up to 520 °C) of High Magadi Bed cherts (a–c), and Green Bed cherts (d, e). $\delta^{13}\text{C}_{\text{V-PDB}}$ values are given for selected compounds. Note different n -alkane distributions in the kerogens, with LM-1698 showing the broadest range ($n\text{-C}_{15}$ to $n\text{-C}_{46}$). Also note that the regular acyclic isoprenoids phytane and 2,6,10,14,18-pentamethyl icosane are only present in High Magadi Bed chert kerogens (a, b, c). Furthermore, farnesane, norpristane and pristane appear in LM-1695, while biphytane is visible in LM-1693 and LM-1695.

The presence of only small amounts of typical algal sterols (cholesterol and sitosterol; cf., Taipale et al., 2016) in the Lake Magadi cherts indicates minor contributions from these primary producers. Long-chain alkanolic acids and alkan-1-ols with an OEP29 of $\ll 1$ in bitumens as well as the corresponding n -alkanes with an OEP31 of 0.7–0.9 in kerogens (Tab. 2.3) indicate inputs from higher land plants (Eglinton & Hamilton, 1967). Further biomarker evidence for plant input is provided by functionalized sesqui- and diterpenoids (e.g., Otto & Simoneit, 2002; Hautevelle et al., 2006; Fig. 2.3a). However, the overall predominance of prokaryotic biomarkers (2.4.4.2) and the

petrographic observations of silicified microbial mat remains and microbial cells (2.3.1; Fig. 2.1e–h) suggest a minor importance of eukaryotes in the lake ecosystem.

The $\delta^{13}\text{C}$ signals of long-chain *n*-alkanoic acids from Lake Magadi (between -22.4 and -29.6 ‰; Tab. 2.4) are in the range of the short-chain homologues (Δ between $+2.4$ and -2.6 ‰), while the Icelandic reference sample (-32.5 ‰) shows a pronounced $\delta^{13}\text{C}$ depletion ($\Delta +7.3$ ‰). All $\delta^{13}\text{C}$ values are in the range of C_3 plants (Schidlowski, 1988, 2001). The slightly heavier $\delta^{13}\text{C}$ values of compounds in the Magadi cherts may indicate additional contributions by C_4 plants (cf., Schidlowski, 1988, 2001; Chikaraishi et al., 2004) which are common in latitudes of the Magadi area (Still et al., 2003). Unlike the *n*-alkanoic acids, long-chain *n*-alkanes in LM-1695–1697 bitumens reveal more depleted $\delta^{13}\text{C}$ values around -31 ‰, pointing at a different origin (unknown).

2.4.2.3 Hydrothermal impact on organic matter

In all Lake Magadi cherts a narrow, bell-shaped pattern of *n*-alkanes with a maximum around *n*- C_{21} is dominant in the bitumens (Figs. 2.3a–e, 2.5a, A1a–h). This *n*-alkane distribution is also present in the bitumen from the Great Geysir reference sample (IC-1700; Figs. 2.3f, A1i) and has been frequently reported from other hydrothermal sites (e.g., Simoneit, 1984; Weston & Woolhouse, 1987; Clifton et al., 1990; Simoneit et al., 2009). As the hydrothermal system of the Magadi basin consists of a dilute ground water reservoir, deep brines, and recycled lake brines (Eugster, 1970; Jones et al., 1977), it appears plausible that immature organic compounds from the lake environment have been thermally altered by hydrothermal cycling, resulting, *inter alia*, in a loss of functional groups (cf., McCollom & Seewald, 2003; Hawkes et al., 2016; Rossel et al., 2017). Consequently, the *n*-alkanes from bitumens might represent stable thermal alteration products of originally functionalized compounds, such as linear fatty acids and *n*-alkanols.

Such hydrothermal processes may also yield compounds through the *in-situ* cracking of macromolecular organic matter from the cherts (e.g., alkanes and hopanes, see 2.3.2.2). However, temperatures of hydrothermal waters from present springs at Lake Magadi are not higher than 86 °C (Eugster, 1970, 1986; Jones et al., 1977). Furthermore, two kerogens from the Green Bed cherts still show relatively low Raman-derived T_{max} values (ca. 40 – 50 °C; Tab. 2.2). *In-situ* maturation near hot springs within the lake may therefore not sufficiently explain the presence of thermally mature organic components in all cherts analyzed.

Alternatively, organic matter from older lake sediments (Oloronga Beds) may have been penetrated by hot fluids, resulting in the formation of hydrothermal petroleum, a process known from other hydrothermal environments (e.g., Clifton et al., 1990; Weston & Woolhouse, 1987; Czochanska et al., 1986; Leif & Simoneit, 1995). This is in good accordance with the early to peak oil window maturity of some bitumen compounds as e.g. indicated by the MPI-1 ratios (≤ 1.02) and C_{31} S/(S+R) ratios (≤ 0.61 ; Peters et al., 2005; Tab. 2.2). Cooling and pressure decline of ascending hydrothermal fluids would have led to decreasing solubility of the compounds entrained, resulting in precipitation and thus, fractionation (cf., Simoneit, 1984; Clifton et al., 1990). Such hydrothermal “geochromatography” (Krooss et al., 1991) may explain the narrow distribution of medium-chain *n*-alkanes present in the chert bitumens. Hydrothermal petroleum generation may furthermore be supported by the unimodal distribution patterns of medium-chain *n*-alkan-2-ones and *n*-alkan-2-ols in bitumens, although the exact origin of these compounds is difficult to elucidate. *n*-Alkan-2-ones with similar distributions have previously been reported from hydrothermal oils and may originate from pyrolysis of aliphatic moieties (with *n*-alkan-2-ols as intermediates; Leif & Simoneit, 1995) or pyrolysis of fatty acids with subsequent β -oxidation and decarboxylation (George & Jardin, 1994). Further, both, *n*-alkan-2-ones and *n*-alkan-2-ols were experimentally produced by Fischer–Tropsch-type reactions under hydrothermal conditions (Rushdi & Simoneit, 2001; Mißbach et al., 2018). In addition to these thermally driven reactions, *n*-alkan-2-ones may also derive from microbial oxidation of *n*-alkanes (e.g., Cranwell et al., 1987; van Bergen et al., 1998), potentially also with *n*-alkan-2-ol intermediates (Allen et al., 1971; Cranwell et al., 1987).

The relatively low abundance of PAHs in the bitumens may indicate low formation temperatures of hydrothermal petroleum (cf., Simoneit, 1984; Simoneit et al., 1987; Clifton et al., 1990). This could be due to a shallow sedimentary source which is well in line with the geological situation at Lake Magadi. The Oloronga Beds (maximal thickness of 45 m; Behr, 2002) are the oldest sediments in the young rift basin (ca. 7 Ma; Baker 1958, 1986; geothermal gradient of ca. 200 °C/km; Wheildon et al., 1994) and were not deeply buried at the time of the Green Bed chert deposition. PAHs are common in dissolved organic matter from hydrothermal fluids (e.g., Konn et al., 2009, 2012; McCollom et al., 2015; Rossel et al., 2017), but may also derive from wildfires. Incomplete combustion of biomass may be a relevant source particularly in LM-1694 and LM-1699, as Flu/(Flu+Py) ratios of about 0.61 (see Tab. 2.2) are considered indicative for a wildfire origin (Yunker et al., 2002).

Hydrothermal activity may not only have impacted the bitumens. Kerogen from LM-1697 shows highly mature graphitic particles (Raman-based T_{\max} of ca. 440 °C; Fig. 2.2; Tab. 2.2). These particles may either originate from hydrothermal processes (Luque et al., 2009; van Zuilen et al., 2012), or alternatively from wildfires (Cope & Chaloner, 1980; Schmidt & Noack, 2000 and references therein). As the Flu/(Flu+Py) ratio in the LM-1697 kerogen is substantially lower as expected for a wildfire source (0.23 vs. 0.61; Yunker et al., 2002) and also the bitumen fraction shows no indication of biomass combustion (Flu/(Flu+Py) = 0.79; Tab. 2.2), the high temperature particles in LM-1697 most likely do not originate from combustion.

We propose that the graphite was produced at depth through the hydrothermally mediated alteration (cf., Luque et al., 2009) of the surrounding trachyte and/or by mineral-templated growth (cf., van Zuilen et al., 2012) during hydrothermal circulation of bitumen-rich fluids. The hydrothermal fluids may then have transported graphite particles into the lake. Like graphite, thermally altered macromolecular particles from older lake sediments may have also been introduced by hydrothermal fluids which would explain the elevated mean Raman temperatures of LM-1692–1693 and LM-1696 kerogens (Raman-based T_{\max} of 100–110 °C; Tab. 2.2), the high MPI-1 (up to 1.69) and R_c (up to 1.41 %; Tab. 2.2) in all kerogens and the strong aromatic character of LM-1692 and 1693 kerogens (see 2.3.3).

The occurrence of thermally mature organic components in the studied materials is therefore most likely due to syndepositional hydrothermal processes and reflects an environmental signature.

2.4.3 Organic signatures from the Magadi cherts: implications for the Archean

A fraction of the organic matter preserved in the Magadi cherts may have been introduced by hydrothermal fluids. Such hydrothermally driven redistribution of organic matter has recently been proposed as an important process for kerogen in Archean hydrothermal vein cherts (“hydrothermal pump hypothesis”; Duda et al., 2018). Another similar feature to findings from Archean cherts is the variability of organic matter characteristics on a small spatial scale observed in the Lake Magadi samples (i.e., heterogeneous thermal maturities of organic matter within a given sample; appearance of organic matter in clots, layers or carbonate rhombs; see Ueno et al., 2004; Allwood et al., 2006; Tice & Lowe, 2006; Glikson et al., 2008; Morag et al., 2016). In case of ancient cherts, such heterogeneities are generally interpreted as a result of post-depositional metamorphic processes (e.g., Ueno et al., 2004; Tice & Lowe, 2006; Morag et al., 2016) rather than syndepositional hydrothermal activity (e.g., Allwood et al., 2006; Glikson et al., 2008). Our results highlight the possibility that organic matter of very different nature and maturity may be enclosed into hydrothermal chert precipitates *a priori*. Such *in-situ* mixing of different organic components should also be considered in the interpretation of Archean environments (see Allwood et al., 2006; Glikson et al., 2008; Morag et al., 2016; Duda et al., 2018). Of course, the heterogeneous maturity signals still have to be in accordance with the overall metamorphic history of the host rock.

In addition, our kerogen data show that archaeal lipid biomarkers are preserved in the macromolecular network (Fig. 2.6). Their presence in the kerogens that show a high thermal overprint (LM-1692–1693; Tab. 2.2) implies a rapid incorporation into macromolecular organic matter, while hydrothermal alteration is active. The kerogen matrix can form an effective shield against oxidation, biodegradation and thermal maturation, thus promoting the preservation of bound compounds over geological time. It has been shown that archaeal lipids can be bound rapidly into macromolecular networks in non-hydrothermal marine sediments (Pancost et al., 2008). The fact that archaeal lipid biomarkers were yielded during the high temperature HyPy step (up to 520 °C) of the Magadi kerogens evidences that these compounds may survive mild diagenetic influences. In this view, a conservation of kerogen-bound molecular biosignatures also in early Archean hydrothermal cherts (see Marshall et al., 2007; Duda et al., 2018) appears plausible. Our results, together with current findings from Archean hydrothermal systems (Duda et al., 2016, 2018; Djokic et al., 2017), therefore underline the enormous potential of hydrothermal cherts as valuable archives for biosignatures of early life on Earth.

2.5 Conclusions

The depositional record of Lake Magadi (Kenya) contains cherts with different organic matter, remarkably similar to Archean cherts from the Pilbara Craton (Western Australia) and the Barberton Greenstone Belt (South Africa). We found that a significant portion of the bitumens (extractable) and kerogens (non-extractable) in cherts from Lake Magadi is thermally immature and contains biomarkers of various prokaryotic microorganisms (e.g., thermophilic cyanobacteria, sulfate reducers, and haloarchaea). The presence of thermophilic organisms is well in line with a hydrothermal environment. At the same time, both the bitumens and kerogens also exhibit a thermally

mature fraction. We explain this apparent offset between different maturity parameters in the Lake Magadi cherts (immature vs. mature) as a result of a syndepositional hydrothermal alteration (e.g., defunctionalization, pre-maturation) and redistribution of organic matter in the environment. These processes include hydrothermal petroleum expulsion in underlying sedimentary units (Oloronga Beds) and a subsequent introduction of the thermally mature cracking products into the lake. Our findings aid in the interpretation of heterogeneous organic signatures in Archean rocks, which may reflect original environmental conditions in some cases. In addition, the preservation of archaeal lipid biomarkers in Magadi chert kerogens demonstrates that biomolecules can survive destructive hydrothermal processes through rapid polymerization and condensation. In this view, a preservation of kerogen-bound molecular biosignatures even in early Archean hydrothermal cherts appears plausible.

Acknowledgements

We thank G. Arp, W. Dröse, J. Dyckmans, A. Hackmann, D. Hause-Reitner, H. Mißbach, A. Reimer, and B. Röring for scientific and technical support. We furthermore thank A. Schito for providing Raman fitting parameters. This work was financially supported by the International Max Planck Research School (IMPRS) for Solar System Science at the University of Göttingen, the Deutsche Forschungsgemeinschaft (grants DU 1450/3-1 and DU 1450/4-1), and the Göttingen Academy of Sciences and Humanities.

References

- Allen, J. E., Forney, F. W., & Markovetz, A. J. (1971). Microbial subterminal oxidation of alkanes and alk-1-enes. *Lipids*, *6*, 448–452. <https://doi.org/10.1007/BF02531227>
- Allwood, A. C., Walter, M. R., & Marshall, C. P. (2006). Raman spectroscopy reveals thermal palaeoenvironments of c. 3.5 billion-year-old organic matter. *Vib. Spectrosc.*, *41*, 190–197. <https://doi.org/10.1016/j.vibspec.2006.02.006>
- Baker, B. H. (1958). *Geology of the Magadi area*. Geological Survey of Kenya.
- Baker, B. H. (1986). Tectonics and volcanism of the southern Kenya Rift Valley and its influence on rift sedimentation. In L. E. Frostick et al. (Eds.), *Sedimentation in the African Rifts* (pp. 45–57). London: Geol. Soc. Spec. Publ.
- Banta, A. B., Wei, J. H., & Welander, P. V. (2015). A distinct pathway for tetrahymanol synthesis in bacteria, *PNAS*, *112*, 13478–13483. <https://doi.org/10.1073/pnas.1511482112>
- Barker, C. E., & Pawlewicz, M. J. (1994). Calculation of Vitrinite Reflectance from Thermal Histories and Peak Temperatures. In P. K. Mukhopadhyay & W. G. Dow (Eds.), *Vitrinite Reflectance as a Maturity Parameter* (pp. 216–229). Washington, DC: Am. Chem. Soc.
- Becker, K. W., Elling, F. J., Yoshinaga, M. Y., Söllinger, A., Urich, T., & Hinrichs, K.-U. (2016). Unusual butane- and pentanetriol-based tetraether lipids in *Methanomassiliicoccus luminyensis*, a representative of the seventh order of methanogens. *Appl. Environ. Microbiol.*, *82*, 4505–4516. <https://doi.org/10.1128/AEM.00772-16>
- Behr, H.-J. (2002). Magadiite and Magadi chert: a critical analysis of the silica sediments in the Lake Magadi Basin, Kenya. In R. W. Renaut & G. M. Ashley (Eds.), *Sedimentation in Continental Rifts* (pp. 257–273). Tulsa, Oklahoma: SEPM Spec. P.
- Behr, H.-J., & Röhrlich, C. (2000). Record of seismotectonic events in siliceous cyanobacterial sediments (Magadi cherts), Lake Magadi, Kenya. *Int. J. Earth Sci.*, *89*, 268–283. <https://doi.org/10.1007/s005319900070>
- van Bergen, P. F., Nott, C. J., Bull, I. D., Poulton, P. R., & Evershed, R. P. (1998). Organic geochemical studies of soils from the Rothamsted Classical Experiments—IV. Preliminary results from a study of the effect of soil pH on organic matter decay. *Org. Geochem.*, *29*, 1779–1795. [https://doi.org/10.1016/S0146-6380\(98\)00188-0](https://doi.org/10.1016/S0146-6380(98)00188-0)
- Beyssac, O., Goffé, B., Chopin, C., & Rouzaud, J. N. (2002). Raman spectra of carbonaceous material in metasediments: a new geothermometer. *J. Metamorph. Geol.*, *20*, 859–871. <https://doi.org/10.1046/j.1525-1314.2002.00408.x>
- Birgel, D., Guido, A., Liu, X., Hinrichs, K.-U., Gier, S., & Peckmann, J. (2014). Hypersaline conditions during deposition of the Calcare di Base revealed from archaeal di- and tetraether inventories. *Org. Geochem.*, *77*, 11–21. <https://doi.org/10.1016/j.orggeochem.2014.09.002>
- Bishop, A. N., Love, G. D., McAulay, A. D., Snape, C. E., & Farrimond, P. (1998). Release of kerogen-bound hopanoids by hydrolysis. *Org. Geochem.*, *29*, 989–1001. [https://doi.org/10.1016/S0146-6380\(98\)00140-5](https://doi.org/10.1016/S0146-6380(98)00140-5)

- van den Boorn, S. H. J. M., van Bergen, M. J., Nijman, W., & Vroon, P. Z. (2007). Dual role of seawater and hydrothermal fluids in Early Archean chert formation: Evidence from silicon isotopes. *Geology*, *35*, 939–942. <https://doi.org/10.1130/G24096A.1>
- Boreham, C. J., Crick, I. H., & Powell, T. G. (1988). Alternative calibration of the Methylphenanthrene Index against vitrinite reflectance: Application to maturity measurements on oils and sediments. *Org. Geochem.*, *12*, 289–294. [https://doi.org/10.1016/0146-6380\(88\)90266-5](https://doi.org/10.1016/0146-6380(88)90266-5)
- Brasier, M. D., Green, O. R., Jephcoat, A. P., Kleppe, A. K., Van Kranendonk, M. J., Lindsay, J. F., Steele, A., & Grassineau, N. V. (2002). Questioning the evidence for Earth's oldest fossils. *Nature*, *416*, 76–81. <https://doi.org/10.1038/416076a>
- Brenna, B. L. (2016). *The Chemical, Physical, and Microbial Origins of Pleistocene Cherts at Lake Magadi, Kenya Rift Valley*. M.Sc. thesis, Department of Geological Sciences, University of Saskatchewan, Saskatoon.
- Brocks, J. J., Buick, R., Logan, G. A., & Summons, R. E. (2003a). Composition and syngeneity of molecular fossils from the 2.78 to 2.45 billion-year-old Mount Bruce Supergroup, Pilbara Craton, Western Australia. *Geochim. Cosmochim. Acta*, *67*, 4289–4319. [https://doi.org/10.1016/S0016-7037\(03\)00208-4](https://doi.org/10.1016/S0016-7037(03)00208-4)
- Brocks, J. J., Love, G. D., Snape, C. E., Logan, G. A., Summons, R. E., & Buick, R. (2003b). Release of bound aromatic hydrocarbons from late Archean and Mesoproterozoic kerogens via hydropyrolysis. *Geochim. Cosmochim. Acta*, *67*, 1521–1530. [https://doi.org/10.1016/S0016-7037\(02\)01302-9](https://doi.org/10.1016/S0016-7037(02)01302-9)
- Campbell, K. A., Buddle, T. F., & Browne, P. R. L. (2003). Late Pleistocene siliceous sinter associated with fluvial, lacustrine, volcanoclastic and landslide deposits at Tahunaatara, Taupo Volcanic Zone, New Zealand. *Trans. R. Soc. Edinburgh: Earth Sci.*, *94*, 485–501. <https://doi.org/10.1017/S0263593300000833>
- Chikaraishi, Y., Naraoka, H., & Poulson, S. R. (2004). Hydrogen and carbon isotopic fractionations of lipid biosynthesis among terrestrial (C3, C4 and CAM) and aquatic plants. *Phytochemistry*, *65*, 1369–1381. <https://doi.org/10.1016/j.phytochem.2004.03.036>
- Clifton, C. G., Walters, C. C., & Simoneit, B. R. T. (1990). Hydrothermal petroleum from Yellowstone National Park, Wyoming, U.S.A. *Appl. Geochem.*, *5*, 169–191. [https://doi.org/10.1016/0883-2927\(90\)90047-9](https://doi.org/10.1016/0883-2927(90)90047-9)
- Coates, R. C., Podell, S., Korobeynikov, A., Lapidus, A., Pevzner, P., Sherman, D. H., Allen, E. E., Gerwick, L., & Gerwick, W. H. (2014). Characterization of Cyanobacterial Hydrocarbon Composition and Distribution of Biosynthetic Pathways. *PLoS ONE*, *9*, e85140. <https://doi.org/10.1371/journal.pone.0085140>
- Cope, M. J., & Chaloner, W. G. (1980). Fossil charcoal as evidence of past atmospheric composition. *Nature*, *283*, 647–649. <https://doi.org/10.1038/283647a0>
- Cranwell, P. A., Eglinton, G., & Robinson, N. (1987). Lipids of aquatic organisms as potential contributors to lacustrine sediments—II. *Org. Geochem.*, *11*, 513–527. [https://doi.org/10.1016/0146-6380\(87\)90007-6](https://doi.org/10.1016/0146-6380(87)90007-6)
- Czochanska, Z., Sheppard, C. M., Weston, R. J., Woolhouse, A. D., & Cook, R. A. (1986). Organic geochemistry of sediments in New Zealand. Part I. A biomarker study of the petroleum seepage at the geothermal region of Waiotapu. *Geochim. Cosmochim. Acta*, *50*, 507–515. [https://doi.org/10.1016/0016-7037\(86\)90100-6](https://doi.org/10.1016/0016-7037(86)90100-6)
- Dawson, K. S., Freeman, K. H., & Macalady, J. L. (2012). Molecular characterization of core lipids from halophilic archaea grown under different salinity conditions. *Org. Geochem.*, *48*, 1–8. <https://doi.org/10.1016/j.orggeochem.2012.04.003>
- De Rosa, M., Gambacorta, A., Nicolaus, B., Ross, H. N. M., Grant, W. D., & Bu'Lock, J. D. (1982). An Asymmetric Archaeobacterial Diether Lipid from Alkaliphilic Halophiles. *J. Gen. Microbiol.*, *128*, 343–348. <https://doi.org/10.1099/00221287-128-2-343>
- Des Marais, D. J., Cohen, Y., Nguyen, H., Cheatham, M., Cheatham, T., & Munoz, E. (1989). Carbon isotopic trends in the hypersaline ponds and microbial mats at Guerrero Negro, Baja California Sur, Mexico: Implications for Precambrian stromatolites. In Y. Cohen & E. Rosenberg (Eds.), *Microbial Mats: Physiological Ecology of Benthic Microbial Communities* (pp. 191–203). Washington, DC: American Society for Microbiology.
- Djokic, T., Van Kranendonk, M. J., Campbell, K. A., Walter, M. R., & Ward, C. R. (2017). Earliest signs of life on land preserved in ca. 3.5 Ga hot spring deposits. *Nat. Commun.*, *8*, e15263. <https://doi.org/10.1038/ncomms15263>
- Duda, J.-P., Van Kranendonk, M. J., Thiel, V., Ionescu, D., Strauss, H., Schäfer, N., & Reitner, J. (2016). A Rare Glimpse of Paleoarchean Life: Geobiology of an Exceptionally Preserved Microbial Mat Facies from the 3.4 Ga Strelley Pool Formation, Western Australia. *PLoS ONE*, *11*, e0147629. <https://doi.org/10.1371/journal.pone.0147629>

- Duda, J.-P., Thiel, V., Bauersachs, T., Mißbach, H., Reinhardt, M., Schäfer, N., Van Kranendonk, M. J., & Reitner, J. (2018). Ideas and perspectives: hydrothermally driven redistribution and sequestration of early Archaean biomass – the “hydrothermal pump hypothesis”. *Biogeosciences*, *15*, 1535–1548. <https://doi.org/10.5194/bg-15-1535-2018>
- Durand, B. (1980). Sedimentary organic matter and kerogen. Definition and quantitative importance of kerogen. In B. Durand (Ed.), *Kerogen: Insoluble organic matter from sedimentary rocks* (pp. 13–34). Paris: Editions Technip.
- Eglinton, G., & Hamilton, R. J. (1967). Leaf Epicuticular Waxes. *Science*, *156*, 1322–1335. <https://doi.org/10.1126/science.156.3780.1322>
- Eugster, H. P. (1967). Hydrous Sodium Silicates from Lake Magadi, Kenya: Precursors of Bedded Chert. *Science*, *157*, 1177–1180. <https://doi.org/10.1126/science.157.3793.1177>
- Eugster, H. P. (1969). Inorganic bedded cherts from the Magadi area, Kenya. *Contrib. Mineral. Petrol.*, *22*, 1–31. <https://doi.org/10.1007/BF00388011>
- Eugster, H. P. (1970). Chemistry and origin of the brines of Lake Magadi, Kenya. *Mineral. Soc. Amer. Spec. Pap.*, *3*, 213–235.
- Eugster, H. P. (1986). Lake Magadi, Kenya: a model for rift valley hydrochemistry and sedimentation?. *Geol. Soc. Spec. Publ.*, *25*, 177–189. <https://doi.org/10.1144/GSL.SP.1986.025.01.15>
- Eugster, H. P., & Jones, B. F. (1968). Gels Composed of Sodium-Aluminium Silicate, Lake Magadi, Kenya. *Science*, *161*, 160–163. <https://doi.org/10.1126/science.161.3837.160>
- Fairhead, J. D., Mitchell, J. G., & Williams, L. A. J. (1972). New K/Ar Determinations on Rift Volcanics of S. Kenya and their Bearing on Age of Rift Faulting. *Nature Physical Science*, *238*, 66–69. <https://doi.org/10.1038/physci238066a0>
- Farrimond, P., Griffiths, T., & Evdokiadis, E. (2002). Hopanoic acids in Mesozoic sedimentary rocks: their origin and relationship with hopanes. *Org. Geochem.*, *33*, 965–977. [https://doi.org/10.1016/S0146-6380\(02\)00059-1](https://doi.org/10.1016/S0146-6380(02)00059-1)
- George, S. C., and Jardine, D. R. (1994). Ketones in a Proterozoic dolerite sill. *Org. Geochem.*, *21*, 829–839. [https://doi.org/10.1016/0146-6380\(94\)90042-6](https://doi.org/10.1016/0146-6380(94)90042-6)
- Glikson, M., Duck, L. J., Golding, S. D., Hofmann, A., Bolhar, R., Webb, R., Baiano, J. C. F., & Sly, L. I. (2008). Microbial remains in some earliest Earth rocks: Comparison with a potential modern analogue. *Precambrian Res.*, *164*, 187–200. <https://doi.org/10.1016/j.precamres.2008.05.002>
- Goetz, C., & Hillaire-Marcel, C. (1992). U-series disequilibria in early diagenetic minerals from Lake Magadi sediments, Kenya: Dating potential. *Geochim. Cosmochim. Acta*, *56*, 1331–1341. [https://doi.org/10.1016/0016-7037\(92\)90065-Q](https://doi.org/10.1016/0016-7037(92)90065-Q)
- Golubic, S., Friedmann, E. I., & Schneider, J. (1981). The lithobiontic ecological niche, with special reference to microorganisms. *J. Sediment. Petrol.*, *51*, 475–478. <https://doi.org/10.1306/212F7CB6-2B24-11D7-8648000102C1865D>
- Goñi, M. A., & Eglinton, T. I. (1996). Stable carbon isotopic analyses of lignin-derived CuO oxidation products by isotope ratio monitoring-gas chromatography-mass spectrometry (irm-GC-MS). *Org. Geochem.*, *24*, 601–615. [https://doi.org/10.1016/0146-6380\(96\)00052-6](https://doi.org/10.1016/0146-6380(96)00052-6)
- Grant, W. D., Pinch, G., Harris, J. E., De Rosa, M., & Gambacorta, A. (1985). Polar Lipids in Methanogen Taxonomy. *J. Gen. Microbiol.*, *131*, 3277–3286. <https://doi.org/10.1099/00221287-131-12-3277>
- Greenwood, P. F., & Summons, R. E. (2003). GC–MS detection and significance of crocetane and pentamethylcosane in sediments and crude oils. *Org. Geochem.*, *34*, 1211–1222. [https://doi.org/10.1016/S0146-6380\(03\)00062-7](https://doi.org/10.1016/S0146-6380(03)00062-7)
- Hallmann, C., Friedenberger, H., Hause-Reitner, D., & Hoppert, M. (2015). Depth profiles of microbial colonization in sandstones. *Geomicrobiol. J.*, *32*, 365–379. <https://doi.org/10.1080/01490451.2014.929762>
- Hamilton-Brehm, S. D., Gibson, R. A., Green, S. J., Hopmans, E. C., Schouten, S., van der Meer, M. T. J., Shields, J. P., Sinninghe Damsté, J. S., & Elkins, J. G. (2013). *Thermodesulfobacterium geofontis* sp. nov., a hyperthermophilic, sulfate-reducing bacterium isolated from Obsidian Pool, Yellowstone National Park. *Extremophiles*, *17*, 251–263. <https://doi.org/10.1007/s00792-013-0512-1>
- Harvey, H. R., & McManus, G. B. (1991). Marine ciliates as a widespread source of tetrahymanol and hopan-3 β -ol in sediments. *Geochim. Cosmochim. Acta*, *55*, 3387–3390. [https://doi.org/10.1016/0016-7037\(91\)90496-R](https://doi.org/10.1016/0016-7037(91)90496-R)
- Hauteville, Y., Michels, R., Malartre, F., & Trouiller, A. (2006). Vascular plant biomarkers as proxies for palaeoflora and palaeoclimatic changes at the Dogger/Malm transition of the Paris Basin (France). *Org. Geochem.*, *37*, 610–625. <https://doi.org/10.1016/j.orggeochem.2005.12.010>

- ten Haven, H. L., de Leeuw, J. W., Rullkötter, J., & Sinninghe Damsté, J. S. (1987). Restricted utility of the pristane/phytane ratio as a palaeoenvironmental indicator. *Nature*, *330*, 641–643. <https://doi.org/10.1038/330641a0>
- ten Haven, H. L., Rohmer, M., Rullkötter, J., & Bisserset, P. (1989). Tetrahymanol, the most likely precursor of gammacerane, occurs ubiquitously in marine sediments. *Geochim. Cosmochim. Acta*, *53*, 3073–3079. [https://doi.org/10.1016/0016-7037\(89\)90186-5](https://doi.org/10.1016/0016-7037(89)90186-5)
- Hawkes, J. A., Rossel, P. E., Stubbins, A., Butterfield, D., Connelly, D. P., Achterberg, E. P., Koschinsky, A., Chavagnac, V., Hansen, C. T., Bach, W., & Dittmar, T. (2015). Efficient removal of recalcitrant deep-ocean dissolved organic matter during hydrothermal circulation. *Nat. Geosci.*, *8*, 856–860. <https://doi.org/10.1038/ngeo2543>
- Hawkes, J. A., Hansen, C. T., Goldhammer, T., Bach, W., & Dittmar, T. (2016). Molecular alteration of marine dissolved organic matter under experimental hydrothermal conditions. *Geochim. Cosmochim. Acta*, *175*, 68–85. <https://doi.org/10.1016/j.gca.2015.11.025>
- Hay, R. L. (1968). Chert and its sodium-silicate precursors in sodium-carbonate lakes of East Africa. *Contrib. Mineral. Petrol.*, *17*, 255–274. <https://doi.org/10.1007/BF00380740>
- Hickman-Lewis, K., Cavalazzi, B., Foucher, F., & Westall, F. (2018). Most ancient evidence for life in the Barberton greenstone belt: Microbial mats and biofabrics of the ~3.47 Ga Middle Marker horizon. *Precambrian Res.*, *312*, 45–67. <https://doi.org/10.1016/j.precamres.2018.04.007>
- Huber, R., Wilharm, T., Huber, D., Tricone, A., Burggraf, S., König, H., Reinhard, R., Rockinger, I., Fricke, H., & Stetter, K. O. (1992). *Aquifex pyrophilus* gen. nov. sp. nov., Represents a Novel Group of Marine Hyperthermophilic Hydrogen-Oxidizing Bacteria. *Syst. Appl. Microbiol.*, *15*, 340–351. [https://doi.org/10.1016/S0723-2020\(11\)80206-7](https://doi.org/10.1016/S0723-2020(11)80206-7)
- Jahnke, L., Eder, W., Huber, R., Hope, J. M., Hinrichs, K.-U., Hayes, J. M., Des Marais, D. J., Cady, S. L., & Summons, R. E. (2001). Signature Lipids and Stable Carbon Isotope Analyses of Octopus Spring Hyperthermophilic Communities Compared with Those of *Aquificales* Representatives. *Appl. Environ. Microbiol.*, *67*, 5179–5189. <https://doi.org/10.1128/AEM.67.11.5179-5189.2001>
- Jones, B., & Renaut, R. W. (1997). Formation of silica oncoids around geysers and hot springs at El Tatio, northern Chile. *Sedimentology*, *44*, 287–304. <https://doi.org/10.1111/j.1365-3091.1997.tb01525.x>
- Jones, B., & Renaut, R. W. (2010). Impact of Seasonal Changes on the Formation and Accumulation of Soft Siliceous Sediments on the Discharge Apron of Geysir, Iceland. *J. Sediment. Res.*, *80*, 17–35. <https://doi.org/10.2110/jsr.2010.008>
- Jones, B., Renaut, R. W., Torfason, H., & Owen, R. B. (2007). The geological history of Geysir, Iceland: a tephrochronological approach to the dating of sinter. *J. Geol. Soc. (London, U.K.)*, *164*, 1241–1252. <https://doi.org/10.1144/0016-76492006-178>
- Jones, B. F., Eugster, H. P., & Rettig, S. L. (1977). Hydrochemistry of the Lake Magadi basin, Kenya. *Geochim. Cosmochim. Acta*, *41*, 53–72. [https://doi.org/10.1016/0016-7037\(77\)90186-7](https://doi.org/10.1016/0016-7037(77)90186-7)
- Kambura, A. K., Mwirichia, R. K., Kasili, R. W., Karanja, E. N., Makonde, H. M., & Boga, H. I. (2016). Bacteria and Archaea diversity within the hot springs of Lake Magadi and Little Magadi in Kenya. *BMC Microbiol.*, *16*. <https://doi.org/10.1186/s12866-016-0748-x>
- Kemp, P., Lander, D. J., & Orpin, C. G. (1984). The Lipids of the Rumen Fungus *Piromonas communis*. *J. Gen. Microbiol.*, *139*, 27–37. <https://doi.org/10.1099/00221287-130-1-27>
- Killops, S., & Killops, V. (2005). *Introduction to Organic Geochemistry*, 2nd edn. Oxford: Blackwell Publishing.
- Kleemann, G., Poralla, K., Englert, G., Kjösen, H., Liaaen-Jensen, S., Neunlist, S., & Rohmer, M. (1990). Tetrahymanol from the phototrophic bacterium *Rhodospseudomonas palustris*: first report of a gammacerane triterpene from a prokaryote. *J. Gen. Microbiol.*, *136*, 2551–2553. <https://doi.org/10.1099/00221287-136-12-2551>
- Koga, Y., Nishihara, M., Morii, H., & Akagawa-Matsushita, M. (1993). Ether polar lipids of methanogenic bacteria: structures, comparative aspects, and biosynthesis. *Microbiol. Mol. Biol. Rev.*, *57*, 164–182.
- Kolattukudy, P. E. (1980). Biopolyester Membranes of Plants: Cutin and Suberin. *Science*, *208*, 990–1000. <https://doi.org/10.1126/science.208.4447.990>
- Konn, C., Charlou, J. L., Donval, J. P., Holm, N. G., Dehairs, F., & Bouillon, S. (2009). Hydrocarbons and oxidized organic compounds in hydrothermal fluids from Rainbow and Lost City ultramafic-hosted vents. *Chem. Geol.*, *258*, 299–314. <https://doi.org/10.1016/j.chemgeo.2008.10.034>

- Konn, C., Charlou, J. L., Donval, J. P., Holm, N. G. (2012). Characterisation of dissolved organic compounds in hydrothermal fluids by stir bar sorptive extraction-gas chromatography-mass spectrometry. Case study: the Rainbow field (36°N, Mid-Atlantic Ridge). *Geochem. Trans.*, 13. <https://doi.org/10.1186/1467-4866-13-8>
- Krooss, B. M., Brothers, L., & Engel, M. H. (1991). Geochromatography in petroleum migration: a review. In W. A. England & A. J. Fleet (Eds.), *Petroleum Migration* (pp. 149–163). London: Geol. Soc. Spec. Publ.
- Langworthy, T. A., Holzer, G., Zeikus, J. G., & Tornabene, T. G. (1983). Iso- and Anteiso-Branched Glycerol Diethers of the Thermophilic Anaerobe *Thermodesulfotobacterium commune*. *Syst. Appl. Microbiol.*, 4, 1–17. [https://doi.org/10.1016/S0723-2020\(83\)80029-0](https://doi.org/10.1016/S0723-2020(83)80029-0)
- Leif, R. N., & Simoneit, B. R. T. (1995). Ketones in hydrothermal petroleums and sediment extracts from Guaymas Basin, Gulf of California. *Org. Geochem.*, 23, 889–904. [https://doi.org/10.1016/0146-6380\(95\)00085-2](https://doi.org/10.1016/0146-6380(95)00085-2)
- Love, G. D., Snape, C. E., Carr, A. D., & Houghton, R. C. (1995). Release of covalently-bound alkane biomarkers in high yields from kerogen via catalytic hydrolysis. *Org. Geochem.*, 23, 981–986. [https://doi.org/10.1016/0146-6380\(95\)00075-5](https://doi.org/10.1016/0146-6380(95)00075-5)
- Love, G. D., McAulay, A. D., & Snape, C. E. (1997). Effect of Process Variables in Catalytic Hydrolysis on the Release of Covalently Bound Aliphatic Hydrocarbons from Sedimentary Organic Matter. *Energy Fuels*, 11, 522–531. <https://doi.org/10.1021/ef960194x>
- Luque, F. J., Ortega, L., Barrenechea, J. F., Millward, D., Beyssac, O., & Huizenga, J.-M. (2009). Deposition of highly crystalline graphite from moderate-temperature fluids. *Geology*, 37, 275–278. <https://doi.org/10.1130/G25284A.1>
- Mallory, F. B., Gordon, J. T., & Conner, R. L. (1963). The isolation of a pentacyclic triterpenoid alcohol from a protozoan. *J. Am. Chem. Soc.*, 85, 1362–1363.
- Marshall, C. P., Love, G. D., Snape, C. E., Hill, A. C., Allwood, A. C., Walter, M. R., Van Kranendonk, M. J., Bowden, S. A., Sylva, S. P., & Summons, R. E. (2007). Structural characterization of kerogen in 3.4 Ga Archaean cherts from the Pilbara Craton, Western Australia. *Precambrian Res.*, 155, 1–23. <https://doi.org/10.1016/j.precamres.2006.12.014>
- McCullom, T. M., & Seewald, J. S. (2003). Experimental study of the hydrothermal reactivity of organic acids and acid anions: II. Acetic acid, acetate, and valeric acid. *Geochim. Cosmochim. Acta*, 67, 3645–3664. [https://doi.org/10.1016/S0016-7037\(03\)00135-2](https://doi.org/10.1016/S0016-7037(03)00135-2)
- McCullom, T. M., Seewald, J. S., & German, C. R. (2015). Investigation of extractable organic compounds in deep-sea hydrothermal vent fluids along the Mid-Atlantic Ridge. *Geochim. Cosmochim. Acta*, 156, 122–144. <https://doi.org/10.1016/j.gca.2015.02.022>
- Meredith, W., Russell, C. A., Cooper, M., Snape, C. E., Love, G. D., Fabbri, D., & Vane, C. H. (2004). Trapping hydrolysis products on silica and their subsequent thermal desorption to facilitate rapid fingerprinting by GC–MS. *Org. Geochem.*, 35, 73–89. <https://doi.org/10.1016/j.orggeochem.2003.07.002>
- Meredith, W., Snape, C. E., & Love, G. D. (2014). Development and Use of Catalytic Hydrolysis (HyPy) as an Analytical Tool for Organic Geochemical Applications. In K. Grice (Ed.), *Principles and Practice of Analytical Techniques in Geosciences* (pp. 171–208). Royal Society of Chemistry.
- Mißbach, H., Schmidt, B. C., Duda, J.-P., Lünsdorf, N. K., Goetz, W., & Thiel, V. (2018). Assessing the diversity of lipids formed via Fischer–Tropsch-type reactions. *Org. Geochem.*, 119, 110–121. <https://doi.org/10.1016/j.orggeochem.2018.02.012>
- Morag, N., Williford, K. H., Kitajima, K., Philippot, P., Van Kranendonk, M. J., Lepot, K., Thomazo, C., & Valley, J. W. (2016). Microstructure-specific carbon isotopic signatures of organic matter from ~3.5 Ga cherts of the Pilbara Craton support a biogenic origin. *Precambrian Res.*, 275, 429–449. <https://doi.org/10.1016/j.precamres.2016.01.014>
- Nicolau, C., Reich, M., & Lynne, B. (2014). Physico-chemical and environmental controls on siliceous sinter formation at the high-altitude El Tatio geothermal field, Chile. *J. Volcanol. Geotherm. Res.*, 282, 60–76. <https://doi.org/10.1016/j.jvolgeores.2014.06.012>
- Otto, A., & Simoneit, B. R. T. (2002). Biomarkers of Holocene buried conifer logs from Bella Coola and north Vancouver, British Columbia, Canada. *Org. Geochem.*, 33, 1241–1251. [https://doi.org/10.1016/S0146-6380\(02\)00139-0](https://doi.org/10.1016/S0146-6380(02)00139-0)
- Pancost, R. D., Coleman, J. M., Love, G. D., Chatzi, A., Bouloubassi, I., & Snape, C. E. (2008). Kerogen-bound glycerol dialkyl tetraether lipids released by hydrolysis of marine sediments: A bias against incorporation of sedimentary organisms?. *Org. Geochem.*, 39, 1359–1371. <https://doi.org/10.1016/j.orggeochem.2008.05.002>

- Pancost, R. D., McClymont, E. L., Bingham, E. M., Roberts, Z., Charman, D. J., Hornibrook, E. R. C., Blundell, A., Chambers, F. M., Lim, K. L. H., & Evershed, R. P. (2011). Archaeol as a methanogen biomarker in ombrotrophic bogs. *Org. Geochem.*, *42*, 1279–1287. <https://doi.org/10.1016/j.orggeochem.2011.07.003>
- Parkes, R. J., & Taylor, J. (1983). The relationship between fatty acid distributions and bacterial respiratory types in contemporary marine sediments. *Eстуarine Coastal Shelf Sci.*, *16*, 175–189. [https://doi.org/10.1016/0272-7714\(83\)90139-7](https://doi.org/10.1016/0272-7714(83)90139-7)
- Peters, K. E., Walters, C. C., & Moldowan, J. M. (2005). *The biomarker guide: II. Biomarkers and Isotopes in petroleum exploration and earth history*, 2nd edn. Cambridge: Cambridge University Press.
- Pirajno, F., & van Kranendonk, M. J. (2005). Review of hydrothermal processes and systems on Earth and implications for Martian analogues. *Aust. J. Earth Sci.*, *52*, 329–351. <https://doi.org/10.1080/08120090500134571>
- Radke, M., & Welte, D. H. (1983). The Methylphenanthrene Index (MPI): A maturity parameter based on aromatic hydrocarbons. In M. Bjorøy, et al. (Eds.), *Adv. org. geochem. 1981* (pp. 504–512). Hoboken, NJ: Wiley.
- Rebello, S. L. H., Guedes, A., Szefczyk, M. E., Pereira, A. M., Araújo, J. P., & Freire, C. (2016). Progress in the Raman spectra analysis of covalently functionalized multiwalled carbon nanotubes: unraveling disorder in graphitic materials. *Phys. Chem. Chem. Phys.*, *18*, 12784–12796. <https://doi.org/10.1039/C5CP06519D>
- Renaut, R. W., Jones, B., Tiercelin, J.-J., & Tarits, C. (2002). Sublacustrine precipitation of hydrothermal silica in rift lakes: evidence from Lake Baringo, central Kenya Rift Valley. *Sediment. Geol.*, *148*, 235–257. [https://doi.org/10.1016/S0037-0738\(01\)00220-2](https://doi.org/10.1016/S0037-0738(01)00220-2)
- Risatti, J. B., Rowland, S. J., Yon, D. A., & Maxwell, J. R. (1984). Stereochemical studies of acyclic isoprenoids—XII. Lipids of methanogenic bacteria and possible contributions to sediments. *Org. Geochem.*, *6*, 93–104. [https://doi.org/10.1016/0146-6380\(84\)90030-5](https://doi.org/10.1016/0146-6380(84)90030-5)
- Roberts, N., Taieb, M., Barker, P., Damnati, B., Icole, M., & Williamson, D. (1993). Timing of the Younger Dryas event in East Africa from lake-level changes, *Nature*, *366*, 146–148. <https://doi.org/10.1038/366146a0>
- Rossel, P. E., Stubbins, A., Rebling, T., Koschinsky, A., Hawkes, J. A., & Dittmar, T. (2017). Thermally altered marine dissolved organic matter in hydrothermal fluids. *Org. Geochem.*, *110*, 73–86. <https://doi.org/10.1016/j.orggeochem.2017.05.003>
- Rushdi, A. I., & Simoneit, B. R. T. (2001). Lipid Formation by Aqueous Fischer–Tropsch-Type Synthesis over a Temperature Range of 100 to 400 °C. *Origins Life Evol. Biosphere*, *31*, 103–118. <https://doi.org/10.1023/A:1006702503954>
- Röhrlich, C. (1999). *Lithologie und Genese der Chertserien des Magadi Beckens, Lake Magadi, Kenia*. Clausthal-Zellerfeld: Papierflieger.
- Scalan, E. S., & Smith, J. E. (1970). An improved measure of the odd-even predominance in the normal alkanes of sediment extracts and petroleum. *Geochim. Cosmochim. Acta*, *34*, 611–620. [https://doi.org/10.1016/0016-7037\(70\)90019-0](https://doi.org/10.1016/0016-7037(70)90019-0)
- Schidlowski, M. (1988). A 3,800-million-year isotopic record of life from carbon in sedimentary rocks. *Nature*, *333*, 313–318. <https://doi.org/10.1038/333313a0>
- Schidlowski, M. (2001). Carbon isotopes as biogeochemical recorders of life over 3.8 Ga of Earth history: evolution of a concept. *Precambrian Res.*, *106*, 117–134. [https://doi.org/10.1016/S0301-9268\(00\)00128-5](https://doi.org/10.1016/S0301-9268(00)00128-5)
- Schidlowski, M., Matzigkeit, U., & Krumbein, W. E. (1984). Superheavy Organic Carbon from Hypersaline Microbial Mats. *Naturwissenschaften*, *71*, 303–308.
- Schidlowski, M., Gorzawski, H., & Dor, I. (1994). Carbon isotope variations in a solar pond microbial mat: Role of environmental gradients as steering variables. *Geochim. Cosmochim. Acta*, *58*, 2289–2298. [https://doi.org/10.1016/0016-7037\(94\)90011-6](https://doi.org/10.1016/0016-7037(94)90011-6)
- Schito, A., Romano, C., Corrado, S., Grigo, D., & Poe, B. (2017). Diagenetic thermal evolution of organic matter by Raman spectroscopy. *Org. Geochem.*, *106*, 57–67. <https://doi.org/10.1016/j.orggeochem.2016.12.006>
- Schmidt, M. W. I., & Noack, A. G. (2000). Black carbon in soils and sediments: Analysis, distribution, implications, and current challenges. *Global Biogeochem. Cycles*, *14*, 777–793. <https://doi.org/10.1029/1999GB001208>
- Schouten, S., Hartgers, W. A., López, J. F., Grimalt, J. O., & Sinninghe Damsté, J. S. (2001). A molecular isotopic study of ¹³C-enriched organic matter in evaporitic deposits: recognition of CO₂-limited ecosystems. *Org. Geochem.*, *32*, 277–286. [https://doi.org/10.1016/S0146-6380\(00\)00177-7](https://doi.org/10.1016/S0146-6380(00)00177-7)
- Simoneit, B. R. T. (1984). Hydrothermal effects on organic matter—high vs low temperature components. *Org. Geochem.*, *6*, 857–864. [https://doi.org/10.1016/0146-6380\(84\)90108-6](https://doi.org/10.1016/0146-6380(84)90108-6)

- Simoneit, B. R. T., Grimalt, J. O., Hayes, J. M., & Hartman, H. (1987). Low temperature hydrothermal maturation of organic matter in sediments from the Atlantis II Deep, Red Sea. *Geochim. Cosmochim. Acta*, *51*, 879–894. [https://doi.org/10.1016/0016-7037\(87\)90101-3](https://doi.org/10.1016/0016-7037(87)90101-3)
- Simoneit, B. R. T., Deamer, D. W., & Kompanichenko, V. (2009). Characterization of hydrothermally generated oil from the Uzon caldera, Kamchatka. *Appl. Geochem.*, *24*, 303–309. <https://doi.org/10.1016/j.apgeochem.2008.10.007>
- Still, C. J., Berry, J. A., Collatz, G. J., & DeFries, R. S. (2003). Global distribution of C3 and C4 vegetation: Carbon cycle implications. *Global Biogeochem. Cycles*, *17*, 6-1–6-14. <https://doi.org/10.1029/2001GB001807>
- Sugitani, K., Yamamoto, K., Wada, H., Binu-Lal, S. S., & Yoneshige, M. (2002). Geochemistry of Archean carbonaceous cherts deposited at immature island-arc setting in the Pilbara Block, Western Australia. *Sediment. Geol.*, *151*, 45–66. [https://doi.org/10.1016/S0037-0738\(01\)00230-5](https://doi.org/10.1016/S0037-0738(01)00230-5)
- Taipale, S. J., Strandberg, U., Peltomaa, E., Galloway, A. W. E., Ojala, A., & Brett, M. T. (2013). Fatty acid composition as biomarkers of freshwater microalgae: analysis of 37 strains of microalgae in 22 genera and in seven classes. *Aquat. Microb. Ecol.*, *71*, 165–178. <https://doi.org/10.3354/ame01671>
- Taipale, S. J., Hiltunen, M., Vuorio, K., & Peltomaa, E. (2016). Suitability of Phytosterols Alongside Fatty Acids as Chemotaxonomic Biomarkers for Phytoplankton. *Front. Plant Sci.*, *7*. <https://doi.org/10.3389/fpls.2016.00212>
- Teixidor, P., Grimalt, J. O., Pueyo, J. J., & Rodriguez-Valera, F. (1993). Isopranyl glycerol diethers in non-alkaline evaporitic environments. *Geochim. Cosmochim. Acta*, *57*, 4479–4489. [https://doi.org/10.1016/0016-7037\(93\)90497-K](https://doi.org/10.1016/0016-7037(93)90497-K)
- Thiel, V., Jenisch, A., Landmann, G., Reimer, A., & Michaelis, W. (1997). Unusual distributions of long-chain alkenones and tetrahymanol from the highly alkaline Lake Van, Turkey. *Geochim. Cosmochim. Acta*, *61*, 2053–2064. [https://doi.org/10.1016/S0016-7037\(97\)00038-0](https://doi.org/10.1016/S0016-7037(97)00038-0)
- Tice, M. M., & Lowe, D. R. (2006). The origin of carbonaceous matter in pre-3.0 Ga greenstone terrains: A review and new evidence from the 3.42 Ga Buck Reef Chert. *Earth Sci. Rev.*, *76*, 259–300. <https://doi.org/10.1016/j.earscirev.2006.03.003>
- Tindall, B. J. (1985). Qualitative and Quantitative Distribution of Diether Lipids in Haloalkaliphilic Archaeobacteria. *Syst. Appl. Microbiol.*, *6*, 243–246. [https://doi.org/10.1016/S0723-2020\(85\)80025-4](https://doi.org/10.1016/S0723-2020(85)80025-4)
- Tindall, B. J., Ross, H. N. M., & Grant, W. D. (1984). *Natronobacterium* gen. nov. and *Natronococcus* gen. nov., Two New Genera of Haloalkaliphilic Archaeobacteria. *Syst. Appl. Microbiol.*, *5*, 41–57. [https://doi.org/10.1016/S0723-2020\(84\)80050-8](https://doi.org/10.1016/S0723-2020(84)80050-8)
- Ueno, Y., Yoshioka, H., Maruyama, S., & Isozaki, Y. (2004). Carbon isotopes and petrography of kerogens in ~3.5-Ga hydrothermal silica dikes in the North Pole area, Western Australia. *Geochim. Cosmochim. Acta*, *68*, 573–589. [https://doi.org/10.1016/S0016-7037\(03\)00462-9](https://doi.org/10.1016/S0016-7037(03)00462-9)
- Villanueva, L., Sinninghe Damsté, J. S., & Schouten, S. (2014). A re-evaluation of the archaeal membrane lipid biosynthetic pathway. *Nat. Rev. Microbiol.*, *12*, 438–448. <https://doi.org/10.1038/nrmicro3260>
- Vinçon-Laugier, A., Grossi, V., Pacton, M., Escarguel, G., & Cravo-Laureau, C. (2016). The alkyl glycerol ether lipid composition of heterotrophic sulfate reducing bacteria strongly depends on growth substrate. *Org. Geochem.*, *98*, 141–154. <https://doi.org/10.1016/j.orggeochem.2016.05.015>
- Weston, R. J., & Woolhouse, A. D. (1987). Organic geochemistry of the sedimentary basins of New Zealand part IV. A biomarker study of the petroleum seepage and some well core bitumens from the geothermal region of Ngawha Springs. *Appl. Geochem.*, *2*, 305–319. [https://doi.org/10.1016/0883-2927\(87\)90046-1](https://doi.org/10.1016/0883-2927(87)90046-1)
- Wheildon, J., Morgan, P., Williamson, K. H., Evans, T. R., & Swanberg, C. A. (1994). Heat flow in the Kenya rift zone. *Tectonophysics*, *236*, 131–149. [https://doi.org/10.1016/0040-1951\(94\)90173-2](https://doi.org/10.1016/0040-1951(94)90173-2)
- Williamson, D., Taieb, M., Damnati, B., Icole, M., & Thouveny, N. (1993). Equatorial extension of the younger Dryas event: rock magnetic evidence from Lake Magadi (Kenya). *Global Planet. Change*, *7*, 235–242. [https://doi.org/10.1016/0921-8181\(93\)90053-Q](https://doi.org/10.1016/0921-8181(93)90053-Q)
- Yang, H., Zheng, F., Xiao, W., & Xie, S. (2015). Distinct distribution revealing multiple bacterial sources for 1-O-monoalkyl glycerol ethers in terrestrial and lake environments. *Sci. China Earth Sci.*, *58*, 1005–1017. <https://doi.org/10.1007/s11430-014-5016-z>
- Yunker, M. B., Macdonald, R. W., Vingarzan, R., Mitchell, R. H., Goyette, D., & Sylvestre, S. (2002). PAHs in the Fraser River basin: a critical appraisal of PAH ratios as indicators of PAH source and composition. *Org. Geochem.*, *33*, 489–515. [https://doi.org/10.1016/S0146-6380\(02\)00002-5](https://doi.org/10.1016/S0146-6380(02)00002-5)
- Zander, J. M., Caspi, E., Pandey, G. N., & Mitra, C. R. (1969). The presence of tetrahymanol in *Oleandra wallichii*. *Phytochemistry*, *8*, 2265–2267. [https://doi.org/10.1016/S0031-9422\(00\)88195-9](https://doi.org/10.1016/S0031-9422(00)88195-9)

3 Ideas and perspectives: hydrothermally driven redistribution and sequestration of early Archean biomass—the “hydrothermal pump hypothesis”

Jan-Peter Duda, Volker Thiel, Thorsten Bauersachs, Helge Mißbach, Manuel Reinhardt, Nadine Schäfer, Martin J. Van Kranendonk, & Joachim Reitner

Biogeosciences (2018), 15, 1535–1548

Archean hydrothermal chert veins commonly contain abundant organic carbon of uncertain origin (abiotic vs. biotic). In this study, we analyzed kerogen contained in a hydrothermal chert vein from the ca. 3.5 Ga Dresser Formation (Pilbara Craton, Western Australia). Catalytic hydrothermal pyrolysis (HyPy) of this kerogen yielded n-alkanes up to n-C₂₂, with a sharp decrease in abundance beyond n-C₁₈. This distribution ($\leq n-C_{18}$) is very similar to that observed in HyPy products of recent bacterial biomass, which was used as reference material, whereas it differs markedly from the unimodal distribution of abiotic compounds experimentally formed via Fischer–Tropsch-type synthesis. We therefore propose that the organic matter in the Archean chert veins has a primarily microbial origin. The microbially derived organic matter accumulated in anoxic aquatic (surface and/or subsurface) environments and was then assimilated, redistributed and sequestered by the hydrothermal fluids (“hydrothermal pump hypothesis”).

3.1 Introduction

Extensive hydrothermal chert vein systems containing abundant organic carbon are a unique phenomenon of early Archean successions worldwide (Lindsay et al., 2005; Van Kranendonk, 2006; Hofmann, 2011). A dense stockwork of several hundred kerogen-rich hydrothermal chert veins that penetrate footwall pillowed komatiitic basalts of the ca. 3.5 Ga Dresser Formation (Pilbara Craton, Western Australia; Fig. 3.1) are up to 2 km deep by 25 m wide (Hickman, 1973, 1983; Nijman et al., 1999; Van Kranendonk & Pirajno, 2004; Lindsay et al., 2005; Van Kranendonk, 2006; Van Kranendonk et al., 2008; Fig. B1). Depleted stable carbon isotope signatures ($\delta^{13}\text{C}$) of bulk kerogens (-38.1 to -24.3 ‰) and of organic microstructures (-33.6 to -25.7 ‰) in these hydrothermal chert veins, as well as remnants of what appear to be microbial remains, are consistent with a biological origin of the organic matter (Ueno et al., 2001, 2004; Glikson et al., 2008; Pinti et al., 2009; Morag et al., 2016). Problematically, however, similarly depleted $\delta^{13}\text{C}$ values (partly down to ca. -36 ‰ relative to the initial substrate) can also be formed through abiotic processes, for instance via Fischer–Tropsch-type synthesis (McCollom et al., 1999; McCollom & Seewald, 2006), and putative microbial remains are not always reliable (Schopf, 1993; Brasier et al., 2002, 2005; Schopf et al., 2002; Bower et al., 2016).

Organic biomarkers can help to trace life and biological processes through deep time and add important information on the origin of the organic matter, even in very old sedimentary rocks (Brocks & Summons, 2003; Summons & Hallmann, 2014). In Archean rocks, however, molecular fingerprints in the conventionally analyzed bitumen (i.e., the extractable portion of organic matter) are commonly blurred by thermal maturation and/or ancient or modern contamination (Brocks et al., 2008; Gérard et al., 2009; Brocks, 2011; French et al., 2015). In contrast, the non-extractable portion of organic matter, known as kerogen, tends to be less affected by thermal maturation and contamination and is considered to be syngenetic with the host rock (Love et al., 1995; Brocks et al., 2003b; Marshall et al., 2007; Lockhart et al., 2008). Catalytic hydrothermal pyrolysis (HyPy) is a powerful tool for sensitively releasing kerogen-bound hydrocarbon moieties with little structural alteration (Love et al., 1995). HyPy has been successfully applied to Archean kerogens in rocks from the Pilbara Craton, liberating syngenetic organic compounds consistent with a biogenic origin (Brocks et al., 2003b; Marshall et al., 2007). However, this technique has not yet been used on kerogens contained in hydrothermal chert veins of this age.

Here, we present the results of analyses of kerogen embedded in a freshly exposed hydrothermal chert vein of the ca. 3.5 Ga Dresser Formation. Our analyses include field and petrographic observations, Raman spectroscopy and organic geochemistry ($\delta^{13}\text{C}_{\text{TOC}}$; kerogen-bound molecules via HyPy followed by gas chromatography–mass spectrometry (GC–MS) and gas chromatography–combustion–isotope ratio mass spectrometry (GC–C–IRMS)). To further constrain potential sources of the Dresser kerogen, we additionally applied HyPy on (i) excessively pre-extracted cyanobacterial biomass and (ii) produced abiotic organic matter via Fischer–Tropsch-type synthesis using a hydrothermal reactor. Results of these investigations suggest that the Dresser kerogen has a primarily microbial origin. We hypothesize that biomass-derived organic compounds accumulated in anoxic aquatic environments and were then redistributed and sequestered by subsurface hydrothermal fluids (“hydrothermal pump hypothesis”).

3.2 Material and methods

3.2.1 Sample preparation

A fresh decimeter-sized sample of a Dresser chert vein was obtained from a recent cut wall of the abandoned Dresser Mine in the Pilbara Craton, Western Australia (GPS: $21^{\circ}09'04.13''\text{S}$; $119^{\circ}26'15.21''\text{E}$; Figs. 3.1, B1d; for geological maps, see Hickman, 1983; Van Kranendonk, 1999; Hickman & Van Kranendonk, 2012). The external surfaces (ca. 1–2 cm) of the sample block were removed using an acetone-cleaned rock saw and then used for the preparation of thin sections. The surfaces of the resulting inner block were extensively rinsed with acetone and then removed (ca. 1–2 cm) with an acetone-cleaned high precision saw (Buehler; Isomet 1000, Germany). The surfaces of the resulting sample were again rinsed with acetone and then crushed and powdered using a carefully acetone-cleaned pebble mill (Retsch MM 301, Germany).

3.2.2 Petrography and Raman spectroscopy

Petrographic analysis was conducted using a Zeiss SteREO Discovery.V8 stereomicroscope (transmitted and reflected light) linked to an AxioCam MRc5 5-megapixel camera.

Raman spectra were recorded using a Horiba Jobin Yvon LabRam-HR 800 UV spectrometer (focal length of 800 mm) attached to an Olympus BX41 microscope. For excitation an Argon ion laser (Melles Griot IMA 106020B0S) with a laser strength of 20 mW was used. The laser beam was focused onto the sample using an Olympus MPlane 100x objective with a numerical aperture of 0.9 and dispersed by a 600 L/mm grating on a charge-couple device (CCD) detector with 1024 x 256 pixels. This yielded a spectral resolution of $< 2 \text{ cm}^{-1}$ per pixel. Data were acquired over 10 to 30 s for a spectral range of 100–4000 cm^{-1} . The spectrometer was calibrated by using a silicon standard with a major peak at 520.4 cm^{-1} . All spectra were recorded and processed using the LabSpec™ database (version 5.19.17; Jobin Yvon, Villeneuve d'Ascq, France).

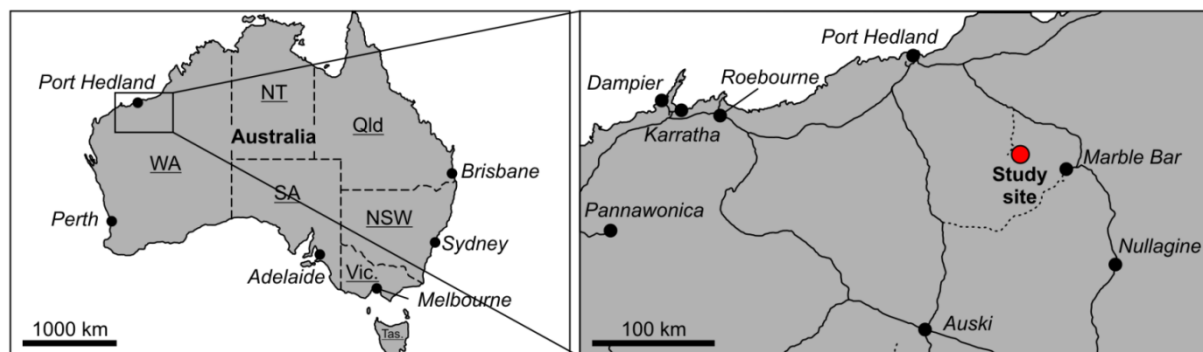


Fig. 3.1: Location of the study site in Western Australia. The hydrothermal chert vein analysed occurs in a recent cut wall of the abandoned Dresser Mine close to Marble Bar.

3.2.3 Raman-derived H/C data

H/C values were calculated based on integrated peak intensities of Raman spectra using the formula $H/C = 0.871 \cdot I_{D5}/(I_{G+D2}) - 0.0508$ (Ferralis et al., 2016). The peaks were fitted in the LabSpec™ software (see 3.2.2) using the Gauss/Lorentz function.

3.2.4 Molecular analysis of the Dresser kerogen

All materials used for preparation were heated to 500 °C for 3 h and/or extensively rinsed with acetone prior to sample contact. A laboratory blank was prepared and analyzed in parallel to monitor laboratory contaminations. We applied catalytic hydropyrolysis (HyPy) to release molecules from the Dresser kerogen and pre-extracted biomass of the heterocystous cyanobacterium *Anabaena cylindrica* SAG 1403-2 following previously published protocols (Snape et al., 1989; Love et al., 1995, 2005). HyPy allows the breaking of covalent bonds by progressive heating under high hydrogen pressure (150 bar). The released products are immediately removed from the hot zone by a constant hydrogen flow and trapped downstream on clean, combusted silica powder cooled with dry ice (Meredith et al., 2004). All hydropyrolysates were eluted from the silica trap with high-purity dichloromethane (DCM), desulfurized overnight using activated copper and subjected to gas chromatography–mass spectrometry (GC–MS). Before all experiments, the empty HyPy system was heated (ambient temperature to 520 °C, held for 30 min) to remove any residual molecules.

Isolation of the Dresser kerogen followed standard procedures (cf., Brocks et al., 2003b). 57 g of powdered sample was first demineralized with hydrochloric acid (24 h) and then hydrofluoric acid (11 days). The purified organic matter was then exhaustively extracted using three excess volumes of DCM and *n*-hexane, respectively (x3), ultrasonic swelling in pyridine (2 x 20 min at 80 °C), and ultrasonic extraction with methanol, DCM (x3) and DCM/methanol (1/1; v/v). The kerogen was subsequently extracted with *n*-hexane until no more compounds were detected via GC–MS. The pure kerogen was used for HyPy following an experimental protocol optimized for the analysis of Archean kerogens (Brocks et al., 2003b; Marshall et al., 2007).

In order to monitor potential contamination, we applied HyPy to blanks before and after the kerogen run. The Dresser kerogen (131.06 mg) and blanks were sequentially heated in the presence of a sulfided molybdenum catalyst (10 wt%) and under a constant hydrogen flow (5 L/min) using a two-step approach (cf., Brocks et al., 2003b; Marshall et al., 2007; Fig. B2). The low-temperature step included heating from ambient temperature to 250 °C (300 °C/min) and then to 330 °C (8 °C/min) to release any molecules that were strongly adsorbed to the kerogen and not accessible to solvent extraction. The silica powder was subsequently recovered from the product trap, and the trap was refilled with clean, combusted silica powder for the following high-temperature step. This

step included heating from ambient temperature to 520 °C (8 °C/min) to release molecules covalently bound to the kerogen.

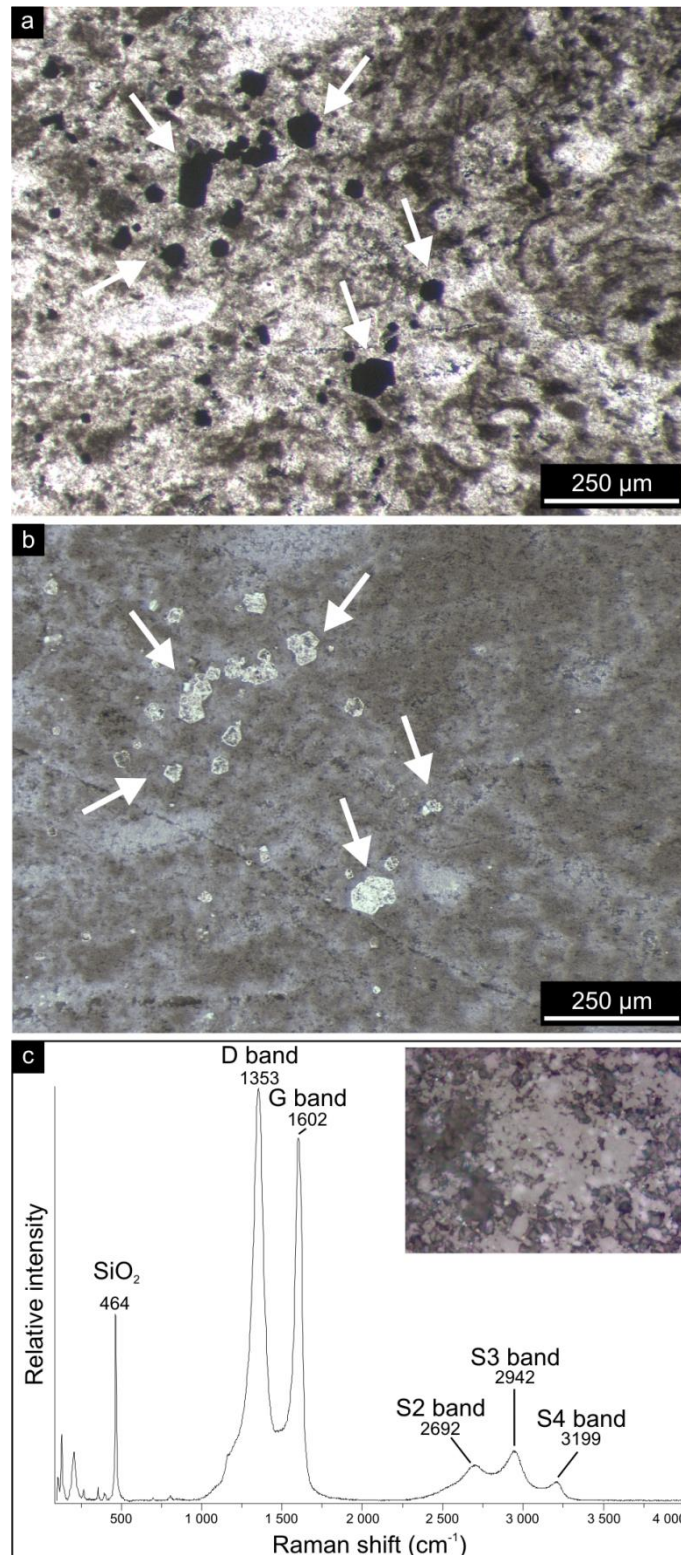


Fig. 3.2: Petrographic observations on the hydrothermal chert vein. (a, b) Thin section photographs (a: transmitted light; b: reflected light) showing kerogen (brownish colours) and pyrite (arrows, black colours in a, bright colours in b) embedded within a fine grained chert matrix. Note that the pyrite crystals (arrows) are excellently preserved and show no evidence of oxidation. (c) Representative Raman spectrum of kerogen (D band at 1353 cm^{-1} and G band at 1602 cm^{-1}) present in the hydrothermal chert vein. Note the wide D and G bands (82 and 55 cm^{-1} width, respectively), pointing to thermally mature and structurally disordered kerogen, and the absence of a S1 band (at 2450 cm^{-1}) being consistent with prehnite-pumpellyite to lower greenschist metamorphism and a temperature of ca. 300 °C (cf., Yui et al., 1996; Delarue et al., 2016).

3.2.5 Molecular analysis of pre-extracted cyanobacterial biomass (*Anabaena cylindrica*)

We used cell material of the heterocystous cyanobacterium *Anabaena cylindrica* strain SAG 1403-2 as it fulfils all criteria for reference material (availability, well characterized, etc.). The material was obtained from the Culture Collection of Algae at the Georg-August-Universität Göttingen (Germany) and grown at the Christian-Albrechts-Universität Kiel (Germany). The axenic batch culture was maintained in 250 mL of BG110 medium free of combined nitrogen sources (Rippka et al., 1979) at 29 °C. A light V dark regime of 14 h : 10 h with a photon flux density of 135 $\mu\text{mol photons m}^{-2} \text{s}^{-1}$ was provided by a white fluorescent light bulb. At the end of the logarithmic growth phase, cells were harvested by centrifugation, and they were lyophilized thereafter. Subsequently, an aliquot of the freeze-dried biomass was exhaustively extracted following the methodology described by Bauersachs et al. (2014).

HyPy was performed following an experimental protocol optimized for biomass applications (Love et al., 2005). Briefly, the material was heated in the presence of a sulfided molybdenum catalyst (1.5 times the weight of the bacterial extraction residue) and under a constant hydrogen flow (6 mL/min). The HyPy program included heating from ambient temperature to 260 °C (300 °C/min) and then to 500 °C (8 °C/min).

3.2.6 Fischer–Tropsch-type synthesis of organic matter under hydrothermal conditions

Fischer–Tropsch-type reactions were carried out based on McCollom et al. (1999). A mixture of 2.5 g oxalic acid (dihydrate, suprapur®, Merck KGaA), 1 g montmorillonite (K10, Sigma Aldrich; pre-extracted with DCM; x4) and ca. 11 mL ultrapure water was heated to 175 °C for 66 to 74 h in a sealed Morey-type stainless steel autoclave. The autoclave was rapidly (≤ 15 min) cooled to room temperature with compressed air.

Fluid and solid phases were collected and extracted with DCM (x4). The montmorillonite was removed by centrifugation and filtration with silica powder and sea sand (which were combusted prior to use). The obtained extracts were then concentrated by rotary evaporation (40 °C, 670 mbar) and subjected to GC–MS analysis. Analytical blank experiments were carried out with all reactants to keep track of contamination.

3.2.7 Gas chromatography–mass spectrometry

GC–MS analysis of HyPy products was carried out with a Thermo Scientific Trace 1310 GC coupled to a Thermo Scientific Quantum XLS Ultra MS. The GC instrument was equipped with a capillary column (Phenomenex Zebron ZB-5, 30 m, 0.25 μm film thickness, 0.25 mm inner diameter). Fractions were injected into a splitless injector and transferred to the GC column at 270 °C. He was used as carrier gas with a constant flow rate of 1.5 mL/min. The GC oven temperature was held isothermal at 80 °C for 1 min and then ramped to 310 °C at 5 °C/min, at which it was kept for 20 min. Electron ionization mass spectra were recorded in full-scan mode at an electron energy of 70 eV with a mass range of m/z 50–600 and scan time of 0.42 s.

3.2.8 Polyaromatic hydrocarbon ratios

Polyaromatic hydrocarbons (PAHs) are organic compounds consisting of multiple fused benzene rings. Methylation and isomerization characteristics of various GC-amenable PAHs are altered during maturation and thus provide a measure for assessing the thermal maturity of organic matter (Killops & Killops, 2005; Peters et al., 2005). The following PAH maturity parameters were used in this study:

1. methylnaphthalene ratio (MNR) = 2-MN/1-MN (Radke et al., 1984),
2. methylphenanthrene index (MPI-I) = $1.5 \cdot (2\text{-MP} + 3\text{-MP}) / (P + 1\text{-MP} + 9\text{-MP})$ (Radke and Welte, 1983), and
3. computed vitrinite reflectance [R_c (MPI-I)] = $0.7 \cdot \text{MPI-I} + 0.22$ (according to $P/\text{MP} > 1$; Boreham et al., 1988).

MN stands for methylnaphthalene, P for phenanthrene and MP for methylphenanthrene.

3.2.9 Total organic carbon (TOC) and $\delta^{13}\text{C}$ analyses (TOC and compound specific)

TOC, $\delta^{13}\text{C}_{\text{TOC}}$ and compound-specific $\delta^{13}\text{C}$ analyses were conducted at the Centre for Stable Isotope Research and Analysis (KOSI) at the Georg-August-Universität Göttingen, Germany. Stable carbon isotope data are expressed as delta values relative to the Vienna Pee Dee Belemnite (VPDB) reference standard.

The TOC content and $\delta^{13}\text{C}_{\text{TOC}}$ values were determined in duplicate using an elemental analyzer (NA-2500 CE-Instruments) coupled to an isotope ratio mass spectrometer (Finnigan MAT Delta plus). Ca. 100 mg of powdered and homogenized whole rock material were analyzed in each run. For internal calibration an acetanilide standard

was used ($\delta^{13}\text{C} = -29.6 \text{ ‰}$; SD = 0.1 ‰). TOC content measurements showed a mean deviation of 0.1 wt%. The average $\delta^{13}\text{C}_{\text{TOC}}$ value had a standard deviation of 0.3 ‰.

Compound-specific $\delta^{13}\text{C}$ analyses were conducted with a Trace GC coupled to a Delta Plus isotope ratio mass spectrometer (IRMS) via a combustion interface (all Thermo Scientific). The combustion reactor contained CuO, Ni and Pt and was operated at 940 °C. The GC was equipped with two serially coupled capillary columns (Agilent DB-5 and DB-1; each 30 m, 0.25 μm film thickness, 0.25 mm inner diameter). Fractions were injected into a splitless injector and transferred to the GC column at 290 °C. The carrier gas was He at a flow rate of 1.2 mL/min. The GC oven temperature program was identical to the one used for GC–MS analysis (see above). CO_2 with a known $\delta^{13}\text{C}$ value was used for internal calibration. Instrument precision was checked using laboratory standards. Standard deviations of duplicate measurements were better than 1.7 ‰.

Tab. 3.1: Stable carbon isotopic composition ($\delta^{13}\text{C}$) of the total organic carbon (TOC) and *n*-alkanes released from high temperature HyPy of the Dresser kerogen

	<i>n</i> -C ₁₂	<i>n</i> -C ₁₃	<i>n</i> -C ₁₄	<i>n</i> -C ₁₅	<i>n</i> -C ₁₆	<i>n</i> -C ₁₇	<i>n</i> -C ₁₈	<i>n</i> -C _{12–18} (mean)	TOC
$\delta^{13}\text{C}$	-30.3	-33.3	-32.7	-31.1	-29.4	-31.2	-31.7	-31.4	-32.8
SD	0.5	1.4	0.2	1.7	0.3	0.8	0.1	1.2	0.3

3.3 Results

The studied hydrothermal chert vein is hosted in komatiitic pillow basalt that has undergone severe hydrothermal acid–sulfate alteration, producing a kaolinite–illite–quartz mineral assemblage (Van Kranendonk & Pirajno, 2004; Van Kranendonk, 2006; Fig. B1). The sampled vein crops out in a recent cut wall of the abandoned Dresser Mine (Fig. B1) and consists of a dense chert (microquartz) matrix of deep black color that contains kerogen and local concentrations of fresh (unweathered) pyrite crystals (Fig. 3.2a, b). There is no field and/or petrographic evidence for fluid-flow events that postdate the initial vein formation (brecciation textures, etc.).

Petrographic analysis and Raman spectroscopy revealed that kerogen (D bands at 1353 cm^{-1} , G bands at 1602 cm^{-1}) is embedded in the chert matrix (SiO_2 band at 464 cm^{-1} ; see Fig. 3.2c, for a representative Raman spectrum). The organic matter occurs as small clots (< 50 μm) of variable shape. Raman spectra of the organic matter exhibit relatively wide D and G bands (82 and 55 cm^{-1} width, respectively; Fig. 3.2c). The total organic carbon (TOC) content is 0.2 wt%, and the $\delta^{13}\text{C}_{\text{TOC}}$ value is $-32.8 \pm 0.3 \text{ ‰}$ (Tab. 3.1). Raman-derived H/C ratios range between 0.03 and 0.14.

HyPy was applied to the isolated Dresser kerogen, as well as to preceding and subsequent analytical blanks (combusted sea sand). Hydropyrolysates of the preceding blank contained a series of *n*-alkanes $\leq n\text{-C}_{24}$, with maximum abundances at *n*-C₁₅ (Figs. 3.3, B2–B4). Sulfur (only after low-temperature HyPy), traces of siloxanes and a phenol (Figs. 3.3, B2, B4) were also present. The blank runs also contained traces of aromatic hydrocarbons (Fig. B5).

Low-temperature HyPy of the Dresser kerogen produced traces of C_{14–18} *n*-alkanes, with a maximum at *n*-C₁₅ (Fig. B3). However, these compounds were significantly less abundant than those released during high-temperature HyPy (see below). Other compounds observed in the low-temperature step pyrolysate were elemental sulfur, phenols, phthalic acid, siloxanes and traces of aromatic hydrocarbons (Figs. B2, B4–B5).

High-temperature HyPy of the Dresser kerogen yielded *n*-alkanes ranging from *n*-C₁₁ to *n*-C₂₂ with a notable decrease (“step”) in the abundance of homologues above *n*-C₁₈ (Figs. 3.3b, B2, B3), which remained virtually unaffected by blank subtraction (Fig. 3.3c). Apart from that step, no carbon number preference is evident. The *n*-alkanes have $\delta^{13}\text{C}$ values ranging from -29.4 to -33.3 ‰ (mean $-31.4 \pm 1.2 \text{ ‰}$; Fig. 3.3b; Tab. 3.1). The hydropyrolysate also contained isomeric mixtures of C_{12–18} monomethyl alkanes (Fig. B3) and a variety of aromatic hydrocarbons, including (dimethyl-, methyl-) naphthalene(s), (methyl-) biphenyl(s), (methyl-) acenaphthene(s), dibenzofuran and (methyl-) phenanthrene(s) (Figs. 3.3b, c, B4–B6). Biologically diagnostic hydrocarbons such as hopanoids or steroids were absent.

HyPy treatment of excessively pre-extracted biomass of the heterocystous cyanobacterium *Anabaena cylindrica* SAG 1403-2 yielded a variety of organic compounds, but also included *n*-alkanes with a clear restriction in carbon number to homologues $\leq n\text{-C}_{18}$ (Fig. 3.3d). In contrast, our experimental synthesis of abiotic *n*-alkanes through Fischer–Tropsch-type reactions under hydrothermal conditions produced a unimodal distribution of homologues ranging from *n*-C₁₂ to *n*-C₄₁ without any carbon number preference (Fig. 3.3e).

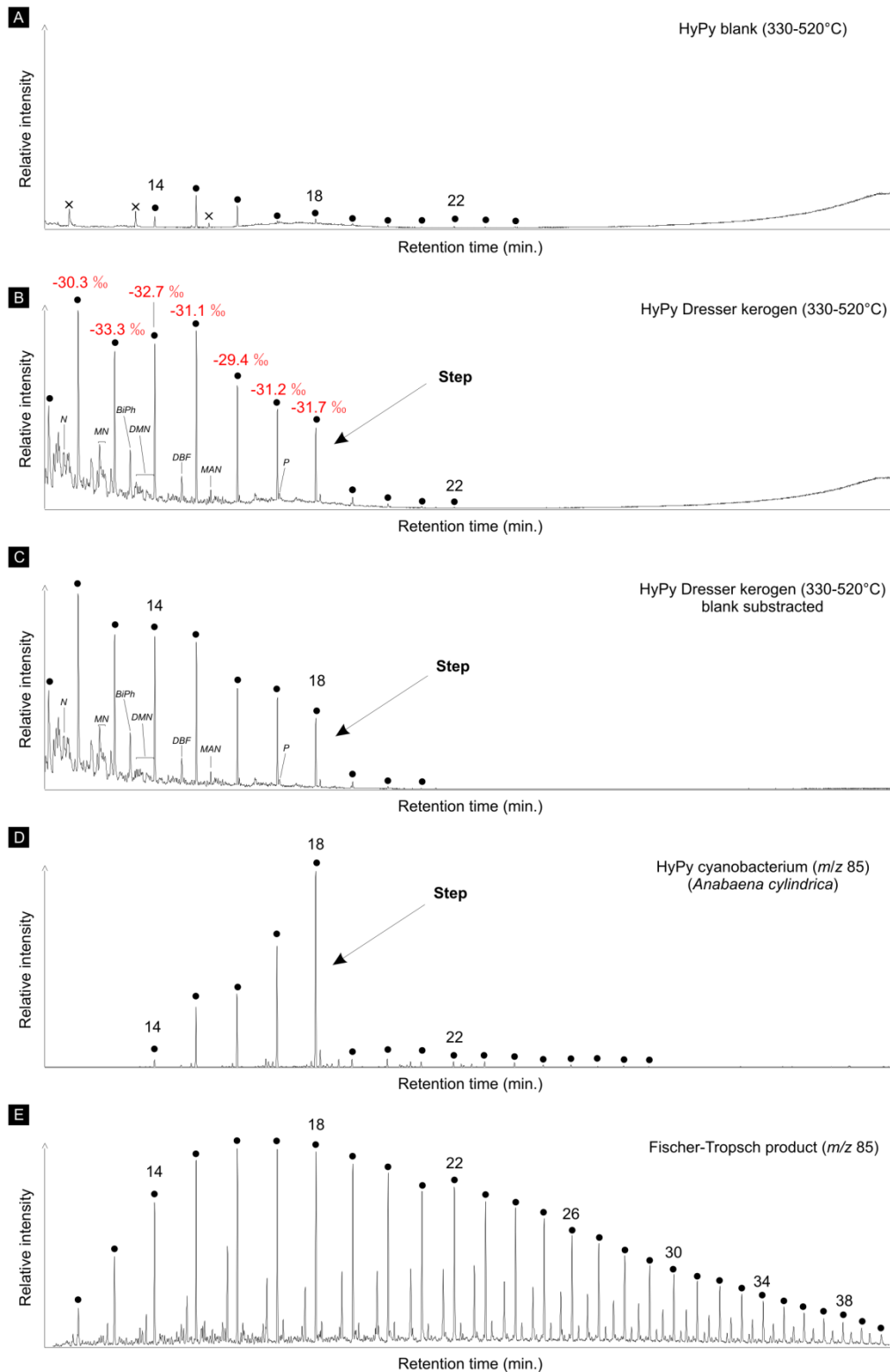


Fig. 3.3: Total ion currents (a–c; in the same scale) and ion chromatograms selective for alkanes (d–f; m/z 85). (a) High temperature HyPy (330–520 °C) product of analytical blank (combusted sea sand) obtained prior to HyPy of the Dresser kerogen. n -Alkanes in the range of n -C₁₄ to n -C₂₄ (maxima at n -C₁₅) represent HyPy background contamination. (b) High temperature HyPy (330–520 °C) product of the Dresser kerogen. Note the sharp decrease in abundance of n -alkanes beyond n -C₁₈ (see arrows). $\delta^{13}\text{C}$ values of n -C₁₂ to n -C₂₈ show a high similarity to the $\delta^{13}\text{C}_{\text{TOC}}$ value (-32.8 ± 0.3 ‰), further confirming syngeneity. (c) Blank subtraction (b minus a) showing that contaminants have no major impact on the n -alkane pattern yielded during the high temperature HyPy step of the Dresser kerogen (b). (d) HyPy products of cell material of the heterocystous cyanobacterium *Anabaena cylindrica*. Note the sharp decrease in abundance of n -alkanes beyond n -C₁₈ (see arrows), similar to the n -alkane distribution of the Dresser kerogen (b). (e) Products of experimental Fischer–Tropsch-type synthesis under hydrothermal conditions; abiogenic n -alkanes show a unimodal distribution that is distinctly different from the Dresser kerogen.

Black dots: *n*-alkanes (numbers refer to carbon chain-lengths); N: naphthalene; MN: methylnaphthalenes; BiPh: 1,1'-biphenyl; DMN: dimethylnaphthalenes; DBF: dibenzofuran; MAN: methylacenaphthene; P: phenanthrene; crosses: siloxanes (GC column or septum bleeding).

3.4 Discussion

3.4.1 Maturity of the Dresser kerogen

The organic record of Archean rocks is commonly affected by thermal maturation (Brocks et al., 2008; Brocks, 2011; French et al., 2015). The kerogen within the analyzed Dresser sample is thermally mature and structurally disordered, as evidenced by relatively wide D and G bands in the Raman spectra (see Fig. 3.2c for a representative Raman spectrum). This is also supported by the absence of S1 bands at 2450 cm⁻¹, high R1 ratios (0.98–1.05) and low FWHM-D1 values (68.64–76.12), consistent with prehnite–pumpellyite to lower greenschist metamorphism at a temperature of ca. 300 °C (cf., Yui et al., 1996; Delarue et al., 2016). All of these observations are well in line with published Raman spectra of Archean organic matter from the same region (Ueno et al., 2001; Marshall et al., 2007; Delarue et al., 2016) and the general thermal history of the host rock (regional prehnite–pumpellyite to lower greenschist metamorphism; Hickman, 1975, 1983, 2012; Terabayashi et al., 2003).

Fitting of D5 peaks can be difficult for Raman spectra of highly mature organic matter (Ferralis et al., 2016). Therefore, the H/C ratios calculated herein (0.03–0.14) should be treated with caution. However, the Raman-based H/C ratios and the methylphenanthrene/phenanthrene value (MP/P = 0.33; Tab. 3.2) of the Dresser kerogen are in good accordance with data reported from more mature kerogens from the same region (ca. 3.4 Ga Strelley Pool Formation: 0.08–0.14 and 0.24–0.37, respectively; Marshall et al., 2007). The low methylphenanthrene index (MPI-I = 0.23) and high phenanthrene/methylphenanthrene index (P/MP = 3.01) result in a computed vitrinite reflectance (R_c (MPI-I)) of 2.87 (Tab. 3.2), indicating a thermal maturity far beyond the oil-generative stage (Radke & Welte, 1983; Boreham et al., 1988). However, it has to be considered that the MPI-I is potentially affected by (de-)methylation reactions (Brocks et al., 2003a). The calculated methylnaphthalene ratio (MNR = 2.52; Tab. 3.2) corresponds to a somewhat lower mean vitrinite reflectance of ca. 1.5, which is again in line with a post-oil window maturity (cf., Radke et al., 1984). The mismatches between single aromatic maturity parameters are negligible, as these indices have limited application for highly mature Archean organic matter (Brocks et al., 2003a). The putative offset between the indices and the metamorphic overprint indicated by Raman data is most likely due to the protection of kerogen-bound moieties even under elevated thermal stress (Love et al., 1995; Lockhart et al., 2008). Furthermore, it has been shown that kerogen isolated from the Strelley Pool Formation also contains larger PAH clusters which are not GC-amenable (> 10–15 rings; Marshall et al., 2007). Consequently, it can be anticipated that the compounds detected in the HyPy pyrolysate of the Dresser kerogen represent only a small fraction of the bulk macromolecular organic matter.

The distribution of monomethyl alkanes ≤ *n*-C₁₈ (Figs. B3, B4) released from the Dresser kerogen resembles high-temperature HyPy products from the Strelley Pool kerogen (Marshall et al., 2007; their Fig. 15). Such isomeric mixtures are typically formed during thermal cracking of alkyl moieties (Kissin, 1987) and are in good agreement with the estimated maturity range. Methylated aromatics such as methyl naphthalenes and methyl phenanthrenes have also been observed in other hydropyrolysates from Archean kerogens that experienced low-grade metamorphism (Brocks et al., 2003b; Marshall et al., 2007; French et al., 2015). In all of these cases, the degree of alkylation varied with the exact thermal alteration of the respective kerogens (Marshall et al., 2007; French et al., 2015).

Tab. 3.2: Maturity indices (based on aromatic hydrocarbons) of the Dresser kerogen. MP/P: Methylphenanthrene/phenanthrene ratio; MPI-I: Methylphenanthrene index [$1.5 \times (2\text{-MP} + 3\text{-MP}) / (P + 1\text{-MP} + 9\text{-MP})$; Radke & Welte, 1983]; P/MP: Phenanthrene/methylphenanthrene ratio; R_c (MPI-I): computed vitrinite reflectance ($0.7 \times \text{MPI-I} + 0.22$, according to P/MP > 1; Boreham et al., 1988); MNR: Methylnaphthalene ratio ($2\text{-MN}/1\text{-MN}$; Radke et al., 1984)

MP/P	MPI-I	P/MP	R _c (MPI-I)	MNR
0.33	0.23	3.01	2.87	2.52

3.4.2 Syngeneity of the Dresser kerogen-derived compounds

The kerogen of the Dresser Formation exclusively occurs in the form of fluffy aggregates and clots embedded within a very dense chert matrix that is, once solidified, highly impermeable to fluids. The depositional age of the

formation is constrained to 3481 ± 3.6 Ma (Van Kranendonk et al., 2008), and the investigated chert vein shows no evidence for disruption by post-depositional hydrothermal fluids. This has also been described for other hydrothermal chert veins of the Dresser Formation, where the kerogen has been interpreted as being syngenetic (i.e., formed prior to host rock lithification; Ueno et al., 2001, 2004; Morag et al., 2016). Furthermore, the maturity of the embedded kerogen is in good accordance with the thermal history of the host rock. An introduction of solid macromolecular organic matter from stratigraphically younger units in this region during later fluid-flow phases, as proposed for the younger Apex chert (Olcott-Marshall et al., 2014), can therefore be excluded.

As the bitumen fractions of Precambrian rocks are easily biased by the incorporation of contaminants during later stages of rock history (Brocks et al., 2008; Brocks, 2011; French et al., 2015), studies have increasingly focused on kerogen-bound compounds that are more likely to be syngenetic to the host rock (Love et al., 1995; Brocks et al., 2003b; Marshall et al., 2007; French et al., 2015). Potential volatile organic contaminants adhering to the kerogen are removed through excessive extraction and a thermal desorption step (~ 350 °C) prior to high-temperature HyPy (550 °C; cf. Brocks et al., 2003b; Marshall et al., 2007). The recurrence of few *n*-alkanes in the range of *n*-C₁₄ to *n*-C₂₄ (maximum at *n*-C₁₅) in high-temperature HyPy blank runs obtained immediately before and after the actual sample run (Figs. 3.3a, B2, B3) indicates minor background contamination during pyrolysis, with a source most likely within the HyPy system. However, these contaminants do not significantly affect the *n*-alkane pattern yielded by high-temperature HyPy of the Dresser kerogen, as evidenced by blank subtraction (Fig. 3.3c).

Contamination of the sample can be further deciphered by the presence of polar additives or hydrocarbons that are not consistent with the thermal history of the host rock. Plastic-derived branched alkanes with quaternary carbon centers (BAQCs), a common contaminant in Precambrian rock samples (Brocks et al., 2008), have not been detected (Fig. B7). Traces of functionalized plasticizers (phenols and phthalic acid; Figs. B2, B6, B8) are unlikely to survive (or result from) HyPy treatment. These compounds are therefore considered as background contamination introduced during sample preparation and analysis after HyPy. The observed siloxanes (Fig. 3.3, B2) probably originate from the GC column or septum bleeding and are unlikely to be contained in the sample. All of these compounds occur only in low or trace abundances and can be clearly distinguished from the ancient aliphatic and aromatic hydrocarbons contained in the Dresser kerogen.

Contamination by (sub-)recent endoliths can be excluded as sample surfaces have been carefully removed and there is no petrographic indication for borings or fissures containing recent organic material (Fig. 3.2). HyPy of untreated or extracted biomass would yield a variety of acyclic and cyclic biomarkers (cf., Love et al., 2005). However, high-temperature HyPy of the Dresser kerogen almost exclusively yielded *n*-alkanes, minor amounts of monomethyl alkanes and various aromatic hydrocarbons (Figs. 3.3b, c, B2–B6), while hopanoids or steroids were absent (Figs. B8, B9). This is in good agreement with the maturity of the Dresser kerogen and previous HyPy studies of Archean rocks (Brocks et al., 2003b; Marshall et al., 2007; French et al., 2015).

Accidental contamination of the kerogen by mono-, di- and triglycerides (e.g., dust, skin surface lipids) can also be ruled out as HyPy treatment of these compounds typically results in *n*-alkane distributions with a distinct predominance of *n*-C₁₆ and *n*-C₁₈ homologues, corresponding to the *n*-C₁₆ and *n*-C₁₈ fatty acid precursors (Craig et al., 2004; Love et al., 2005; unpublished data from our own observations). At the same time, the observed distribution of kerogen-derived *n*-alkanes, with a distinct decrease beyond *n*-C₁₈ (Fig. 3.3b, c), is notably similar to high-temperature HyPy products of kerogens isolated from the ca. 3.4 Ga Strelley Pool Formation of the Pilbara Craton (Marshall et al., 2007; their Fig. 14). Marshall and co-workers considered these *n*-alkanes unlikely to be contaminants as they were released only in the high-temperature HyPy step. Furthermore, the stable carbon isotopic composition of *n*-alkanes in the Dresser high-temperature pyrolysate (-29.4 to -33.3 ‰; mean -31.4 ± 1.2 ‰) is very similar to the $\delta^{13}\text{C}_{\text{TOC}}$ signature of the sample (-32.8 ± 0.3 ‰; Figs. 3.3, B10; Tab. 3.1), indicating that these compounds were generated from the kerogen. Hence, we consider the compounds released from the Dresser kerogen during high-temperature HyPy (Fig. 3.3b, c) as syngenetic.

High-temperature HyPy of the Dresser kerogen yielded a variety of aromatic hydrocarbons, which are orders of magnitudes lower or absent in all other pyrolysates (Figs. 3.3, B2, B4–B6). It also produced significantly higher amounts of *n*-alkanes than the low-temperature step, and these further showed a distinct distribution pattern (i.e., a step $\leq n$ -C₁₈; Figs. 3.3, B2, B3). The lack of even low quantities of *n*-alkenes that typically accompany bond cleavage in kerogen pyrolysis was also observed by Marshall et al. (2007) in their HyPy analysis of cherts from the Strelley Pool Formation. As a possible explanation for the lack of *n*-alkenes, these authors suggested that the *n*-alkanes were not cracked from the kerogen but were rather trapped in closed micropores until the organic host matrix was pyrolytically disrupted. Alternatively, however, unsaturated cleavage products may have been

immediately reduced during HyPy by the steadily available hydrogen and catalysts. Indeed, it has been demonstrated that double bonds in linear alkyl chains are efficiently hydrogenated during HyPy, even in the case of pre-extracted microbial biomass (e.g., Love et al., 2005; our Fig. 3.3d). We consider both as plausible scenarios to explain the absence of *n*-alkenes in the Dresser chert hydropyrolysate.

3.4.3 Origin of the Dresser kerogen: hydrothermal vs. biological origin

The $\delta^{13}\text{C}_{\text{TOC}}$ value of $-32.8 \pm 0.3 \text{ ‰}$ is consistent with carbon fixation by photo- or chemoautotrophs (cf., Schidlowski, 2001). However, organic compounds exhibiting similar ^{13}C depletions (partly down to ca. -36 ‰ relative to the initial substrate) could also be formed abiotically during the serpentinization of ultramafic rocks (Fischer–Tropsch-type synthesis; McCollom et al., 1999; McCollom & Seewald, 2006; Proskurowski et al., 2008). A further constraint on the origin of the Dresser kerogen is provided by the distinct decrease in *n*-alkane abundance beyond *n*-C₁₈ observed in the high-temperature HyPy pyrolysate (Fig. 3.3b, c). This distribution resembles HyPy products of pre-extracted recent cyanobacterial biomass, which also shows a very pronounced restriction in carbon number to homologues $\leq n\text{-C}_{18}$ (Fig. 3.3d).

The pre-extracted cyanobacterial cell material and the abiotically produced *n*-alkanes studied as reference samples experienced no thermal maturation. It can nevertheless be expected that burial, and thus heating, of *Anabaena* biomass (Fig. 3.3d) would initially liberate lower *n*-alkane homologues from their predominant *n*-alkyl moieties while, up to a certain point, retaining the distinct step at *n*-C₁₈. Experimental maturation of an immature kerogen revealed the preservation of distinct alkyl-chain length preferences even after 100 days at 300 °C (Mißbach et al., 2016; e.g., a step beyond *n*-C₃₁ in their Fig. 3.2). Further maturation would ultimately lead to a unimodal distribution of short-chain *n*-alkanes and erase the biologically inherited pattern (cf., Mißbach et al., 2016). In contrast, abiotically synthesized extractable organic compounds show a unimodal homologue distribution from the beginning (Fig. 3.3e) and will retain it, while thermal maturation would gradually shift the *n*-alkane pattern towards shorter homologues. It can therefore be expected that organic compounds cleaved from an abiotic “Fischer–Tropsch-kerogen” – whose existence has not been proven yet – would also exhibit a unimodal distribution. Consequently, the distinctive distribution of *n*-alkanes released from the Dresser kerogen (i.e., the step $\leq n\text{-C}_{18}$; Figs. 3.3b, c) can be regarded as a molecular fingerprint relating to a biosynthetic origin of the organic matter.

Highly ^{13}C -depleted methane in primary fluid inclusions in hydrothermal chert veins of the Dresser Formation ($\delta^{13}\text{C} < 56 \text{ ‰}$) was taken as evidence for biological methanogenesis and thus the presence of Archaea (Ueno et al., 2006). Our $\delta^{13}\text{C}_{\text{TOC}}$ value ($-32.8 \pm 0.3 \text{ ‰}$; Tab. 3.1; Fig. B10) would generally be consistent with both bacterial and archaeal sources (cf., Schidlowski, 2001). Archaea only synthesize isoprene-based compounds (Koga & Morii, 2007; Matsumi et al., 2011). Straight-chain (acetyl-based) hydrocarbon moieties such as fatty acids – the potential precursors of the kerogen-derived *n*-alkanes – are to current knowledge being formed only by Bacteria and Eukarya, where they typically function as constituents of membranes or storage lipids (cf., Erwin, 1973; Kaneda, 1991). The formation of these lipids is tightly controlled by different biosynthetic pathways resulting in characteristic chain-length distributions. In bacterial lipids, carbon chain lengths typically do not extend above *n*-C₁₈ (cf., Kaneda, 1991). Consequently, given the lack of convincing evidence for the presence of Eukarya as early as 3.5 Ga (cf., Parfrey et al., 2011; Knoll, 2014; French et al., 2015), the most plausible source of kerogen-occluded *n*-alkanes in the Dresser hydrothermal chert is Bacteria. Strongly reducing conditions during the deposition of the Dresser Formation are indicated by widespread pyrite, Fe-rich carbonates and trace element signatures (Van Kranendonk et al., 2003, 2008). Potential microbial sources for the Dresser kerogen therefore may have included anoxygenic photoautotrophic, chemoautotrophic and heterotrophic microorganisms.

3.4.4 The “hydrothermal pump hypothesis”

Our results strongly support a biological origin of the kerogen found in the early Archean hydrothermal chert veins of the Dresser Formation. We explain this finding by the redistribution and sequestration of microbial organic matter that may have formed in a variety of Dresser environments through hydrothermal circulation (proposed herein as the “hydrothermal pump hypothesis”; Fig. 3.4). Higher geothermal gradients prior to the onset of modern-type plate tectonics at ca. 3.2–3.0 Ga (Smithies et al., 2005; Shirey & Richardson, 2011) were possibly important drivers of early Archean hydrothermal systems. In fact, the Dresser Formation was formed in a volcanic caldera environment affected by strong hydrothermal circulation, where voluminous fluid circulation locally caused intense acid–sulfate alteration of basalts and the formation of a dense hydrothermal vein swarm (Nijman et al., 1999; Van Kranendonk & Pirajno, 2004; Van Kranendonk, 2006; Van Kranendonk et al., 2008; Harris et al., 2009).

In addition to the high crustal heat flow, the absence of thick sedimentary cover may have facilitated the intrusion of seawater into the hydrothermal system. The associated large-scale assimilation of particulate and dissolved organic matter and its transport and alteration by hydrothermal fluids (Fig. 3.4) therefore appears to be a plausible mechanism that may, at least partly, explain the high amounts of kerogen in early Archean hydrothermal veins.

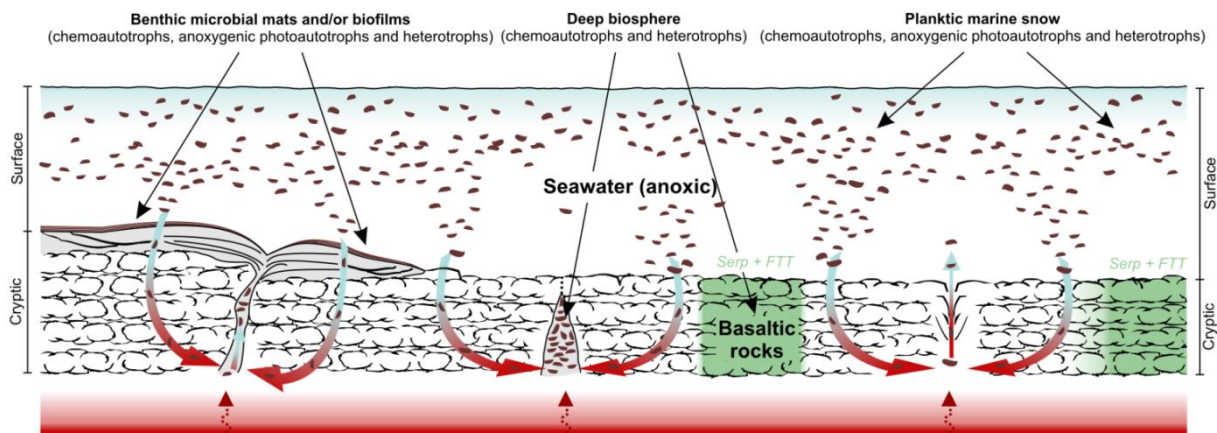


Fig. 3.4: The ‘hydrothermal pump hypothesis’. Organic matter was predominantly biologically produced and heterotrophically processed by Bacteria and, possibly, Archaea. Additionally, Fischer–Tropsch-type synthesis of organic matter linked to the serpentinisation of ultramafic rocks (McCollom et al., 1999; McCollom & Seewald, 2006) may have occurred locally. Primary producers (chemoautotrophs, anoxygenic photoautotrophs) and heterotrophs may have flourished in surface waters (planktic ‘marine snow’), at the water/rock interface (microbial mats and/or biofilms), and in cryptic environments (e.g., within basalts and hydrothermal vent systems). After accumulating in different Dresser environments, the organic matter was redistributed and sequestered in veins by hydrothermal fluids.

The hydrothermal pump hypothesis requires a source of organic matter during the deposition of the Dresser Formation (Fig. 3.4). Whereas contributions from extraterrestrial sources, as well as from Fischer–Tropsch-type synthesis linked to the serpentinization of ultramafic rocks, cannot be excluded, our results indicate a primarily biological origin for the kerogen contained in the chert veins (Fig. 3.4). The inferred biogenicity is also in line with the consistent $\delta^{13}\text{C}$ offset between bulk kerogens (ca. -20 to -30 ‰) and carbonate (ca. ± 2 ‰) in Archean rocks (Hayes, 1983; Schidlowski, 2001). Prokaryotic primary producers and heterotrophs may have flourished in microbial mats (Dresser stromatolites; Walter et al., 1980; Van Kranendonk, 2006, 2011; Philippot et al., 2007; Van Kranendonk et al., 2008), the water column (planktic “marine snow”; Brasier et al., 2006; Blake et al., 2010) and even hot springs on land (Djokic et al., 2017). Another biological source for the ancient organic matter could have been chemoautotrophs and heterotrophs thriving in subsurface environments, such as basalts (Banerjee et al., 2007; Furnes et al., 2008) and hydrothermal vent systems (Shen et al., 2001; Ueno et al., 2001, 2004, 2006; Pinti et al., 2009; Morag et al., 2016; Fig. 3.4). All of these systems are not mutually exclusive and the largely anoxic conditions would have encouraged a high steady-state abundance of organic matter in the aquatic environment (Fig. 3.4).

Dissolved organic matter (DOM) in modern seawater may resist decomposition over millennial timescales (Druffel & Griffin, 2015). In recent hydrothermal fields, however, organic matter becomes thermally altered and redistributed (Simoneit, 1993; Delacour et al., 2008; Konn et al., 2009). Laboratory experiments using marine DOM indicate that thermal alteration already occurs at temperatures > 68 – 100 °C and efficient removal of organic molecules at 212 – 401 °C (Hawkes et al., 2015, 2016). It has been argued, however, that such DOM removal may also be due to transformation into immiscible material through, for example, condensation (Castello et al., 2014) and/or defunctionalization reactions (Hawkes et al., 2016). These processes, however, are as yet poorly understood. In the Dresser Formation, hydrothermal temperatures ranged from ca. 300 °C at depth to 120 °C near the palaeosurface, causing propylitic (ca. 250 – 350 °C) and argillic (including advanced argillic: ca. 100 – 200 °C) alteration of the host rocks (Van Kranendonk & Pirajno, 2004; Van Kranendonk et al., 2008; Harris et al., 2009). Given this variety of thermal regimes, and the generally anoxic nature of early Archaean seawater (e.g., Van Kranendonk et al., 2003, 2008; Li et al., 2013), it is likely that some of the organic substances underwent in situ alteration, but not complete oxidation, during hydrothermal circulation. The entrained organics would have been trapped in the chert that instantaneously precipitated from the ascending hydrothermal fluids due to subsurface cooling (cf., Van Kranendonk, 2006).

In summary, the hydrothermal pump hypothesis proposed here (Fig. 3.4) includes (i) a net build-up of organic matter in different Dresser environments under largely anoxic conditions, (ii) a large-scale assimilation of particulate and dissolved organic matter from various biological sources and its subsurface transport and alteration by hydrothermal fluids, and (iii) its sequestration within hydrothermal chert veins as kerogen. This model explains the presence of abundant organic carbon in early Archean hydrothermal veins, as well as its morphological, structural and isotopic variability observed in the Dresser hydrothermal chert veins (Ueno et al., 2001, 2004; Pinti et al., 2009; Morag et al., 2016). It does not, however, help to pinpoint the formation pathways of distinct carbonaceous structures, as for instance those preserved in the Dresser Formation (Glikson et al., 2008) or the younger Apex chert (e.g., Schopf, 1993; Brasier et al., 2002, 2005; Schopf et al., 2002; Bower et al., 2016). Further work is necessary to test whether consistent molecular and compound-specific isotopic patterns can be generated from a larger set of Archean kerogens.

3.5 Conclusions

Kerogen embedded in a hydrothermal chert vein from the ca. 3.5 Ga Dresser Formation (Pilbara Craton, Western Australia) is syngenetic. A biological origin is inferred from the presence of short-chain *n*-alkanes in high-temperature HyPy pyrolysates, showing a sharp decrease in homologue abundance beyond *n*-C₁₈. HyPy products of pre-extracted recent bacterial biomass exhibited a similar restriction to carbon chain lengths $\leq n$ -C₁₈, whereas abiotic compounds experimentally formed via Fischer–Tropsch-type synthesis exhibited a unimodal distribution. A biological interpretation for Dresser organics is further consistent with the $\delta^{13}\text{C}_{\text{TOC}}$ value (-32.8 ± 0.3 ‰) and the stable carbon isotopic composition of *n*-alkanes in the Dresser high-temperature pyrolysate (-29.4 to -33.3 ‰; mean -31.4 ± 1.2 ‰). Based on these observations, we propose that the original organic matter was primarily biologically synthesized. We hypothesize that microbially derived organic matter accumulating in anoxic aquatic (surface and/or subsurface) environments was assimilated, redistributed and sequestered by hydrothermal fluids (“hydrothermal pump hypothesis”).

Acknowledgements

This work was financially supported by the Deutsche Forschungsgemeinschaft (grant Du 1450/3-1, DFG Priority Programme 1833 “Building a Habitable Earth”, to Jan-Peter Duda and Joachim Reitner; grant Th 713/11-1 to Volker Thiel), the Courant Research Centre of the Georg-August-Universität Göttingen (DFG, German Excellence Program), the Göttingen Academy of Sciences and Humanities (to Jan-Peter Duda and Joachim Reitner), the International Max Planck Research School for Solar System Science at the Georg-August-Universität Göttingen (to Manuel Reinhardt and Helge Mißbach) and the ARC Centre of Excellence for Core to Crust Fluid Systems (Martin J. Van Kranendonk). We thank Martin Blumenberg, Cornelia Conradt, Wolfgang Dröse, Jens Dyckmans, Axel Hackmann, Merve Öztoprak and Burkhard C. Schmidt for scientific and technical support. Josh Rochelmeier is thanked for assistance during sample extraction of *A. cylindrica*. We are indebted to Malcolm Walter and Mark A. van Zuilen for helpful comments on the manuscript and Jack Middelburg for editorial handling. This is publication number 5 of the Early Life Research Group (Department of Geobiology, Georg-August-Universität Göttingen; Göttingen Academy of Sciences and Humanities) and contribution 980 from the ARC Centre of Excellence for Core to Crust Fluid Systems.

We acknowledge support by the German Research Foundation and the Open Access Publication Funds of Georg-August-Universität Göttingen.

References

- Banerjee, N. R., Simonetti, A., Furnes, H., Muehlenbachs, K., Staudigel, H., Heaman, L., & Van Kranendonk, M. J. (2007). Direct dating of Archean microbial ichnofossils. *Geology*, 35, 487–490. <https://doi.org/10.1130/g23534a.1>
- Bauersachs, T., Mudimu, O., Schulz, R., & Schwark, L. (2014). Distribution of long chain heterocyst glycolipids in N₂-fixing cyanobacteria of the order Stigonematales. *Phytochemistry*, 98, 145–150. <https://doi.org/10.1016/j.phytochem.2013.11.007>
- Blake, R. E., Chang, S. J., & Lepland, A. (2010). Phosphate oxygen isotopic evidence for a temperate and biologically active Archean ocean. *Nature*, 464, 1029–1032. <https://doi.org/10.1038/nature08952>

- Boreham, C. J., Crick, I. H., & Powell, T. G. (1988). Alternative calibration of the Methylphenanthrene Index against vitrinite reflectance: Application to maturity measurements on oils and sediments. *Org. Geochem.*, *12*, 289–294. [https://doi.org/10.1016/0146-6380\(88\)90266-5](https://doi.org/10.1016/0146-6380(88)90266-5)
- Bower, D. M., Steele, A., Fries, M. D., Green, O. R., & Lindsay, J. F. (2016). Raman Imaging Spectroscopy of a Putative Microfossil from the ~3.46 Ga Apex Chert: Insights from Quartz Grain Orientation. *Astrobiology*, *16*, 169–180. <https://doi.org/10.1089/ast.2014.1207>
- Brasier, M. D., Green, O. R., Jephcoat, A. P., Kleppe, A. K., Van Kranendonk, M. J., Lindsay, J. F., Steele, A., & Grassineau, N. V. (2002). Questioning the evidence for Earth's oldest fossils. *Nature*, *416*, 76–81. <https://doi.org/10.1038/416076a>
- Brasier, M. D., Green, O. R., Lindsay, J. F., McLoughlin, N., Steele, A., & Stoakes, C. (2005). Critical testing of Earth's oldest putative fossil assemblage from the ~3.5 Ga Apex chert, Chinaman Creek, Western Australia. *Precambrian Res.*, *140*, 55–102. <https://doi.org/10.1016/j.precamres.2005.06.008>
- Brasier, M., McLoughlin, N., Green, O., & Wacey, D. (2006). A fresh look at the fossil evidence for early Archaean cellular life. *Philos. T. R. Soc. B*, *361*, 887–902. <https://doi.org/10.1098/rstb.2006.1835>
- Brocks, J. J. (2011). Millimeter-scale concentration gradients of hydrocarbons in Archean shales: Live-oil escape or fingerprint of contamination?. *Geochim. Cosmochim. Acta*, *75*, 3196–3213. <https://doi.org/10.1016/j.gca.2011.03.014>
- Brocks, J. J. & Summons, R. E. (2003). Sedimentary Hydrocarbons, Biomarkers for Early Life. In Holland, H. D. and Turekian, K. K. (Eds.), *Treatise on Geochemistry Vol.8* (pp. 63–115). Amsterdam, the Netherlands: Pergamon.
- Brocks, J. J., Buick, R., Logan, G. A., & Summons, R. E. (2003a). Composition and syngeneity of molecular fossils from the 2.78 to 2.45 billion-year-old Mount Bruce Supergroup, Pilbara Craton, Western Australia. *Geochim. Cosmochim. Acta*, *67*, 4289–4319. [https://doi.org/10.1016/S0016-7037\(03\)00208-4](https://doi.org/10.1016/S0016-7037(03)00208-4)
- Brocks, J. J., Love, G. D., Snape, C. E., Logan, G. A., Summons, R. E., & Buick, R. (2003b). Release of bound aromatic hydrocarbons from late Archean and Mesoproterozoic kerogens via hydrolysis. *Geochim. Cosmochim. Acta*, *67*, 1521–1530. [https://doi.org/10.1016/S0016-7037\(02\)01302-9](https://doi.org/10.1016/S0016-7037(02)01302-9)
- Brocks, J. J., Grosjean, E., & Logan, G. A. (2008). Assessing biomarker syngeneity using branched alkanes with quaternary carbon (BAQCs) and other plastic contaminants. *Geochim. Cosmochim. Acta*, *72*, 871–888. <https://doi.org/10.1016/j.gca.2007.11.028>
- Castello, D., Kruse, A., & Fiori, L. (2014). Supercritical water gasification of hydrochar. *Chem. Eng. Res. Des.*, *92*, 1864–1875. <https://doi.org/10.1016/j.cherd.2014.05.024>
- Craig, O. E., Love, G. D., Isaksson, S., Taylor, G., & Snape, C. E. (2004). Stable carbon isotopic characterisation of free and bound lipid constituents of archaeological ceramic vessels released by solvent extraction, alkaline hydrolysis and catalytic hydrolysis. *J. Anal. Appl. Pyrol.*, *71*, 613–634. <https://doi.org/10.1016/j.jaap.2003.09.001>
- Delacour, A., Früh-Green, G. L., Bernasconi, S. M., Schaeffer, P., & Kelley, D. S. (2008). Carbon geochemistry of serpentinites in the Lost City Hydrothermal System (30° N, MAR). *Geochim. Cosmochim. Acta*, *72*, 3681–3702. <https://doi.org/10.1016/j.gca.2008.04.039>
- Delarue, F., Rouzaud, J.-N., Derenne, S., Bourbin, M., Westall, F., Kremer, B., Sugitani, K., Deldicque, D., & Robert, F. (2016). The Raman-derived carbonization continuum: A tool to select the best preserved molecular structures in Archean kerogens. *Astrobiology*, *16*, 407–417. <https://doi.org/10.1089/ast.2015.1392>
- Djokic, T., Van Kranendonk, M. J., Campbell, K. A., Walter, M. R., & Ward, C. R. (2017). Earliest signs of life on land preserved in ca. 3.5 Ga hot spring deposits. *Nature Comm.*, *8*, e15263. <https://doi.org/10.1038/ncomms15263>
- Druffel, E. R. M. & Griffin, S. (2015). Radiocarbon in dissolved organic carbon of the South Pacific Ocean. *Geophys. Res. Lett.*, *42*, 4096–4101. <https://doi.org/10.1002/2015gl063764>
- Erwin, J. (1973). *Lipids and biomembranes of eukaryotic microorganisms*. New York, USA: Academic Press.
- Ferralis, N., Matys, E. D., Knoll, A. H., Hallmann, C., & Summons, R. E. (2016). Rapid, direct and non-destructive assessment of fossil organic matter via microRaman spectroscopy. *Carbon*, *108*, 440–449. <https://doi.org/10.1016/j.carbon.2016.07.039>
- French, K. L., Hallmann, C., Hope, J. M., Schoon, P. L., Zumberge, J. A., Hoshino, Y., Peters, C. A., George, S. C., Love, G. D., Brocks, J. J., & Buick, R. (2015). Reappraisal of hydrocarbon biomarkers in Archean rocks. *P. Natl. Acad. Sci. USA*, *112*, 5915–5920. <https://doi.org/10.1073/pnas.1419563112>

- Furnes, H., McLoughlin, N., Muehlenbachs, K., Banerjee, N., Staudigel, H., Dilek, Y., de Wit, M., Van Kranendonk, M. J., & Schiffman, P. (2008). Oceanic pillow lavas and hyaloclastites as habitats for microbial life through time – a review. In Dilek, Y., Furnes, H., and Muehlenbachs, K. (Eds.), *Links Between Geological Processes, Microbial Activities & Evolution of Life* (pp. 1–68). The Netherlands: Springer.
- Gérard, E., Moreira, D., Philippot, P., Van Kranendonk, M., & López-García, P. (2009). Modern subsurface bacteria in pristine 2.7 Ga-old fossil stromatolite drillcore samples from the Fortescue Group, Western Australia. *PLoS ONE*, *4*, e5298. <https://doi.org/10.1371/journal.pone.0005298>
- Glikson, M., Duck, L. J., Golding, S. D., Hofmann, A., Bolhar, R., Webb, R., Baiano, C. F., & Sly, L. I. (2008). Microbial remains in some earliest Earth rocks: Comparison with a potential modern analogue. *Precambrian Res.*, *164*, 187–200. <https://doi.org/10.1016/j.precamres.2008.05.002>
- Harris, A. C., White, N. C., McPhie, J., Bull, S. W., Line, M. A., Skrzeczynski, R., Mernagh, T. P., & Tosdal, R. M. (2009). Early Archean Hot Springs above Epithermal Veins, North Pole, Western Australia: New Insights from Fluid Inclusion Microanalysis. *Econ. Geol.*, *104*, 793–814. <https://doi.org/10.2113/gsecongeo.104.6.793>
- Hawkes, J. A., Rossel, P. E., Stubbins, A., Butterfield, D., Connelly, D. P., Achterberg, E. P., Koschinsky, A., Chavagnac, V., Hansen, C. T., Bach, W., & Dittmar, T. (2015). Efficient removal of recalcitrant deep-ocean dissolved organic matter during hydrothermal circulation. *Nat. Geosci.*, *8*, 856–860. <https://doi.org/10.1038/ngeo2543>
- Hawkes, J. A., Hansen, C. T., Goldhammer, T., Bach, W., and Dittmar, T. (2016). Molecular alteration of marine dissolved organic matter under experimental hydrothermal conditions. *Geochim. Cosmochim. Acta*, *175*, 68–85. <https://doi.org/10.1016/j.gca.2015.11.025>
- Hayes, J. M. (1983). Geochemical evidence bearing on the origin of aerobiosis, a speculative hypothesis. In Schopf, J.W. (Ed.), *The Earth's Earliest Biosphere: Its Origin and Evolution* (pp. 291–301). New York: Princeton University Press.
- Hickman, A. H. (1973). The North Pole barite deposits, Pilbara Goldfield. *Geol. Surv. West. Aust. Ann. Rep.*, *1972*, 57–60.
- Hickman, A. H. (1975). Precambrian structural geology of part of the Pilbara region. *Geol. Surv. West. Aust. Ann. Rep.*, 68–73.
- Hickman, A. H. (1983). Geology of the Pilbara block and its environs. *Geol. Surv. West. Aust. Bull.*, *127*.
- Hickman, A. H. (2012). Review of the Pilbara Craton and Fortescue Basin, Western Australia: crustal evolution providing environments for early life. *Island Arc*, *21*, 1–31.
- Hickman, A. H. & Van Kranendonk, M. J. (2012). A Billion Years of Earth History: A Geological Transect Through the Pilbara Craton and the Mount Bruce Supergroup – a field guide to accompany 34th IGC ExcursionWA-2. *Geol. Surv. West. Aust., Record 2012/10*.
- Hofmann, A. (2011). Archaean Hydrothermal Systems in the Barberton Greenstone Belt and Their Significance as a Habitat for Early Life. In Golding, S. and Glikson, M. (Eds.), *Earliest Life on Earth: Habitats, Environments and Methods of Detection* (pp. 51–78). Dordrecht: Springer. https://doi.org/10.1007/978-90-481-8794-2_3
- Kaneda, T. (1991). Iso- and Anteiso-Fatty Acids in Bacteria: Biosynthesis, Function, and Taxonomic significance. *Microbiol. Rev.*, *55*, 288–302.
- Killops, S. & Killops, V. (2005). *Introduction to organic geochemistry*, 2nd edn. Oxford: Blackwell Publishing.
- Kissin, Y. V. (1987). Catagenesis and composition of petroleum: origin of *n*-alkanes and isoalkanes in petroleum crudes. *Geochim. Cosmochim. Acta*, *51*, 2445–2457. [https://doi.org/10.1016/0016-7037\(87\)90296-1](https://doi.org/10.1016/0016-7037(87)90296-1)
- Knoll, A. H. (2014). Paleobiological perspectives on early eukaryotic evolution. *CSH Perspect. Biol.*, *6*, a016121. <https://doi.org/10.1101/cshperspect.a016121>
- Koga, Y. & Morii, H. (2007). Biosynthesis of Ether-Type Polar Lipids in Archaea and Evolutionary Considerations. *Microbiol. Mol. Biol. R.*, *71*, 97–120. <https://doi.org/10.1128/membr.00033-06>
- Konn, C., Charlou, J. L., Donval, J. P., Holm, N. G., Dehairs, F., & Bouillon, S. (2009). Hydrocarbons and oxidized organic compounds in hydrothermal fluids from Rainbow and Lost City ultramafic-hosted vents. *Chem. Geol.*, *258*, 299–314. <https://doi.org/10.1016/j.chemgeo.2008.10.034>
- Li, W., Czaja, A. D., Van Kranendonk, M. J., Beard, B. L., Roden, E. E., & Johnson, C. M. (2013). An anoxic, Fe(II)-rich, U-poor ocean 3.46 billion years ago. *Geochim. Cosmochim. Acta*, *120*, 65–79. <https://doi.org/10.1016/j.gca.2013.06.033>

- Lindsay, J. F., Brasier, M. D., McLoughlin, N., Green, O. R., Fogel, M., Steele, A., & Mertzman, S. A. (2005). The problem of deep carbon—An Archean paradox. *Precambrian Res.*, *143*, 1–22. <https://doi.org/10.1016/j.precamres.2005.09.003>
- Lockhart, R. S., Meredith, W., Love, G. D., & Snape, C. E. (2008). Release of bound aliphatic biomarkers via hydrolysis from Type II kerogen at high maturity. *Org. Geochem.*, *39*, 1119–1124. <https://doi.org/10.1016/j.orggeochem.2008.03.016>
- Love, G. D., Snape, C. E., Carr, A. D., & Houghton, R. C. (1995). Release of covalently-bound alkane biomarkers in high yields from kerogen via catalytic hydrolysis. *Org. Geochem.*, *23*, 981–986. [https://doi.org/10.1016/0146-6380\(95\)00075-5](https://doi.org/10.1016/0146-6380(95)00075-5)
- Love, G. D., Bowden, S. A., Jahnke, L. L., Snape, C. E., Campbell, C. N., Day, J. G., & Summons, R. E. (2005). A catalytic hydrolysis method for the rapid screening of microbial cultures for lipid biomarkers. *Org. Geochem.*, *36*, 63–82. <https://doi.org/10.1016/j.orggeochem.2004.07.010>
- Marshall, C. P., Love, G. D., Snape, C. E., Hill, A. C., Allwood, A. C., Walter, M. R., Van Kranendonk, M. J., Bowden, S. A., Sylva, S. P., & Summons, R. E. (2007). Structural characterization of kerogen in 3.4 Ga Archean cherts from the Pilbara Craton, Western Australia. *Precambrian Res.*, *155*, 1–23. <https://doi.org/10.1016/j.precamres.2006.12.014>, 2007
- Matsumi, R., Atomi, H., Driessen, A. J. M., & van der Oost, J. (2011). Isoprenoid biosynthesis in Archaea – Biochemical and evolutionary implications. *Res. Microbiol.*, *162*, 39–52. <https://doi.org/10.1016/j.resmic.2010.10.003>
- McCullom, T. M. & Seewald, J. S. (2006). Carbon isotope composition of organic compounds produced by abiotic synthesis under hydrothermal conditions. *Earth Planet. Sci. Lett.*, *243*, 74–84. <https://doi.org/10.1016/j.epsl.2006.01.027>
- McCullom, T. M., Ritter, G., & Simoneit, B. R. T. (1999). Lipid Synthesis Under Hydrothermal Conditions by Fischer–Tropsch-Type Reactions. *Origins Life Evol. B.*, *29*, 153–166. <https://doi.org/10.1023/a:1006592502746>
- Meredith, W., Russell, C. A., Cooper, M., Snape, C. E., Love, G. D., Fabbri, D., & Vane, C. H. (2004). Trapping hydrolysis products on silica and their subsequent thermal desorption to facilitate rapid fingerprinting by GC-MS. *Org. Geochem.*, *35*, 73–89. <https://doi.org/10.1016/j.orggeochem.2003.07.002>
- Mißbach, H., Duda, J.-P., Lünsdorf, N. K., Schmidt, B. C., & Thiel, V. (2016). Testing the preservation of biomarkers during experimental maturation of an immature kerogen. *Int. J. Astrobiol.*, *15*, 165–175. <https://doi.org/10.1017/S1473550416000069>
- Morag, N., Williford, K. H., Kitajima, K., Philippot, P., Van Kranendonk, M. J., Lepot, K., Thomazo, C., & Valley, J. W. (2016). Microstructure-specific carbon isotopic signatures of organic matter from ~3.5 Ga cherts of the Pilbara Craton support a biogenic origin. *Precambrian Res.*, *275*, 429–449. <https://doi.org/10.1016/j.precamres.2016.01.014>
- Nijman, W., de Bruijne, K. H., & Valkering, M. E. (1999). Growth fault control of Early Archean cherts, barite mounds and chert-barite veins, North Pole Dome, Eastern Pilbara, Western Australia. *Precambrian Res.*, *98*, 247–274. [https://doi.org/10.1016/S0301-9268\(97\)00062-4](https://doi.org/10.1016/S0301-9268(97)00062-4)
- Olcott-Marshall, A., Jehlička, J., Rouzaud, J. N., & Marshall, C. P. (2014). Multiple generations of carbonaceous material deposited in Apex chert by basin-scale pervasive hydrothermal fluid flow. *Gondwana Res.*, *25*, 284–289. <https://doi.org/10.1016/j.gr.2013.04.006>
- Parfrey, L. W., Lahr, D. J., Knoll, A. H., & Katz, L. A. (2011). Estimating the timing of early eukaryotic diversification with multigene molecular clocks. *P. Natl. Acad. Sci. USA*, *108*, 13624–13629. <https://doi.org/10.1073/pnas.1110633108>
- Peters, K. E., Walters, C. C., & Moldowan, J. M. (2005). *The biomarker guide: II. Biomarkers and Isotopes in petroleum exploration and earth history*, 2nd edn. Cambridge: Cambridge University Press.
- Philippot, P., Van Zuilen, M., Lepot, K., Thomazo, C., Farquhar, J., & Van Kranendonk, M. J. (2007). Early Archean microorganisms preferred elemental sulfur, not sulfate. *Science*, *317*, 1534–1537. <https://doi.org/10.1126/science.1145861>
- Pinti, D. L., Hashizume, K., Sugihara, A., Massault, M., & Philippot, P. (2009). Isotopic fractionation of nitrogen and carbon in Paleoproterozoic cherts from Pilbara craton, Western Australia: Origin of ¹⁵N-depleted nitrogen. *Geochim. Cosmochim. Acta*, *73*, 3819–3848. <https://doi.org/10.1016/j.gca.2009.03.014>

- Proskurowski, G., Lilley, M. D., Seewald, J. S., Früh-Green, G. L., Olson, E. J., Lupton, J. E., Sylva, S. P., & Kelley, D. S. (2008). Abiogenic hydrocarbon production at Lost City hydrothermal field. *Science*, *319*, 604–607.
- Radke, M., & Welte, D. H. (1983). The Methylphenanthrene Index (MPI): A maturity parameter based on aromatic hydrocarbons. In M. Bjorøy, et al. (Eds.), *Adv. org. geochem. 1981* (pp. 504–512). Hoboken, NJ: Wiley.
- Radke, M., Leythaeuser, D., & Teichmüller, M. (1984). Relationship between rank and composition of aromatic hydrocarbons for coals of different origins. *Org. Geochem.*, *6*, 423–430., [https://doi.org/10.1016/0146-6380\(84\)90065-2](https://doi.org/10.1016/0146-6380(84)90065-2)
- Rippka, R., Deruelles, J., Waterbury, J. B., Herdman, M., & Stanier, R. Y. (1979). Generic assignments, strain histories and properties of pure cultures of cyanobacteria. *J. Gen. Microbiol.*, *111*, 1–61. <https://doi.org/10.1099/00221287-111-1-1>
- Schidlowski, M. (2001). Carbon isotopes as biogeochemical recorders of life over 3.8 Ga of Earth history: evolution of a concept. *Precambrian Res.*, *106*, 117–134. [https://doi.org/10.1016/S0301-9268\(00\)00128-5](https://doi.org/10.1016/S0301-9268(00)00128-5)
- Schopf, J. W. (1993). Microfossils of the Early Archean Apex chert: new evidence of the antiquity of life. *Science*, *260*, 640–646. <https://doi.org/10.1126/science.260.5108.640>
- Schopf, J. W., Kudryavtsev, A. B., Agresti, D. G., Wdowiak, T. J., & Czaja, A. D. (2002). Laser-Raman imagery of Earth's earliest fossils. *Nature*, *416*, 73–76. <https://doi.org/10.1038/416073a>
- Shen, Y., Buick, R., & Canfield, D. E. (2001). Isotopic evidence for microbial sulphate reduction in the early Archean era. *Nature*, *410*, 77–81. <https://doi.org/10.1038/35065071>
- Shirey, S. B. & Richardson, S. H. (2011). Start of the Wilson Cycle at 3 Ga Shown by Diamonds from Subcontinental Mantle. *Science*, *333*, 434–436. <https://doi.org/10.1126/science.1206275>
- Simoneit, B. R. T. (1993). Aqueous high-temperature and high-pressure organic geochemistry of hydrothermal vent systems. *Geochim. Cosmochim. Acta*, *57*, 3231–3243. [https://doi.org/10.1016/0016-7037\(93\)90536-6](https://doi.org/10.1016/0016-7037(93)90536-6)
- Smithies, R. H., Champion, D. C., Van Kranendonk, M. J., Howard, H. M., & Hickman, A. H. (2005). Modern-style subduction processes in the Mesoarchean: Geochemical evidence from the 3.12 Ga Whundo intra-oceanic arc. *Earth Planet. Sci. Lett.*, *231*, 221–237. <https://doi.org/10.1016/j.epsl.2004.12.026>
- Snape, C. E., Bolton, C., Dosch, R. G., & Stephens, H. P. (1989). High liquid yields from bituminous coal via hydropyrolysis with dispersed catalysts. *Ener. Fuel.*, *3*, 421–425. <https://doi.org/10.1021/ef00015a028>
- Summons, R. E. & Hallmann, C. (2014). Organic geochemical signatures of early life on earth. In Falkowski, P. and Freeman, K. (Eds.), *Treatise on geochemistry 2nd edn.* (pp. 33–46). The Netherlands: Elsevier. <https://doi.org/10.1016/B978-0-08-095975-7.01005-6>
- Terabayashi, M., Masada, Y., & Ozawa, H. (2003). Archean oceanfloor metamorphism in the North Pole area, Pilbara Craton, Western Australia. *Precambrian Res.*, *127*, 167–180. [https://doi.org/10.1016/S0301-9268\(03\)00186-4](https://doi.org/10.1016/S0301-9268(03)00186-4)
- Ueno, Y., Isozaki, Y., Yurimoto, H., & Maruyama, S. (2001). Carbon Isotopic Signatures of Individual Archean Microfossils(?) from Western Australia. *Int. Geol. Rev.*, *43*, 196–212. <https://doi.org/10.1080/00206810109465008>
- Ueno, Y., Yoshioka, H., Maruyama, S., & Isozaki, Y. (2004). Carbon isotopes and petrography of kerogens in ~3.5-Ga hydrothermal silica dikes in the North Pole area, Western Australia. *Geochim. Cosmochim. Acta*, *68*, 573–589. [https://doi.org/10.1016/S0016-7037\(03\)00462-9](https://doi.org/10.1016/S0016-7037(03)00462-9)
- Ueno, Y., Yamada, K., Yoshida, N., Maruyama, S., & Isozaki, Y. (2006). Evidence from fluid inclusions for microbial methanogenesis in the early Archean era. *Nature*, *440*, 516–519. <https://doi.org/10.1038/nature04584>
- Van Kranendonk, M. J. (1999). North Shaw, W.A. Sheet 2755. *West. Aust. Geol. Surv. 1 : 100 000, Geol. Series.*
- Van Kranendonk, M. J. (2006). Volcanic degassing, hydrothermal circulation and the flourishing of early life on Earth: A review of the evidence from c. 3490–3240 Ma rocks of the Pilbara Supergroup, Pilbara Craton, Western Australia. *Earth-Sci. Rev.*, *74*, 197–240. <https://doi.org/10.1016/j.earscirev.2005.09.005>
- Van Kranendonk, M. J. (2011). Morphology as an Indicator of Biogenicity for 3.5–3.2 Ga Fossil Stromatolites from the Pilbara Craton, Western Australia. In Reitner, J., Quéric, N.-V., and Arp, G. (Eds.), *Advances in Stromatolite Geobiology* (pp. 537–554). Berlin, Heidelberg: Springer.
- Van Kranendonk, M. J. & Pirajno, F. (2004). Geochemistry of metabasalts and hydrothermal alteration zones associated with c. 3.45 Ga chert and barite deposits: implications for the geological setting of the Warrawoona Group, Pilbara Craton, Australia. *Geochem.-Explor. Env. A.*, *4*, 253–278. <https://doi.org/10.1144/1467-7873/04-205>

- Van Kranendonk, M. J., Webb, G. E., & Kamber, B. S. (2003). Geological and trace element evidence for a marine sedimentary environment of deposition and biogenicity of 3.45 Ga stromatolitic carbonates in the Pilbara Craton, and support for a reducing Archaean ocean. *Geobiology*, *1*, 91–108. <https://doi.org/10.1046/j.1472-4669.2003.00014.x>
- Van Kranendonk, M. J., Philippot, P., Lepot, K., Bodorkos, S., & Pirajno, F. (2008). Geological setting of Earth's oldest fossils in the ca. 3.5 Ga Dresser Formation, Pilbara Craton, Western Australia. *Precambrian Res.*, *167*, 93–124. <https://doi.org/10.1016/j.precamres.2008.07.003>
- Walter, M. R., Buick, R., & Dunlop, J. S. R. (1980). Stromatolites 3,400–3,500 Myr old from the North Pole area, Western Australia. *Nature*, *284*, 443–445.
- Yui, T. F., Huang, E., & Xu, J. (1996). Raman spectrum of carbonaceous material: a possible metamorphic grade indicator for lowgrade metamorphic rocks. *J. Metamorph. Geol.*, *14*, 115–124. <https://doi.org/10.1046/j.1525-1314.1996.05792.x>

4 The taphonomic fate of isorenieratene in Lower Jurassic shales—controlled by iron?

Manuel Reinhardt, Jan-Peter Duda, Martin Blumenberg, Christian Ostertag-Henning, Joachim Reitner, Christine Heim, & Volker Thiel

Geobiology (2018), 16, 237–251

Fossil derivatives of isorenieratene, an accessory pigment in brown-colored green sulfur bacteria, are often used as tracers for photic zone anoxia through Earth's history, but their diagenetic behavior is still incompletely understood. Here, we assess the preservation of isorenieratene derivatives in organic-rich shales (1.5–8.4 wt.% TOC) from two Lower Jurassic anoxic systems (Bächental oil shale, Tyrol, Austria; Posidonia Shale, Baden-Württemberg, Germany). Bitumens and kerogens were investigated using catalytic hydrothermal pyrolysis (HyPy), closed-system hydrous pyrolysis (in gold capsules), gas chromatography–mass spectrometry (GC–MS) and gas chromatography–combustion–isotope ratio mass spectrometry (GC–C–IRMS). Petrography and biomarkers indicate a syngenetic relationship between bitumens and kerogens. All bitumens contain abundant isorenieratane, diverse complex aromatized isorenieratene derivatives, and a pseudohomologous series of 2,3,6-trimethyl aryl isoprenoids. In contrast, HyPy and mild closed-system hydrous pyrolysis of the kerogens yielded only minor amounts of these compounds. Given the overall low maturity of the organic matter (below oil window), it appears that isorenieratene and its abundant derivatives from the bitumen had not been incorporated into the kerogens. Accordingly, sulfur cross-linking, the key mechanism for sequestration of functionalized lipids into kerogens in anoxic systems, was not effective in the Jurassic environments studied. We explain this by (i) early cyclization/aromatization and (ii) hydrogenation reactions that have prevented effective sulfurization. In addition, (iii) sulfide was locally removed via anoxygenic photosynthesis and efficiently trapped by the reaction with sedimentary iron, as further indicated by elevated iron contents (4.0–8.7 wt.%) and the presence of abundant pyrite aggregates in the rock matrix. Although the combined processes have hampered the kerogen incorporation of isorenieratene and its derivatives, they may have promoted the long-term preservation of these biomarkers in the bitumen fraction via early defunctionalization. This particular taphonomy of aromatic carotenoids has to be considered in studies of anoxic iron-rich environments (e.g., the Proterozoic ocean).

4.1 Introduction

The aromatic carotenoid isorenieratene (**I**, see Fig. C1) is an unambiguous biosynthetic product serving as accessory pigment in the brown-colored strain of green sulfur bacteria (Chlorobiaceae) that thrive under low light intensities in the photic zone of stratified, anoxic water columns (e.g., Takahashi & Ichimura, 1970; Overmann & Pfennig, 1989; Overmann et al., 1992). Chlorobiaceae use the reductive (reverse) tricarboxylic acid (TCA) cycle for CO₂ fixation (Sirevåg & Ormerod, 1970; *Chlorobaculum tepidum* can also use the oxidative (forward) TCA cycle (Tang & Blankenship, 2010)), resulting in lipids enriched in ¹³C as compared to algal biomass ($\delta^{13}\text{C} = -8$ to -22 ‰ vs. Vienna Pee Dee Belemnite (V-PDB) standard; Quandt et al., 1977; Sirevåg et al., 1977; van der Meer et al., 1998; Schidlowski, 2001).

Diagenetic products of isorenieratene and also their stable carbon isotopic signals are commonly used for tracking photic zone anoxia through the Phanerozoic (e.g., Summons & Powell, 1986; Sinninghe Damsté & Köster, 1998; Grice et al., 2005; Hays et al., 2007; Heimhofer et al., 2008; Marynowski et al., 2008, 2011; Blumenberg et al., 2016). Anoxic conditions with potential photic zone anoxia have probably also been widespread during the Proterozoic (e.g., Canfield, 1998; Poulton et al., 2004; Scott et al., 2008; Planavsky et al., 2011; Poulton & Canfield, 2011). Anoxygenic phototrophs, including purple and green sulfur bacteria, may have contributed to the overall primary production and influenced biogeochemical cycles (Johnston et al., 2009). However, there are only few reports of aromatic carotenoid biomarkers dating back to this time (see French et al., 2015), most noteworthy the 1.64 Ga old Barney Creek Formation (Brocks et al., 2005; Brocks & Schaeffer, 2008). In these rocks, aromatic carotenoid biomarkers only occur in the bitumen phase and disappear down section due to thermal degradation (Lee & Brocks, 2011).

In the presence of reduced sulfur (a requirement for Chlorobiaceae), aromatic carotenoids such as isorenieratene should be rapidly incorporated into the kerogen (i.e., the non-extractable fraction of organic matter; Durand, 1980) via sulfur cross-linking (e.g., Sinninghe Damsté et al., 1989a; Sinninghe Damsté & de Leeuw, 1990; Kohnen et al., 1991; Hartgers et al., 1994). Even though sulfur bonds (S–S, C–S) are thermally less stable than carbon bonds (C–C; Cottrell, 1954), such early sequestration would promote long-term preservation, as kerogen-bound moieties are typically less affected by thermal degradation and biodegradation as compared to the soluble bitumen fraction (e.g., Brocks et al., 2003b; Marshall et al., 2007; Love et al., 2008). However, mechanisms controlling the incorporation of aromatic carotenoids into kerogens are still poorly constrained. Iron, for instance, may outcompete organic matter as a binding partner for reduced sulfur in anoxic settings, thus hindering organo-sulfurization (e.g., Gransch & Posthuma, 1974; Canfield, 1989; Sinninghe Damsté et al., 1989b; Hartgers et al., 1997).

To evaluate the taphonomic behavior of isorenieratene, we assess its derivatives in bitumens and the corresponding kerogens from two Lower Jurassic oil shale successions (Bächental, Allgäu Formation; Ohmden, Posidonienschiefer Formation). These units have previously been reported to contain abundant isorenieratene derivatives in their bitumens (e.g., Köster et al., 1995; Koopmans et al., 1996a; Schouten et al., 2000; Schwark & Frimmel, 2004). The analytical approach comprises detailed petrographic observations, bulk rock analyses (e.g., organic carbon, sulfur and iron contents, Rock-Eval pyrolysis), two different qualitative pyrolysis techniques (catalytic hydrolysis, HyPy; closed-system hydrous pyrolysis), gas chromatography–mass spectrometry (GC–MS) and gas chromatography–combustion–isotope ratio mass spectrometry (GC–C–IRMS). Our data reveal (i) early cyclization/aromatization and hydrogenation processes, and (ii) iron as major obstacles for the incorporation of aromatic carotenoids into kerogen.

4.2 Material and methods

4.2.1 Geological setting and sample material

We obtained three organic-rich rock samples (Bäch-1382, Bäch-1383, and Bäch-1385; Reinhardt, 2015) from an active quarry, located in the Bächental valley (Karwendel Mountains, Tyrol, Austria) close to Achenkirch (GPS: 047°30'31.01"N; 011°37'45.83"E; Fig. 4.1a, b). In this area, limestones and marls of the Middle Allgäu Formation (or Sachrang Formation *sensu* Jacobshagen, 1965) contain a ca. 15 m thick bituminous intercalation (Bächental oil shale; Reinhardt, 2015; Fig. 4.1c). The Bächental oil shale is of Pliensbachian to Toarcian (Lower Jurassic) age and was probably deposited in a local basin on the former Tethyan shelf (Kodina et al., 1988; Spieler & Brandner, 1989; Neumeister et al., 2015). Today, the oil shale is mined to produce cosmetics and pharmaceuticals (Tiroler Steinölwerke Albrecht GmbH & CoKG).

An additional sample (Ohm-1387) was analyzed from the quarry “Kromer” (Ohmden, Baden-Württemberg, Germany; GPS: 048°39'05.64"N; 009°32'30.27"E; Fig. 4.1a). The outcrop is dominated by bituminous marlstones of the Posidonienschiefer Formation (Posidonia Shale, Lower Toarcian; see Arp & Heyng, 2013) deposited under anoxic conditions in a stratified shelf sub-basin (SW-German Basin) of the Tethys Ocean (e.g., Röhl et al., 2001; Frimmel et al., 2004).

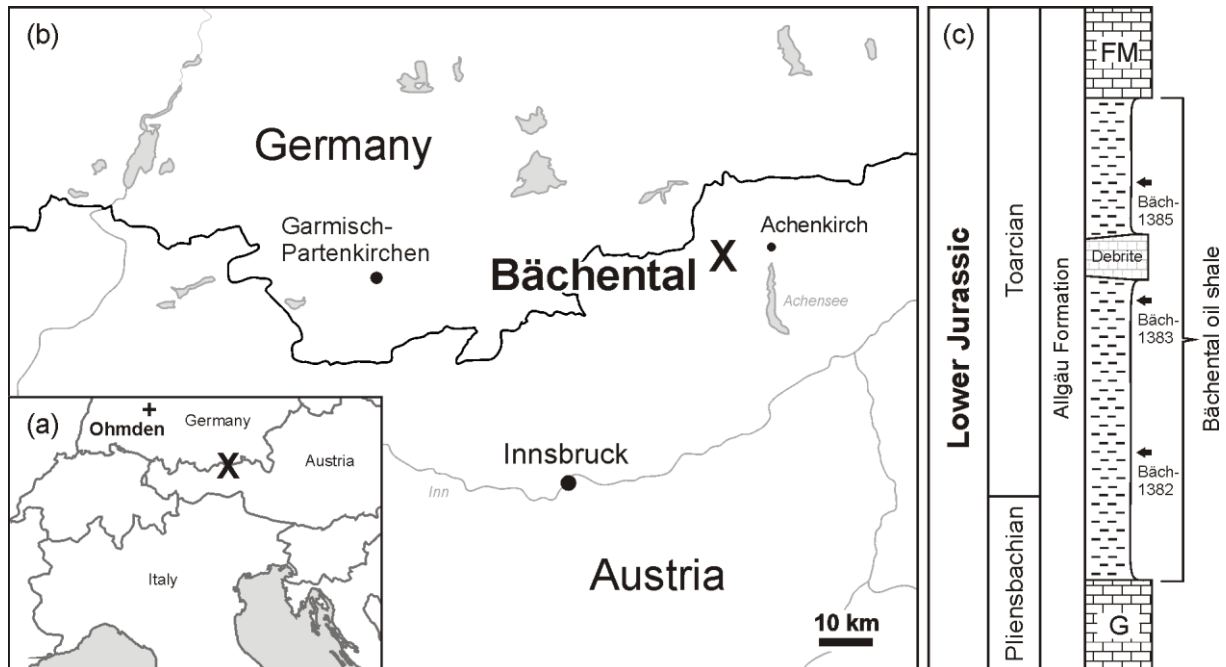


Fig. 4.1: Outcrop locations (a, b; + = Ohmden, X = Bächtental) and stratigraphic overview (c) of the Bächtental oil shale (thickness ca. 15 m) with approximate sample positions (arrows); brick pattern = limestone, dashed pattern = bituminous shale, G = gray nodular limestone, FM = Fleckenmergel.

4.2.2 Petrography and bulk analyses

Petrographic analyses were performed on thin sections (60 μm) using a Zeiss SteREO Discovery.V8 stereomicroscope (using transmitted and reflected light) connected to an AxioCam MRc5 5-megapixel camera. Bulk analyses (total organic carbon, TOC; total inorganic carbon, C_{inorg} ; total sulfur) were executed using a Leco RC612 carbon analyzer and a Hekatech Euro EA elemental analyzer. Iron contents were determined with a Bruker M4 Tornado micro-X-ray fluorescence ($\mu\text{-XRF}$) scanner. X-ray diffraction was conducted on a Philips X'Pert MPD with a PW3050 Goniometer and $\text{CuK}\alpha$ radiation to identify iron-containing mineral phases.

Rock-Eval pyrolysis was executed with a Rock-Eval 6 following the method described by Espitalié et al. (1977). The temperature program started at 300 $^{\circ}\text{C}$ (held for 3 min) with subsequent heating to 650 $^{\circ}\text{C}$ at 25 $^{\circ}\text{C}/\text{min}$. The free hydrocarbons released during the isotherm phase are represented by the S1 peak, the hydrocarbons released during pyrolysis by the S2, and the sum of the released CO_2 up to 400 $^{\circ}\text{C}$ by the S3. The maximum of hydrocarbon generation during pyrolysis is given by T_{max} that also reflects thermal maturity. Measurements of pyrolysis products were conducted with a flame ionization detector (FID), and released CO_2 was analyzed with an infrared cell. Hydrogen index (HI; $\text{S2}/\text{TOC}$), oxygen index (OI; $\text{S3}/\text{TOC}$), and production index (PI; $\text{S1}/(\text{S1}+\text{S2})$) were calculated from the generated data.

4.2.3 Organic geochemical preparation

All materials used for preparation were combusted (500 $^{\circ}\text{C}$ for 3 hr) and/or extensively rinsed with acetone. Additionally, a blank (pre-combusted sea sand) was prepared and analyzed in parallel to keep track of laboratory contamination.

4.2.3.1 Bitumen

Sample surfaces were removed using a rock saw. The remaining blocks (ca. 3 \times 3 \times 5 cm) were crushed and powdered with a Retsch MM 301 pebble mill. Sample powders (5 g) were extracted three times with 50 mL dichloromethane/methanol (DCM/MeOH; 3/1; v/v), 50 mL DCM, and 50 mL *n*-hexane via ultrasonication (20 $^{\circ}\text{C}$,

10 min). Elemental sulfur was removed from the resulting total organic extracts (TOEs) overnight with activated copper. TOEs were concentrated to near dryness using a rotary evaporator and a gentle stream of N₂. The TOEs were subsequently vapor-deposited onto a small amount of dry silica gel (ca. 500 mg) and fractionated into an aliphatic (F1), aromatic (F2), and polar fraction (F3) by column chromatography (1.5 cm internal diameter; 7 g of dry silica gel). F1 was eluted with 27 mL *n*-hexane, F2 with 32 mL *n*-hexane/DCM (1/1; v/v), and F3 with 40 mL DCM/MeOH (1/1; v/v). All fractions were concentrated with a rotary evaporator and N₂.

4.2.3.2 Kerogen

The extraction residues were demineralized following Brocks et al. (2003b). In brief, the extraction residues were first decalcified with concentrated HCl (37 %; 20 °C, 24 hr), and silica phases were subsequently dissolved with HF (48 %; 20 °C, ca. one week including stepwise neutralization with distilled water). The concentrated organic residues were then gently dried (50 °C, 72 hr) and rigorously extracted to remove any residual bituminous materials trapped in the complex molecular structure of the kerogen (Behar & Vandenbroucke, 1988). This step included a double passage of extraction with 30 mL DCM/*n*-hexane (1/1; v/v; 20 °C, 10-min ultrasonication), swelling with pyridine using ultrasonication (80 °C, 20 min), and extraction with 30 mL DCM/MeOH (1/1; v/v; 20°C, 10-min ultrasonication). The organic residues were subsequently extracted with DCM/*n*-hexane and DCM/MeOH until no more compounds were detected via gas chromatography–mass spectrometry (GC–MS). The resulting kerogens were used for pyrolysis experiments (4.2.4 and 4.2.5).

4.2.4 Catalytic hydropyrolysis (HyPy, open system)

Catalytic hydropyrolysis (HyPy; Love et al., 1995) was conducted following existing protocols (Snape et al., 1989; Love et al., 1995, 2005) using a device from Strata Technology Ltd. (Nottingham, UK). Briefly, the system was heated from ambient temperature to 500 °C (held for 30 min) prior to each sample run to eliminate potential contaminants. 50 mg of each kerogen was pyrolyzed in the presence of 5 mg sulfided molybdenum catalyst (ammonium dioxodithiomolybdate, [(NH₄)₂MoO₂S₂]) and 50 mg pre-combusted sea sand. The kerogens were progressively heated (ambient temperature to 250 °C at 50°C/min, 250–500 °C at 8 °C/min) under a constant pressure (15 MPa) and H₂ flow (5 L/min). The generated pyrolysates were trapped on silica gel cooled with dry ice (Meredith et al., 2004). The HyPy pyrolysates were then eluted from the silica gel with DCM and desulfurized overnight with activated copper. Subsequently, all pyrolysates were fractionated into an aliphatic (F1), aromatic (F2), and polar fraction (F3) using column chromatography (see 4.2.3.1).

4.2.5 Hydrous pyrolysis in gold capsules (closed system)

Closed-system hydrous pyrolysis was applied to the Bäch-1383 and Ohm-1387 kerogens to corroborate the HyPy results by investigating the biomarkers released during thermal maturation in the presence of water. Therefore, 31 mg (Bäch-1383) and 29 mg (Ohm-1387) of the kerogens and 200 µL of N₂-purged water were weighed into a gold capsule under an inert N₂ atmosphere, respectively. The thermal maturation was achieved by heating the sealed gold capsules at 30 MPa and 315 °C in a high-pressure reactor resulting in a calculated EASY-R0 maturity of 0.81 % (after Burnham & Sweeney, 1989) for the organic matter. After the pyrolysis experiment, the gold capsules were opened and extracted with DCM. The extracts were then fractionated via column chromatography (see 4.2.3.1).

4.2.6 Gas chromatography–mass spectrometry (GC–MS)

Aliphatic (F1) and aromatic fractions (F2) were analyzed by GC–MS using a Thermo Trace 1310 GC coupled to a Thermo TSQ Quantum Ultra triple quadrupole MS. The GC was equipped with a fused silica capillary column (Phenomenex Zebron ZB-5MS, 30 m length, 250 µm internal diameter, and 0.25 µm film thickness). The carrier gas was He (flow rate 1.5 mL/min). Fractions were injected into a splitless injector using a Thermo TriPlus RSH autosampler and transferred to the GC column at 300 °C. The GC oven temperature was ramped up from 80 °C (1 min) to 310 °C at 5 °C/min (held for 20 min). The MS source operated at 240 °C in electron impact mode at 70 eV. Biomarkers were analyzed in full-scan mode (scan range 50–600 amu) and identified by comparison with published retention times and mass spectra (e.g., Goodwin et al., 1988; Koopmans et al., 1996a; Peters et al., 2005a; Brocks & Schaeffer, 2008). Anthracene-d₁₀ was used as a standard for quantification of isorenieratene derivatives.

4.2.7 Compound-specific stable carbon isotope ($\delta^{13}\text{C}_{\text{V-PDB}}$) analysis

Compound-specific stable carbon isotope ratios ($\delta^{13}\text{C}_{\text{V-PDB}}$) were determined for aliphatic and aromatic fractions from bitumens and HyPy-pyrolysates. Analyses were executed with a Thermo Scientific Trace gas chromatograph (GC) coupled to a Delta Plus isotope ratio mass spectrometer (IRMS). The combustion reactor was equipped with CuO, Ni, and Pt and operated at 940 °C. The columns used in the GC unit were an Agilent DB-5 coupled to an Agilent DB-1 (each with 30 m length, 250 μm internal diameter, and 0.25 μm film thickness). He was used as carrier gas at a flow rate of 1.2 mL/min. Fractions were injected into a splitless injector and transferred to the GC column at 290 °C. The temperature program for analyses of the aliphatic fractions started at 80 °C, followed by heating to 310 °C at 5 °C/min (held for 40 min). For aromatic fractions, the maximum temperature was 325 °C (heating rate 5 °C/min, held for 60 min). Laboratory standards were analyzed to control the reproducibility of measuring conditions and CO_2 gas of known isotopic composition was used for calibration.

4.3 Results

4.3.1 Petrographic observations and bulk geochemical data

The analyzed samples consisted of fresh, unweathered material. The organic matter occurred exclusively in thin layers (Fig. 4.2a–d; Fig. C2a, b). Pyrite (crystal size ca. 7 μm) was observed in all samples in the form of layered aggregates (Fig. 4.2a, c, e; Fig. C2c) or finely dispersed within the rock matrix (Fig. 4.2b, d, f; Fig. C2c, d). Generally, the samples showed virtually no fissures and signs of migrating bituminous substances. Bäch-1382, however, contained few local millimeter-scale extensional structures (Fig. 4.2a, c), but these did not transect the whole sample block (a $3 \times 3 \times 5$ cm block was used for crushing and powdering; see 4.2.3.1).

All samples revealed moderate to high TOC (1.5–8.4 wt.%), sulfur (1.1–4.6 wt.%), and C_{inorg} (3.0–7.5 wt.%, equating to 25.2–62.6 wt.% CaCO_3 ; Tab. 4.1). Bäch-1383 showed the highest TOC (8.4 wt.%) and Ohm-1387 contained the lowest C_{inorg} (3.0 wt.%). Iron contents ranged from 4.0 to 8.7 wt.% (Tab. 4.1), originating from pyrite (FeS_2), ankerite ($\text{Ca}(\text{Mg,Fe,Mn})(\text{CO}_3)_2$), and siderite (FeCO_3) (Fig. C3). S-Fe ratios (S/Fe) varied between 0.13 and 0.95 (Tab. 4.1). Rock-Eval pyrolysis revealed low T_{max} (426–430 °C) and PI (0.03–0.05; Tab. 4.1). HI ranged from 503 to 681 mg HC/g TOC and OI from 6 to 38 mg CO_2 /g TOC.

Tab. 4.1: Bulk rock geochemical data

Sample	TOC ^a [wt.%]	C _{carb} ^b [wt.%]	S ^c [wt.%]	Fe ^d [wt.%]	S/Fe ^e	S1 ^f [mg/g]	S2 ^g [mg/g]	T _{max} ^h [°C]	HI ⁱ [mg HC/g TOC]	OI ^j [mg CO ₂ /g TOC]	PI ^k
Bäch-1382	1.6	5.8	4.6	7.0	0.66	0.42	8.74	428	546	21	0.05
Bäch-1383	8.4	4.4	3.8	4.0	0.95	1.80	57.22	426	681	11	0.03
Bäch-1385	1.5	7.5	1.1	8.7	0.13	0.20	7.55	426	503	38	0.03
Ohm-1387	8.0	3.0	3.6	7.3	0.49	2.06	51.15	430	639	6	0.04

^aTotal organic carbon

^bTotal inorganic carbon

^cTotal sulfur

^dTotal iron

^eTotal sulfur vs. total iron

^fFree hydrocarbons released during the isotherm phase at 300 °C (Rock-Eval)

^gHydrocarbons released during pyrolysis (Rock-Eval)

^hMaximum of hydrocarbon generation during pyrolysis (Rock-Eval)

ⁱHydrogen index (HI = S2 / TOC × 100)

^jOxygen index (OI = S3 / TOC × 100)

^kProduction index (PI = S1 / (S1 + S2))

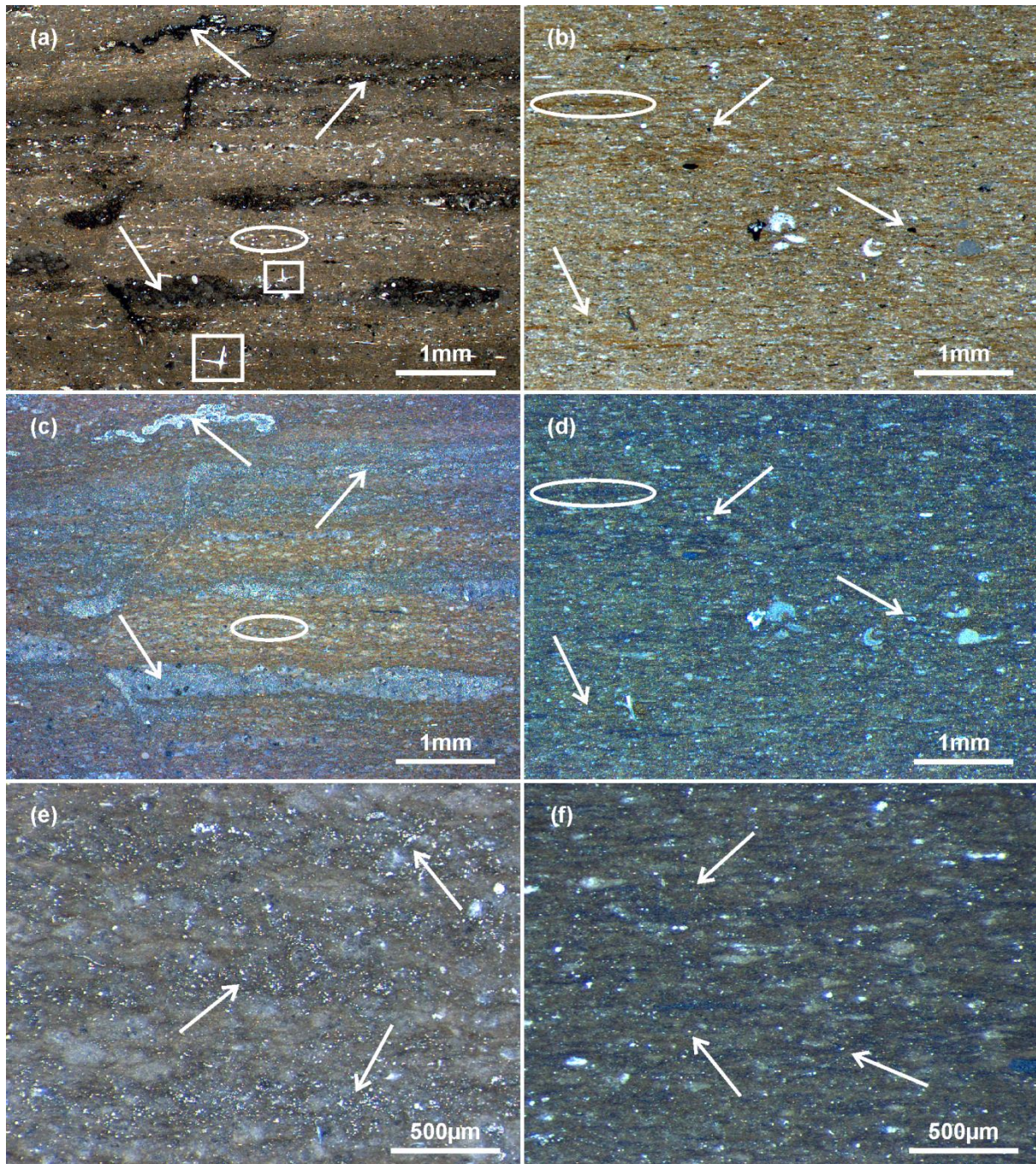


Fig. 4.2: Microscopic thin section images from Bäch-1382 (a, c, e) and Bäch-1383 (b, d, f) under transmitted (a, b) and reflected light (c–f) illustrating the microfacies. Organic matter (indicated by ovals) occurs in thin layers within the facies. Pyrite (indicated by arrows; black under transmitted light, bright colors under reflected light) is highly abundant and occurs either in layered aggregates (a, c, e) or finely dispersed (b, d, f). Few hexactinellid sponge spicules were observed in Bäch-1382 (squares in a). Please note that the rock matrix shows no major structural defects or indications for fluid migration, except millimeter scale extensional features in Bäch-1382 (a, c) that do, however, not transect the complete sample block (3 × 3 × 5 cm blocks were used).

4.3.2 Biomarkers from bitumens and kerogens

4.3.2.1 Aliphatic hydrocarbons

n-Alkanes in all bitumens and kerogens ranged from *n*-C₁₁ to *n*-C₄₀, with maxima between *n*-C₁₅ and *n*-C₁₇ (Fig. 4.3). Concentrations of *n*-alkanes were higher in the kerogen pyrolysates (e.g., *n*-C₁₇; Tab. C1). All kerogen pyrolysates after HyPy also contained *n*-alkenes in corresponding distributions (Fig. 4.3). Carbon preference indices (CPI; Bray & Evans, 1961) varied from 0.91 to 1.28 in bitumens and from 0.97 to 1.04 in kerogens (Tab.

4.2). All bitumens and kerogens furthermore contained the acyclic isoprenoids farnesane (Far), norpristane (Nor), pristane (Pr), and phytane (Ph) (Fig. 4.3).

4-Desmethylsteranes in all bitumens and kerogens ranged from C₂₇ to C₂₉ and included a variety of isomers. The most prominent compounds were 5 α ,14 α ,17 α (H)-cholestane (C₂₇) 20R and 5 α ,14 α ,17 α (H)-stigmastane (C₂₉) 20R (Fig. 4.3). Calculated 5 α ,14 α ,17 α (H)-C₂₉ 20S/(S+R) ratios ranged from 0.16 to 0.27 in bitumens and from 0.10 to 0.17 in kerogens (Tab. 4.2). All bitumens and kerogens also contained varying amounts of 4-methylsteranes (e.g., the 4 α -methyl- 5 α (H)-cholestane (C₂₈); Fig. 4.3; Tab. C1), including the 4 α ,23,24-trimethylcholestanes (dinosteranes).

C₂₇ to C₃₅ hopanes were observed in all bitumens and kerogens, and were dominated by the 17 α ,21 β (H)-series (Fig. 4.3). The most prominent compounds were 17 α ,21 β (H)-30-norhopane (C₂₉), 17 α ,21 β (H)-hopane (C₃₀), and C₃₁ to C₃₅ homohopanes (S+R isomers). The 17 α ,21 β (H)-C₃₁ 22S/(S+R) ratios ranged from 0.50 to 0.57 in bitumens and from 0.25 to 0.37 in kerogens (Tab. 4.2). The 18 α -22,29,30-trisnorhopane (Ts) to 17 α -22,29,30-trisnorhopane (Tm) ratio (Ts/(Ts+Tm)) showed values between 0.27 and 0.34 in bitumens and between 0.20 and 0.23 in kerogens. 17 β ,21 α (H)-Hopanes (moretanes), namely the 17 β ,21 α (H)-30-norhopane (C₂₉; normoretane) and the 17 β ,21 α (H)-hopane (C₃₀; moretane), were also present and showed, with one exception (Bäch-1385), higher concentrations in kerogens (Tab. C1). Furthermore, 28,30-bisnorhopane was identified in all samples, along with additional terpenoids, including cheilanthanes and gammacerane (Gam).

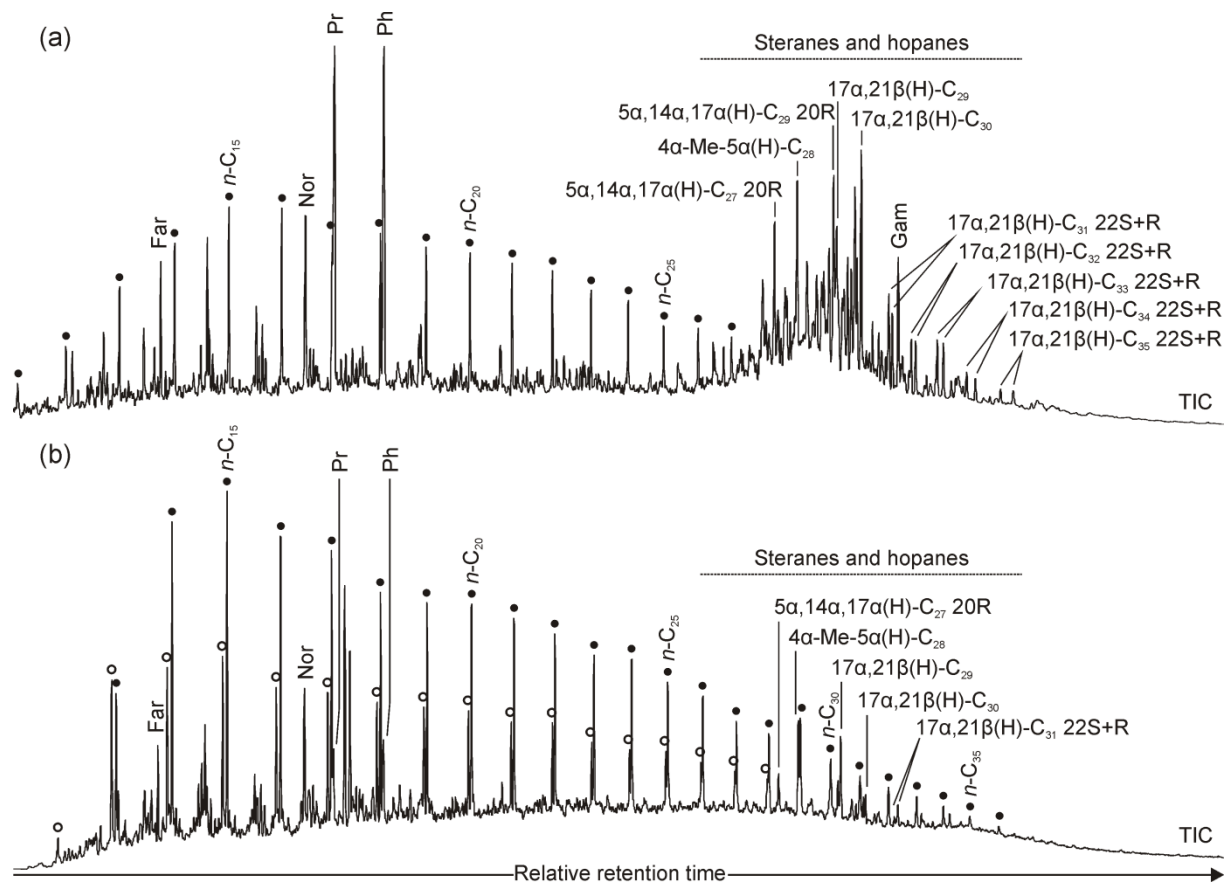


Fig. 4.3: Total ion chromatograms (TICs) of the aliphatic hydrocarbons (F1) in the bitumen (a) and kerogen (b, HyPy) from Bäch-1383. Dots mark *n*-alkanes, circles denote *n*-alkenes. Steranes are represented by 5 α ,14 α ,17 α (H)-C₂₇ 20R, 4 α -Me-5 α (H)-C₂₈ and 5 α ,14 α ,17 α (H)-C₂₉ 20R, and hopanes by 17 α ,21 β (H)-C₂₉/C₃₀ plus 17 α ,21 β (H) 22S+R isomers. Far = farnesane, Nor = norpristane, Pr = pristane, Ph = phytane, Gam = gammacerane.

4.3.2.2 Aromatic hydrocarbons

All aromatic fractions from bitumens and kerogens contained a variety of non-isoprenoidal aromatic hydrocarbons, including (methyl-) naphthalenes, (methyl-) phenanthrenes, and (methyl-) dibenzothiophenes (Fig. 4.4). The dibenzothiophene-phenanthrene ratio (DBT/Phe; Tab. 4.2) varied between 0.07 and 0.32 in bitumens and between 0.32 and 0.41 in kerogens. The methylphenanthrene index (MPI-1; Radke & Welte, 1983) ranged from 0.51 to

0.77 in bitumens and from 0.73 to 1.03 in kerogens (Tab. 4.2). Computed vitrinite reflectance (R_c ; Boreham, Crick, & Powell, 1988) varied between 0.58 and 0.76 in bitumens and 0.73 and 0.94 in kerogens.

The bitumens of all analyzed samples revealed isorenieratane (**II**), with highest amounts in Bäch-1383 (17.1 $\mu\text{g/g}$ TOC; Fig. 4.4; Tab. 4.3). In case of the kerogens, however, only the pyrolysates (both, HyPy and closed-system hydrous pyrolysis in gold capsules) of sample Bäch-1383 showed trace amounts of isorenieratane (0.6 and 0.5 $\mu\text{g/g}$ TOC, respectively; Fig. 4.5; Tab. 4.3). All bitumens and corresponding kerogens contained a pseudohomologous series of 2,3,6-trimethyl aryl isoprenoids (C_{10} to C_{25} ; Fig. 4.5).

A variety of medium to high molecular weight isorenieratene derivatives was identified exclusively in the bitumens, including C_{40} moieties with up to three additional aromatic rings (**III** to **XII**), C_{33} compounds with up to one additional aromatic ring (**XIV** and **XV**), and C_{32} moieties with either one (**XVI** and **XVII**) or two additional aromatic rings (**XVIII** and **XIX**). Aryl isoprenoids with either one or three additional aromatic rings (referred to as short-chain compounds; **XX** to **XXII**), a pseudohomologous series of 2,3,5',6'-tetramethyl-2'-alkylbiphenyls (C_{19} to C_{22} ; Fig. 4.6), and traces of three sulfur-containing diagenetic products of isorenieratene (**XXIII** to **XXV**; Fig. C4) were also observed. Bitumens additionally contained the aromatic carotenoid biomarkers β -isorenieratane (**XXVI**) and chlorobactane (**XXVII**). In Bäch-1383 **III**, **XX** and **XXI** were also found in the aromatic fractions from kerogen pyrolysates (both, HyPy and closed-system hydrous pyrolysis in gold capsules; Fig. 4.5).

4.3.2.3 Compound-specific stable carbon isotopes

$\delta^{13}\text{C}$ values of *n*-alkanes varied roughly between -31 and -37‰ in all samples (Figs. C5, C6; Tab. C2). Steranes and hopanes showed more enriched signatures, ranging between -25 and -37‰ . Phenanthrene and methyl phenanthrenes revealed $\delta^{13}\text{C}$ values around -32‰ in bitumens and kerogens. Isorenieratane (**II**) and a C_{40} isorenieratene derivative (**III**) from bitumens showed strong ^{13}C enrichments (-17.4 to -20.3‰ ; Tab. C2). Most compounds from bitumens were slightly ^{13}C depleted as compared to kerogens (Figs. C5, C6; Tab. C2). Standard deviations of all measurements were below 1.0‰ (see Tab. C2).

Tab. 4.2: Biomarker indices of bitumens (Bit) and kerogens (Ker)

Sample		CPI ^a	DBT/ Phe ^b	C_{29} 20S/ (S+R) ^c	C_{31} 22S/ (S+R) ^d	Ts/ (Ts+Tm) ^e	MPI-1 ^f	P/MP ^g	R_c ^h
Bäch-1382	Bit	0.91	0.32	0.22	0.54	0.33	0.77	0.59	0.76
	Ker (HyPy)	1.01	0.32	0.13	0.28	0.22	1.03	0.49	0.94
Bäch-1383	Bit	1.00	0.15	0.27	0.56	0.27	0.74	0.63	0.74
	Ker (HyPy)	1.02	0.39	0.17	0.37	0.20	0.95	0.42	0.88
Bäch-1385	Bit	1.28	0.15	0.16	0.50	0.34	0.69	0.71	0.71
	Ker (HyPy)	1.04	0.41	0.10	0.25	0.23	0.99	0.53	0.92
Ohm-1387	Bitumen	1.01	0.07	0.21	0.57	0.28	0.51	0.57	0.58
	Ker (HyPy)	0.97	0.33	0.14	0.33	0.20	0.73	0.71	0.73

^aCarbon preference index (Bray & Evans, 1961)

^bDibenzothiophene(DBT)-phenanthrene(Phe) ratio

^c $5\alpha,14\alpha,17\alpha(\text{H})\text{-}C_{29}$ 20S/(S+R)

^d $17\alpha,21\beta(\text{H})\text{-}C_{31}$ 22S/(S+R)

^e $18\alpha\text{-}22,29,30\text{-trisnorhopane}$ (Ts), $17\alpha\text{-}22,29,30\text{-trisorhopane}$ (Tm)

^fMethylphenanthrene index = $1.5 \times (2\text{-MP} + 3\text{-MP}) / (\text{Phe} + 1\text{-MP} + 9\text{MP})$; Radke & Welte, 1983

^gPhenanthrene(Phe)-methylphenanthrene(MP) ratio = $\text{Phe} / (3\text{-MP} + 2\text{-MP} + 9\text{-MP} + 1\text{-MP})$

^hComputed vitrinite reflectance = $0.7 \times \text{MPI-1} + 0.22$ (Boreham et al., 1988; if Phe/MP < 1 (Brocks et al., 2003a))

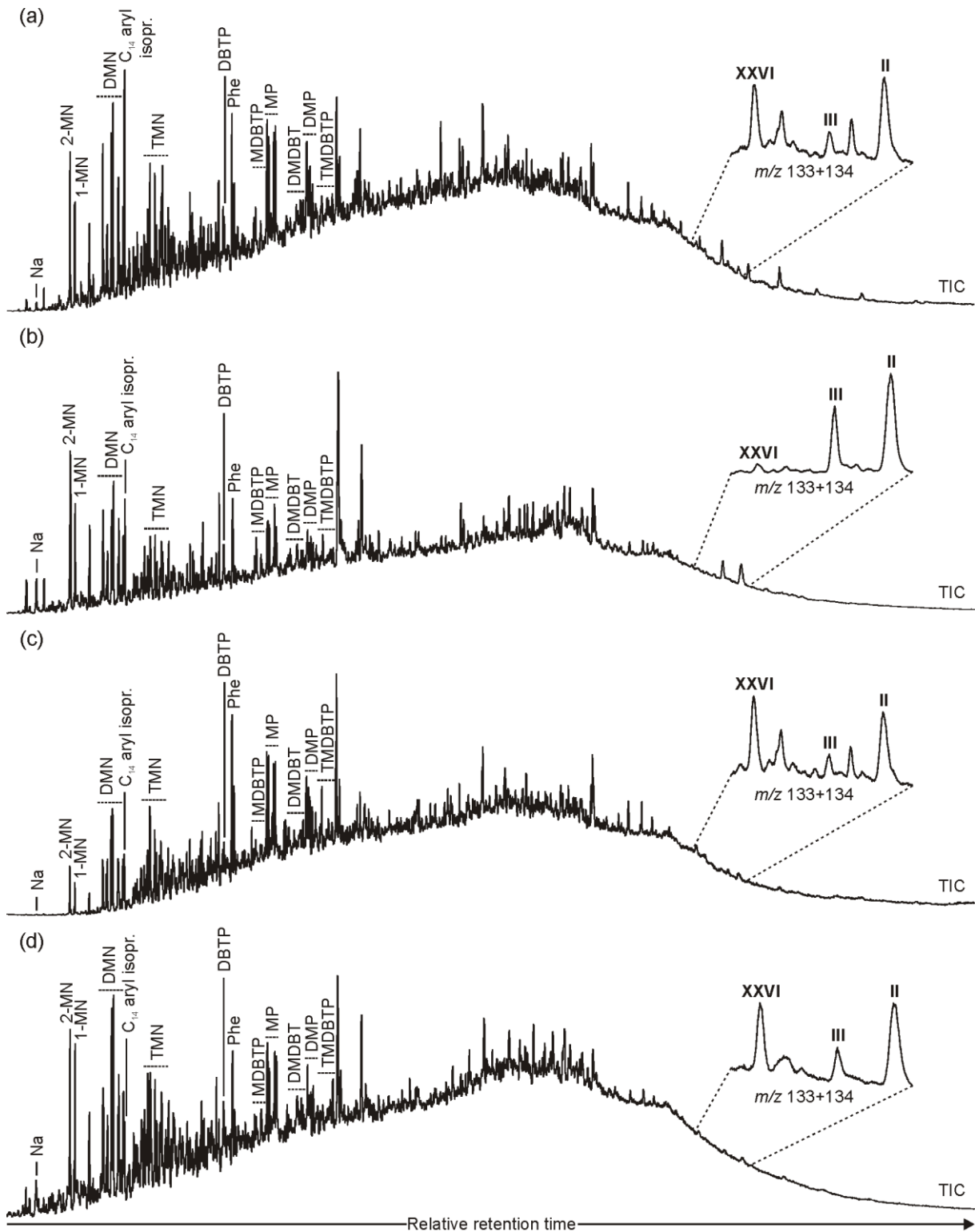


Fig. 4.4: Total ion chromatograms (TICs) of the aromatic hydrocarbons (F2) in the bitumens from Bäch-1382 (a), Bäch-1383 (b), Bäch-1385 (c), and Ohm-1387 (d). Enlargements show partial ion chromatograms (m/z 133 + 134), illustrating the distribution of key isorenieratene derivatives (**II** = isorenieratane, **III** = C_{40} isorenieratene derivative with one additional aromatic ring, **XXVI** = β -isorenieratane). Na = naphthalene, MN = methylnaphthalene, DMN = dimethylnaphthalenes, TMN = trimethylnaphthalenes, Phe = phenanthrene, MP = methylphenanthrenes, DMP = dimethylphenanthrenes, DBTP = dibenzothiophene, MDBTP = methyldibenzothiophenes, DMDBTP = dimethyldibenzothiophenes, TMDDBTP = trimethyldibenzothiophenes.

4.4 Discussion

4.4.1 Syngeneity and maturity of the organic matter

Molecular inventories of sedimentary rocks are potentially modified by secondary processes such as migration. However, the analyzed samples reveal no major fabric defects indicating petroleum migration (Fig. 4.2) and this is well supported by the Rock-Eval data (PI correspond to T_{\max} ; Tab. 4.1). Syngeneity can further be tested by comparing the motile bitumen with the corresponding immotile kerogen (e.g., Brocks et al., 2003b; Love et al., 2008). Indeed, bitumens and corresponding kerogens (type I–II; see HI and OI, Tab. 4.1; Tissot & Welte, 1984) from the Bächtental oil shale and Posidonia Shale exhibit similar compounds and calculated biomarker maturity indices (Fig. 4.3; Tab. 4.2). Aliphatic fractions from bitumens and kerogens of all samples contain C_{27} – C_{29} 4-desmethylsteranes, dinosteranes, $17\alpha,21\beta(H)$ -30-norhopane (C_{29}), $17\alpha,21\beta(H)$ -hopane (C_{30}), C_{31} to C_{35} homohopanes, moretanes, and gammacerane in similar patterns. One of the samples (Bäch-1383) furthermore reveals isorenieratane (II) and a C_{40} isorenieratene derivative (III) in the aromatic fractions from bitumen and kerogen (Tab. 4.3; Fig. 4.5). In addition, $\delta^{13}C$ values of biomarkers in bitumens vs. kerogens show a typical offset between 1 and 4‰, with some outliers being probably caused by coelutions (Figs. C5, C6; Tab. C2). This provides further evidence for the syngeneity of the molecular inventories (Tissot & Welte, 1984).

Thermal overprint may blur primary biomarker distribution patterns. In the Bächtental and Ohmden bitumens, C_{29} 20S/(S+R), C_{31} 22S/(S+R) and Ts/(Ts+Tm) all suggest an early oil window maturity (Tab. 4.2; Peters et al., 2005b and references therein). These indices are generally lower in the kerogen pyrolysates, which is in line with the often observed higher thermal stability of macromolecular-bound molecules (e.g., Love et al., 1995, 2008; Bishop et al., 1998) and further supports that the bitumens and the kerogens are syngenetic. A low thermal maturity is furthermore supported by the presence of moretanes, which are unstable under elevated thermal conditions (Peters et al., 2005b). MPI-1 and R_c of the bitumens and corresponding kerogens indicate a somewhat higher maturity (early to peak oil; Tab. 4.2; Killips & Killips, 2005), except Ohm-1387. However, elevated MPI-1 and R_c values are a well-known phenomenon for marine, hydrogen-rich organic matter (Radke et al., 1986; Boreham et al., 1988), which may lead to overestimations of the maturity level.

With $PI < 0.06$ and $T_{\max} < 431^\circ C$ (Tab. 4.1), Rock-Eval data clearly indicate immature organic matter (below oil window; Peters & Cassa, 1994). Furthermore, most biomarkers other than isorenieratene derivatives are more abundant in the kerogens than in the corresponding bitumens (Tab. C1). We therefore suggest a maturity below oil window for the organic matter from our samples. This is in good accordance with results obtained for other materials from Bächtental (Neumeister et al., 2015; their $PI < 0.1$ and $T_{\max} < 428^\circ C$) and the Posidonia Shale from South Germany (Littke et al., 1991; Schwark & Frimmel, 2004).

Tab. 4.3: Concentrations of isorenieratane in bitumens (Bit) and kerogens (Ker)

Sample	[$\mu g/g$ sample]	[$\mu g/g$ TOC]
Bäch-1382 Bit	<0.1	1.7
Ker (HyPy)	-	-
Bäch-1383 Bit	1.4	17.1
Ker (HyPy)	<0.1	0.6
Ker (gold capsule)	<0.1	0.5
Bäch-1385 Bit	<0.1	1.1
Ker (HyPy)	-	-
Ohm-1387 Bit	0.2	2.4
Ker (HyPy)	-	-
Ker (gold capsule)	-	-

Hyphen (-) = not

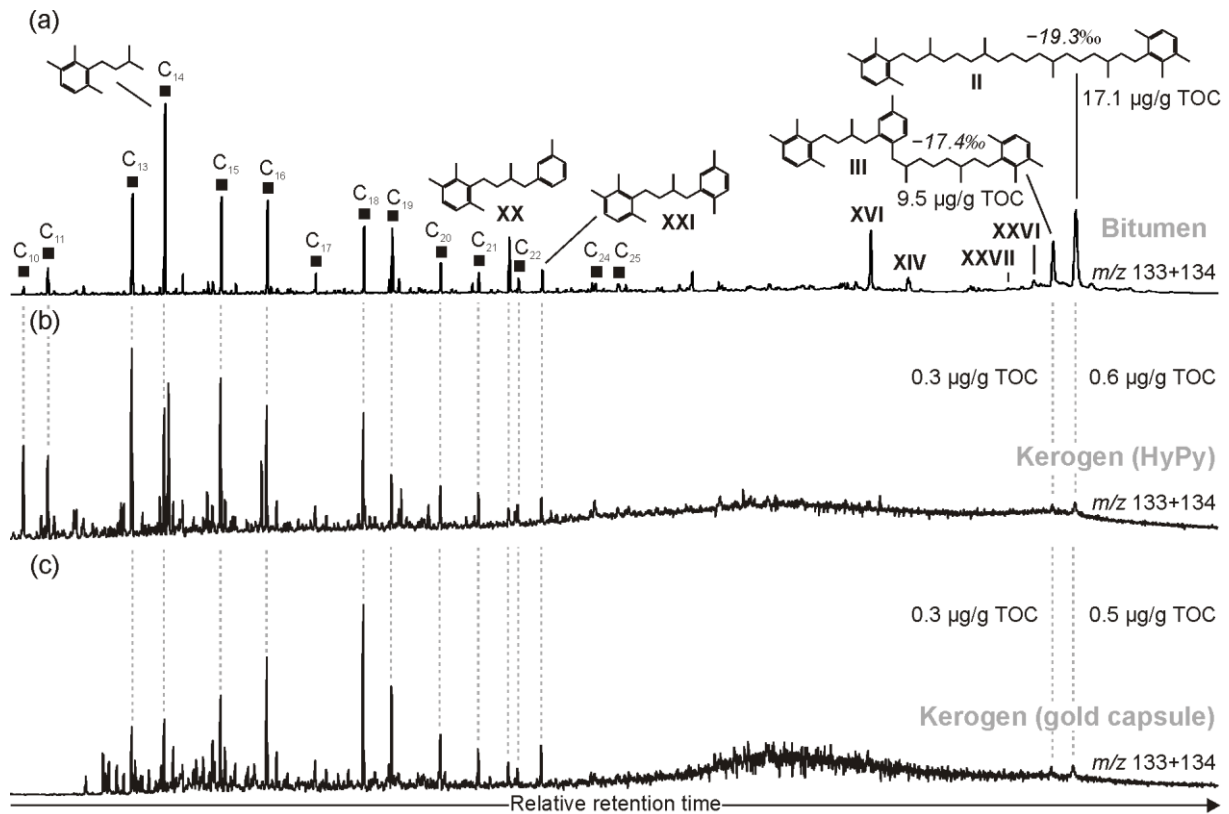


Fig. 4.5: Partial ion chromatograms (m/z 133 + 134) of the aromatic hydrocarbons (F2) in the bitumen (a), kerogen (b, HyPy) and kerogen (c, closed system hydrous pyrolysis in gold capsules) from Bäch-1383. Squares mark a pseudohomologous series of 2,3,6-trimethyl aryl isoprenoids. **II** = isorenieratane, **III** = C₄₀ isorenieratene derivative with one additional aromatic ring, **XVI** = C₃₂ isorenieratene derivative with one additional aromatic ring, **XX** and **XXI** = short-chain isorenieratene derivatives with one additional aromatic ring. Note the $\delta^{13}\text{C}$ values of -19.3‰ for **II** and -17.4‰ for **III**, evidencing Chlorobiaceae as source.

4.4.2 Bächental kerogens—archives for isorenieratene derivatives?

In anoxic environments, aromatic carotenoids can react with sulfur via the available double bonds in the isoprenoid chains (see e.g., **I** in Fig. C1). Consequently, these molecules should be efficiently sequestered in macromolecules by intermolecular sulfur cross-linkages (e.g., Sinnighe Damsté et al., 1989a; Sinnighe Damsté & de Leeuw, 1990; Kohnen et al., 1991), thus enhancing their preservation potential over geological timescales. Indeed, isorenieratane and further diaromatic carotenoids from Upper Devonian organic-rich carbonates appear to be preserved rather within the kerogen than in the free bitumen (Duvernay Formation, Western Canada Basin and Williston Basin; Hartgers et al., 1994). The Bächental basin was also periodically anoxic (Köster et al., 1995; Neumeister et al., 2015, 2016) and thus expectedly favorable for the production and preservation of aromatic carotenoids via sulfur bonds in kerogen. However, kerogen pyrolysis yields only very low amounts of isorenieratene derivatives (Fig. 4.5) and sulfurized compounds are virtually absent (except small amounts of **XXIII** to **XXV** in bitumens; see 3.2.2 and Fig. C4).

Several aspects support the idea that this discrepancy is an indigenous signal, and not caused by secondary effects:

- The syngeneity of bitumens and kerogens (see 4.1) implies that isorenieratene derivatives have not been introduced by migrating petroleum fluids.
- Under laboratory conditions, expulsion of isorenieratane from the kerogen may occur below 200°C (Koopmans et al., 1996a, b). Consequently, thermal expulsion may explain the occurrence of isorenieratene derivatives exclusively in the bitumen fraction. However, the very low thermal maturity of our samples (see also 4.1) renders it unlikely that this process had already transferred, more or less completely, the isorenieratene derivatives from the kerogen into the bitumen.

- A selective destruction of isorenieratene derivatives during hydropyrolysis appears unlikely, as HyPy is a relatively gentle pyrolysis approach (e.g., Love et al., 1995, 1997; Bishop et al., 1998). Furthermore, the HyPy results were independently confirmed by (similarly mild) closed-system hydrous pyrolysis (Fig. 4.5).

The absence of isorenieratene derivatives in kerogen pyrolysates from Bächental is therefore regarded as an authentic signal, likely resulting from an ineffective sequestration into the kerogen during early diagenesis. Interestingly, the same observation was made for the reference sample from the Posidonienschiefer Formation (Ohm-1387; Tab. 4.3), suggesting that the scarcity in Bächental kerogens is not a local phenomenon.

4.4.3 Implications for the diagenetic fate of isorenieratene

Sulfur-containing isorenieratene derivatives are scarce in the studied environments. Given that sulfurization is typically an early process, as it has been shown for example for recent Black Sea sediments (Sinninghe Damsté et al., 1993; Wakeham et al., 1995), it may be argued that other early diagenetic effects might have competed with this reaction mechanism.

Our samples contain various C₄₀ intermediates on the proposed diagenetic path from isorenieratene (**I**) to the fully aromatized tetracyclic end product (**XIII**, not detected in our samples). These compounds (**III** to **XII**) originate from cyclization and subsequent aromatization of the conjugated double-bond system in the isoprenoid chain (Koopmans et al., 1996a). In addition, the samples reveal C₃₃ and C₃₂ compounds that probably result from expulsion reactions (i.e., shortening of the isoprenoid chain by expulsion of *m*-xylene or toluene; e.g., Byers & Erdman, 1983; Koopmans et al., 1996a). Like the C₄₀ derivatives, these compounds can undergo aromatization, and this is well documented in the samples analyzed (**XV** to **XIX**). Consequently, cyclization/aromatization reactions must have played a major role during isorenieratene diagenesis in these settings.

Moreover, the presence of the fully reduced C₄₀ carotenoids isorenieratane (**II**), β-isorenieratane (**XXVI**), and chlorobactane (**XXVII**) in all bitumens testifies that the carotenoid precursors additionally underwent an effective hydrogenation. In anoxic systems, such a reduction of double bonds can be induced abiotically via reduced sulfur species (Hebting et al., 2006; Brocks & Banfield, 2009), and probably also biologically via microbial degradation. The abiotic process has been reported to occur early during diagenesis, even in the water column (Hebting et al., 2006).

All these processes (sulfurization, cyclization/aromatization, and hydrogenation) depend on, and compete for, available double bonds in the isoprenoid chains (e.g., Hartgers et al., 1994; Koopmans et al., 1996a; van Duin & Sinninghe Damsté, 2003). Accordingly, cyclization/aromatization and hydrogenation must have been important in the ancient depositional settings, whereas sulfurization has obviously been minimized. Simultaneously, these factors plausibly explain the sparse findings of isorenieratene derivatives in the kerogens.

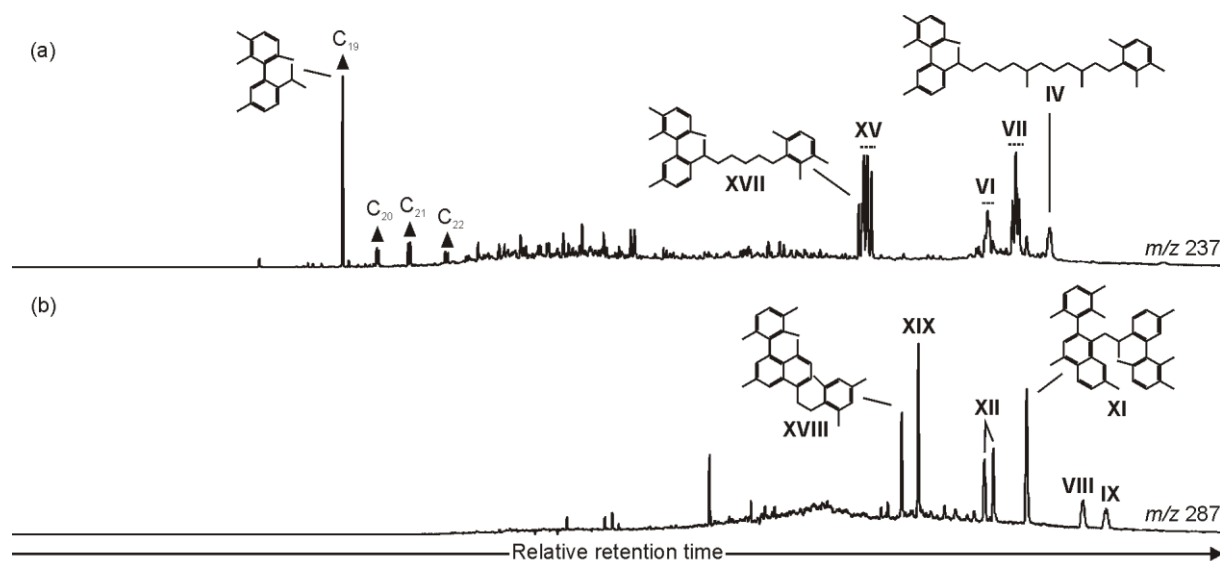


Fig. 4.6: Partial ion chromatograms (a = m/z 237; b = m/z 287) of the aromatic hydrocarbons (F2) in the bitumen from Bäch-1383. Triangles represent 2,3,5,6-tetramethyl-2'-alkylbiphenyls; **IV**, **VI**, **VII**, **VIII**, **IX**, **XI** and **XII** = C₄₀ isorenieratene derivatives with up to three additional aromatic rings; **XV** = C₃₃ isorenieratene derivative with one additional aromatic ring; **XVII**, **XVIII** and **XIX** = C₃₂ isorenieratene derivatives with either one or two additional aromatic rings.

4.4.4 A competition for sulfur: Iron vs. organics

In all samples studied, pyrite coexists with ankerite and/or siderite (Fig. C3). These iron carbonates are unstable in the presence of free H₂S (see Eh-pH diagram for oxides, carbonates and sulfides in Maynard (1983)), proving that free H₂S was temporarily limited in the microenvironment. In anoxic systems, pyrite formation may effectively buffer sulfide concentrations to low levels, even in sediments where sulfate reduction is active (Canfield, 1989; Hartgers et al., 1997). As a consequence, sulfur cross-linking of organic substances can be hampered. Only high sulfide concentrations may overcome this effect (Farrimond et al., 2003), and an S/Fe of 1.15 (stoichiometric pyrite) is considered as the threshold for iron limitation during pyrite formation (Dean & Arthur, 1989). However, S/Fe in our samples is always lower (Tab. 4.1; see also Neumeister et al., 2015, 2016 for Bächental), implying that excess iron may have outcompeted organic matter in the reaction with reduced sulfur.

Taking into account the presence of abundant pyrite aggregates, low DBT/Phe ratios (Tab. 4.2; cf., Hughes et al., 1995) and the rare findings of sulfurized biomarkers (see 3.2.2 and 4.2), sulfide trapping by iron seems a critical factor for the non-incorporation of isorenieratene derivatives into the kerogens. This model might be transferred to the Proterozoic ocean, where anoxic and ferruginous conditions may have coexisted (e.g., Planavsky et al., 2011; Poulton & Canfield, 2011). It should also be noted that reactive iron may interact with organic matter by forming complexes, thus enhancing the preservation potential of the organic compounds (Lalonde et al., 2012; Barber et al., 2017).

4.4.5 The fate of isorenieratene in the Bächental basin: Controlled by iron?

The Bächental oil shales were deposited under temporarily anoxic conditions (Köster et al., 1995; Neumeister et al., 2015, 2016) prevailing in a local basin on the Tethys shelf (Spieler & Brandner, 1989). The findings of ¹³C enriched isorenieratane (about 15‰ compared to algal biomass, Köster et al., 1995; this study, Tab. C2) confirm brown-colored green sulfur bacteria as the biological source and also imply photic zone anoxia.

We suggest that (i) at the oxic-anoxic boundary, H₂S was metabolized by brown-colored green sulfur bacteria as a hydrogen donor in anoxygenic photosynthesis. This resulted in a local removal of reduced sulfur which in turn gave way to cyclization/aromatization reactions of isorenieratene. (ii) Subsequently, during settling, at the sediment-water interface, or within the surface sediment, hydrogenation may have occurred (cf., Hebling et al., 2006). (iii) Eventually, precipitation of the remaining sulfide with sedimentary iron (pyrite formation) largely inhibited diagenetic sulfurization of the remaining functionalized isorenieratene derivatives, even though sulfate reduction was active. According to this model, the incorporation of aromatic carotenoids into kerogens was effectively suppressed. This scenario might also apply to the Ohmden setting, but to confirm this, more data are required.

The observations made for the Bächental and Ohmden kerogens provide fundamental implications for the geological record of carotenoid biomarkers. A rapid sequestration of the polyunsaturated precursors into the macromolecular network is considered crucial for preserving these important biomarkers over large geological timescales. Our study demonstrates that such early kerogen incorporation may not always be the case, particularly as controlling processes and environmental parameters may change rapidly in space and time (e.g., Repeta, 1993; Sinninghe Damsté et al., 1993; Del Don et al., 2001). The proposed pathway, including early cyclization/aromatization, hydrogenation, and sulfide buffering via sedimentary iron, may represent an alternative mechanism enabling the preservation of highly functionalized aromatic carotenoids without kerogen sequestration. Investigations of additional settings rich in carotenoids, including also high-sulfur-, low-iron- environments, would be of great interest to test this hypothesis.

4.5 Conclusions

Isorenieratene derivatives are highly abundant in bitumens from organic-rich shales of the temporarily anoxic Bächental basin (Lower Jurassic), but are virtually absent in the corresponding kerogens. Analysis of an additional sample from the Toarcian Posidonia Shale revealed the same result. Given the syngeneity and low maturity of the organic matter, it is likely that these compounds were never efficiently incorporated into the kerogen. We propose that the taphonomic fate of isorenieratene is largely controlled by (i) fast cyclization/aromatization, (ii) hydrogenation processes, and (iii) sulfide removal via anoxygenic photosynthesis and precipitation with sedimentary iron. From our results, it can be inferred that in iron-rich environments (e.g., the Proterozoic ocean)

aromatic carotenoids might preferentially be preserved in the bitumen phase, although iron is not the sole controlling factor.

Acknowledgments

We kindly thank J. J. Brocks for editorial handling and two anonymous reviewers for helpful comments. We also would like to thank G. Arp, W. Dröse, J. Dyckmans, A. Hackmann, V. Karius, A. Reimer, B. Röring, G. Scheeder, and T. Weger for scientific and technical support. We are indebted to Tiroler Steinölwerke Albrecht GmbH & CoKG for providing access to the Bächental oil shales. This work was financially supported by the International Max Planck Research School for Solar System Science at the University of Göttingen, the Deutsche Forschungsgemeinschaft (grants Th 713/13-1; Du 1450/3-1, DFG Priority Program 1833 “Building a Habitable Earth”), the Göttingen Academy of Sciences and Humanities, and the Courant Research Centre of the University of Göttingen (DFG, German Excellence Program). This is publication number 6 of the Early Life Research Group (Department of Geobiology, University of Göttingen; Göttingen Academy of Sciences and Humanities).

References

- Arp, G., & Heyng, A. M. (2013). Jurassic fossil Lagerstätten of Southern Germany. In J. Reitner & M. Reich (Eds.), *Palaeobiology and geobiology of fossil lagerstätten through earth history. A joint conference of the “paläontologische gesellschaft” and the “palaeontological society of China”* (pp. 57). Göttingen: Geowissenschaftliches Museum.
- Barber, A., Brandes, J., Leri, A., Lalonde, K., Balind, K., Wirick, S., Wang, J., & Gélinas, Y. (2017). Preservation of organic matter in marine sediments by inner-sphere interactions with reactive iron. *Sci. Rep.*, *7*. <https://doi.org/10.1038/s41598-017-00494-0>
- Behar, F., & Vandenbroucke, M. (1988). Characterization and quantification of saturates trapped inside kerogen: implications for pyrolysate composition. *Org. Geochem.*, *13*, 927–938. [https://doi.org/10.1016/0146-6380\(88\)90246-X](https://doi.org/10.1016/0146-6380(88)90246-X)
- Bishop, A. N., Love, G. D., McAulay, A. D., Snape, C. E., & Farrimond, P. (1998). Release of kerogen-bound hopanoids by hydrolysis. *Org. Geochem.*, *29*, 989–1001. [https://doi.org/10.1016/S0146-6380\(98\)00140-5](https://doi.org/10.1016/S0146-6380(98)00140-5)
- Blumenberg, M., Heunisch, C., Lückge, A., Scheeder, G., & Wiese, F. (2016). Photic zone euxinia in the central Rhaetian Sea prior the Triassic-Jurassic boundary. *Palaeogeogr. Palaeoclimatol. Palaeoecol.*, *461*, 55–64. <https://doi.org/10.1016/j.palaeo.2016.08.007>
- Boreham, C. J., Crick, I. H., & Powell, T. G. (1988). Alternative calibration of the Methylphenanthrene Index against vitrinite reflectance: Application to maturity measurements on oils and sediments. *Org. Geochem.*, *12*, 289–294. [https://doi.org/10.1016/0146-6380\(88\)90266-5](https://doi.org/10.1016/0146-6380(88)90266-5)
- Bray, E. E., & Evans, E. D. (1961). Distribution of *n*-paraffins as a clue to recognition of source beds. *Geochim. Cosmochim. Acta*, *22*, 2–15. [https://doi.org/10.1016/0016-7037\(61\)90069-2](https://doi.org/10.1016/0016-7037(61)90069-2)
- Brocks, J. J., & Banfield, J. (2009). Unravelling ancient microbial history with community proteogenomics and lipid geochemistry. *Nat. Rev. Microbiol.*, *7*, 601–609. <https://doi.org/10.1038/nrmicro2167>
- Brocks, J. J., & Schaeffer, P. (2008). Okenane, a biomarker for purple sulfur bacteria (Chromatiaceae), and other new carotenoid derivatives from the 1640 Ma Barney Creek Formation. *Geochim. Cosmochim. Acta*, *72*, 1396–1414. <https://doi.org/10.1016/j.gca.2007.12.006>
- Brocks, J. J., Buick, R., Logan, G. A., & Summons, R. E. (2003a). Composition and syngeneity of molecular fossils from the 2.78 to 2.45 billion-year-old Mount Bruce Supergroup, Pilbara Craton, Western Australia. *Geochim. Cosmochim. Acta*, *67*, 4289–4319. [https://doi.org/10.1016/S0016-7037\(03\)00208-4](https://doi.org/10.1016/S0016-7037(03)00208-4)
- Brocks, J. J., Love, G. D., Snape, C. E., Logan, G. A., Summons, R. E., & Buick, R. (2003b). Release of bound aromatic hydrocarbons from late Archean and Mesoproterozoic kerogens via hydrolysis. *Geochim. Cosmochim. Acta*, *67*, 1521–1530. [https://doi.org/10.1016/S0016-7037\(02\)01302-9](https://doi.org/10.1016/S0016-7037(02)01302-9)
- Brocks, J. J., Love, G. D., Summons, R. E., Knoll, A. H., Logan, G. A., & Bowden, S. A. (2005). Biomarker evidence for green and purple sulphur bacteria in a stratified Palaeoproterozoic sea. *Nature*, *437*, 866–870. <https://doi.org/10.1038/nature04068>
- Burnham, A. K., & Sweeney, J. J. (1989). A chemical kinetic model of vitrinite maturation and reflectance. *Geochim. Cosmochim. Acta*, *53*, 2649–2657. [https://doi.org/10.1016/0016-7037\(89\)90136-1](https://doi.org/10.1016/0016-7037(89)90136-1)

- Byers, J. D., & Erdman, J. G. (1983). Low temperature degradation of carotenoids as a model for early diagenesis in recent sediments. In M. Bjørøy, et al. (Eds.), *Adv. org. geochem. 1981* (pp. 725–732). Hoboken, NJ: Wiley.
- Canfield, D. E. (1989). Reactive iron in marine sediments. *Geochim. Cosmochim. Acta*, *53*, 619–632. [https://doi.org/10.1016/0016-7037\(89\)90005-7](https://doi.org/10.1016/0016-7037(89)90005-7)
- Canfield, D. E. (1998). A new model for Proterozoic ocean chemistry. *Nature*, *396*, 450–453. <https://doi.org/10.1038/24839>
- Cottrell, T. L. (1954). *The strengths of chemical bonds*. London: Butterworth Scientific Publications.
- Dean, W. E., & Arthur, M. A. (1989). Iron-sulfur- carbon relationships in organic-carbon- rich sequences I: Cretaceous Western Interior seaway. *Am. J. Sci.*, *289*, 708–743. <https://doi.org/10.2475/ajs.289.6.708>
- Del Don, C., Hanselmann, K. W., Peduzzi, R., & Bachofen, R. (2001). The meromictic alpine Lake Cadagno: Orographical and biogeochemical description. *Aquat. Sci.*, *63*, 70–90. <https://doi.org/10.1007/PL00001345>
- van Duin, A. C. T., & Sinninghe Damsté, J. S. (2003). Computational chemical investigation into isorenieratene cyclisation. *Org. Geochem.*, *34*, 515–526. [https://doi.org/10.1016/S0146-6380\(02\)00247-4](https://doi.org/10.1016/S0146-6380(02)00247-4)
- Durand, B. (1980). Sedimentary organic matter and kerogen. Definition and quantitative importance of kerogen. In B. Durand (Ed.), *Kerogen: Insoluble organic matter from sedimentary rocks* (pp. 13–34). Paris: Editions Technip.
- Espitalié, J., Laporte, J. L., Madec, M., Marquis, F., Leplat, P., Paulet, J., & Boutefeu, A. (1977). Méthode rapide de caractérisation des roches mères, de leur potentiel pétrolier et de leur degré d'évolution. *Revue de l'Institut Français du Pétrole*, *32*, 23–42.
- Farrimond, P., Love, G. D., Bishop, A. N., Innes, H. E., Watson, D. F., & Snape, C. E. (2003). Evidence for the rapid incorporation of hopanoids into kerogen. *Geochim. Cosmochim. Acta*, *67*, 1383–1394. [https://doi.org/10.1016/S0016-7037\(02\)01287-5](https://doi.org/10.1016/S0016-7037(02)01287-5)
- French, K. L., Rocher, D., Zumberge, J. E., & Summons, R. E. (2015). Assessing the distribution of sedimentary C₄₀ carotenoids through time. *Geobiology*, *13*, 139–151. <https://doi.org/10.1111/gbi.12126>
- Frimmel, A., Oschmann, W., & Schwark, L. (2004). Chemostratigraphy of the Posidonia Black Shale, SW Germany: I. Influence of sea-level variation on organic facies evolution. *Chem. Geol.*, *206*, 199–230. <https://doi.org/10.1016/j.chemgeo.2003.12.007>
- Goodwin, N. S., Mann, A. L., & Patience, R. L. (1988). Structure and significance of C₃₀ 4-methyl steranes in lacustrine shales and oils. *Org. Geochem.*, *12*, 495–506. [https://doi.org/10.1016/0146-6380\(88\)90159-3](https://doi.org/10.1016/0146-6380(88)90159-3)
- Gransch, J. A., & Posthuma, J. (1974). On the origin of sulphur in crudes. In B. P. Tissot & F. Biennier (Eds.), *Adv. org. geochem. 1973* (pp. 727–739). Paris, France: Editions Technip.
- Grice, K., Cao, C., Love, G. D., Böttcher, M. E., Twitchett, R. J., Grosjean, E., Summons, R. E., Turgeon, S. C., Dunning, W., & Jin, Y. (2005). Photic zone euxinia during the permian-triassic superanoxic event. *Science*, *307*, 706–709. <https://doi.org/10.1126/science.1104323>
- Hartgers, W. A., Sinninghe Damsté, J. S., Requejo, A. G., Allan, J., Hayes, J. M., Ling, Y., Xie, T.-M., Primack, J., & de Leeuw, J. W. (1994). A molecular and carbon isotopic study towards the origin and diagenetic fate of diaromatic carotenoids. *Org. Geochem.*, *22*, 703–725. [https://doi.org/10.1016/0146-6380\(94\)90134-1](https://doi.org/10.1016/0146-6380(94)90134-1)
- Hartgers, W. A., Lòpez, J. F., Sinninghe Damsté, J. S., Reiss, C., Maxwell, J. R., & Grimalt, J. O. (1997). Sulfur-binding in recent environments: II. Speciation of sulfur and iron and implications for the occurrence of organo-sulfur compounds. *Geochim. Cosmochim. Acta*, *61*, 4769–4788. [https://doi.org/10.1016/S0016-7037\(97\)00279-2](https://doi.org/10.1016/S0016-7037(97)00279-2)
- Hays, L. E., Beatty, T., Henderson, C. M., Love, G. D., & Summons, R. E. (2007). Evidence for photic zone euxinia through the end-Permian mass extinction in the Panthalassic Ocean (Peace River Basin, Western Canada). *Palaeoworld*, *16*, 39–50. <https://doi.org/10.1016/j.palwor.2007.05.008>
- Hebting, Y., Schaeffer, P., Behrens, A., Adam, P., Schmitt, G., Schneckenburger, P., Bernasconi, S. M., & Albrecht, P. (2006). Biomarker evidence for a major preservation pathway of sedimentary organic carbon. *Science*, *312*, 1627–1631. <https://doi.org/10.1126/science.1126372>
- Heimhofer, U., Hesselbo, S. P., Pancost, R. D., Martill, D. M., Hochuli, P. A., & Guzzo, J. V. P. (2008). Evidence for photic-zone euxinia in the early Albian Santana formation (Araripe Basin, NE Brazil). *Terra Nova*, *20*, 347–354. <https://doi.org/10.1111/j.1365-3121.2008.00827.x>
- Hughes, W. B., Holba, A. G., & Dzou, L. I. P. (1995). The ratios of dibenzothiophene to phenanthrene and pristane to phytane as indicators of depositional environment and lithology of petroleum source rocks. *Geochim. Cosmochim. Acta*, *59*, 3581–3598. [https://doi.org/10.1016/0016-7037\(95\)00225-O](https://doi.org/10.1016/0016-7037(95)00225-O)

- Jacobshagen, V. (1965). *Die Allgäu-Schichten (Jura-Fleckenmergel) zwischen Wettersteingebirge und Rhein*. Wien: Geol. Bundesanstalt.
- Johnston, D. T., Wolfe-Simon, F., Pearson, A., & Knoll, A. H. (2009). Anoxygenic photosynthesis modulated Proterozoic oxygen and sustained Earth's middle age. *PNAS*, *106*, 16925–16929. <https://doi.org/10.1073/pnas.0909248106>
- Killops, S., & Killops, V. (2005). *Introduction to organic geochemistry*, 2nd edn. Oxford: Blackwell Publishing.
- Kodina, L. A., Bogatcheva, M. P., & Lobitzer, H. (1988). An organic geochemical study of Austrian bituminous rocks. *Jahrb. Geol. Bundesanst.*, *131*, 291–300.
- Kohnen, M. E. L., Sinninghe Damsté, J. S., Kock-van Dalen, A. C., & de Leeuw, J. W. (1991). Di- or polysulphide-bound biomarkers in sulphur-rich geomacromolecules as revealed by selective chemolysis. *Geochim. Cosmochim. Acta*, *55*, 1375–1394. [https://doi.org/10.1016/0016-7037\(91\)90315-V](https://doi.org/10.1016/0016-7037(91)90315-V)
- Koopmans, M. P., Köster, J., van Kaam-Peters, H. M. E., Kenig, F., Schouten, S., Hartgers, W. A., de Leeuw, J. W., & Sinninghe Damsté, J. S. (1996a). Diagenetic and catagenetic products of isorenieratene: Molecular indicators for photic zone anoxia. *Geochim. Cosmochim. Acta*, *60*, 4467–4496. [https://doi.org/10.1016/S0016-7037\(96\)00238-4](https://doi.org/10.1016/S0016-7037(96)00238-4)
- Koopmans, M. P., de Leeuw, J. W., Lewan, M. D., & Sinninghe Damsté, J. S. (1996b). Impact of dia- and catagenesis on sulphur and oxygen sequestration of biomarkers as revealed by artificial maturation of an immature sedimentary rock. *Org. Geochem.*, *25*, 391–426. [https://doi.org/10.1016/S0146-6380\(96\)00144-1](https://doi.org/10.1016/S0146-6380(96)00144-1)
- Köster, J., Schouten, S., Sinninghe Damsté, J. S., & de Leeuw, J. W. (1995). Reconstruction of the depositional environment of Toarcian marlstones (Allgäu Formation, Tyrol/Austria) using biomarkers and compound specific carbon isotope analyses. In J. O. Grimalt & C. Dorronsoro (Eds.), *Org. Geochem.: Developments and applications to energy, climate, environment and human history - selected papers from the 17th international meeting on organic geochemistry* (pp. 76–78). San Sebastián: AIGOA.
- Lalonde, K., Mucci, A., Ouellet, A., & Gélinas, Y. (2012). Preservation of organic matter in sediments promoted by iron. *Nature*, *483*, 198–200. <https://doi.org/10.1038/nature10855>
- Lee, C., & Brocks, J. J. (2011). Identification of carotane breakdown products in the 1.64 billion year old Barney Creek Formation, McArthur Basin, northern Australia. *Org. Geochem.*, *42*, 425–430. <https://doi.org/10.1016/j.orggeochem.2011.02.006>
- Littke, R., Leythaeuser, D., Rullkötter, J., & Baker, D. R. (1991). Keys to the depositional history of the Posidonia Shale (Toarcian) in the Hils Syncline, northern Germany. In R. V. Tyson & T. H. Pearson (Eds.), *Modern and ancient continental shelf anoxia* (pp. 311–333). London: Geological Society Special Publications.
- Love, G. D., Snape, C. E., Carr, A. D., & Houghton, R. C. (1995). Release of covalently-bound alkane biomarkers in high yields from kerogen via catalytic hydrolysis. *Org. Geochem.*, *23*, 981–986. [https://doi.org/10.1016/0146-6380\(95\)00075-5](https://doi.org/10.1016/0146-6380(95)00075-5)
- Love, G. D., McAulay, A., Snape, C. E., & Bishop, A. N. (1997). Effect of process variables in catalytic hydrolysis on the release of covalently bound aliphatic hydrocarbons from sedimentary organic matter. *Energy Fuels*, *11*, 522–531. <https://doi.org/10.1021/ef960194x>
- Love, G. D., Bowden, S. A., Jahnke, L. L., Snape, C. E., Campbell, C. N., Day, J. G., & Summons, R. E. (2005). A catalytic hydrolysis method for the rapid screening of microbial cultures for lipid biomarkers. *Org. Geochem.*, *36*, 63–82. <https://doi.org/10.1016/j.orggeochem.2004.07.010>
- Love, G. D., Stalvies, C., Grosjean, E., Meredith, W., & Snape, C. E. (2008). Analysis of molecular biomarkers covalently bound within neoproterozoic sedimentary kerogen. In P. H. Kelley & R. K. Bambach (Eds.), *From evolution to geobiology: Research questions driving paleontology at the start of a new century* (pp. 67–83). New Haven: Paleontological Society Papers.
- Marshall, C. P., Love, G. D., Snape, C. E., Hill, A. C., Allwood, A. C., Walter, M. R., Van Kranendonk, M. J., Bowden, S. A., Sylva, S. P., & Summons, R. E. (2007). Structural characterization of kerogen in 3.4 Ga Archean cherts from the Pilbara Craton, Western Australia. *Precambrian Res.*, *155*, 1–23. <https://doi.org/10.1016/j.precamres.2006.12.014>
- Marynowski, L., Filipiak, P., & Piszczowska, A. (2008). Organic geochemistry and palynofacies of the Early-Middle Frasnian transition (Late Devonian) of the Holy Cross Mountains, Southern Poland. *Palaeogeogr. Palaeoclimatol. Palaeoecol.*, *269*, 152–165. <https://doi.org/10.1016/j.palaeo.2008.04.033>
- Marynowski, L., Rakociński, M., Borcuch, E., Kremer, B., Schubert, B. A., & Hope Jahren, A. (2011). Molecular and petrographic indicators of redox conditions and bacterial communities after the F/F mass extinction

- (Kowala, Holy Cross Mountains, Poland). *Palaeogeogr. Palaeoclimatol. Palaeoecol.*, 306, 1–14. <https://doi.org/10.1016/j.palaeo.2011.03.018>
- Maynard, J. B. (1983). *Geochemistry of sedimentary ore deposits*, 1st edn. New York: Springer. <https://doi.org/10.1007/978-1-4613-9493-8>
- van der Meer, M. T. J., Schouten, S., & Sinninghe Damsté, J. S. (1998). The effect of the reversed tricarboxylic acid cycle on the ^{13}C contents of bacterial lipids. *Org. Geochem.*, 28, 527–533. [https://doi.org/10.1016/S0146-6380\(98\)00024-2](https://doi.org/10.1016/S0146-6380(98)00024-2)
- Meredith, W., Russell, C. A., Cooper, M., Snape, C. E., Love, G. D., Fabbri, D., & Vane, C. H. (2004). Trapping hydropyrolsates on silica and their subsequent thermal desorption to facilitate rapid fingerprinting by GC–MS. *Org. Geochem.*, 35, 73–89. <https://doi.org/10.1016/j.orggeochem.2003.07.002>
- Neumeister, S., Gratzner, R., Algeo, T. J., Bechtel, A., Gawlick, H.-J., Newton, R. J., & Sachsenhofer, R. F. (2015). Oceanic response to Pliensbachian and Toarcian magmatic events: Implications from an organic-rich basal succession in the NW Tethys. *Global Planet. Change*, 126, 62–83. <https://doi.org/10.1016/j.gloplacha.2015.01.007>
- Neumeister, S., Algeo, T. J., Bechtel, A., Gawlick, H.-J., Gratzner, R., & Sachsenhofer, R. F. (2016). Redox conditions and depositional environment of the Lower Jurassic Bächental bituminous marls (Tyrol, Austria). *Austrian J. Earth Sci.*, 109, 142–159. <https://doi.org/10.17738/ajes.2016.0010>
- Overmann, J., & Pfennig, N. (1989). *Pelodictyon phaeoclathratiforme* sp. nov., a new brown-colored member of the Chlorobiaceae forming net-like colonies. *Arch. Microbiol.*, 152, 401–406. <https://doi.org/10.1007/BF00425181>
- Overmann, J., Cypionka, H., & Pfennig, N. (1992). An extremely low-light- adapted phototrophic sulfur bacterium from the Black Sea. *Limnol. Oceanogr.*, 37, 150–155. <https://doi.org/10.4319/lo.1992.37.1.0150>
- Peters, K. E., & Cassa, M. R. (1994). Applied source rock geochemistry. In L. B. Magoon & W. G. Dow (Eds.), *The petroleum system—from source to trap* (pp. 93–120). Tulsa, OK: AAPG Memoir.
- Peters, K. E., Walters, C. C., & Moldowan, J. M. (2005a). *The biomarker guide: I. Biomarkers and isotopes in the environment and human history*, 2nd edn. Cambridge: Cambridge University Press.
- Peters, K. E., Walters, C. C., & Moldowan, J. M. (2005b). *The biomarker guide: II. Biomarkers and Isotopes in petroleum exploration and earth history*, 2nd edn. Cambridge: Cambridge University Press.
- Planavsky, N. J., McGoldrick, P., Scott, C. T., Li, C., Reinhard, C. T., Kelly, A. E., Chu, X., Bekker, A., Love, G. D., & Lyons, T. W. (2011). Widespread iron-rich conditions in the mid-Proterozoic ocean. *Nature*, 477, 448–451. <https://doi.org/10.1038/nature10327>
- Poulton, S. W., & Canfield, D. E. (2011). Ferruginous conditions: A dominant feature of the ocean through earth's history. *Elements*, 7, 107–112. <https://doi.org/10.2113/gselements.7.2.107>
- Poulton, S. W., Fralick, P. W., & Canfield, D. E. (2004). The transition to a sulphidic ocean ~1.84 billion years ago. *Nature*, 431, 173–177. <https://doi.org/10.1038/nature02912>
- Quandt, L., Gottschalk, G., Ziegler, H., & Stichler, W. (1977). Isotope discrimination by photosynthetic bacteria. *FEMS Microbiol. Lett.*, 1, 125–128. <https://doi.org/10.1111/j.1574-6968.1977.tb00596.x>
- Radke, M., & Welte, D. H. (1983). The Methylphenanthrene Index (MPI): A maturity parameter based on aromatic hydrocarbons. In M. Bjørøy, et al. (Eds.), *Adv. org. geochem. 1981* (pp. 504–512). Hoboken, NJ: Wiley.
- Radke, M., Welte, D. H., & Willsch, H. (1986). Maturity parameters based on aromatic hydrocarbons: Influence of the organic matter type. *Org. Geochem.*, 10, 51–63. [https://doi.org/10.1016/0146-6380\(86\)90008-2](https://doi.org/10.1016/0146-6380(86)90008-2)
- Reinhardt, M. (2015). *Biomarkers in bitumens and kerogens from Lower Jurassic oil shales in the Northern Calcareous Alps (Bächental)*. MSc thesis, University of Göttingen, Göttingen. (unpublished)
- Repeta, D. J. (1993). A high resolution historical record of Holocene anoxygenic primary production in the Black Sea. *Geochim. Cosmochim. Acta*, 57, 4337–4342. [https://doi.org/10.1016/0016-7037\(93\)90334-S](https://doi.org/10.1016/0016-7037(93)90334-S)
- Röhl, H.-J., Schmid-Röhl, A., Oschmann, W., Frimmel, A., & Schwark, L. (2001). The Posidonia Shale (Lower Toarcian) of SW-Germany: An oxygen-depleted ecosystem controlled by sea level and palaeoclimate. *Palaeogeogr. Palaeoclimatol. Palaeoecol.*, 165, 27–52. [https://doi.org/10.1016/S0031-0182\(00\)00152-8](https://doi.org/10.1016/S0031-0182(00)00152-8)
- Schidlowski, M. (2001). Carbon isotopes as biogeochemical recorders of life over 3.8 Ga of Earth history: Evolution of a concept. *Precambrian Res.*, 106, 117–134. [https://doi.org/10.1016/S0301-9268\(00\)00128-5](https://doi.org/10.1016/S0301-9268(00)00128-5)
- Schouten, S., van Kaam-Peters, H. M. E., Rijpstra, W. I. C., Schoell, M., & Sinninghe Damsté, J. S. (2000). Effects of an oceanic anoxic event on the stable carbon isotopic composition of early Toarcian carbon. *Am. J. Sci.*, 300, 1–22. <https://doi.org/10.2475/ajs.300.1.1>

- Schwark, L., & Frimmel, A. (2004). Chemostratigraphy of the Posidonia Black Shale, SW-Germany: II. Assessment of extent and persistence of photic-zone anoxia using aryl isoprenoid distributions. *Chem. Geol.*, *206*, 231–248. <https://doi.org/10.1016/j.chemgeo.2003.12.008>
- Scott, C., Lyons, T. W., Bekker, A., Shen, Y., Poulton, S. W., Chu, X., & Anbar, A. D. (2008). Tracing the stepwise oxygenation of the Proterozoic ocean. *Nature*, *452*, 456–459. <https://doi.org/10.1038/nature06811>
- Sinninghe Damsté, J. S., & Köster, J. (1998). A euxinic southern North Atlantic Ocean during the Cenomanian/Turonian oceanic anoxic event. *Earth Planet. Sci. Lett.*, *158*, 165–173. [https://doi.org/10.1016/S0012-821X\(98\)00052-1](https://doi.org/10.1016/S0012-821X(98)00052-1)
- Sinninghe Damsté, J. S., & de Leeuw, J. W. (1990). Analysis, structure and geochemical significance of organically-bound sulphur in the geosphere: State of the art and future research. *Org. Geochem.*, *16*, 1077–1101. [https://doi.org/10.1016/0146-6380\(90\)90145-P](https://doi.org/10.1016/0146-6380(90)90145-P)
- Sinninghe Damsté, J. S., Rijpstra, W. I. C., Kock-van Dalen, A. C., de Leeuw, J. W., & Schenck, P. A. (1989a). Quenching of labile functionalised lipids by inorganic sulphur species: Evidence for the formation of sedimentary organic sulphur compounds at the early stages of diagenesis. *Geochim. Cosmochim. Acta*, *53*, 1343–1355. [https://doi.org/10.1016/0016-7037\(89\)90067-7](https://doi.org/10.1016/0016-7037(89)90067-7)
- Sinninghe Damsté, J. S., Rijpstra, W. I. C., de Leeuw, J. W., & Schenck, P. A. (1989b). The occurrence and identification of series of organic sulphur compounds in oils and sediment extracts: II. Their presence in samples from hypersaline and non-hypersaline palaeoenvironments and possible application as source, palaeoenvironmental and maturity indicators. *Geochim. Cosmochim. Acta*, *53*, 1323–1341. [https://doi.org/10.1016/0016-7037\(89\)90066-5](https://doi.org/10.1016/0016-7037(89)90066-5)
- Sinninghe Damsté, J. S., Wakeham, S. G., Kohnen, M. E. L., Hayes, J. M., & de Leeuw, J. W. (1993). A 6,000-year sedimentary molecular record of chemocline excursions in the Black Sea. *Nature*, *362*, 827–829. <https://doi.org/10.1038/362827a0>
- Sirevåg, R., & Ormerod, J. G. (1970). Carbon dioxide fixation in green sulphur bacteria. *Biochem. J.*, *120*, 399–408. <https://doi.org/10.1042/bj1200399>
- Sirevåg, R., Buchanan, B. B., Berry, J. A., & Troughton, J. H. (1977). Mechanisms of CO₂ fixation in bacterial photosynthesis studied by the carbon isotope fractionation technique. *Arch. Microbiol.*, *112*, 35–38. <https://doi.org/10.1007/BF00446651>
- Snape, C. E., Bolton, C., Dosch, R. G., & Stephens, H. P. (1989). High liquid yields from bituminous coal via hydrolysis with dispersed catalysts. *Energy Fuels*, *3*, 421–425. <https://doi.org/10.1021/ef00015a028>
- Spieler, A., & Brandner, R. (1989). Vom jurassischen Pull-Apart Becken zur Westüberschiebung der Achantaler Schubmasse (Tirol, Österreich). *Geologisch-Paläontologische Mitteilungen Innsbruck*, *16*, 191–194.
- Summons, R. E., & Powell, T. G. (1986). Chlorobiaceae in Palaeozoic seas revealed by biological markers, isotopes and geology. *Nature*, *319*, 763–765. <https://doi.org/10.1038/319763a0>
- Takahashi, M., & Ichimura, S.-E. (1970). Photosynthetic properties and growth of photosynthetic sulfur bacteria in lakes. *Limnol. Oceanogr.*, *15*, 929–944. <https://doi.org/10.4319/lo.1970.15.6.0929>
- Tang, K.-H., & Blankenship, R. E. (2010). Both forward and reverse TCA cycles operate in green sulfur bacteria. *The Journal of Biological Chemistry*, *285*, 35848–35854. <https://doi.org/10.1074/jbc.M110.157834>
- Tissot, B. P., & Welte, D. H. (1984). *Petroleum formation and occurrence*, 2nd edn. Berlin: Springer. <https://doi.org/10.1007/978-3-642-87813-8>
- Wakeham, S. G., Sinninghe Damsté, J. S., Kohnen, M. E. L., & de Leeuw, J. W. (1995). Organic sulfur compounds formed during early diagenesis in Black Sea sediments. *Geochim. Cosmochim. Acta*, *59*, 521–533. [https://doi.org/10.1016/0016-7037\(94\)00361-O](https://doi.org/10.1016/0016-7037(94)00361-O)

5 Testing MOMA flight-like pyrolysis GC–MS on analog samples from Earth (iron-rich shale and opaline chert)—implications for MOMA pyrolysis during the ExoMars 2020 rover mission

Manuel Reinhardt, Walter Goetz, & Volker Thiel

Manuscript in preparation, to be submitted to *Astrobiology*

The Mars Organic Molecule Analyzer (MOMA) onboard the ExoMars 2020 rover utilizes pyrolysis gas chromatography–mass spectrometry (GC–MS) to detect organic molecules in Martian (sub-)surface materials. Pyrolysis, however, may thermally destruct and transform organic matter, obliterating original molecular signatures. In this study, we tested MOMA flight-like pyrolysis GC–MS on natural mineralogical analog samples for Oxia Planum (the designated ExoMars 2020 landing site), namely an iron-rich shale (that is rich in Fe-Mg-smectites) and an opaline chert, with known organic matter compositions. Two hydrocarbon standards (n-octadecane and phytane) were also analyzed. The experiments show that during stepwise pyrolysis (300 °C, 500 °C, 700 °C), (i) low molecular weight hydrocarbon biomarkers (like acyclic isoprenoids and aryl isoprenoids) can be analyzed intact, (ii) discrimination between free and complex molecules (macromolecules) is principally possible, (iii) secondary pyrolysis products and carryover may affect the 500 °C and 700 °C runs, and (iv) the difference in mineralogy between the two samples had no significant effect on the pyrolysis outcome. Although pyrosynthesis reactions and carryover clearly have to be considered in data interpretation, our results demonstrate that pyrolysis GC–MS onboard MOMA will be capable of providing important information on potential organic matter found on Mars, particularly when used in conjunction with other techniques on MOMA (derivatization and thermochemolysis GC–MS, laser desorption/ionization–MS).

5.1 Introduction

The ExoMars 2020 rover mission has been designed to investigate the Martian (sub-)surface for biosignatures of present or past life (Vago et al., 2017). The key instrument onboard that rover is the Mars Organic Molecule Analyzer (MOMA; Goetz et al., 2016; Goesmann et al., 2017). MOMA is capable of detecting molecular organics by performing pyrolysis and derivatization (including thermochemolysis) gas chromatography–mass spectrometry (GC–MS), as well as laser desorption/ionization–mass spectrometry (LDI–MS; Li et al., 2017). To assess potential molecular biosignatures in the subsurface, the rover will be drilling as deep as 2 m for sample material (Vago et al., 2017). Such a technical approach is necessary, as the surface of Mars is characterized by harsh conditions for the preservation of organic materials, including UV radiation (e.g., Pavlov et al., 2012; Hassler et al., 2014) and the presence of oxidants, particularly perchlorates (e.g., Hecht et al., 2009; Steininger et al., 2012; Goetz et al., 2016).

The designated landing site for ExoMars 2020 is Oxia Planum, a potential fluvio-deltaic area at the eastern margin of Chryse Planitia (Carter et al., 2016; Quantin, et al., 2016; Vago et al., 2017). The geology is characterized by Late to Middle Noachian (i.e., ca. 3.9 Ga old) deposits, mainly Fe/Mg phyllosilicates, like Fe/Mg smectite (Carter et al., 2016; Quantin et al., 2016), as well as Al phyllosilicates and hydrated silica (opal) in minor abundances (Carter et al., 2016). Noachian deposits may be suitable targets for the search of molecular biosignatures, as this time period may have been favorable for the emergence of life on Mars (cf., Westall et al., 2015; Vago et al., 2017). However, the Oxia Planum area was cratered by impacts and volcanic deposits were also found (see Carter et al., 2016; Quantin, et al., 2016). Under these circumstances, organic matter would have been altered as a result of enhanced temperatures or thermal gradients. The search for molecular biosignatures on Oxia Planum therefore should focus on energetically stabilized, i.e., de-functionalized “molecular fossils”, like hydrocarbons.

In Earth’s oldest rocks, organic matter is present as graphite (e.g., Ueno et al., 2002; van Zuilen et al., 2003, 2005) or as geomacromolecules (e.g., Marshall et al., 2007; Duda et al., 2016, 2018; Hickman-Lewis et al., 2018). The latter have often been termed “kerogen”, i.e., the immobile non-extractable fraction of organic matter (Durand, 1980), as opposed to “bitumen” (i.e., the mobile, extractable fraction). Kerogen is commonly regarded as syngenetic to the host rock and may, to some extent, shield incorporated biologically derived organic moieties from thermal alteration, thus favoring preservation over large geological time scales (cf., Brocks et al., 2003; Marshall et al., 2007; Love et al., 2008; Hallmann et al., 2011). Kerogen may also be present on the Martian surface, e.g., delivered by meteoritic infall (see Flynn, 1996; Sephton et al., 2002) or geological processes, like diagenetic sulfurization (cf., Eigenbrode et al., 2018), a process commonly involved in kerogen formation in anoxic environments on Earth (e.g., Sinninghe Damsté & de Leeuw, 1990; Wakeham et al., 1995).

The pyrolysis GC–MS device on the MOMA instrument can analyze both, free organic molecules and macromolecular organic matter (tested with other organic-bearing rocks; Goesmann et al., 2017; Mißbach, 2018). Pyrolysis, however, may decompose and transform organic matter (e.g., Hartgers, 1994a; Moldoveanu, 2010), thus obliterating original biosignatures. It is therefore necessary to study pyrolytic effects that may occur during MOMA pyrolysis on complex organic matter in greater detail.

In our study we investigated two geological samples with a MOMA flight analog system (FAS; Goesmann et al., 2017; Mißbach, 2018, Fig. 6.1 therein), an iron-rich shale (high smectite) and an opaline chert that both contain minerals detected on Oxia Planum. The organic matter of both samples includes bitumen and kerogen and was pre-characterized by various organic geochemical techniques (Reinhardt et al., 2018, 2019). In addition, two hydrocarbon standards, *n*-octadecane and phytane, were analyzed using the FAS. The main questions addressed by our study are the following:

- (i) Do potential molecular biomarkers stay intact during MOMA flight-like pyrolysis?
- (ii) Does MOMA flight-like pyrolysis form ambiguous secondary products?
- (iii) Is it possible to discriminate between bitumen- and kerogen-derived moieties?
- (iv) Do differences in mineralogy influence the pyrolysis result?

The results of this study will inform the use of MOMA during operations on Oxia Planum and will also support interpretation of returned data.

5.2 Material and methods

5.2.1 Sample material

Two Earth analog samples that are dominated by minerals found on Oxia Planum were analyzed, a fossil iron-rich shale (Bäch-1383, Bächental, Austria, Lower Jurassic; TOC = 8.3 wt.%, Fe_{tot} = 4.0 wt.%, Fe-Mg-smectite = 10.0 wt.%; Reinhardt et al., 2018) and a modern opaline chert (LM-1693, Lake Magadi, Kenya, Pleistocene; TOC = 0.3 wt.%; Reinhardt et al., 2019). Their molecular organic inventories are detailed elsewhere (Reinhardt et al., 2018, 2019). In brief, Bäch-1383 mainly contains aliphatic and aromatic hydrocarbons, including abundant biomarkers, like hopanes, steranes, acyclic isoprenoids, and derivatives of aromatic carotenoids (e.g., aryl isoprenoids; see Reinhardt et al., 2018). LM-1693 is characterized by more polar compounds, like alkanic acids, alkanols, glycerol mono- and diethers, as well as aliphatic and aromatic components (e.g., *n*-alkanes and PAHs). Important biomarkers from LM-1693 are the glycerol mono- and diethers (e.g., archaeol and extended archaeol), as well as acyclic isoprenoids (phytane, 2,6,10,14,18-pentamethylcosane; see Reinhardt et al., 2019).

For MOMA-like pyrolysis GC–MS whole rock powders were used. Two hydrocarbon standards, namely *n*-octadecane (Sigma-Aldrich) and phytane (Dr. Ehrenstorfer GmbH), were pyrolyzed in addition. Perchlorates were intentionally not added, to avoid blurring of thermal pyrolysis effects.

5.2.2 MOMA flight-like pyrolysis GC–MS

Pyrolysis experiments were conducted with a MOMA flight analog system (FAS; Goesmann et al., 2017; Mißbach, 2018, Fig. 6.1 therein), an open pyrolysis system (flushed by helium) consisting of a reusable MOMA pyrolysis oven, a tapping station, and an absorption trap filled with Tenax® GR. The FAS was coupled to a commercial Varian CP-3800 GC that in turn was connected to a Varian 240-MS/4000 MS. The major differences between FAS and the MOMA flight system are listed in Tab. 5.1 (see also Goesmann et al., 2017; Mißbach, 2018). Up to now, the FAS pyrolysis unit is the most flight-analog pyrolysis unit available (until a MOMA flight-identical testbed will be ready for use; not before launch of ExoMars 2020). However, the trap does not support flow inversion. Volatile compounds have to pass the whole trap on their way to the GC, increasing the chance of cross contamination considerably. The FAS GC–MS therefore possesses a lower resolution and an overall degraded performance as compared to the MOMA flight instrument.

Tab. 5.1: Major technical differences between the MOMA flight system and the flight analog system (FAS)

	Flight system	FAS
Trap temperature	300 °C	160 °C
Temperature of transfer lines	≥ 135 °C	110 °C
Trap flow mode	supports flow inversion	no flow inversion

To check for contamination and to ensure constant measuring conditions, the FAS and GC–MS were cleaned by heating, and blanks were run regularly. Sample powders (19.32 mg for LM-1693, 0.33 mg for Bäch-1383; pre-dried in the MOMA oven at 80 °C for 10 min before pyrolysis; oven not connected to tapping station) were pyrolyzed using stepwise pyrolysis (300 °C, 10 s; 500 °C, 10s; 700 °C, 10 s; Goesmann et al., 2017). The trap was cooled by a Peltier element to ca. 5 °C and trap heating was initiated after 10 s (at the end of pyrolysis) to ca. 160 °C (with 200 °C/min). The GC–MS was started after additional 45 s. To transfer compounds from the trap into the GC injector, the FAS transfer lines were heated to ca. 110 °C.

Standard compounds (100 ng of *n*-octadecane and phytane, respectively) were deposited on ca. 20 mg of annealed silica gel (at 550 °C), and pyrolyzed via stepwise (see above) and single-step pyrolysis (separated heating to 300 °C (10 s), 500 °C (10 s), and 700 °C (10 s), respectively).

5.2.3 GC–MS configuration

The GC (Varian CP-3800) was equipped with a Varian Factor Four VF-5ms column (length = 30 m, inner diameter = 0.25 mm, film thickness = 0.25 µm). The VF-5ms column is comparable to the MOMA Restek MXT 5 column (see Goesmann et al., 2017). The carrier gas was He with a flow rate of 2 L/min. The injector temperature was 250 °C, and a split ratio of 30 was used. The GC temperature program started at 30 °C and heated to 250 °C with 10 °C/min (hold time = 5 min).

The MS (Varian 240-MS/4000) operated in full-scan mode with a scan time of 0.58 s. The scanned mass range covered m/z 35 to 1000. Compounds were identified by comparison with the NIST mass spectral library and/or the retention times of standard compounds (*n*-octadecane, phytane).

5.3 Results

5.3.1 Iron-rich shale (Bäch-1383)

Stepwise pyrolysis of the iron-rich shale predominantly yields low molecular weight aliphatic and aromatic hydrocarbons, especially *n*-alkanes and *n*-alkenes, as well as mono- and polyaromatic compounds.

n-Alkanes appear in all temperature fractions. At 300 °C *n*-C_{10–15} are released (Fig. 5.1a; 1.2 % of total *n*-alkanes with 9–17 carbons; Tab. 5.2). At 500 °C the *n*-alkane diversity increases significantly to *n*-C_{7–21} (Fig. 5.1b; 64.0 % of total *n*-alkanes with 9–17 carbons and 34.8 % of total *n*-alkanes with 18–22 carbons; Tab. 5.2). Additionally the acyclic isoprenoid phytane appears (11.9 % of total phytane; Tab. 5.2), and *n*-alkenes occur together with the corresponding alkanes (Fig. 5.1b; 55.6 % of total *n*-alkenes; Tab. 5.2). At 700 °C *n*-alkanes up to *n*-C₂₂ are visible, and for greater chain-length (*n*-C₁₈ to *n*-C₂₂) the pyrolysis yields increase drastically as compared to 500 °C (89.8 % of total *n*-alkanes with 18–22 carbons; Tab. 2). Phytane shows the same effect (88.1 % of total phytane at 700 °C; Tab. 5.2).

The monoaromatic 2,6,10-trimethyl aryl isoprenoids appear in all temperature steps (C_{10–14} at 300 °C, C_{10–16} at 500 °C, C_{10–11} and C_{15–19} at 700 °C; Fig. 5.2) with highest amounts at 500 °C (82.8 % of total aryl isoprenoids with 10–16 carbons; Tab. 5.2). C_{18–19} aryl isoprenoids only occur at 700 °C. Other monoaromatic compounds are alkyl benzenes (mono-, di-, and trimethyl-; all temperature steps; Fig. D1), and the heteroaromatic alkyl thiophenes (mono- and dimethyl; at 500 and 700 °C; Fig. D1). Again, the highest amounts were generated at 500 °C (82.5 % of total alkyl thiophenes; Tab. 5.2). Furthermore, low molecular weight polycyclic aromatic hydrocarbons (PAHs) are represented in all temperature steps, including the 2-ring PAHs naphthalene, alkyl naphthalenes (mono-, di-, and trimethyl), and the 3-ring PAH phenanthrene. While the alkyl naphthalenes mainly appear at 500 °C (60.6 % of total alkyl naphthalenes; Tab. 5.2), naphthalene and phenanthrene show highest amounts at 700 °C (55.3 and 52.6 %, respectively; Tab. 5.2).

Tab. 5.2: Stepwise pyrolysis of Bäch-1383; relative abundances of selected compounds ([%] of the total).

	Pyrolysis T		
	300 °C	500 °C	700 °C
<u><i>n</i>-Alkenes</u>			
<i>n</i> -C _{9:1–17:1}		55.6	44.4
<u><i>n</i>-Alkanes</u>			
<i>n</i> -C _{9–17}	1.2	64.0	34.8
<i>n</i> -C _{18–22}		10.2	89.8
<u>Isoprenoids</u>			
phytane		11.9	88.1
<u>Aromatics</u>			
aryl isopr. (C _{10–16})	6.6	82.8	10.5
aryl isopr. (C _{18–19})			100.0
Alkyl benzenes	1.2	53.6	45.2
Alkyl thiophenes		82.5	17.5
<u>PAHs</u>			
Alkyl naphthalenes	2.9	60.6	36.4
naphthalene	7.8	37.0	55.3
phenanthrene	19.6	27.7	52.6

5.3.2 Opaline chert (LM-1693)

Ketones are the main pyrolysis products of the opaline chert. At 300 °C furanones and a few *n*-alkan-2-ones (C_{7–12}, C_{14–15}) occur (Fig. 5.3a; D2). *n*-Alkan-2-ones (C_{6–15}) then dominate at 500 and 700 °C (Fig. 5.3b, c; D2). At

500 °C the majority of C₆₋₁₃ *n*-alkan-2-ones appear (62.3 % of total C₆₋₁₃ *n*-alkan-2-ones; Tab. 5.3), while at 700 °C the amount of C₁₄₋₁₅ increases, as compared to 500 °C (49.8 % of total C₁₄₋₁₅ *n*-alkan-2-ones; Tab. 5.3). Two structurally unidentified furanones (Fur1 and Fur2) show highest abundances at 500 °C (63.5 % of total Fur1 and 2; Tab. 5.3), while the structurally unidentified furanones Fur3 and Fur4 appear in higher amounts at 700 °C (65.5 % of total Fur3 and 4; Tab. 5.3).

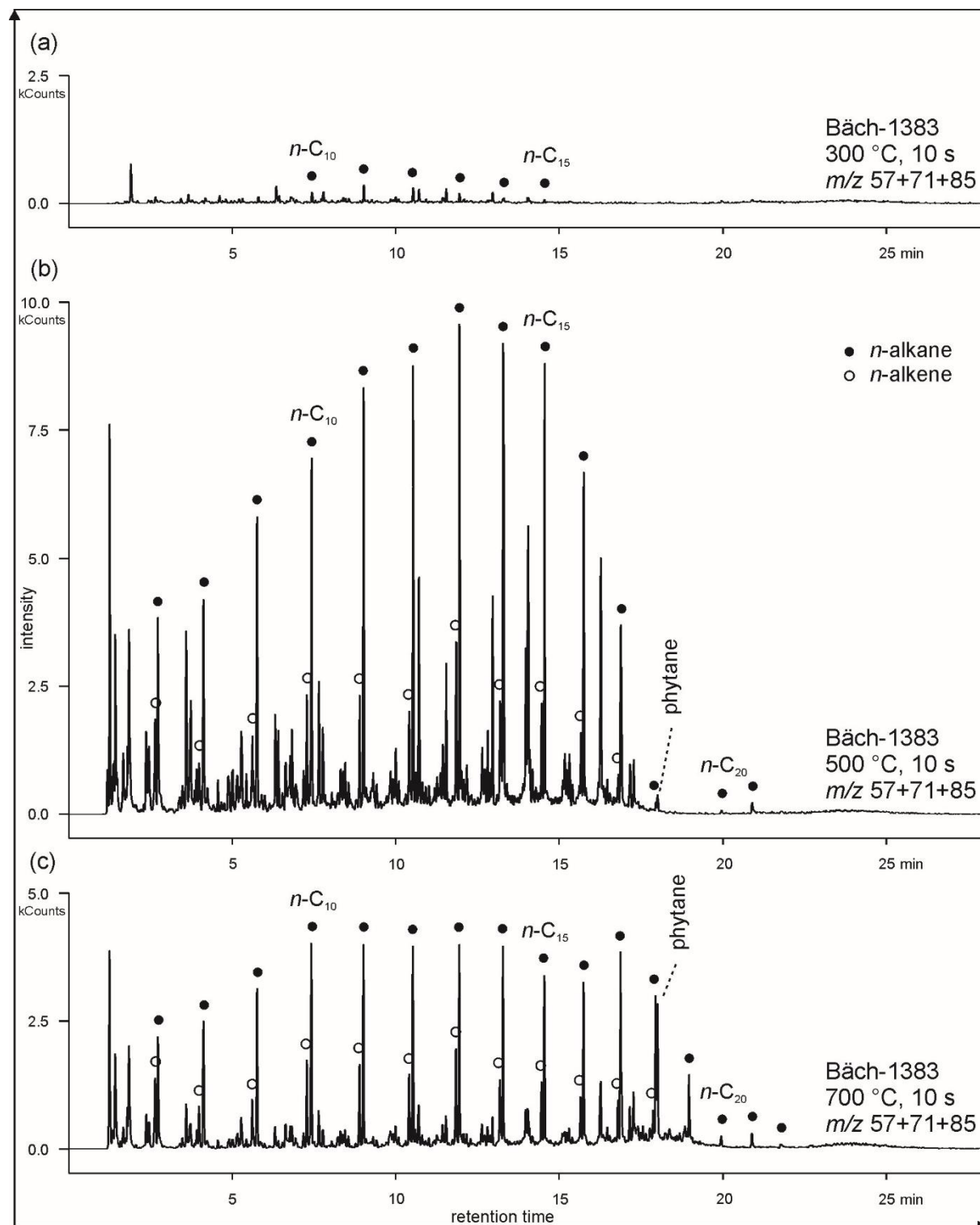


Fig. 5.1: GC-MS ion chromatograms (m/z 57+71+85) from stepwise pyrolysis (300 °C, 500 °C, 700 °C, held for 10 s, respectively; a-c) of Bäch-1383. *n*-Alkanes (filled circles) appear only marginally at 300 °C and show highest abundances at 500 °C. *n*-Alkenes (open circles) co-occur with *n*-alkanes at 500 °C and 700 °C. Note that the acyclic isoprenoid phytane shows highest amounts at 700 °C.

A few *n*-alkanes (*n*-C_{16–22}) and phytane occur at 500 and 700 °C (Fig. 5.3b, c). *n*-C_{16–17} are most abundant at 500 °C (71.3 % of total *n*-alkanes with 16 or 17 carbons), while *n*-C_{18–22} and phytane dominate at 700 °C (88.7 % of total *n*-alkanes with 18–22 carbons, and 76.1 % of total phytane; Tab. 5.3). Additionally, we tentatively identified a diterpene at 500 °C.

Aromatic compounds, including (methyl) benzene, (methyl) naphthalenes, and dibenzofuran only appear at 700 °C in low abundances (Fig. D2).

5.3.3 Hydrocarbon standards (*n*-octadecane and phytane)

n-Octadecane (*n*-C₁₈) was subjected to stepwise and single step pyrolysis. During stepwise pyrolysis the abundance of *n*-octadecane increases significantly from 300 °C to 700 °C (Fig. 5.4), with 69.9 % of the total *n*-octadecane being transferred at 700 °C (Tab. 5.3). However, no secondary pyrolysis products from potential fragmentation/destruction appear in both, stepwise and single step pyrolysis runs. Phytane (only pyrolyzed at 700 °C) also remains virtually intact, and does not produce breakdown products detectable with this setup (Fig. D3).

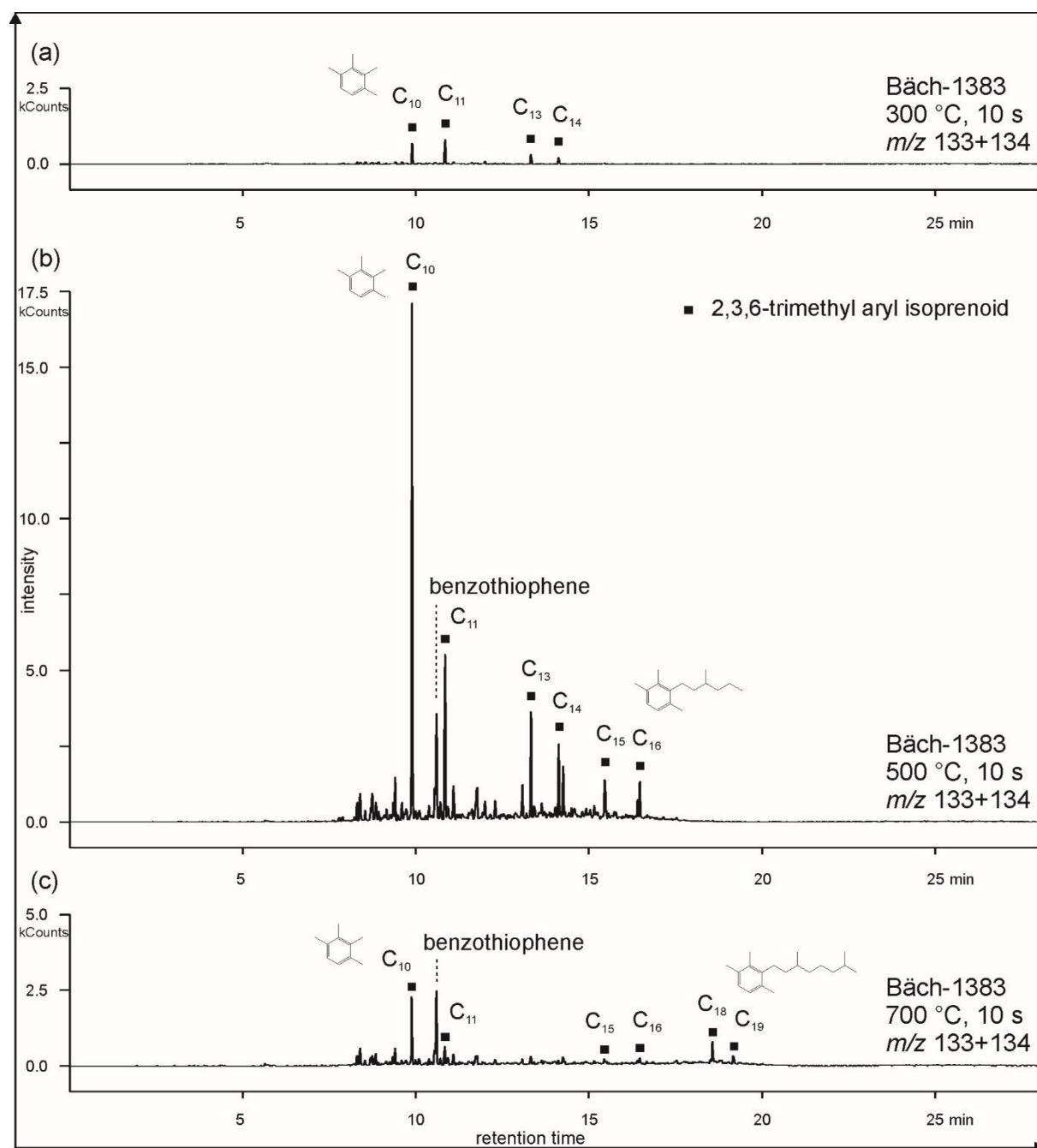


Fig. 5.2: GC–MS ion chromatograms (*m/z* 133+134) from stepwise pyrolysis (300 °C, 500 °C, 700 °C, held for 10 s, respectively; a–c) of Bäch-1383. 2,3,6-trimethyl aryl isoprenoids (squares) are present in all three temperature fractions, with

only four homologs at 300 °C. At 500 °C highest amounts of aryl isoprenoids were generated, while the diversity is greatest at 700 °C.

5.4 Discussion

5.4.1 Intact biomarkers in MOMA FAS pyrolysates

Pyrolysis leads to destruction and transformation (including pyrosynthesis) of organic matter via various reaction mechanisms (see Moldoveanu, 2010). Signals from the original organic molecules present in the samples are thereby blurred. MOMA pyrolysis, however, is an open-system technique, where thermal heating is achieved under a constant flow of inert helium (cf., Goesmann et al., 2017). It is therefore likely that some organic moieties stay intact during the pyrolysis process.

Stepwise pyrolysis GC–MS of Bäch-1383 and LM-1693 revealed the acyclic isoprenoid phytane (Fig. 5.1b, c, 5.3b, c), a biomarker that derives e.g., from (i) the side chain of chlorophyll (e.g., Brooks et al., 1969; Didyk et al., 1978), or (ii) archaeal membrane lipids, like archaeol (Nishihara & Koga, 1995). Phytane did not decompose during heating up to 700 °C (held for 10 s), as shown by the phytane standard test (5.3.3; Fig. D3). Consequently, the amounts of phytane in the pyrolysates probably reflect a minimum amount of phytane in the samples. The intensity of released phytane, however, is very low (see Fig. 5.3, D2), corroborating pre-characterization results (Reinhardt et al., 2019). It may therefore be indicated that no pyrolytic phytane (from decomposition of archaeol or extended archaeol that are abundant in LM-1693 (Reinhardt et al., 2019)) was generated during stepwise pyrolysis.

Tab. 5.3: Stepwise pyrolysis of LM-1693 and the *n*-octadecane standard; relative abundances of selected compounds ([%] of the total). The labels Fur1, Fur2, Fur3 and Fur4 denote structurally unidentified furanones.

	Pyrolysis T		
	300 °C	500 °C	700 °C
<u><i>n</i>-Alkanes</u>			
<i>n</i> -C ₁₆₋₁₇		71.3	28.7
<i>n</i> -C ₁₈₋₂₂		11.3	88.7
<u>Isoprenoids</u>			
phytane		23.9	76.1
<u><i>n</i>-Alkan-2-ones</u>			
C ₆₋₁₃	0.3	62.3	37.4
C ₁₄₋₁₅	7.7	42.5	49.8
<u>Furanones</u>			
Fur1+Fur2	9.6	63.5	26.9
Fur3+Fur4	1.2	33.3	65.5
Standard			
<i>n</i> -C ₁₈ (100 ng)	4.3	25.8	69.9

Additionally, 2,3,6-trimethyl aryl isoprenoids occur in all temperature steps during pyrolysis of Bäch-1383 (Fig. 5.3; Tab. 5.2). Aryl isoprenoids are diagenetic products of aromatic carotenoids, biomarkers for anoxygenic phototrophic bacteria, and are commonly found in ancient rocks on Earth (e.g., Summons & Powell, 1986; Koopmans et al., 1996a; Grice et al., 2005; Reinhardt et al., 2018). The observed aryl isoprenoid pattern detected in the pyrolysates, however, only comprises a fraction of the complete aryl isoprenoid inventory from bitumen in Bäch-1383 (up to C₂₅; Reinhardt et al., 2018). Further abundant biomarkers known from Bäch-1383 (intact aromatic carotenoids, steranes, hopanes) and LM-1693 (glycerol mono- and diethers, sterols, branched alkanolic acids and alcohols) were also not detected by MOMA flight analog pyrolysis GC–MS. This analytical gap demonstrates the limits of MOMA pyrolysis GC–MS that is especially designed to detect low to medium molecular weight compounds (up to C₂₅; see Goesmann et al., 2017). Most of the biomarkers in Bäch-1383 (Reinhardt et al., 2018) and LM-1693 (Reinhardt et al., 2019), including aryl isoprenoids with long side chains, however, possess higher molecular weights (> C₂₅; e.g., hopanes, glycerol mono- and diethers) and are therefore out of the FAS

analytical window. But even though the detection of intact compounds from Bäch-1383 and LM-1696 is limited due to technical constraints, the low molecular weight biomarkers detected with the FAS are still highly diagnostic for their biological precursors.

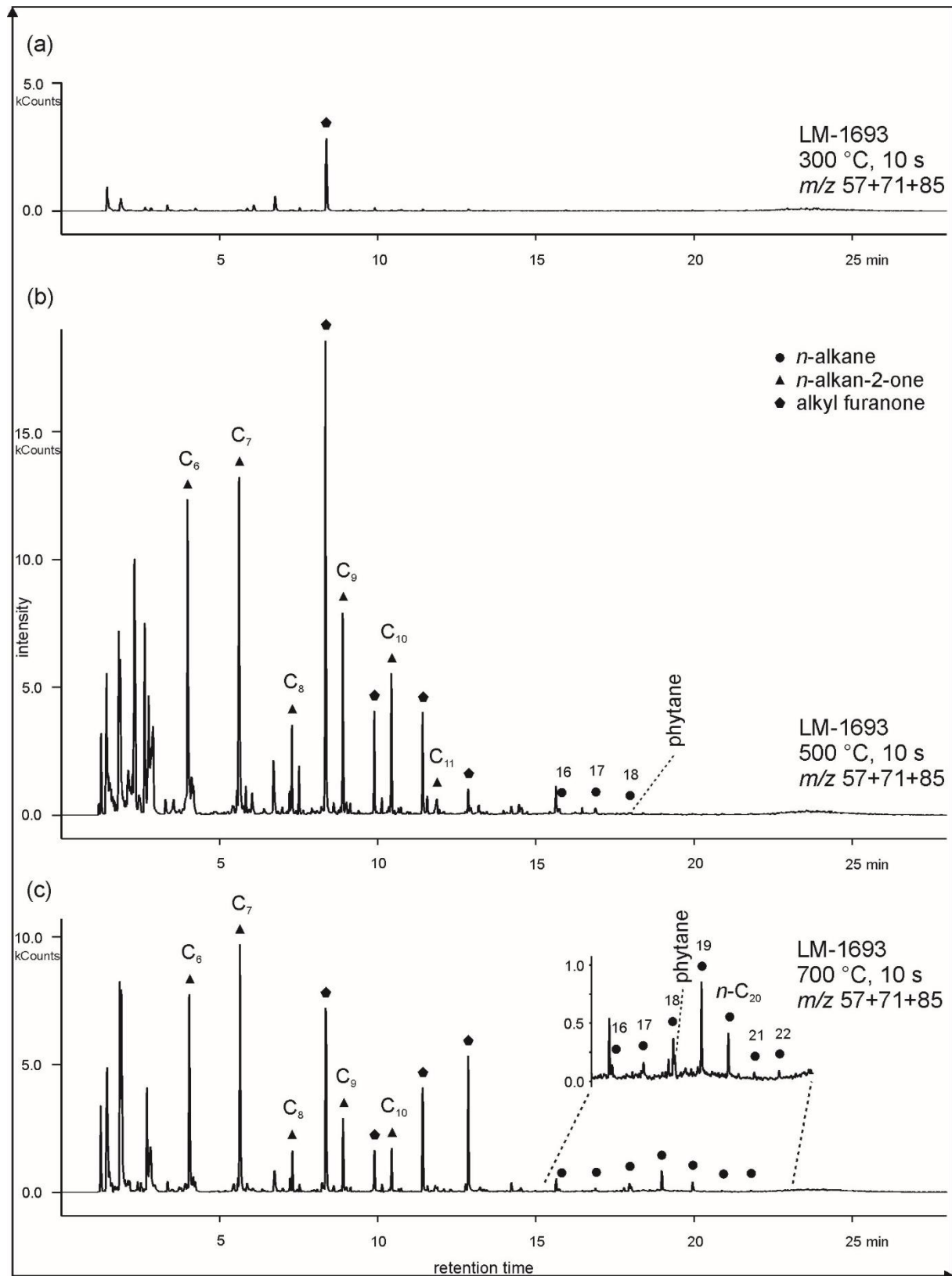


Fig. 5.3: GC-MS ion chromatograms (m/z 57+71+85) from stepwise pyrolysis (300 °C, 500 °C, 700 °C, held for 10 s, respectively; a-c) of LM-1693. At 300 °C a furanone (pentagon) is dominant, while n -alkanes (filled circles) and n -alkan-2-ones (triangles) are missing. n -Alkan-2-ones show highest amounts at 500 °C. n -Alkanes with 18–22 carbons and phytane, on the other hand, are most abundant at 700 °C.

5.4.2 Secondary pyrolysis products

Aryl isoprenoids may not only represent alteration products of aromatic carotenoids formed during geological alteration (diagenesis), they may potentially also be generated from breakdown of aromatic carotenoids or their molecular fossils during pyrolysis (Hartgers et al., 1994a, b; Koopmans et al., 1996a, b). For Bäch-1383 both possibilities are principally possible, as Bäch-1383 contains both, diagenetically produced aryl isoprenoids and also intact aromatic carotenoid biomarkers, like isorenieratane (Reinhardt et al., 2018) that may decompose during pyrolysis. The samples, however, revealed also other potential secondary pyrolysis products that are commonly observed in organic pyrolysates and may form by different reaction pathways:

(i) *Polycyclic aromatic hydrocarbons (PAHs)*, like *naphthalene* and *phenanthrene* especially occur in the 700 °C fractions (see chapter 5.3; Tab. 5.2), indicating pyrolytic formation. De-alkylated PAHs can form through pyrosynthesis from various educts, e.g., *n*-alkanes, *n*-alkenes or simple monoaromatics like benzene (e.g., Appel et al., 2000; Moldoveanu, 2010). Phenanthrene may also derive from pyrolytic conversion of terpenes (abundant in Bäch-1383) via de-alkylation of dimehtyl phenanthrenes (e.g., McCollom et al., 1999; Britt et al., 2004). Such de-alkylation may also plausibly explain the decrease in abundance of alkyl naphthalenes from 500 °C to 700 °C that is accompanied by an increase in naphthalene concentration at 700 °C (Tab. 5.2). A formation of naphthalene and phenanthrene from *n*-alkanes and *n*-alkenes, however, would require high temperatures or long heating time (Moldoveanu, 2010), which is not in line with MOMA pyrolysis conditions.

(ii) *n*-Alkenes may also be generated through pyrolytic decomposition reactions. Free *n*-alkanes may lose a carbon atom during pyrolysis and form radicals (Moldoveanu, 2010). Such a process would additionally lead to the formation of alkadienes that were, however, not detected in the pyrolysates. Moreover, the *n*-octadecane standard pyrolysis did not show any destruction of the hydrocarbon chain even under 700 °C (held for 10 s; Fig. 5.4). The *n*-alkenes may therefore not derive from decomposition of free *n*-alkanes. A further potential origin is discussed in section 5.4.3.

(iii) *Alkyl benzenes* represent typical pyrolysis products that may derive from various potential organic precursors (e.g., Hartgers et al., 1994a; Moldoveanu, 2010). Together with naphthalene they were also detected as contaminants from Tenax® heating in the SAM instrument on board the Curiosity rover (Freissinet et al., 2015). It is therefore likely that alkyl benzenes and also naphthalene may partly derive from Tenax decomposition.

(iv) *n*-Alkan-2-ones may form via dehydrogenation of *n*-alkan-2-ols (see Leif & Simoneit, 1995) that are abundant in LM-1693 (Reinhardt et al., 2019). Furthermore, *n*-alkan-2-ones may derive from the pyrolysis of carboxylic acids through radical formation and the loss of one carbon atom (e.g., Regtop et al., 1985). This mechanism seems likely here, as LM-1693 is known to contain abundant extractable alkanolic acids (Reinhardt et al., 2019). The odd-over-even chain length preference of *n*-alkan-2-ones in the pyrolysates from LM-1693 therefore may correspond to the even-over-odd preference of the precursor *n*-alkanoic acids.

(v) *Furanones* were tentatively identified in pyrolysates from LM-693 and may derive from pyrolysis of glucose or glucose-containing polymers, like cellulose (cf., Steinbeiss et al., 2006; Moldoveanu, 2010; Lv & Wu, 2012). A pyrolytic origin is further indicated by non-detection with conventional organic geochemical techniques (Reinhardt et al., 2019).

The pyrolysis results show the difficulty to clearly identify secondary products in the pyrolysates and work out their corresponding formation pathways. It is planned, however, that LDI–MS will typically be performed before GC–MS on Mars (see Goesmann et al., 2017). The combination of data from all analytical techniques available on MOMA, including also derivatization and thermochemolysis, can therefore help to corroborate results from MOMA pyrolysis.

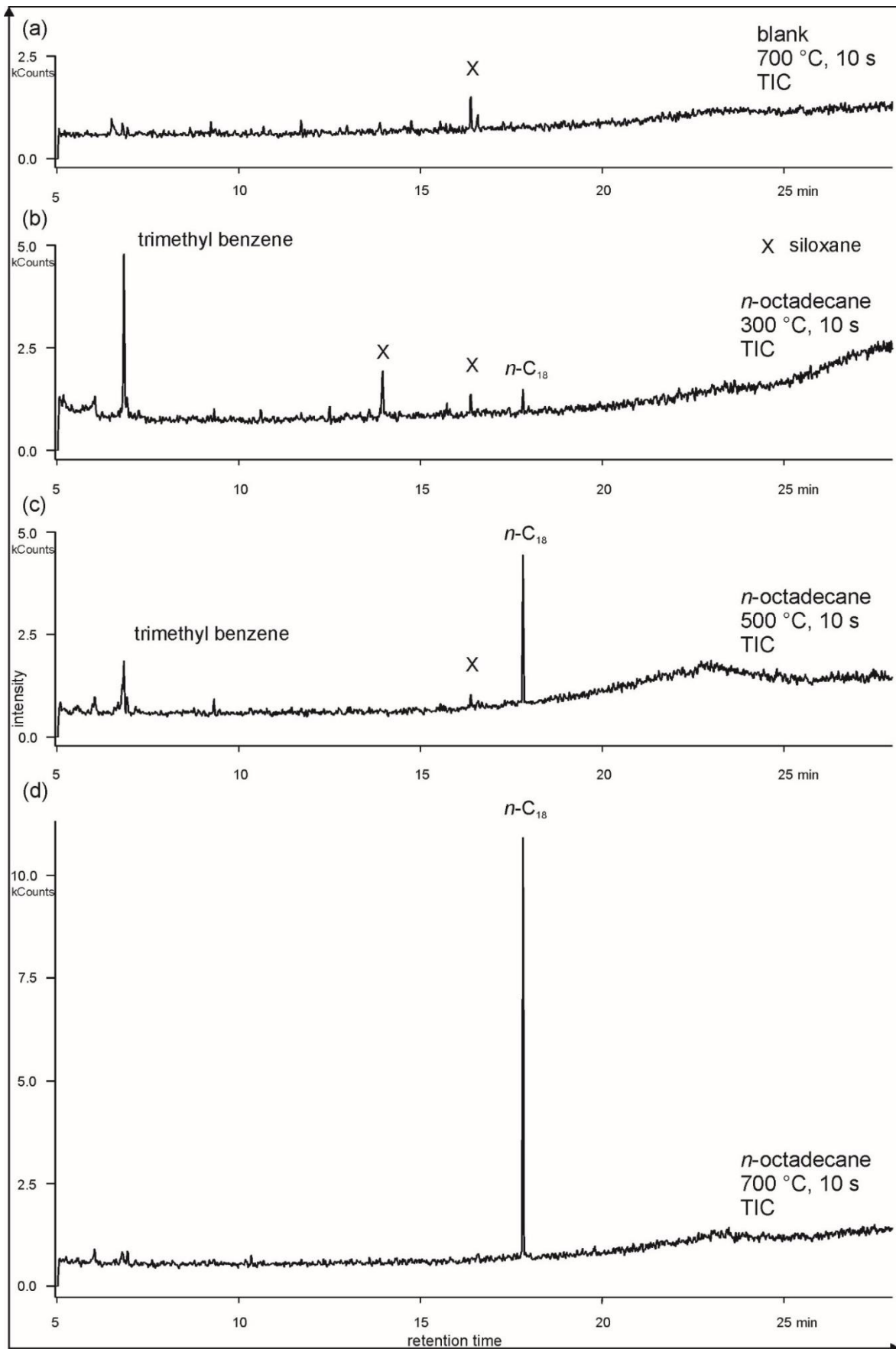


Fig. 5.4: Total ion chromatograms (TICs) from a blank run (700 °C, held for 10 s; a) and stepwise pyrolysis of *n*-octadecane (100 ng; 300 °C, 500 °C, 700 °C, held for 10 s, respectively; b–d) deposited on ca. 20 mg of silica gel. The abundance of free *n*-octadecane in the pyrolysates constantly increases from 300 °C to 700 °C. ‘X’ denotes siloxane contaminants.

5.4.3 Pyrolysis products from macromolecules

Pyrolysis can furthermore be used to investigate the composition of organic macromolecules like biopolymers or kerogen (e.g., van de Meent et al., 1980; Horsfield, 1989; Eglinton et al., 1992; Reinhardt et al., 2018, 2019). Particularly kerogen is of high interest for the reconstruction of palaeo-ecosystems, as it is syngenetic to the host rock and may enhance the preservation of biomarkers over large geological time scales by incorporating and shielding the components against mild thermal maturation (cf., Brocks et al., 2003; Marshall et al., 2007; Love et al., 2008; Hallmann et al., 2011).

Cracking of macromolecular networks (O–C, C–C bonds) under artificial pyrolytic conditions normally starts above 300 °C, while unbound moieties generally volatilized already at low temperatures (ca. 100–300 °C; e.g., Scrima et al., 1974; Tissot & Welte, 1984; Huizinga et al., 1988). The *n*-alkanes released during the 300 °C run of Bäch-1383 most likely represent free hydrocarbons from bitumen or were adsorbed to macromolecules. Decomposition of kerogen or other complex organic moieties (e.g., polymers) may then contribute significantly to the *n*-alkane pool of the 500 °C and 700 °C runs. Indeed, in addition to *n*-alkanes, *n*-alkenes appear at 500 and 700 °C (Fig. 5.1; Tab. 5.2). Such alkane/alkene pairs are commonly observed during kerogen maturation (e.g., Leif & Simoneit, 2000) and may be attributed to the degradation of ester-bound alkanolic acids or alkanols (e.g., van de Meent et al., 1980; Burnham et al., 1982; Huizinga et al., 1988).

However, it appears that after FAS pyrolysis not all free hydrocarbons may have been transferred initially from the trap into the GC. As trap and transfer line temperatures were only 160 °C and 110 °C, respectively (Tab. 5.1), higher molecular weight compounds (e.g., C₁₈₊ *n*-alkanes) may have condensed in the FAS tubing system and were transferred to the GC-injector only during subsequent heating pulses. Such “carryover” was indeed observed during stepwise pyrolysis of the *n*-octadecane standard (see Fig. 5.4). During the 700 °C step, 70 % of total *n*-octadecane were detected. It is therefore very likely that the 500 °C and even the 700 °C runs contain significant amounts of free hydrocarbons that had already been volatilized at lower temperature. Thus, the predominance of long-chain *n*-alkanes (*n*-C_{18–22}) in the 700 °C fraction (89.9 %, Tab. 5.2; 88.7 %, Tab. 5.3) obviously results from a delayed transfer of unbound compounds into the GC injector after repeated heating of trap and transfer lines.

In this view, the significant relative amount of aryl isoprenoids observed in the 500 °C step may represent a mixture of free bitumen and compounds released during breakdown of kerogen. However, alkyl thiophenes show similarly high relative abundances at 500 °C (82.5 %; Tab. 5.2) and do not occur at 300 °C (despite boiling points way below 300 °C, e.g., ca. 120 °C for 2-methyl thiophene; Katritzky et al., 1998). We explain this finding by decomposition of sulfur bonds (S–S, S–C) from kerogen that need lower temperatures to decompose than C–O or C–C bonds (cf., Cottrell, 1954; Koopmans et al., 1996b). Some aryl isoprenoids and thiophenes were likely bound into the kerogen network through sulfurization (e.g., Sinnighe Damsté & de Leeuw, 1990; Hartgers et al., 1994b; Wakeham et al., 1995), a diagenetic process that was likely minimized, but active in the Bächental environment (Reinhardt et al., 2018). Koopmans et al. (1996b) have shown that sulfur-bound aromatic carotenoid biomarkers, like aryl isoprenoids, are released early from macromolecules during pyrolysis, which would plausibly explain the higher relative amounts of aryl isoprenoids and alkyl thiophenes as compared to *n*-alkanes in the 500 °C fraction of Bäch-1383. Although the observed carryover effects call for caution in the interpretation of the high temperature pyrolysates produced during MOMA FAS pyrolysis, it may therefore still be possible to distinguish between free molecules (bitumen) and compounds bound to macromolecules (e.g., kerogen or polymers).

5.4.4 Effects of mineral matrix on the pyrolysis outcome

Mineral surfaces can adsorb organic molecules, preventing fast volatilization during pyrolysis. Such effects may decrease pyrolysis yields and lead to enhanced thermocatalysis, as well as elevated aromaticity of pyrolysates already at low temperatures (e.g., Horsfield & Douglas, 1980; Huizinga et al., 1987). Especially under dry pyrolysis conditions (like MOMA pyrolysis) clay minerals adsorb free molecules (from the bituminous organic fraction of the sample) in the reaction zone of the pyrolysis device (Huizinga et al., 1987).

Both, Bäch-1383 (rich in clay minerals, e.g., smectite) and LM-1693 (poor in clay minerals) contain *n*-alkanes, phytane and low molecular weight PAHs. Specifically the following features common to both materials were observed:

- (i) The majority of *n*-alkanes were released at 500 °C (Figs. 5.1, 5.3; Tabs. 5.2, 5.3).
- (ii) *n*-Alkanes with longer chains (C_{18–22}) preferentially occur at higher temperatures (Figs. 5.1, 5.3; Tabs. 5.2, 5.2).

(iii) PAH release (naphthalene and phenanthrene) is highest at 700 °C (Tabs. 5.2, 5.3).

Elevated aromaticity at low temperatures that would indicate retention of free molecules on mineral surfaces was not observed in both samples. Also increased thermocatalysis in the presence of clay minerals (Bäch-1383) that preferentially produces C₁₋₉ hydrocarbons (e.g., Tannenbaum & Kaplan, 1985) is not evident (see Fig. 5.1).

It therefore seems that the presence or absence of clay minerals does not produce major qualitative variations in MOMA pyrolysates. This finding may be explained by short heating times during individual temperature steps. However, quantitative changes of compound release during pyrolysis cannot be assessed with our experimental set-up, as both samples contain very different types of organic matter (hydrocarbons vs. functionalized lipids) and no pure kerogen was tested as a reference.

5.4.5 Implications for MOMA pyrolysis GC–MS on Mars

If organic matter can be detected in Oxia Planum samples, it will be of interest to assess (i) the source (meteoritic, insitu abiogenic synthesis, biogenic) and (ii) the structural preservation (simple molecules vs. complex macromolecules) with the MOMA instrument. Especially the presence of macromolecules in Martian sediments should be investigated, as their protective networks may encase organic biomarkers and shield them from the harsh oxidative conditions on the surface of Mars (cf., McDonald et al., 1998).

Organic sulfur compounds (e.g., thiophene) were recently detected by the SAM instrument onboard the Curiosity rover during pyrolysis > 500 °C. Their occurrence was interpreted as cracking from macromolecules that formed through diagenetic sulfurization (Eigenbrode et al., 2018). However, it cannot completely be excluded that the thiophenes and other organic sulfur compounds detected by SAM were generated during the disproportionation of sulfur-bearing minerals that were likely present in the samples from Gale Crater (Hurowitz et al., 2017; Eigenbrode et al., 2018). The presence of macromolecules formed through sulfurization on Mars therefore is questionable. Our study shows that MOMA pyrolysis GC–MS is also capable to decipher such signals. The assessment of sulfurization on Mars should consequently be re-addressed by MOMA onboard the ExoMars rover.

While the distinction between bitumen and kerogen will be possible with MOMA pyrolysis, a source evaluation may be more difficult. MOMA pyrolysis GC–MS will be able to detect low molecular weight aliphatic and aromatic hydrocarbons (including low molecular weight biomarkers as we know them from Earth, like acyclic isoprenoids from archaeal lipids and aryl isoprenoids from pigments of anoxygenic phototrophs) without significant decomposition and transformation during pyrolysis (see 5.4.1). The origin of many molecules formed as secondary products during pyrolysis (see 5.4.2), such as PAHs, will be difficult to elucidate. These compounds are major constituents of carbonaceous chondrite organic matter (e.g., Sephton et al., 2004, 2005), appear in thermally altered rocks (e.g., Brocks et al., 2003; Marshall et al., 2007) and are furthermore likely formed during pyrosynthesis in the MOMA oven (our study). The combined use of all available MOMA techniques will therefore be necessary to properly interpret potential organic signatures from Oxia Planum.

5.5 Conclusions

MOMA flight-like pyrolysis GC–MS (including MOMA oven, tapping station and trap) was tested on two organic-bearing samples with bulk mineral compositions relevant to Oxia Planum, Mars (smectite-rich shale, opaline chert), as well as two hydrocarbon standards (*n*-octadecane and phytane), to assess pyrolytic effects that may obliterate original organic signatures in the samples. MOMA flight analog pyrolysis tests revealed that:

- (i) Low molecular weight hydrocarbon biomarkers (like acyclic isoprenoids and aryl isoprenoids) are not decomposed during stepwise pyrolysis (300 °C, 500 °C, 700 °C) and stay highly diagnostic for their precursors.
- (ii) A range of secondary pyrolysis products (such as PAHs) can hardly be discriminated from similar molecules produced by natural rock alteration (diagenesis), complicating their interpretation.
- (iii) Carryover of compounds affect the 500 °C and 700 °C pyrolysis steps.
- (iv) Discrimination between free bitumen and molecules released from macromolecular networks may be possible despite carryover between different temperature runs.
- (v) The presence or absence of clay minerals did not show significant qualitative differences on the composition of the pyrolysates. Differences between the samples are mainly dictated by the type of organic matter (defunctionalized hydrocarbons vs. functionalized lipid remains).

Our study demonstrates that MOMA pyrolysis benefits from pre-characterization of potential organic matter on Oxia Planum by LDI–MS, as carryover effects and pyrosynthesis may lead to misinterpretations. The stepwise pyrolysis approach, however, is suitable to gain important data on structural organic matter characteristics, while keeping the extent of thermal decomposition low.

Acknowledgements

We kindly thank F. Goesmann and H. Mißbach for help with the MOMA flight analog pyrolysis unit at the Max Planck Institute for Solar System Research, Göttingen. Financial support from the International Max Planck Research School (IMPRS) for Solar System Science is gratefully acknowledged.

References

- Appel, J., Bockhorn, H., & Frenklach, M. (2000). Kinetic modeling of soot formation with detailed chemistry and physics: laminar premixed flames of C₂ hydrocarbons. *Combust. Flame*, *121*, 122–136. [https://doi.org/10.1016/S0010-2180\(99\)00135-2](https://doi.org/10.1016/S0010-2180(99)00135-2)
- Britt, P. F., Buchanan III, A. C., & Owens Jr., C. V. (2004). Mechanistic investigation into the formation of polycyclic aromatic hydrocarbons from the pyrolysis of terpenes. *Prepr. Pap.-Am. Chem. Soc., Div. Fuel Chem*, *49*, 868–871.
- Brocks, J. J., Love, G. D., Snape, C. E., Logan, G. A., Summons, R. E., & Buick, R. (2003). Release of bound aromatic hydrocarbons from late Archean and Mesoproterozoic kerogens via hydrolysis. *Geochim. Cosmochim. Acta*, *67*, 1521–1530. [https://doi.org/10.1016/S0016-7037\(02\)01302-9](https://doi.org/10.1016/S0016-7037(02)01302-9)
- Brooks, J. D., Gould, K., & Smith, J. W. (1969). Isoprenoid Hydrocarbons in Coal and Petroleum. *Nature*, *222*, 257–259. <https://doi.org/10.1038/222257a0>
- Burnham, A. K., Clarkson, J. E., Singleton, M. F., Wong, C. M., & Crawford, R. W. (1982). Biological markers from Green River kerogen decomposition. *Geochim. Cosmochim. Acta*, *46*, 1243–1251. [https://doi.org/10.1016/0016-7037\(82\)90009-6](https://doi.org/10.1016/0016-7037(82)90009-6)
- Carter, J., Quantin, C., Thollot, P., Loizeau, D., Ody, A., & Lozach, L. (2016). Oxia Planum: A Clay-Laden Landing Site Proposed for the ExoMars Rover Mission: Aqueous Mineralogy and Alteration Scenarios. Paper presented at the 47th Lunar and Planetary Science Conference, The Woodlands, Texas.
- Cottrell, T. L. (1954). *The strengths of chemical bonds*. London: Butterworth Scientific Publications.
- Didyk, B. M., Simoneit, B. R. T., Brassell, S. C., & Eglinton, G. (1978). Organic geochemical indicators of palaeoenvironmental conditions of sedimentation. *Nature*, *272*, 216–222. <https://doi.org/10.1038/272216a0>
- Duda, J.-P., Van Kranendonk, M. J., Thiel, V., Ionescu, D., Strauss, H., Schäfer, N., & Reitner, J. (2016). A Rare Glimpse of Paleoarchean Life: Geobiology of an Exceptionally Preserved Microbial Mat Facies from the 3.4 Ga Strelley Pool Formation, Western Australia. *PLoS ONE*, *11*, e0147629. <https://doi.org/10.1371/journal.pone.0147629>
- Duda, J.-P., Thiel, V., Bauersachs, T., Mißbach, H., Reinhardt, M., Schäfer, N., Van Kranendonk, M. J., & Reitner, J. (2018). Ideas and perspectives: hydrothermally driven redistribution and sequestration of early Archaean biomass – the “hydrothermal pump hypothesis”. *Biogeosciences*, *15*, 1535–1548. <https://doi.org/10.5194/bg-15-1535-2018>
- Durand, B. (1980). Sedimentary organic matter and kerogen. Definition and quantitative importance of kerogen. In B. Durand (Ed.), *Kerogen: Insoluble organic matter from sedimentary rocks* (pp. 13–34). Paris: Editions Technip.
- Eglinton, T. I., Sinninghe Damsté, J. S., Pool, W., de Leeuw, J. W., Eijk, G., & Boon, J. J. (1992). Organic sulphur in macromolecular sedimentary organic matter. II. Analysis of distributions of sulphur-containing pyrolysis products using multivariate techniques. *Geochim. Cosmochim. Acta*, *56*, 1545–1560. [https://doi.org/10.1016/0016-7037\(92\)90224-7](https://doi.org/10.1016/0016-7037(92)90224-7)
- Eigenbrode, J. L., Summons, R. E., Steele, A., Freissinet, C., Millan, M., Navarro-González, R., Sutter, B., McAdam, A. C., Franz, H. B., Glavin, D. P., Archer Jr, P. D., Mahaffy, P. R., Conrad, P. G., Hurowitz, J. A., Grotzinger, J. P., Gupta, S., Ming, D. W., Sumner, D. Y., Szopa, C., Malespin, C., Buch, A., & Coll, P. (2018). Organic matter preserved in 3-billion-year-old mudstones at Gale crater, Mars. *Science*, *360*, 1096–1101. <https://doi.org/10.1126/science.aas9185>

- Flynn, G. J. (1996). The Delivery of Organic Matter from Asteroids and Comets to the Early Surface of Mars. In H. Rickman & M. J. Valtonen (Eds.), *Worlds in Interaction: Small Bodies and Planets of the Solar System* (pp. 469–474). Dordrecht: Springer.
- Freissinet, C., Glavin, D. P., Mahaffy, P., Miller, K. E., Eigenbrode, J. L., Summons, R. E., Brunner, A. E., Buch, A., Szopa, C., Archer Jr, P. D., Franz, H. B., Atreya, S. K., Brinckerhoff, W. B., Cabane, M., Coll, P., Conrad, P. G., Des Marais, J., Dworkin, J. P., Fairén, A. G., François, P., Grotzinger, J. P., Kashyap, S., ten Kate, I. L., Leshin, L. A., Malespin, C., Martin, M. G., Martin-Torres, F. J., McAdam, A. C., Ming, D. W., Navarro-González, R., Pavlov, A. A., Prats, B. D., Squyres, S. W., Steele, A., Stern, J. C., Sumner, D. Y., Sutter, B., Zorzano, M.-P., & the MSL Science Team (2015). Organic molecules in the Sheepbed Mudstone, Gale Crater, Mars. *J. Geophys. Res. Planets*, *120*, 495–514. <https://doi.org/10.1002/2014JE004737>
- Gelin, F., Sinninghe Damsté, J. S., Harrison, W. N., Maxwell, J. R., & de Leeuw, J. W. (1995). Molecular indicators for palaeoenvironmental change in a Messinian evaporitic sequence (Vena del Gesso, Italy): III. Stratigraphic changes in the molecular structure of kerogen in a single marl bed as revealed by flash pyrolysis. *Org. Geochem.*, *23*, 555–566. [https://doi.org/10.1016/0146-6380\(95\)00041-C](https://doi.org/10.1016/0146-6380(95)00041-C)
- Grice, K., Cao, C., Love, G. D., Böttcher, M. E., Twitchett, R. J., Grosjean, E., Summons, R. E., Turgeon, S. C., Dunning, W., & Jin, Y. (2005). Photic zone euxinia during the permian-triassic superanoxic event. *Science*, *307*, 706–709. <https://doi.org/10.1126/science.1104323>
- Goesmann, F., Brinckerhoff, W. B., Raulin, F., Goetz, W., Danell, R. M., Getty, S. A., Siljeström, S., Mißbach, H., Steininger, H., Arevalo Jr., R. D., Buch, A., Freissinet, C., Grubisic, A., Meierhenrich, U. J., Pinnick, V. T., Stalport, F., Szopa, C., Vago, J. L., Lindner, R., Schulte, M., Brucato, J. R., Glavin, D. P., Grand, N., Li, X., van Amerom, F. H. W., & the MOMA Science Team (2017). The Mars Organic Molecule Analyzer (MOMA) Instrument: Characterization of Organic Material in Martian Sediments. *Astrobiology*, *17*, 655–685. <https://doi.org/10.1089/ast.2016.1551>
- Goetz, W., Brinckerhoff, W. B., Arevalo Jr., R. D., Freissinet, C., Getty, S. A., Glavin, D. P., Siljeström, S., Buch, A., Stalport, F., Grubisic, A., Li, X., Pinnick, V. T., Danell, R. M., van Amerom, F. H. W., Goesmann, F., Steininger, H., Grand, N., Raulin, F., Szopa, C., Meierhenrich, U. J., Brucato, J. R., & the MOMA Science Team (2016). MOMA: the challenge to search for organics and biosignatures on Mars. *Int. J. Astrobiol.*, *15*, 239–250. <https://doi.org/10.1017/S1473550416000227>
- Hallmann, C., Kelly, A. E., Gupta, S. N., & Summons, R. E. (2011). Reconstructing Deep-Time Biology with Molecular Fossils. In M. Laflamme, J. D. Schiffbauer & S. Q. Dornbos (Eds.), *Quantifying the Evolution of Early Life* (pp. 355–401). Dordrecht: Springer.
- Hartgers, W. A., Sinninghe Damsté, J. S., & de Leeuw, J. W. (1994a). Geochemical significance of alkylbenzene distributions in flash pyrolysates of kerogens, coals, and asphaltenes. *Geochim. Cosmochim. Acta*, *58*, 1759–1775. [https://doi.org/10.1016/0016-7037\(94\)90535-5](https://doi.org/10.1016/0016-7037(94)90535-5)
- Hartgers, W. A., Sinninghe Damsté, J. S., Requejo, A. G., Allan, J., Hayes, J. M., Ling, Y., Xie, T.-M., Primack, J., & de Leeuw, J. W. (1994b). A molecular and carbon isotopic study towards the origin and diagenetic fate of diaromatic carotenoids. *Org. Geochem.*, *22*, 703–725. [https://doi.org/10.1016/0146-6380\(94\)90134-1](https://doi.org/10.1016/0146-6380(94)90134-1)
- Hassler, D. M., Zeitlin, C., Wimmer-Schweingruber, R. F., Ehresmann, B., Rafkin, S., Eigenbrode, J. L., Brinza, D. E., Weigle, G., Böttcher, S., Böhm, E., Burmeister, S., Guo, J., Köhler, J., Martin, C., Reitz, G., Cucinotta, F. A., Kim, M.-H., Grinspoon, D., Bullock, M. A., Posner, A., Gómez-Elvira, J., Vasvada, A., Grotzinger, J. P., & MSL Science Team (2014). Mars' Surface Radiation Environment Measured with the Mars Science Laboratory's Curiosity Rover. *Science*, *343*, 1244797. <https://doi.org/10.1126/science.1244797>
- Hecht, M. H., Kounaves, S. P., Quinn, R. C., West, S. J., Young, S. M. M., Ming, D. W., Catling, D. C., Clark, B. C., Boynton, W. V., Hoffman, J., DeFlores, L. P., Gospodinova, K., Kapit, J., & Smith, P. H. (2009). Detection of Perchlorate and the Soluble Chemistry of Martian Soil at the Phoenix Lander Site. *Science*, *325*, 64–67. <https://doi.org/10.1126/science.1172466>
- Hickman-Lewis, K., Cavalazzi, B., Foucher, F., & Westall, F. (2018). Most ancient evidence for life in the Barberton greenstone belt: Microbial mats and biofabrics of the ~3.47 Ga Middle Marker horizon. *Precambrian Res.*, *312*, 45–67. <https://doi.org/10.1016/j.precamres.2018.04.007>
- Horsfield, B. (1989). Practical criteria for classifying kerogens: Some observations from pyrolysis-gas chromatography. *Geochim. Cosmochim. Acta*, *53*, 891–901. [https://doi.org/10.1016/0016-7037\(89\)90033-1](https://doi.org/10.1016/0016-7037(89)90033-1)
- Horsfield, B., & Douglas, A. G. (1980). The influence of minerals on the pyrolysis of kerogens. *Geochim. Cosmochim. Acta*, *44*, 1119–1131. [https://doi.org/10.1016/0016-7037\(80\)90066-6](https://doi.org/10.1016/0016-7037(80)90066-6)

- Huizinga, B. J., Tannenbaum, E., & Kaplan, I. R. (1987). The role of minerals in the thermal alteration of organic matter—III. Generation of bitumen in laboratory experiments. *Org. Geochem.*, *11*, 591–604. [https://doi.org/10.1016/0146-6380\(87\)90012-X](https://doi.org/10.1016/0146-6380(87)90012-X)
- Huizinga, B. J., Aizenshtat, Z. A., & Peters, K. E. (1988). Programmed Pyrolysis-Gas Chromatography of Artificially Matured Green River Kerogen. *Energy Fuels*, *2*, 74–81.
- Hurowitz, J. A., Grotzinger, J. P., Fischer, W. W., McLennan, S. M., Milliken, R. E., Stein, N., Vasavada, A. R., Blake, D. F., Dehouck, E., Eigenbrode, J. L., Fairén, A. G., Frydenvang, J., Gellert, R., Grant, J. A., Gupta, S., Herkenhoff, K. E., Ming, D. W., Rampe, E. B., Schmidt, M. E., Siebach, K. L., Stack-Morgan, K., Sumner, D. Y., & Wiens, R. C. (2017). Redox stratification of an ancient lake in Gale crater, Mars. *Science*, *356*. <https://doi.org/10.1126/science.aah6849>
- Katritzky, A. R., Lobanov, V. S., & Karelson, M. (1998). Normal Boiling Points for Organic Compounds: Correlation and Prediction by a Quantitative Structure–Property Relationship. *J. Chem. Inf. Comput. Sci.*, *38*, 28–41. <https://doi.org/10.1021/ci970029v>
- Koopmans, M. P., Köster, J., van Kaam-Peters, H. M. E., Kenig, F., Schouten, S., Hartgers, W. A., de Leeuw, J. W., & Sinninghe Damsté, J. S. (1996a). Diagenetic and catagenetic products of isorenieratene: Molecular indicators for photic zone anoxia. *Geochim. Cosmochim. Acta*, *60*, 4467–4496. [https://doi.org/10.1016/S0016-7037\(96\)00238-4](https://doi.org/10.1016/S0016-7037(96)00238-4)
- Koopmans, M. P., de Leeuw, J. W., Lewan, M. D., & Sinninghe Damsté, J. S. (1996b). Impact of dia- and catagenesis on sulphur and oxygen sequestration of biomarkers as revealed by artificial maturation of an immature sedimentary rock. *Org. Geochem.*, *25*, 391–426. [https://doi.org/10.1016/S0146-6380\(96\)00144-1](https://doi.org/10.1016/S0146-6380(96)00144-1)
- Leif, R. N., & Simoneit, B. R. T. (1995). Ketones in hydrothermal petroleum and sediment extracts from Guaymas Basin, Gulf of California. *Org. Geochem.*, *23*, 889–904. [https://doi.org/10.1016/0146-6380\(95\)00085-2](https://doi.org/10.1016/0146-6380(95)00085-2)
- Leif, R. N., & Simoneit, B. R. T. (2000). The role of alkenes produced during hydrous pyrolysis of a shale. *Org. Geochem.*, *31*, 1189–1208. [https://doi.org/10.1016/S0146-6380\(00\)00113-3](https://doi.org/10.1016/S0146-6380(00)00113-3)
- Li, X., Danell, R. M., Pinnick, V. T., Grubisic, A., van Amerom, F. H. W., Arevalo Jr., R. D., Getty, S. A., Brinckerhoff, W. B., Southard, A. E., Gonnensen, Z., D., & Adachi, T. (2017). Mars Organic Molecule Analyzer (MOMA) laser desorption/ionization source design and performance characterization. *Int. J. Mass Spectrom.*, *422*, 177–187. <https://doi.org/10.1016/j.ijms.2017.03.010>
- Love, G. D., Stalvies, C., Grosjean, E., Meredith, W., & Snape, C. E. (2008). Analysis of molecular biomarkers covalently bound within Neoproterozoic sedimentary kerogen. In P. H. Kelley & R. K. Bambach (Eds.), *From Evolution to Geobiology: Research Questions Driving Paleontology at the Start of a New Century* (pp. 67–83). New Haven: Paleontological Society Papers.
- Lv, G., & Wu, S. (2012). Analytical pyrolysis studies of corn stalk and its three main components by TG-MS and Py-GC/MS. *J. Anal. Appl. Pyrolysis*, *97*, 11–18. <https://doi.org/10.1016/j.jaap.2012.04.010>
- Marshall, C. P., Love, G. D., Snape, C. E., Hill, A. C., Allwood, A. C., Walter, M. R., Van Kranendonk, M. J., Bowden, S. A., Sylva, S. P., & Summons, R. E. (2007). Structural characterization of kerogen in 3.4 Ga Archaean cherts from the Pilbara Craton, Western Australia. *Precambrian Res.*, *155*, 1–23. <https://doi.org/10.1016/j.precamres.2006.12.014>
- McCullom, T. M., Simoneit, B. R. T., & Shock, E. L. (1999). Hydrous Pyrolysis of Polycyclic Aromatic Hydrocarbons and Implications for the Origin of PAH in Hydrothermal Petroleum. *Energy Fuels*, *13*, 401–410. <https://doi.org/10.1021/ef980089i>
- McDonald, G. D., de Vanssay, E., & Buckley, J. R. (1998). Oxidation of Organic Macromolecules by Hydrogen Peroxide: Implications for Stability of Biomarkers on Mars. *Icarus*, *132*, 170–175. <https://doi.org/10.1006/icar.1998.5896>
- van de Meent, D., Brown, S. C., Philp, R. P., & Simoneit, B. R. T. (1980). Pyrolysis-high resolution gas chromatography and pyrolysis gas chromatography-mass spectrometry of kerogens and kerogen. *Geochim. Cosmochim. Acta*, *44*, 999–1013. [https://doi.org/10.1016/0016-7037\(80\)90288-4](https://doi.org/10.1016/0016-7037(80)90288-4)
- Mißbach, H. (2018). *Formation and preservation of abiotic organic signatures vs. lipid biomarkers—experimental studies in preparation for the ExoMars 2020 mission*. PhD thesis, University of Göttingen, Göttingen.
- Moldoveanu, S. C. (2010). *Pyrolysis of organic molecules with applications to health and environmental issues*. Amsterdam: Elsevier.
- Nishihara, M., & Koga, Y. (1995). Two new phospholipids, hydroxyarchaetidylglycerol and hydroxyarchaetidylethanolamine, from the Archaea *Methanosarcina barkeri*. *Biochim. Biophys. Acta*, *1254*, 155–160. [https://doi.org/10.1016/0005-2760\(94\)00178-2](https://doi.org/10.1016/0005-2760(94)00178-2)

- Pavlov, A. A., Vasilyev, G., Ostryakov, V. M., Pavlov, A. K., & Mahaffy, P. (2012). Degradation of the organic molecules in the shallow subsurface of Mars due to irradiation by cosmic rays. *Geophys. Res. Lett.*, *39*, L13202. <https://doi.org/10.1029/2012GL052166>
- Quantin, C., Carter, J., Thollot, P., Broyer, J., Lozach, L., Davis, J., Grindrod, P., Pajola, M., Baratti, E., Rossato, S., Allemand, P., Bultel, B., Leyrat, C., Fernando, J., & Ody, A. (2016). Oxia Planum, the landing site for ExoMars 2018. Paper presented at the 47th Lunar and Planetary Science Conference, The Woodlands, Texas.
- Regtop, R. A., Ellis, J., Crisp, P. T., Ekstrom, A., & Fookes, C. J. R. (1985). Pyrolysis of model compounds on spent oil shales, minerals and charcoal: Implications for shale oil composition. *Fuel*, *64*, 1640–1646. [https://doi.org/10.1016/0016-2361\(85\)90387-4](https://doi.org/10.1016/0016-2361(85)90387-4)
- Reinhardt, M., Duda, J.-P., Blumenberg, M., Ostertag-Hennings, C., Reitner, J., Heim, C., & Thiel, V. (2018). The taphonomic fate of isorenieratene in Lower Jurassic shales—controlled by iron? *Geobiology*, *16*, 237–251. <https://doi.org/10.1111/gbi.12284>
- Reinhardt, M., Goetz, W., Duda, J.-P., Heim, C., Reitner, J., & Thiel, V. (2019). Organic signatures in Pleistocene cherts from Lake Magadi (Kenya), analogs for early Earth hydrothermal deposits. *Biogeosci. Discuss.* <https://doi.org/10.5194/bg-2018-513>
- Scrima, D. A., Yen, T. F., & Warren, P. L. (2007). Thermal Chromatography of Green River Oil Shale I. Bitumen and Kerogen. *Energy Sources*, *1*, 312–336. <https://doi.org/10.1080/00908317408945929>
- Sephton, M. A. (2002). Organic compounds in carbonaceous meteorites. *Nat. Prod. Rep.*, *19*, 292–311. <https://doi.org/10.1039/B103775G>
- Sephton, M. A., Love, G. D., Watson, J. S., Verchovsky, A. B., Wright, I. P., Snape, C. E., & Gilmour, I. (2004). Hydropyrolysis of insoluble carbonaceous matter in the Murchison meteorite: new insights into its macromolecular structure. *Geochim. Cosmochim. Acta*, *68*, 1385–1393. <https://doi.org/10.1016/j.gca.2003.08.019>
- Sephton, M. A., Love, G. D., Meredith, W., Snape, C. E., Sun, C.-G., & Watson, J. S. (2005). Hydropyrolysis: A new technique for the analysis of macromolecular material in meteorites. *Planet. Space Sci.*, *53*, 1280–1286. <https://doi.org/10.1016/j.pss.2005.06.008>
- Sinninghe Damsté, J. S., & de Leeuw, J. W. (1990). Analysis, structure and geochemical significance of organically-bound sulphur in the geosphere: State of the art and future research. *Org. Geochem.*, *16*, 1077–1101. [https://doi.org/10.1016/0146-6380\(90\)90145-P](https://doi.org/10.1016/0146-6380(90)90145-P)
- Steinbeiss, S., Schmidt, C. M., Heide, K., & Gleixner, G. (2006). $\delta^{13}\text{C}$ values of pyrolysis products from cellulose and lignin represent the isotope content of their precursors. *J. Anal. Appl. Pyrolysis*, *75*, 19–26. <https://doi.org/10.1016/j.jaap.2005.03.009>
- Steininger, H., Goesmann, F., & Goetz, W. (2012). Influence of magnesium perchlorate on the pyrolysis of organic compounds in Mars analogue soils. *Planet. Space Sci.*, *71*, 9–17. <https://doi.org/10.1016/j.pss.2012.06.015>
- Summons, R. E., & Powell, T. G. (1986). Chlorobiaceae in Palaeozoic seas revealed by biological markers, isotopes and geology. *Nature*, *319*, 763–765. <https://doi.org/10.1038/319763a0>
- Tannenbaum, E., & Kaplan, I. R. (1985). Role of minerals in the thermal alteration of organic matter—I: Generation of gases and condensates under dry condition. *Geochim. Cosmochim. Acta*, *49*, 2589–2604. [https://doi.org/10.1016/0016-7037\(85\)90128-0](https://doi.org/10.1016/0016-7037(85)90128-0)
- Tissot, B. P., & Welte, D. H. (1984). *Petroleum formation and occurrence*, 2nd edn. Berlin: Springer. <https://doi.org/10.1007/978-3-642-87813-8>
- Wakeham, S. G., Sinninghe Damsté, J. S., Kohnen, M. E. L., & de Leeuw, J. W. (1995). Organic sulfur compounds formed during early diagenesis in Black Sea sediments. *Geochim. Cosmochim. Acta*, *59*, 521–533. [https://doi.org/10.1016/0016-7037\(94\)00361-O](https://doi.org/10.1016/0016-7037(94)00361-O)
- Ueno, Y., Yurimoto, H., Yoshioka, H., Komiya, T., & Maruyama, S. (2002). Ion microprobe analysis of graphite from ca. 3.8 Ga metasediments, Isua supracrustal belt, West Greenland: Relationship between metamorphism and carbon isotopic composition. *Geochim. Cosmochim. Acta*, *66*, 1257–1268. [https://doi.org/10.1016/S0016-7037\(01\)00840-7](https://doi.org/10.1016/S0016-7037(01)00840-7)
- Vago, J. L., Westall, F., Pasteur Instrument Teams, Landing Site Selection Working Group, & Other Contributors (2017). Habitability on Early Mars and the Search for Biosignatures with the ExoMars Rover. *Astrobiology*, *17*, 471–510. <https://doi.org/10.1089/ast.2016.1533>
- Westall, F., Foucher, F., Bost, N., Bertrand, M., Loizeau, D., Vago, J. L., Kminek, G., Gaboyer, F., Campbell, K. A., Bréhéret, J.-G., Gautret, P., & Cockell, C. S. (2015). Biosignatures on Mars: What, Where, and How?

- Implications for the Search for Martian Life. *Astrobiology*, 15, 998–1029. <https://doi.org/10.1089/ast.2015.1374>
- van Zuilen, M. A., Lepland, A., Teranes, J., Finarelli, J., Wahlen, M., & Arrhenius, G. (2003). Graphite and carbonates in the 3.8 Ga old Isua Supracrustal Belt, southern West Greenland. *Precambrian Res.*, 126, 331–348. [https://doi.org/10.1016/S0301-9268\(03\)00103-7](https://doi.org/10.1016/S0301-9268(03)00103-7)
- van Zuilen, M. A., Mathew, K., Wopenka, B., Lepland, A., Marti, K., & Arrhenius, G. (2005). Nitrogen and argon isotopic signatures in graphite from the 3.8-Ga-old Isua Supracrustal Belt, Southern West Greenland. *Geochim. Cosmochim. Acta*, 69, 1241–1252. <https://doi.org/10.1016/j.gca.2004.08.033>

6 Assessing the formation and preservation of organic signatures on Oxia Planum

The ExoMars 2020 rover will search for (molecular) biosignatures in Noachian to Hesperian (ca. 3.9–3.0 Ga) sediments at Oxia Planum ([chapter 1](#), Fig. 1.1). The mission success will strongly depend on whether the formation, accumulation and preservation of sufficient amounts of organic matter was possible at this site or still is today. To tackle this question, this thesis is aimed at assessing the formation and preservation of organic matter in analog settings from Earth. The obtained findings are of fundamental meaning for the interpretation of possible organic signatures, including the identification of biosignatures, by the ExoMars 2020 rover.

6.1 Origin of organic matter on Oxia Planum

Organic matter can generally be formed through biological and abiological processes. Abiogenic pathways that are considered relevant for Mars include (i) synthesis in solar nebula (e.g., Anders et al., 1973; Ciesla & Sandford, 2012), (ii) Fischer–Tropsch-type synthesis (e.g., McCollom et al., 1999; Rushdi & Simoneit, 2001; Mißbach et al., 2018), (iii) formation during impacts (Steele et al., 2016) and (iv) the electrochemical reduction of CO₂ (Steele et al., 2018).

6.1.1 Abiogenic processes

Oxia Planum is a cratered terrain (cf., Carter et al., 2016; Quantin et al., 2016) that shaped particularly during the early periods of Martian history when impact rates were high (e.g., Hartmann & Neukum, 2001; Frey, 2006). Chondrites, comets or interplanetary dust particles may have delivered abiogenic organic matter to Oxia Planum that formed in a protoplanetary disk (Flynn, 1996; Ehrenfreund & Charnley, 2000; Westall et al., 2015). Such organic matter potentially includes amino- and carboxylic acids (e.g., Ehrenfreund et al., 2001; Botta & Bada, 2002; Sephton, 2002) and macromolecular moieties mainly consisting of PAHs (e.g., Pendleton & Allamandola, 2002; Sephton et al., 2004, 2005). Furthermore, refractory organic matter like graphite may have been formed during impacts (Steele et al., 2016).

Oxia Planum likely represents a fluvio-deltaic basin that hosted a standing water body during Noachian–Hesperian times (Carter et al., 2016; Quantin et al., 2016; Vago et al., 2017). During these early phases (especially Noachian) Mars was severely affected by widespread volcanism (e.g., Williams et al., 2008; Carr & Head III, 2010; Xiao et al., 2012), and there is further evidence of volcanic activity at Oxia Planum during the Amazonian (ca. 2.6 Ga old lavas; Carter et al., 2016). It appears therefore likely that subaquatic hydrothermal systems have established in some areas (cf., Farmer, 1996; [chapter 1](#); Fig. 6.1). Such environments may have promoted the abiogenic formation of organic matter via Fischer–Tropsch-type reactions or electrochemical reduction of CO₂.

Fischer–Tropsch-type synthesis in natural environments on Earth is associated with serpentinization, a hydrothermal alteration process that typically involves the conversion of olivine to serpentine in the presence of water (Moody, 1976). This reaction yields hydrogen, which can then further react with endogenic CO₂ to form organic molecules (Berndt et al., 1996; Holm & Charlou, 2001). Serpentine was detected on various localities of Mars (Ehlmann et al., 2010), but so far not at Oxia Planum. Electrochemical reduction of CO₂, on the other hand, requires the presence of minerals that exhibit an electrochemical potential (e.g., magnetite and sulfides; Steele et al., 2018), but these have not been detected by orbital observations in Oxia Planum sediments. Consequently, the operation of both processes on Oxia Planum remains questionable.

6.1.2 Biology

Hydrothermal environments are commonly considered as habitats for early life on Earth (e.g., Van Kranendonk, 2006 and references therein; Martin et al., 2008; [chapter 1](#)) and it has therefore been hypothesized that simple prokaryotic life forms may have also evolved in hydrothermal environments on Mars (e.g., Schulte et al., 2006; Westall et al., 2015; Vago et al., 2017). For instance, chemoautotrophs may have lived at hydrothermal vents or in the surrounding crust (Fig. 6.1; see also Vago et al., 2017). It may also be possible that a heterotrophic lifestyle evolved at places of organic carbon availability, including organisms feeding on meteoritic organics (Fig. 6.1). Fermentation, for instance, represents a simple biochemical pathway that uses organic molecules as both, electron

donor and acceptor (see Westall et al., 2015, their Tab. 1). Such heterotrophic lifestyle is also considered as one of the most primitive on Earth (cf., Lazcano & Miller, 1999; Westall et al., 2015). Both scenarios fit into a hypothetical Oxia Planum environment at Noachian-Hesperian times (Fig. 6.1). If life ever evolved on Mars, it may also be possible that it survived in protected subsurface environments until today.

6.1.3 Discrimination between biogenic and abiogenic organic matter

Biology, as we know it from Earth, is selective and synthesizes only a limited variety of what would be chemically possible (see Summons et al., 2008). Distribution patterns or chain-length-preferences that deviate from abiogenic statistical distributions (decrease in abundance with increase in carbon number; see McCollom et al., 1999; Rushdi & Simoneit, 2001; Mißbach et al., 2018) can therefore also be used to trace biological activity. Organic signatures in sub-recent and early Archean rocks exhibit such specific traits ([chapter 2](#), Reinhardt et al., 2019; [chapter 3](#), Duda et al. 2018). These criteria may also be applicable to Mars.

In [chapter 2](#) (Reinhardt et al., 2019) and [chapter 4](#) (Reinhardt et al., 2018) unambiguous biomarkers were identified (e.g. diaryl isoprenoids, like isorenieratane, acyclic isoprenoids, glycerol mono- and diethers) that could be directly linked to precursor organisms. In contrast, other organic compounds, including alkanolic acids, alkanols or alkanes, can be of both, biological or abiotic origin (see [chapter 2](#), Reinhardt et al., 2019; [chapter 3](#), Duda et al., 2018; [chapter 4](#), Reinhardt et al., 2018; Eglinton & Hamilton, 1967; McCollom et al., 1999; Rushdi & Simoneit, 2001; Mißbach et al., 2018). However, the study in [chapter 5](#) (Reinhardt et al., to be submitted) demonstrated that pyrolysis gas chromatography–mass spectrometry (GC–MS) as applied by the Mars Organic Molecule Analyzer (MOMA) produces ambiguous secondary pyrolysis products that may not be linked to a single precursor and blur primary signals. In addition, single temperature steps during pyrolysis may be influenced by carryover effects (Fig. 5.4) and the technique is only able to detect low molecular weight organics (Fig. D1–2; see also Goesmann et al., 2017; Mißbach, 2018). It will therefore be necessary to combine all possible MOMA techniques, including laser desorption/ionization–mass spectrometry (LDI–MS; Li et al., 2017), as well as derivatization and thermochemolysis GC–MS (Goesmann et al., 2017), in order to interpret potential organic signals and identify biosignatures.

6.2 Preservation of organic matter on Oxia Planum

Mars opens a rare window into deep-time geology, as plate tectonics probably did not evolve on that planet (van Thienen et al., 2004). In addition to the scenarios discussed above, organic matter (independent from its origin) could have been transported to Oxia Planum by water through channels from its surroundings (e.g., Cogoon Vallis; see Quantin et al., 2016) and remained near the surface for billions of years. However, the Martian surface represents a highly destructive regime for organic substances, as UV-radiation is strong and oxidants (like perchlorates) are ubiquitous (e.g., Hecht et al., 2009; Pavlov et al., 2012). Therefore, the ExoMars 2020 rover can obtain drill samples from depths ≤ 2 m, but various destructive processes, particularly volcanism and impacts in the early history of Mars, have not been restricted to the surface (see 6.1; cf., Westall et al., 2015). A long-term preservation of organic matter on Mars appears to be challenging.

Clay minerals, as detected on Oxia Planum, may promote organic matter preservation through adsorption onto their surfaces (e.g., Kennedy et al., 2002; Ehlmann et al., 2008; Summons et al., 2011). Furthermore, the formation of macromolecular organic matter, like kerogen, can shield incorporated organic molecules, at least to some extent, against thermal alteration (cf., Brocks et al., 2003; Marshall et al., 2007; Love et al., 2008; Hallmann et al., 2011; Eigenbrode et al., 2018). These macromolecules may also partly survive oxidative degradation under Martian conditions (McDonald et al., 1998; Eigenbrode et al., 2018). However, the formation and preservation of macromolecular organic matter is still incompletely understood, and needs further investigation.

On Earth, organic molecules are already incorporated into the macromolecular network during earliest diagenesis, e.g., through the formation of sulfur bonds (e.g., Sinninghe Damsté & de Leeuw, 1990; Hartgers et al., 1994). Results from the SAM instrument onboard the Curiosity rover suggest that sulfurization may have occurred on Mars in sediments from Gale Crater (Eigenbrode et al., 2018; see Fig. 1.1 for location). It is as yet unknown whether sulfur was available on Oxia Planum during Noachian-Hesperian times, but reduced iron (Fe^{2+}) may have been abundant (cf., Carter et al., 2016). The study in [chapter 4](#) (Reinhardt et al., 2018) showed that abundant Fe^{2+} can hinder the formation of organic sulfur bonds and thus effectively hamper the incorporation of organic biomolecules (e.g., aromatic carotenoids; see Fig. 4.5). In such environments, organic molecules will rather be preserved as free moieties in the bitumen phase and are thus much more prone to secondary degradation processes.

- Botta, O., & Bada, J. L. (2002). Extraterrestrial Organic Compounds in Meteorites. *Surv. Geophys.*, *23*, 411–467. <https://doi.org/10.1023/A:1020139302770>
- Brocks, J. J., Love, G. D., Snape, C. E., Logan, G. A., Summons, R. E., & Buick, R. (2003). Release of bound aromatic hydrocarbons from late Archean and Mesoproterozoic kerogens via hydrolysis. *Geochim. Cosmochim. Acta*, *67*, 1521–1530. [https://doi.org/10.1016/S0016-7037\(02\)01302-9](https://doi.org/10.1016/S0016-7037(02)01302-9)
- Carr, M. H., & Head III, J. W. (2010). Geologic history of Mars. *Earth Planet. Sci. Lett.*, *294*, 185–203. <https://doi.org/10.1016/j.epsl.2009.06.042>
- Carter, J., Quantin, C., Thollot, P., Loizeau, D., Ody, A., & Lozach, L. (2016). Oxia Planum: A Clay-Laden Landing Site Proposed for the ExoMars Rover Mission: Aqueous Mineralogy and Alteration Scenarios. Paper presented at the 47th Lunar and Planetary Science Conference, The Woodlands, Texas.
- Ciesla, F. J., & Sandford, S. A. (2012). Organic Synthesis via Irradiation and Warming of Ice Grains in the Solar Nebula. *Science*, *336*, 452–454. <https://doi.org/10.1126/science.1217291>
- Duda, J.-P., Thiel, V., Bauersachs, T., Mißbach, H., Reinhardt, M., Schäfer, N., Van Kranendonk, M. J., & Reitner, J. (2018). Ideas and perspectives: hydrothermally driven redistribution and sequestration of early Archean biomass – the “hydrothermal pump hypothesis”. *Biogeosciences*, *15*, 1535–1548. <https://doi.org/10.5194/bg-15-1535-2018>
- Eglinton, G., & Hamilton, R. J. (1967). Leaf Epicuticular Waxes. *Science*, *156*, 1322–1335. <https://doi.org/10.1126/science.156.3780.1322>
- Ehlmann, B. L., Mustard, J. F., Fassett, C. I., Schon, S. C., Head III, J. W., Des Marais, J., Grant, J. A., & Murchie, S. L. (2008). Clay minerals in delta deposits and organic preservation potential on Mars. *Nat. Geosci.*, *1*, 355–358. <https://doi.org/10.1038/ngeo207>
- Ehlmann, B. L., Mustard, J. F., & Murchie, S. L. (2010). Geologic setting of serpentine deposits on Mars. *Geophys. Res. Lett.*, *37*, L06201. <https://doi.org/10.1029/2010GL042596>
- Ehrenfreund, P., & Charnley, S. B. (2000). Organic Molecules in the Interstellar Medium, Comets, and Meteorites: A Voyage from Dark Clouds to the Early Earth. *Annu. Rev. Astron. Astrophys.*, *38*, 427–483. <https://doi.org/10.1146/annurev.astro.38.1.427>
- Ehrenfreund, P., Glavin, D. P., Botta, O., Cooper, G., & Bada, J. L. (2001). Extraterrestrial amino acids in Orgueil and Ivuna: Tracing the parent body of CI type carbonaceous chondrites. *PNAS*, *98*, 2138–2141. <https://doi.org/10.1073/pnas.051502898>
- Eigenbrode, J. L., Summons, R. E., Steele, A., Freissinet, C., Millan, M., Navarro-González, R., Sutter, B., McAdam, A. C., Franz, H. B., Glavin, D. P., Archer Jr, P. D., Mahaffy, P. R., Conrad, P. G., Hurowitz, J. A., Grotzinger, J. P., Gupta, S., Ming, D. W., Sumner, D. Y., Szopa, C., Malespin, C., Buch, A., & Coll, P. (2018). Organic matter preserved in 3-billion-year-old mudstones at Gale crater, Mars. *Science*, *360*, 1096–1101. <https://doi.org/10.1126/science.aas9185>
- Farmer, J. D. (1996). Hydrothermal systems on Mars: an assessment of present evidence. In G. R. Bock & J. A. Goode (Eds.), *Evolution of Hydrothermal Ecosystems on Earth (and Mars?)* (pp. 273–299). Chichester: Wiley.
- Flynn, G. J. (1996). The Delivery of Organic Matter from Asteroids and Comets to the Early Surface of Mars. In H. Rickman & M. J. Valtonen (Eds.), *Worlds in Interaction: Small Bodies and Planets of the Solar System* (pp. 469–474). Dordrecht: Springer.
- Frey, H. V. (2006). Impact constraints on, and a chronology for, major events in early Mars history. *J. Geophys. Res. Planets*, *111*, E08S91. <https://doi.org/10.1029/2005JE002449>
- Goemann, F., Brinckerhoff, W. B., Raulin, F., Goetz, W., Danell, R. M., Getty, S. A., Siljeström, S., Mißbach, H., Steininger, H., Arevalo Jr., R. D., Buch, A., Freissinet, C., Grubisic, A., Meierhenrich, U. J., Pinnick, V. T., Stalport, F., Szopa, C., Vago, J. L., Lindner, R., Schulte, M., Brucato, J. R., Glavin, D. P., Grand, N., Li, X., van Amerom, F. H. W., & the MOMA Science Team (2017). The Mars Organic Molecule Analyzer (MOMA) Instrument: Characterization of Organic Material in Martian Sediments. *Astrobiology*, *17*, 655–685. <https://doi.org/10.1089/ast.2016.1551>
- Hallmann, C., Kelly, A. E., Gupta, S. N., & Summons, R. E. (2011). Reconstructing Deep-Time Biology with Molecular Fossils. In M. Laflamme, J. D. Schiffbauer & S. Q. Dornbos (Eds.), *Quantifying the Evolution of Early Life* (pp. 355–401). Dordrecht: Springer.
- Hartgers, W. A., Sinninghe Damsté, J. S., Requejo, A. G., Allan, J., Hayes, J. M., Ling, Y., Xie, T.-M., Primack, J., & de Leeuw, J. W. (1994). A molecular and carbon isotopic study towards the origin and diagenetic fate of diaromatic carotenoids. *Org. Geochem.*, *22*, 703–725. [https://doi.org/10.1016/0146-6380\(94\)90134-1](https://doi.org/10.1016/0146-6380(94)90134-1)

- Hartmann, W. K., & Neukum, G. (2001). Cratering Chronology and the Evolution of Mars. In R. Kallenbach, J. Geiss & W. K. Hartmann (Eds.), *Chronology and Evolution of Mars* (pp. 165–194). Dordrecht: Springer.
- Hecht, M. H., Kounaves, S. P., Quinn, R. C., West, S. J., Young, S. M. M., Ming, D. W., Catling, D. C., Clark, B. C., Boynton, W. V., Hoffman, J., DeFlores, L. P., Gospodinova, K., Kapit, J., & Smith, P. H. (2009). Detection of Perchlorate and the Soluble Chemistry of Martian Soil at the Phoenix Lander Site. *Science*, *325*, 64–67. <https://doi.org/10.1126/science.1172466>
- Holm, N. G., & Charlou, J. L. (2001). Initial indications of abiotic formation of hydrocarbons in the Rainbow ultramafic hydrothermal system, Mid-Atlantic Ridge. *Earth Planet. Sci. Lett.*, *191*, 1–8. [https://doi.org/10.1016/S0012-821X\(01\)00397-1](https://doi.org/10.1016/S0012-821X(01)00397-1)
- Kennedy, M. J., Pevear, D. R., & Hill, R. J. (2002). Mineral Surface Control of Organic Carbon in Black Shale. *Science*, *295*, 657–660. <https://doi.org/10.1126/science.1066611>
- Lalonde, K., Mucci, A., Ouellet, A., & Gélinas, Y. (2012). Preservation of organic matter in sediments promoted by iron. *Nature*, *483*, 198–200. <https://doi.org/10.1038/nature10855>
- Lazcano, A., & Miller, S. L. (1999). On the Origin of Metabolic Pathways. *Journal of Molecular Evolution*, *49*, 424–431. <https://doi.org/10.1007/PL00006565>
- Li, X., Danell, R. M., Pinnick, V. T., Grubisic, A., van Amerom, F. H. W., Arevalo Jr., R. D., Getty, S. A., Brinckerhoff, W. B., Southard, A. E., Gonnens, Z., D., & Adachi, T. (2017). Mars Organic Molecule Analyzer (MOMA) laser desorption/ionization source design and performance characterization. *Int. J. Mass Spectrom.*, *422*, 177–187. <https://doi.org/10.1016/j.ijms.2017.03.010>
- Love, G. D., Stalvies, C., Grosjean, E., Meredith, W., & Snape, C. E. (2008). Analysis of molecular biomarkers covalently bound within Neoproterozoic sedimentary kerogen. In P. H. Kelley & R. K. Bambach (Eds.), *From Evolution to Geobiology: Research Questions Driving Paleontology at the Start of a New Century* (pp. 67–83). New Haven: Paleontological Society Papers.
- Marshall, C. P., Love, G. D., Snape, C. E., Hill, A. C., Allwood, A. C., Walter, M. R., Van Kranendonk, M. J., Bowden, S. A., Sylva, S. P., & Summons, R. E. (2007). Structural characterization of kerogen in 3.4 Ga Archaean cherts from the Pilbara Craton, Western Australia. *Precambrian Res.*, *155*, 1–23. <https://doi.org/10.1016/j.precamres.2006.12.014>
- Martin, W., Baross, J., Kelley, D., & Russell, M. J. (2008). Hydrothermal vents and the origin of life. *Nat. Rev. Microbiol.*, *6*, 805–814. <https://doi.org/10.1038/nrmicro1991>
- McCollom, T. M., Ritter, G., & Simoneit, B. R. T. (1999). Lipid Synthesis Under Hydrothermal Conditions by Fischer–Tropsch-Type Reactions. *Origins Life Evol. Biosphere*, *29*, 153–166. <https://doi.org/10.1023/A:1006592502746>
- McDonald, G. D., de Vanssay, E., & Buckley, J. R. (1998). Oxidation of Organic Macromolecules by Hydrogen Peroxide: Implications for Stability of Biomarkers on Mars. *Icarus*, *132*, 170–175. <https://doi.org/10.1006/icar.1998.5896>
- Mißbach, H. (2018). *Formation and preservation of abiotic organic signatures vs. lipid biomarkers—experimental studies in preparation for the ExoMars 2020 mission*. PhD thesis, University of Göttingen, Göttingen.
- Mißbach, H., Schmidt, B. C., Duda, J.-P., Lünsdorf, N. K., Goetz, W., & Thiel, V. (2018). Assessing the diversity of lipids formed via Fischer–Tropsch-type reactions. *Org. Geochem.*, *119*, 110–121. <https://doi.org/10.1016/j.orggeochem.2018.02.012>
- Moody, 1976
- Pavlov, A. A., Vasilyev, G., Ostryakov, V. M., Pavlov, A. K., & Mahaffy, P. (2012). Degradation of the organic molecules in the shallow subsurface of Mars due to irradiation by cosmic rays. *Geophys. Res. Lett.*, *39*, L13202. <https://doi.org/10.1029/2012GL052166>
- Pendleton, Y. J., & Allamandola, L. J. (2002). The Organic Refractory Material in the Diffuse Interstellar Medium: Mid-Infrared Spectroscopic Constraints. *Astrophys. J. Suppl. Ser.*, *138*, 75–98. <https://doi.org/10.1086/322999>
- Quantin, C., Carter, J., Thollot, P., Broyer, J., Lozach, L., Davis, J., Grindrod, P., Pajola, M., Baratti, E., Rossato, S., Allemand, P., Bultel, B., Leyrat, C., Fernando, J., & Ody, A. (2016). Oxia Planum, the landing site for ExoMars 2018. Paper presented at the 47th Lunar and Planetary Science Conference, The Woodlands, Texas.
- Reinhardt, M., Duda, J.-P., Blumenberg, M., Ostertag-Hennings, C., Reitner, J., Heim, C., & Thiel, V. (2018). The taphonomic fate of isorenieratene in Lower Jurassic shales—controlled by iron? *Geobiology*, *16*, 237–251. <https://doi.org/10.1111/gbi.12284>
- Reinhardt, M., Goetz, W., Duda, J.-P., Heim, C., Reitner, J., & Thiel, V. (2019). Organic signatures in Pleistocene cherts from Lake Magadi (Kenya), analogs for early Earth hydrothermal deposits. *Biogeosci. Discuss.* <https://doi.org/10.5194/bg-2018-513>

- Reinhardt, M., Goetz, W., & Thiel, V.. *Testing MOMA flight-like pyrolysis GC–MS on analog samples from Earth (iron-rich shale and opaline chert)—implications for MOMA pyrolysis during the ExoMars 2020 rover mission.* (unpublished, to be submitted to *Astrobiology*)
- Rushdi, A. I., & Simoneit, B. R. T. (2001). Lipid Formation by Aqueous Fischer–Tropsch-Type Synthesis over a Temperature Range of 100 to 400 °C. *Origins Life Evol. Biosphere*, *31*, 103–118. <https://doi.org/10.1023/A:1006702503954>
- Schulte, M., Blake, D., Hoehler, T., & McCollom, T. M. (2006). Serpentinization and Its Implications for Life on the Early Earth and Mars. *Astrobiology*, *6*, 364–376. <https://doi.org/10.1089/ast.2006.6.364>
- Sephton, M. A. (2002). Organic compounds in carbonaceous meteorites. *Nat. Prod. Rep.*, *19*, 292–311. <https://doi.org/10.1039/B103775G>
- Sephton, M. A., Love, G. D., Watson, J. S., Verchovsky, A. B., Wright, I. P., Snape, C. E., & Gilmour, I. (2004). Hydropyrolysis of insoluble carbonaceous matter in the Murchison meteorite: new insights into its macromolecular structure. *Geochim. Cosmochim. Acta*, *68*, 1385–1393. <https://doi.org/10.1016/j.gca.2003.08.019>
- Sephton, M. A., Love, G. D., Meredith, W., Snape, C. E., Sun, C.-G., & Watson, J. S. (2005). Hydropyrolysis: A new technique for the analysis of macromolecular material in meteorites. *Planet. Space Sci.*, *53*, 1280–1286. <https://doi.org/10.1016/j.pss.2005.06.008>
- Sinninghe Damsté, J. S., & de Leeuw, J. W. (1990). Analysis, structure and geochemical significance of organically-bound sulphur in the geosphere: State of the art and future research. *Org. Geochem.*, *16*, 1077–1101. [https://doi.org/10.1016/0146-6380\(90\)90145-P](https://doi.org/10.1016/0146-6380(90)90145-P)
- Steele, A., McCubbin, F. M., & Fries, M. D. (2016). The provenance, formation, and implications of reduced carbon phases in Martian meteorites. *Meteorit. Planet. Sci.*, *51*, 2203–2225. <https://doi.org/10.1111/maps.12670>
- Steele, A., Benning, L. G., Wirth, R., Siljeström, S., Fries, M. D., Hauri, E., Conrad, P. G., Rogers, K., Eigenbrode, J. L., Schreiber, A., Needham, A., Wang, J. H., McCubbin, F. M., Kiöcoyne, D., & Rodriguez Blanco, J. D. (2018). Organic synthesis on Mars by electrochemical reduction of CO₂. *Sci. Adv.*, *4*, eaat5118. <https://doi.org/10.1126/sciadv.aat5118>
- Summons, R. E., Albrecht, P., McDonald, G. D., & Moldowan, J. M. (2008). Molecular Biosignatures. In O. Botta, J. L. Bada, J. Gomez-Elvira, E. Javaux, F. Selsis & R. E. Summons (Eds.), *Strategies of Life Detection* (pp. 133–159). Boston: Springer.
- Summons, R. E., Amend, J. P., Bish, D., Buick, R., Cody, G. D., Des Marais, J., Dromart, G., Eigenbrode, J. L., Knoll, A. H., & Sumner, D. Y. (2011). Preservation of Martian Organic and Environmental Records: Final Report of the Mars Biosignature Working Group. *Astrobiology*, *11*, 157–181. <https://doi.org/10.1089/ast.2010.0506>
- van Thienen, P., Vlaar, N. J., & van den Berg, A. P. (2004). Plate tectonics on the terrestrial planets. *Phys. Earth Planet. Inter.*, *142*, 61–74. <https://doi.org/10.1016/j.pepi.2003.12.008>
- Vago, J. L., Westall, F., Pasteur Instrument Teams, Landing Site Selection Working Group, & Other Contributors (2017). Habitability on Early Mars and the Search for Biosignatures with the ExoMars Rover. *Astrobiology*, *17*, 471–510. <https://doi.org/10.1089/ast.2016.1533>
- Van Kranendonk, M. J. (2006). Volcanic degassing, hydrothermal circulation and the flourishing of early life on Earth: A review of the evidence from c. 3490–3240 Ma rocks of the Pilbara Supergroup, Pilbara Craton, Western Australia. *Earth Sci. Rev.*, *74*, 197–240. <https://doi.org/10.1016/j.earscirev.2005.09.005>
- Westall, F., Foucher, F., Bost, N., Bertrand, M., Loizeau, D., Vago, J. L., Kminek, G., Gaboyer, F., Campbell, K. A., Bréhéret, J.-G., Gautret, P., & Cockell, C. S. (2015). Biosignatures on Mars: What, Where, and How? Implications for the Search for Martian Life. *Astrobiology*, *15*, 998–1029. <https://doi.org/10.1089/ast.2015.1374>
- Williams, J.-P., Nimmo, F., Moore, W. B., & Paige, D. A. (2008). The formation of Tharsis on Mars: What the line-of-sight gravity is telling us. *J. Geophys. Res. Planets*, *113*. <https://doi.org/10.1029/2007JE003050>
- Xiao, L., Huang, J., Christensen, P. R., Greeley, R., Williams, D. A., Zhao, J., & He, Q. (2012). Ancient volcanism and its implication for thermal evolution of Mars. *Earth Planet. Sci. Lett.*, *323–324*, 9–18. <https://doi.org/10.1016/j.epsl.2012.01.027>

7 Summary, conclusions and outlook

7.1 Summary and conclusions

The primary objective of the ESA/Roscosmos ExoMars program is to determine, if life has ever existed on Mars, particularly in its very early history (Noachian to Hesperian times, ca. 3.9–3.0 Ga; Vago et al., 2017). One central part of this mission is the launch of a solar-powered rover (currently scheduled for 2020) that aims at the identification and interpretation of possible organic (bio-)signatures on the designated ExoMars 2020 landing site Oxia Planum. To tackle this sophisticated goal, the rover is equipped with a drill plus a variety of analytical instruments such as a Raman spectrometer and the Mars Organic Molecule Analyzer (MOMA). This thesis provides a solid basis for the interpretation of expected MOMA data by systematically assessing the fate of organic signatures in various analog materials from Earth (hydrothermal cherts, iron-rich shales). This assessment includes conventional and ExoMars rover relevant techniques like Raman spectroscopy and MOMA flight-like pyrolysis GC–MS. The following questions were specifically addressed:

- (i) What is the origin of the organic matter in the specific analog materials (abiotic vs. biological)?
- (ii) Are unambiguous molecular biosignatures preserved?
- (iii) How are the molecular biosignatures preserved (bitumen vs. kerogen)?
- (iv) Which organic compounds can be detected with MOMA flight-like pyrolysis GC–MS?

Several studies were conducted in order to answer these questions:

The first study focused on organic matter in Pleistocene hydrothermal cherts (Lake Magadi, Kenya), a potential analog for hydrothermal environments on early Mars ([chapter 2](#), Reinhardt et al., 2019). Bitumens contained various immature archaeal and bacterial “biolipids” (e.g., glycerol mono- and diethers, fatty acids and alcohols), but also thermally altered “geolipids” (e.g., *n*-alkanes, hopanes, PAHs). This co-occurrence indicates partial *in-situ* alteration of dissolved organic matter during hydrothermal cycling. Raman spectroscopic features and molecular indices from kerogens also revealed heterogeneities in maturity, indicating admixing of pre-altered macromolecules. Remarkably, isoprenoid biomarkers from archaeal membrane lipids were not hydrothermally degraded, but preserved in kerogen. This demonstrates that lipid biomarkers can survive mild *in-situ* hydrothermal alteration, particularly if incorporated into macromolecular networks.

The second study tackled the origin of kerogen isolated from a ca. 3.5 Ga old hydrothermal vein chert (Dresser Formation, Pilbara Craton, Western Australia), representing fairly the same age as deposits exposed at Oxia Planum ([chapter 3](#), Duda et al., 2018). Raman spectroscopy and molecular maturity parameters demonstrated that the organic matter experienced elevated temperatures (post-oil window maturity). Yet, the kerogen pyrolysate (HyPy) still exhibited *n*-alkanes with a distinct chain-length preference (sharp decrease in abundance $> n-C_{18}$). A similar distribution was found in HyPy pyrolysates of modern bacterial biomass (*Anabaena cylindrica*), but not in products of Fischer–Tropsch-type synthesis. According to these results, the organic matter was likely biologically produced and redistributed by hydrothermal circulation (“hydrothermal pump hypothesis”). This means that organic macromolecules, such as kerogen, may retain molecular traits of biology in mildly thermally matured deposits even over billions of years.

The third study addressed the preservation of aromatic carotenoids, pigments from anoxygenic phototrophs, in anoxic iron- and sulfur-rich shales (Bächental oil shale, Posidonia Shale; Lower Jurassic; [chapter 4](#), Reinhardt et al., 2018). Such anoxic environments are highly beneficial for the preservation of organic matter, e.g., by early diagenetic sulfurization. Despite abundant sulfur (up to 4.6 wt.%), few sulfurized molecules were detected in the samples analyzed. Additionally, the concentration of aromatic carotenoid biomarkers, like isorenieratane, was significantly higher in bitumens as compared to kerogens. The appearance of cyclized isorenieratene derivatives suggests fast aromatization/cyclization processes that hindered sulfurization. In addition, hydrogenation and the reaction of reduced iron with sulfide may have prevented sulfur crosslinking of aromatic carotenoids. In iron-rich environments, like the Fe/Mg-smectite clays of Oxia Planum, organic molecules may therefore rather be preserved in the bitumen than in the kerogen fraction. This finding may have wide implications on long-term organic matter

preservation, as macromolecular networks may facilitate the survival of organic signatures under oxidative conditions on Mars (see McDonald et al., 1998; Eigenbrode et al., 2018).

In the fourth study, organic matter from an opaline chert (pre-characterized in [chapter 2](#), Reinhardt et al., 2019) and an iron-rich shale (pre-characterized in [chapter 4](#), Reinhardt et al., 2018) was further analyzed via MOMA flight-like pyrolysis GC–MS to assess pyrolytic destruction and pyrosynthesis reactions ([chapter 5](#), Reinhardt et al., to be submitted). The experiments indicated that the nature of pyrolysis products is primarily determined by the type of organic matter, rather than differences in mineralogy. Various hydrocarbons that are distinctive for biology (e.g., phytane, aryl isoprenoids) stayed intact during stepwise pyrolysis (300 °C, 500 °C, 700 °C). At the same time, however, pyrolysis caused the artificial formation of products like PAHs, which are per se not specific as life markers and can hardly be related to distinct biological precursors. Products yielded during 500 °C and 700 °C were furthermore obscured through carryover effects. This emphasizes that the interpretation of MOMA-pyrolysis data requires organic matter pre-characterization by LDI–MS (as planned for MOMA operation on Mars), as well as additional input from derivatization and thermochemolysis GC–MS.

[Chapter 6](#) integrates the results from the previous studies to discuss potential scenarios of organic matter preservation (including molecular biosignatures) on Oxia Planum during its early history (Noachian to Hesperian). Based on these findings, it appears likely that depositional controls such as hydrothermal defunctionalization ([chapter 2](#), Reinhardt et al., 2019) and iron-buffering ([chapter 4](#), Reinhardt et al., 2018) may have negatively impacted organic matter preservation at this site (in addition to UV-radiation, perchlorates, early volcanism, and impacts). Despite these restrictions, the formation of macromolecules may still be possible ([chapter 2](#), Reinhardt et al., 2019; [chapter 4](#), Reinhardt et al., 2018), and processes like fast sedimentation or enclosure in dense mineral matrices may further promote the survival of organic molecules over the billions of years after deposition (cf., [chapter 3](#), Duda et al., 2018). In any case, the interpretation of data obtained via MOMA pyrolysis GC–MS will require the integration of findings by all other available MOMA techniques (LDI–MS, derivatization and thermochemolysis GC–MS; [chapter 5](#); Reinhardt et al., to be submitted).

7.2 Outlook

MOMA provides three options to volatilize organic matter for analysis via mass spectrometry (i.e., pyrolysis, chemical derivatization and laser ionization). This thesis includes investigations of MOMA flight-like pyrolysis GC–MS on two samples and two aliphatic hydrocarbon standards ([chapter 5](#), Reinhardt et al., to be submitted). Future MOMA pyrolysis test experiments should include additional analog sample material and organic standard compounds (e.g., carboxylic acids and alcohols). Furthermore, the samples analyzed in [chapter 5](#) should also be tested via MOMA derivatization and thermochemolysis GC–MS, to complement pyrolysis results. The mineralogy of the sample does not appear to significantly affect organic compounds during pyrolysis ([chapter 5](#), Reinhardt et al., to be submitted). However, standard compounds should be spiked on different mineral substrates (e.g., clay vs. opaline silica) to further evaluate potential matrix effects on pyrolysis. Here, it would be particularly important to integrate perchlorates into the experiments (see Mißbach, 2018), as these oxidants may be widespread on the Martian surface.

In conjunction with this thesis, the organic matter of two bulk Magadi chert powders (LM-1692 and LM-1693; [chapter 2](#), Reinhardt et al., 2019) was analyzed via LDI–MS at NASA Goddard Space Flight Center (Greenbelt, USA). These preliminary analyses showed promising results in that LDI produced numerous ions from organic and inorganic compounds in the samples. The identification of these ions, however, is still incomplete and needs further investigation. LDI–MS analysis of standards that contain similar organic molecules as the rock samples will help to pinpoint ion patterns that are characteristic for distinctive individual compounds. This strategy should then be extended to samples from other Mars-relevant environments that contain different organic inventories (e.g., Bächtal; [chapter 4](#), Reinhardt et al., 2018). The expected results will support the validation and interpretation of data obtained during the ExoMars 2020 rover mission.

Future studies should also focus on organic signature preservation in further analog settings, potentially in combination with systematic field experiments. For instance, it would be important to experimentally assess organic matter production and preservation in extremely dry terrestrial environments such as the Atacama Desert (see Navarro-González et al., 2003; Quinn et al., 2005). The impact-related alteration of organic matter (specifically the preservation of organic biosignatures) could be investigated in terrestrial impact craters. One particularly interesting target for such endeavors are organic-rich deposits in the Nördlinger Ries (Bavaria,

Germany), a Miocene crater similar to those found on Mars (e.g., Pohl et al., 1977; Kenkmann & Schönian, 2006; Arp et al., 2019).

References

- Arp, G., Schultz, S., Karius, V., & Head III, J. W. (2019). Ries impact crater sedimentary conglomerates: Sedimentary particle 'impact pre-processing', transport distances and provenance, and implications for Gale crater conglomerates, Mars. *Icarus*, *321*, 531–549. <https://doi.org/10.1016/j.icarus.2018.12.003>
- Duda, J.-P., Thiel, V., Bauersachs, T., Mißbach, H., Reinhardt, M., Schäfer, N., Van Kranendonk, M. J., & Reitner, J. (2018). Ideas and perspectives: hydrothermally driven redistribution and sequestration of early Archaean biomass – the “hydrothermal pump hypothesis”. *Biogeosciences*, *15*, 1535–1548. <https://doi.org/10.5194/bg-15-1535-2018>
- Eigenbrode, J. L., Summons, R. E., Steele, A., Freissinet, C., Millan, M., Navarro-González, R., Sutter, B., McAdam, A. C., Franz, H. B., Glavin, D. P., Archer Jr, P. D., Mahaffy, P. R., Conrad, P. G., Hurowitz, J. A., Grotzinger, J. P., Gupta, S., Ming, D. W., Sumner, D. Y., Szopa, C., Malespin, C., Buch, A., & Coll, P. (2018). Organic matter preserved in 3-billion-year-old mudstones at Gale crater, Mars. *Science*, *360*, 1096–1101. <https://doi.org/10.1126/science.aas9185>
- Kenkmann, T., & Schönian, F. (2006). Ries and Chicxulub: Impact craters on Earth provide insights for Martian ejecta blankets. *Meteorit. Planet. Sci.*, *41*, 1587–1603. <https://doi.org/10.1111/j.1945-5100.2006.tb00437.x>
- McDonald, G. D., de Vanssay, E., & Buckley, J. R. (1998). Oxidation of Organic Macromolecules by Hydrogen Peroxide: Implications for Stability of Biomarkers on Mars. *Icarus*, *132*, 170–175. <https://doi.org/10.1006/icar.1998.5896>
- Mißbach, H. (2018). *Formation and preservation of abiotic organic signatures vs. lipid biomarkers—experimental studies in preparation for the ExoMars 2020 mission*. PhD thesis, University of Göttingen, Göttingen.
- Navarro-González, R., Rainey, F. A., Molina, P., Bagaley, D. R., Hollen, B. J., de la Rosa, J., Small, A. M., Quinn, R. C., Grunthaner, F. J., Cáceres, L., Gomez-Silva, B., & McKay, C. P. (2003). Mars-Like Soils in the Atacama Desert, Chile, and the Dry Limit of Microbial Life. *Science*, *302*, 1018–1021. <https://doi.org/10.1126/science.1089143>
- Pohl, J., Stöffler, D., Gall, H., & Ernstson, K. (1977). The Ries impact crater. In D. J. Roddy, R. O. Pepin & R. B. Merrill (Eds.), *Impact and explosion cratering: Planetary and terrestrial implications* (pp. 343–404). New York: Pergamon Press.
- Quinn, R. C., Zent, A. P., Grunthaner, F. J., Ehrenfreund, P., Tylor, C. L., & Garry, J. R. C. (2005). Detection and characterization of oxidizing acids in the Atacama Desert using the Mars Oxidation Instrument. *Planet. Space Sci.*, *53*, 1376–1388. <https://doi.org/10.1016/j.pss.2005.07.004>
- Reinhardt, M., Duda, J.-P., Blumenberg, M., Ostertag-Hennings, C., Reitner, J., Heim, C., & Thiel, V. (2018). The taphonomic fate of isorenieratene in Lower Jurassic shales—controlled by iron? *Geobiology*, *16*, 237–251. <https://doi.org/10.1111/gbi.12284>
- Reinhardt, M., Goetz, W., Duda, J.-P., Heim, C., Reitner, J., & Thiel, V. (2019). Organic signatures in Pleistocene cherts from Lake Magadi (Kenya), analogs for early Earth hydrothermal deposits. *Biogeosci. Discuss.* <https://doi.org/10.5194/bg-2018-513>
- Reinhardt, M., Goetz, W., & Thiel, V.. *Testing MOMA flight-like pyrolysis GC–MS on analog samples from Earth (iron-rich shale and opaline chert)—implications for MOMA pyrolysis during the ExoMars 2020 rover mission*. (unpublished, to be submitted to *Astrobiology*)
- Vago, J. L., Westall, F., Pasteur Instrument Teams, Landing Site Selection Working Group, & Other Contributors (2017). Habitability on Early Mars and the Search for Biosignatures with the ExoMars Rover. *Astrobiology*, *17*, 471–510. <https://doi.org/10.1089/ast.2016.1533>

Appendices

Appendix A

Supplementary information for chapter 2:

Organic signatures in Pleistocene cherts from Lake Magadi (Kenya), analogs for early Earth hydrothermal deposits

Manuel Reinhardt, Walter Goetz, Jan-Peter Duda, Christine Heim, Joachim Reitner, & Volker Thiel

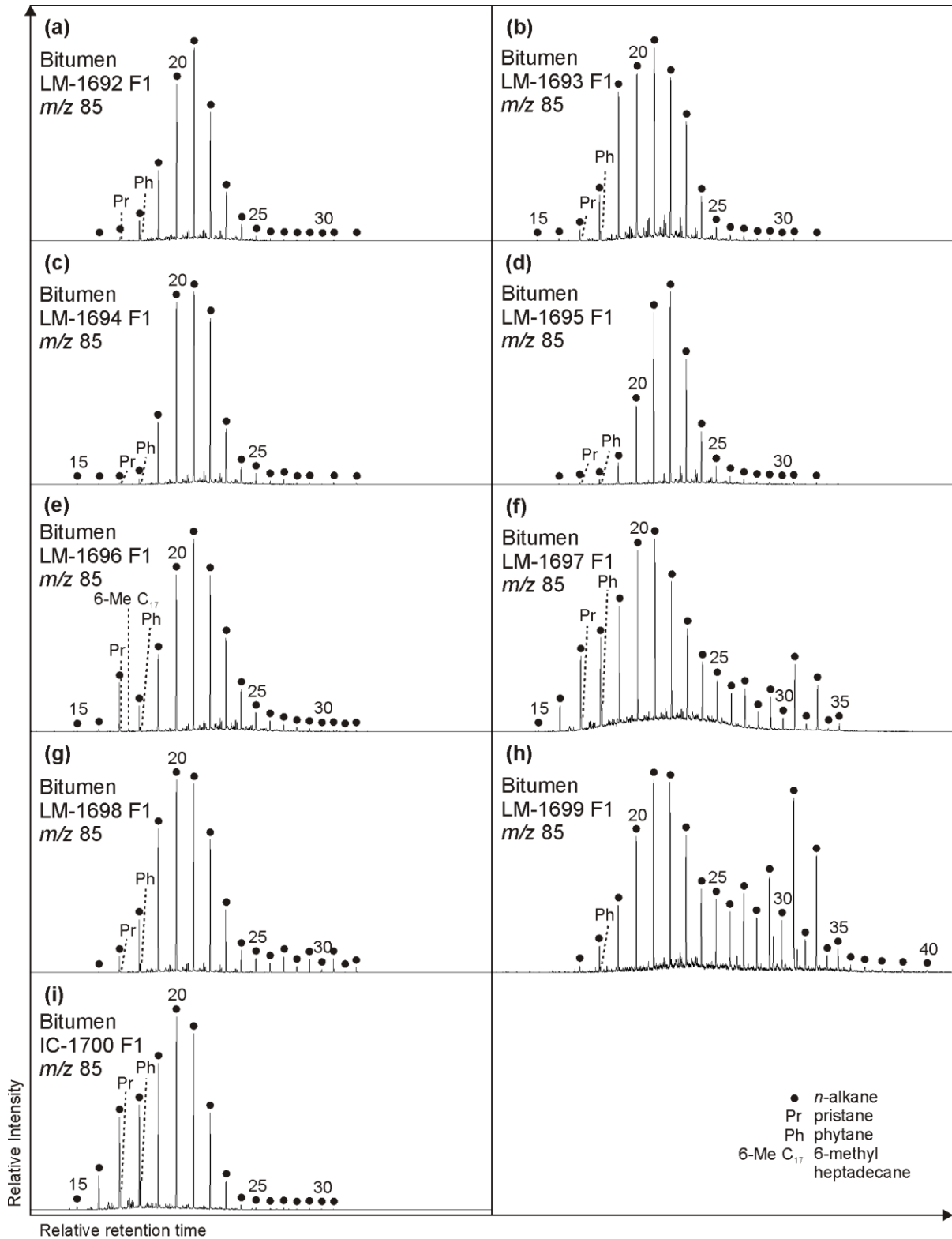


Fig. A1: Partial GC–MS ion chromatograms (m/z 85; 10–60 min) of the hydrocarbon fractions (F1) from bitumens of the Magadi cherts (LM-1692–1699; a–h) and the Great Geysir reference sinter (IC-1700; i). A narrow bell-shaped n -alkane distribution in the mid-chain range (around n -C₂₁) is visible in all samples analyzed. Additionally, odd-numbered long-chain n -alkanes are abundant in bitumens from most of the Green Bed cherts (LM-1697–1699; f–h). Notably, 6-methyl heptadecane appears in LM-1696 (e).

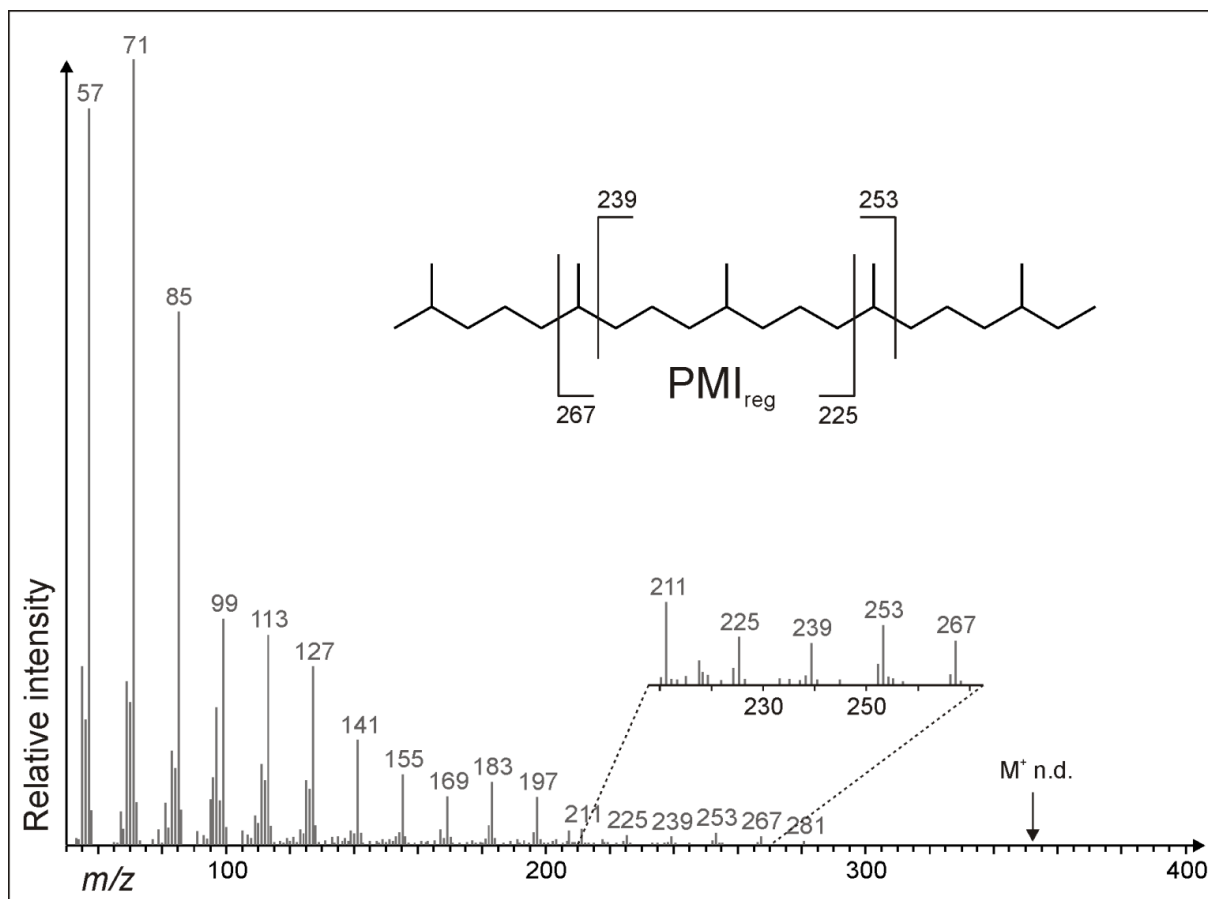


Fig. A2: Mass spectrum of the regular C₂₅ isoprenoid 2,6,10,14,18-pentamethylcosane (PMI_{reg}) from kerogen of LM-1693 (similar in kerogen pyrolysates from LM-1692 and LM-1695). Typical for this C₂₅ isoprenoid isomer is the high abundance of the fragments at 225 and 253 amu, as compared to 239 and 267 amu (Risatti et al., 1984; Greenwood & Summons, 2003). The molecular ion (M⁺) at 352 amu was not detected (n.d.).

Tab. A1: Mean $\delta^{13}\text{C}_{\text{V-PDB}}$ values in ‰ of fatty acids from bitumens

	LM-1692		LM-1693		LM-1694		LM-1695		LM-1696		LM-1697		LM-1698		LM-1699		IC-1700					
	Mean	±	Mean	±																		
C _{12:0}	-25.7	0.1	-25.0	0.1															-26.5	0.1		
C _{13:0}			-26.1	0.5																-21.2	0.2	
C _{14:0}	-26.1	<0.1	-27.5	0.1	-27.4	<0.1	-32.2	0.1			-28.5	0.8								-26.4	0.2	
<i>i</i> -C _{15:0}			-25.3	<0.1	-27.3	0.1															-18.2	<0.1
<i>ai</i> -C _{15:0}	-30.9	<0.1	-28.8	0.1	-29.5	0.1															-21.2	0.7
C _{15:0}	-27.8	0.1	-28.0	0.2	-26.1	0.1	-31.4	0.2			-21.5	0.4	-29.2	<0.1	-23.9	0.1					-24.8	0.2
C _{16:1}													-26.9	0.5								
C _{16:1}													-23.7	0.5								
C _{16:0}	-28.3	<0.1	-25.3	<0.1	-26.4	<0.1	-23.9	0.1	-27.0	0.5	-27.5	0.1	-23.9	<0.1	-25.3	0.1					-26.1	<0.1
<i>ai</i> -C _{17:0}	-34.0	<0.1	-30.0	0.3	-25.7	0.1																
C _{17:0}	-29.4	0.2	-27.3	0.2	-24.8	0.7	-27.3	<0.1	-18.8	0.1	-22.8	0.1	-24.1	0.9	-30.5	0.5					-24.2	0.2
C _{18:2}			-27.8	1.0	-18.3	0.7			-35.2	0.2			-27.5	0.2								
C _{18:1}	-29.1	0.1	-26.5	0.1	-25.8	<0.1			-26.9	<0.1	-28.1	0.5	-23.2	0.2	-30.2	0.1						
C _{18:1}	-21.7	0.2	-22.5	0.1									-21.2	0.2								
C _{18:0}	-28.3	0.2	-26.3	0.1	-29.1	0.1	-29.6	0.1	-26.2	0.4	-28.7	0.1	-25.1	0.2	-28.4	0.7					-27.2	0.1
C _{19:0}											-22.1	0.1	-32.0	0.1							-27.9	<0.1
C _{20:0}	-28.8	0.6	-28.2	<0.1	-27.2	<0.1			-20.2	0.1	-20.8	0.1	-27.3	0.7	-27.5	0.2					-21.1	0.1
C _{21:0}											-21.3	<0.1	-30.9	0.3								
C _{22:0}									-30.5	0.3	-24.3	0.1	-28.0	0.7	-26.7	<0.1					-33.7	0.3
C _{23:0}											-25.7	<0.1	-30.8	0.1							-30.6	<0.1
C _{24:0}	-24.5	0.1	-28.0	0.1	-22.2	0.1	-28.9	0.1	-28.5	0.3	-26.3	0.1	-27.5	0.1	-28.8	<0.1					-29.5	0.1
<i>i</i> -C _{25:0}			-24.8	0.2																		
<i>ai</i> -C _{25:0}			-27.1	0.2																		
C _{25:0}			-22.5	0.2							-26.8	0.1	-24.7	0.7							-33.8	0.1
C _{26:0}	-25.8	0.2	-30.6	<0.1	-30.4	0.4			-16.3	0.2	-24.6	0.2	-30.0	0.3	-30.5	0.3					-35.4	0.1
C _{27:0}											-22.5	0.2									-31.9	0.2
C _{28:0}											-25.4	<0.1									-32.0	<0.1

Tab. A2: Mean $\delta^{13}\text{C}_{\text{V-PDB}}$ values in ‰ of alcohols, ketones, mono- and diethers from bitumens

	LM- 1692	LM- 1693	LM- 1694	LM- 1695	LM- 1696	LM- 1697	LM- 1698	LM- 1699	IC- 1700	
	Mean	±	Mean	±	Mean	±	Mean	±	Mean	±
<i>Alkan-1-ols</i>										
C ₁₂									-29.9	0.4
C ₁₃									-25.2	0.1
C ₁₄	-28.5	0.2	-39.5	0.1	-37.3	0.1	-19.6	0.5	-27.1	0.7
C ₁₅								-19.4	0.2	
C ₁₆	-34.8	0.2	-25.1	<0.1	-35.5	0.4	-36.0	0.3	-35.9	0.2
C ₁₈	-37.2	0.3	-31.9	0.2	-35.0	0.3	-35.9	0.4	-34.8	0.1
C ₂₀	-30.9	0.1	-29.9	0.6	-32.7	0.1	-30.3	0.2	-29.8	0.1
C ₂₁							-33.3	0.2		
C ₂₂	-29.6	0.4	-32.4	0.3	-28.7	0.1	-30.3	0.2	-25.2	0.4
C ₂₃								-34.6	0.2	
C ₂₄	-20.2	0.3	-36.5	0.1	-28.3	0.3	-32.3	0.6	-30.1	0.7
C ₂₅								-22.6	0.8	
C ₂₆	-32.1	0.5	-33.8	0.7	-17.4	0.2	-28.5	0.9	-26.5	0.3
C ₂₇								-29.2	0.1	
C ₂₈	-21.3	1.0	-26.7	0.5	-20.6	0.4	-26.6	1.0	-18.7	0.3
C ₃₀					-14.6	0.3			-22.8	0.1
C ₃₂	-26.4	0.7						-20.3	0.7	
									-25.4	<0.1
									-19.6	0.1
									-29.5	0.5
<i>Glycerol mono- and diethers</i>										
<i>i</i> -C _{16:0}	-21.8	0.1	-20.3	<0.1	-12.2	<0.1				
C _{16:0}	-20.4	0.1	-20.2	0.7	-11.4	0.4				
10Me-C _{16:0}	-21.5	0.1	-23.0	0.1	-19.7	<0.1				
<i>i</i> -C _{17:0}	-25.2	0.2	-21.3	0.5						
<i>ai</i> -C _{17:0}	-17.4	0.1	-25.0	0.7						
C _{17:0}	-19.0	0.1	-26.9	0.1	-10.7	0.2				
Me-C _{17:0}	-22.1	0.1	-17.9	0.4	-10.9	0.1				
Me-C _{17:0}	-22.5	0.3	-9.8	<0.1	-9.4	<0.1	-18.6	0.1		
C _{18:1}	-20.9	0.2	-15.7	0.1						
C _{18:1}	-19.1	0.8	-22.9	0.7	-7.0	0.2				
C _{18:0}	-12.5	0.2	-19.0	0.8	-5.7	0.4				
A	-21.7	0.4	-18.5	0.5	-12.2	0.4	-22.2	0.1	-14.8	0.5
ExA	-18.3	0.6	-19.9	0.2	-15.3	0.4	-19.4	0.5	-19.6	0.5
<i>Other compounds</i>										
Tetrahyd.							-33.3	0.3	-27.7	0.1
							-25.4	0.2	-24.1	0.5
									-29.3	0.2

Tab. A3: Mean $\delta^{13}\text{C}_{\text{V-PDB}}$ values in ‰ of alkanes and isoprenoids from bitumens

	LM-1692		LM-1693		LM-1694		LM-1695		LM-1696		LM-1697		LM-1698		LM-1699		IC-1700				
	Mean	±																			
<i>n</i> -C ₁₆																			-37.1	0.1	
<i>n</i> -C ₁₇			-30.5	0.6					-30.1	0.6	-38.0	1.2								-32.9	<0.1
6Me-C ₁₇									-30.3	0.2											
<i>n</i> -C ₁₈	-32.5	<0.1	-32.1	<0.1	-31.8	0.5	-35.6	0.5	-33.8	<0.1	-34.4	0.1	-34.3	0.1						-33.4	<0.1
<i>n</i> -C ₁₉	-32.0	0.2	-31.6	0.1	-32.0	0.1	-33.3	0.3	-32.9	0.5	-33.3	0.4	-32.9	<0.1	-14.7	0.5				-35.2	0.1
<i>i</i> -C ₂₀	-31.1	0.1	-30.0	<0.1	-34.1	0.3							-29.8	0.2							
<i>ai</i> -C ₂₀	-32.1	0.8	-33.2	0.1	-29.0	0.8							-27.5	0.1							
<i>n</i> -C ₂₀	-31.4	<0.1	-30.7	0.2	-30.9	0.3	-32.3	0.4	-33.2	<0.1	-32.6	0.4	-32.7	0.2	-38.9	0.3				-33.6	<0.1
<i>i</i> -C ₂₁	-32.3	<0.1	-31.2	<0.1	-32.7	<0.1	-30.9	0.1	-34.4	0.7	-35.3	0.5	-33.2	0.3							
<i>ai</i> -C ₂₁	-29.8	<0.1	-31.5	<0.1	-30.5	0.3	-31.9	0.4	-28.6	0.1	-36.5	0.3	-32.2	0.1							
<i>n</i> -C ₂₁	-31.6	<0.1	-31.0	0.2	-31.2	0.4	-31.9	0.1	-32.9	<0.1	-31.6	<0.1	-33.6	<0.1	-35.0	0.7				-34.0	<0.1
<i>i</i> -C ₂₂	-29.9	0.8	-33.2	0.1	-29.6	0.1	-34.0	0.3	-34.1	0.1	-34.9	0.1	-33.6	0.1							
<i>ai</i> -C ₂₂	-29.1	0.2	-37.4	0.8	-28.9	0.1	-34.4	0.2	-33.3	<0.1	-32.6	0.1	-33.3	0.3							
<i>n</i> -C ₂₂	-32.1	0.2	-31.7	<0.1	-32.0	0.3	-32.3	0.1	-32.8	<0.1	-31.6	0.2	-34.4	0.2	-36.7	0.3				-37.5	<0.1
<i>i</i> -C ₂₃	-33.8	0.1	-30.3	0.1	-29.1	0.1	-32.1	<0.1	-31.4	<0.1	-36.5	0.1	-31.3	0.2							
<i>ai</i> -C ₂₃	-33.7	0.2	-27.3	0.1	-28.8	0.1	-33.1	0.1	-32.1	0.1	-39.1	0.4	-30.2	0.4							
<i>n</i> -C ₂₃	-32.1	<0.1	-32.2	0.2	-32.2	<0.1	-32.4	0.1	-32.6	0.3	-34.5	<0.1	-33.4	0.1	-25.4	0.1				-39.6	0.1
<i>i</i> -C ₂₄	-31.8	<0.1	-33.9	0.1	-32.5	<0.1	-29.8	0.4	-35.2	<0.1			-36.3	0.3							
<i>ai</i> -C ₂₄	-26.2	0.5	-32.6	0.2	-31.5	0.1	-29.0	0.1	-34.3	0.3			-29.5	0.7							
<i>n</i> -C ₂₄	-32.7	0.2	-33.7	<0.1	-31.6	<0.1	-31.8	0.2	-32.5	0.5	-30.6	0.2	-32.2	0.1	-27.6	0.2				-39.2	<0.1
<i>i</i> -C ₂₅	-30.8	<0.1	-31.2	0.4	-25.3	<0.1	-34.6	0.1	-28.4	0.4											
<i>ai</i> -C ₂₅	-26.8	0.4	-35.9	0.4	-22.6	0.2	-30.4	0.7	-28.0	0.2											
<i>n</i> -C ₂₅							-32.0	<0.1	-30.2	0.1	-34.7	0.1	-34.9	0.2	-25.6	0.1					
<i>n</i> -C ₂₆							-29.8	0.1	-29.9	0.2			-34.0	0.2	-25.8	<0.1	-34.8	0.3			
<i>n</i> -C ₂₇													-36.3	0.2	-23.7	0.1	-30.8	0.1			
<i>n</i> -C ₂₈													-33.8	0.2	-24.2	0.3	-27.9	0.1			
<i>n</i> -C ₂₉													-28.8	0.4	-23.9	0.5	-21.5	0.2			
<i>n</i> -C ₃₀																	-26.9	0.1			
<i>n</i> -C ₃₁													-20.9	0.6	-24.4	0.1	-21.1	0.4			
<i>n</i> -C ₃₂																	-24.5	0.2			
<i>n</i> -C ₃₃																	-25.8	<0.1			
<i>Isoprenoids</i>																					
Pr			-31.7	0.1					-30.2	0.1	-32.2	0.2	-35.8	0.1						-34.5	0.2
Ph	-33.3	<0.1	-30.9	0.4	-30.0	0.6	-36.1	1.2	-34.7	0.1	-33.8	0.1	-35.3	<0.1						-38.6	0.1

Tab. A4: Mean $\delta^{13}\text{C}_{\text{V-PDB}}$ values in ‰ of alkanes and isoprenoids from kerogens

	LM-1692		LM-1693		LM-1695		LM-1697		LM-1698	
	Mean	±	Mean	±	Mean	±	Mean	±	Mean	±
<i>n</i> -C ₁₅					-30.5	0.6				
<i>n</i> -C ₁₆					-30.4	0.1			-30.9	0.1
<i>n</i> -C ₁₇					-30.3	<0.1	-26.0	0.3	-31.3	<0.1
<i>n</i> -C ₁₈	-36.3	0.7	-35.0	0.9	-31.5	0.2	-25.4	0.4	-34.9	<0.1
<i>n</i> -C ₁₉	-32.0	0.3	-29.2	0.7	-27.2	0.1	-24.0	<0.1	-34.6	0.1
<i>n</i> -C ₂₀	-27.8	0.6	-33.7	0.8	-26.9	0.1	-22.1	<0.1	-35.8	0.2
<i>n</i> -C ₂₁	-28.1	0.4	-31.5	0.3	-27.6	0.7	-22.0	0.2	-34.3	0.8
<i>n</i> -C ₂₂	-31.1	<0.1	-30.9	0.2	-28.8	0.1	-23.0	0.9	-32.9	0.1
<i>n</i> -C ₂₃	-31.8	0.1	-29.3	0.4	-27.3	<0.1	-22.4	0.1	-34.5	0.8
<i>n</i> -C ₂₄	-26.5	0.6	-30.5	0.3	-26.9	0.2	-22.9	0.5	-35.3	0.2
<i>n</i> -C ₂₅	-28.7	0.5	-30.9	1.0	-27.3	<0.1	-24.4	0.3	-34.9	<0.1
<i>n</i> -C ₂₆	-26.6	0.5	-27.4	0.1	-25.4	<0.1	-24.1	0.1	-29.7	0.1
<i>n</i> -C ₂₇	-29.8	0.3	-30.6	0.1	-24.8	<0.1	-22.9	0.4	-28.0	0.1
<i>n</i> -C ₂₈	-30.4	0.4	-28.8	0.7	-23.6	0.3	-22.6	0.3	-28.0	0.1
<i>n</i> -C ₂₉	-25.9	<0.1	-29.1	0.8	-25.8	0.2	-22.8	0.2	-26.3	0.3
<i>n</i> -C ₃₀	-29.6	0.6	-32.3	0.4	-24.3	0.3	-22.1	<0.1	-26.0	0.1
<i>n</i> -C ₃₁	-24.7	0.2	-31.0	0.4	-23.5	<0.1	-22.4	0.1	-27.1	0.6
<i>n</i> -C ₃₂	-26.7	0.4	-31.3	1.0	-22.6	0.4	-21.5	<0.1	-24.1	0.6
<i>n</i> -C ₃₃	-24.8	0.7			-23.6	0.2	-21.4	0.4	-26.2	0.2
<i>n</i> -C ₃₄	-27.6	0.1			-23.2	0.1	-21.2	0.1	-25.4	<0.1
<i>n</i> -C ₃₅	-28.9	0.3			-24.4	0.7	-20.4	0.5	-28.2	0.5
<i>n</i> -C ₃₆					-27.4	0.7	-21.0	0.1	-23.7	0.4
<i>n</i> -C ₃₇					-27.7	0.9	-20.8	0.4	-26.9	0.2
<i>n</i> -C ₃₈					-25.6	<0.1	-19.3	0.6	-25.3	<0.1
<i>n</i> -C ₃₉							-21.8	0.1		
<i>n</i> -C ₄₀							-21.6	0.5		
<i>Isoprenoids</i>										
Far					-33.0	0.2				
Nor					-35.3	0.1				
Pr					-32.3	0.3				
Ph	-25.1	0.3	-26.8	0.2	-28.5	<0.1				
PMI _{req}	-22.0	0.3	-24.0	0.4	-24.6	0.1				

Appendix B

Supplementary information for chapter 3:

Ideas and perspectives: hydrothermally driven redistribution and sequestration of early Archean biomass—the “hydrothermal pump hypothesis”

Jan-Peter Duda, Volker Thiel, Thorsten Bauersachs, Helge Mißbach, Manuel Reinhardt, Nadine Schäfer, Martin J. Van Kranendonk, & Joachim Reitner

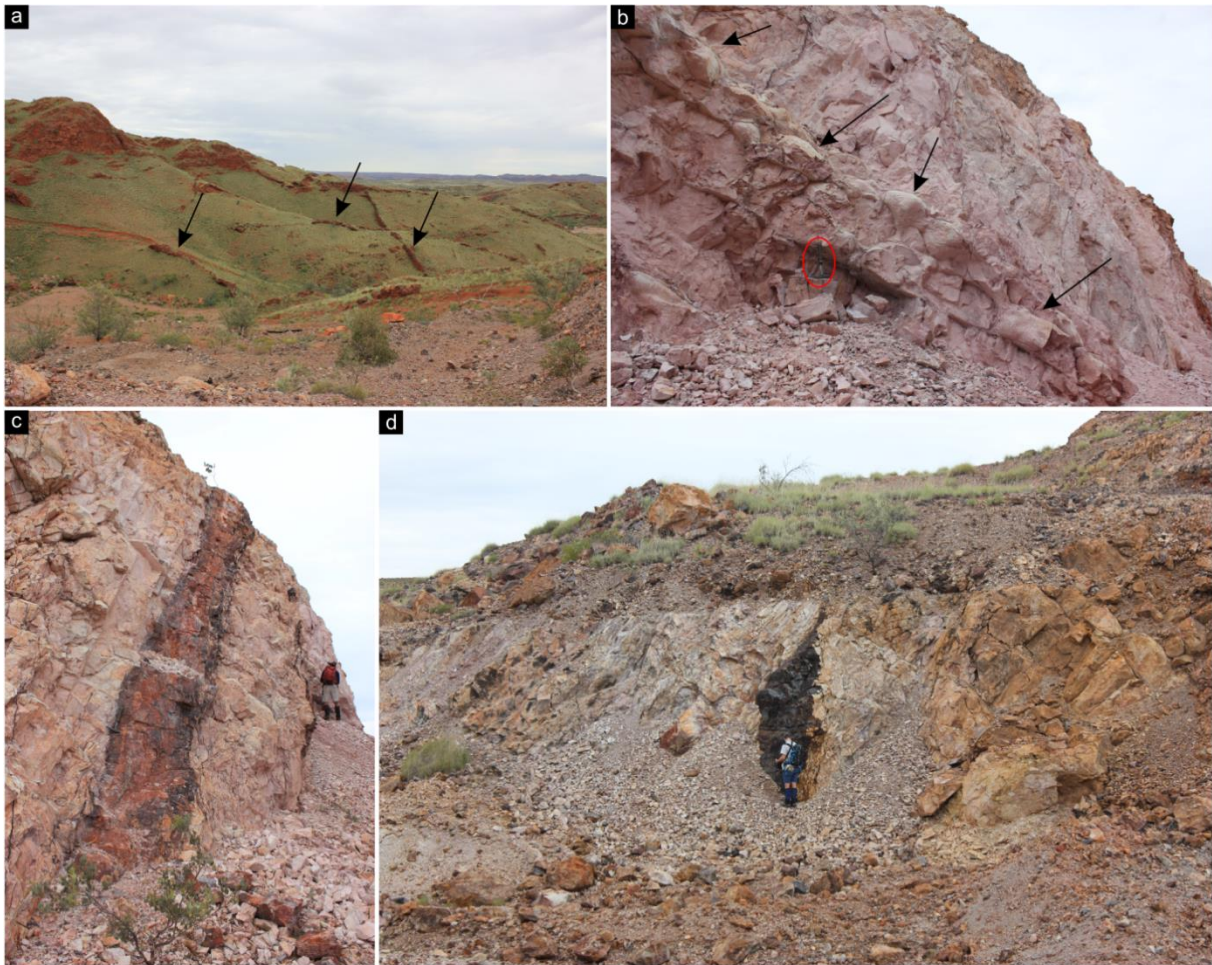


Fig. B1: Hydrothermal chert veins of the ca. 3.5 Ga Dresser Formation (Pilbara Craton, Western Australia). **(a)** Hydrothermal chert veins of the Dresser Formation (ridges, see arrows) forming large-scale networks in their host basalts. **(b)** Hydrothermally altered footwall basalts exhibiting pillow structures (arrows); hammer for scale (red circle). **(c, d)** Hydrothermal chert veins of the Dresser Formation penetrating komatiitic footwall basalts in a recent cut wall of the abandoned Dresser Mine (persons for scale). The analysed hydrothermal chert vein occurs adjacent to the one shown in **(d)**.

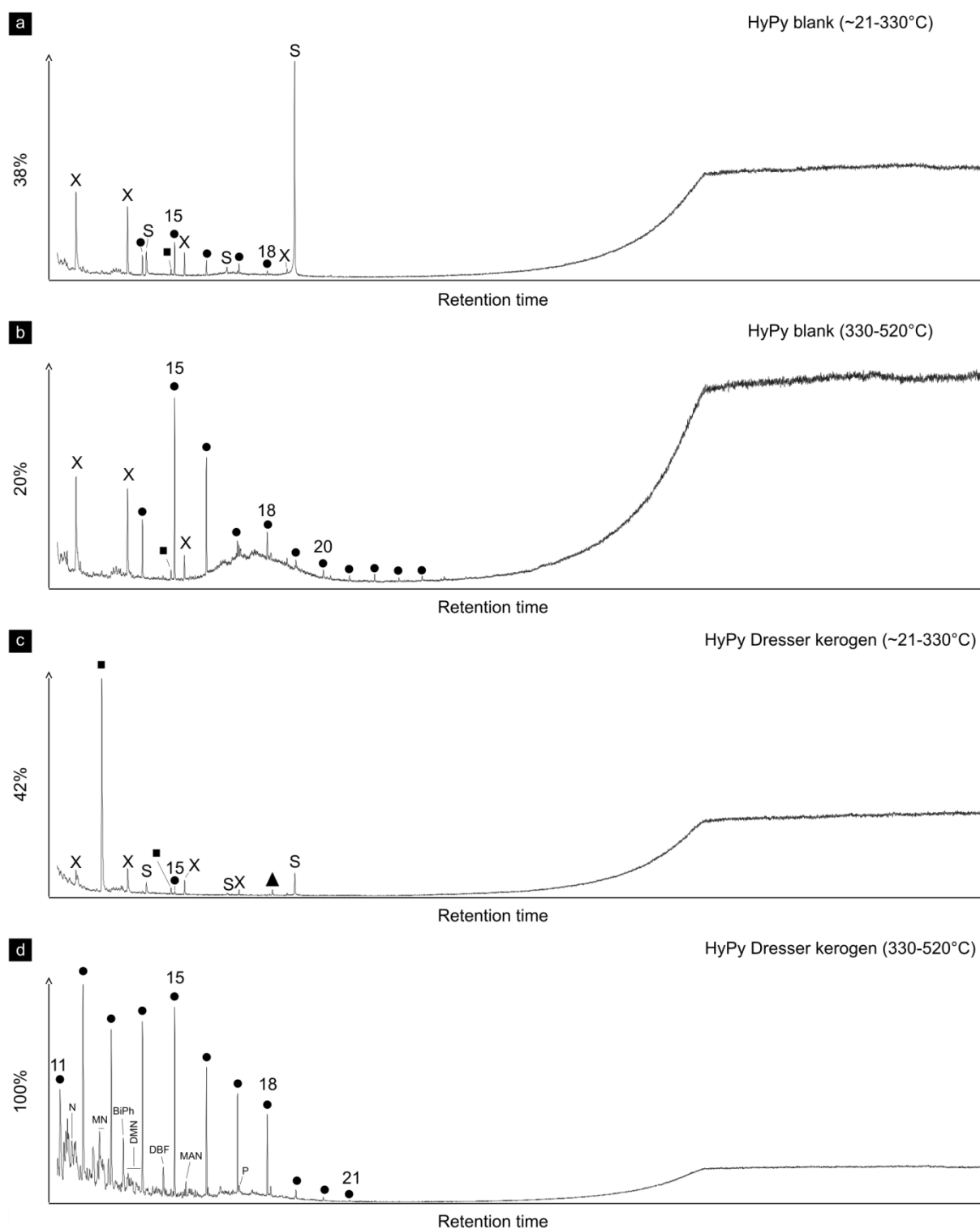


Fig. B2: Total ion current chromatograms. Low temperature (a) and high temperature (b) HyPy products of the analytical blank (combusted sea sand) obtained prior to HyPy of the Dresser kerogen. Low temperature (c) and high temperature (d) HyPy products of the Dresser kerogen. Compounds detected in (a–c) represent background contamination and/or artefacts. Note that high temperature HyPy of the Dresser kerogen yielded significantly higher amounts of products with a distinctly different distribution pattern. Black dots: *n*-alkanes (numbers refer to carbon chain-lengths); triangle: phthalic acid; N: naphthalene; MN: methylnaphthalenes; BiPh: 1,1'-biphenyl; DMN: dimethylnaphthalenes; MAN: methylacenaphthenes; P: phenanthrene; crosses: siloxanes (GC column or septum bleeding); squares: phenols; S: sulphur. Note: Percentage values given on the vertical axes of chromatograms (a–c) relate peak intensities to chromatogram (d) (HyPy Dresser kerogen, 330–520 °C).

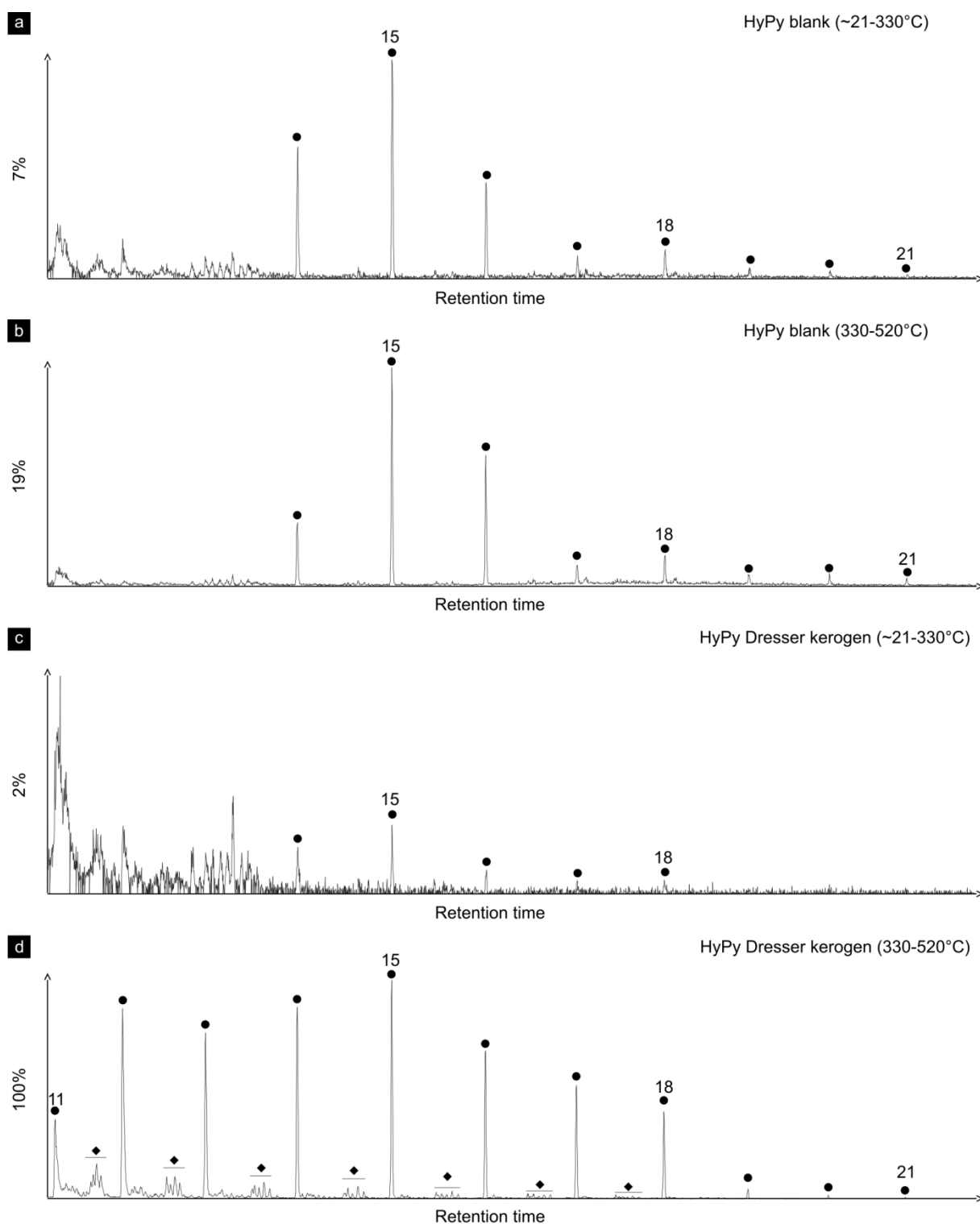


Fig. B3: Partial ion chromatograms selective for alkanes (m/z 85). Low temperature (a) and high temperature (b) HyPy products of the analytical blank (combusted sea sand) obtained prior to HyPy of the Dresser kerogen. Low temperature (c) and high temperature (d) HyPy products of the Dresser kerogen. High temperature HyPy produced the highest yields of n -alkanes and minor clusters of isomeric monomethyl alkanes (diamonds in d). The n -alkanes in the high temperature pyrolysate of the Dresser kerogen (d) furthermore exhibit a distinct distribution different to those observed in (a–c). All compounds detected in (a–c) are considered to represent background contamination. Black dots: n -alkanes (numbers refer to carbon chain-lengths). Note: Percentage values given on the vertical axes of chromatograms (a–c) relate peak intensities to chromatogram (d) (HyPy Dresser kerogen, 330–520 °C).

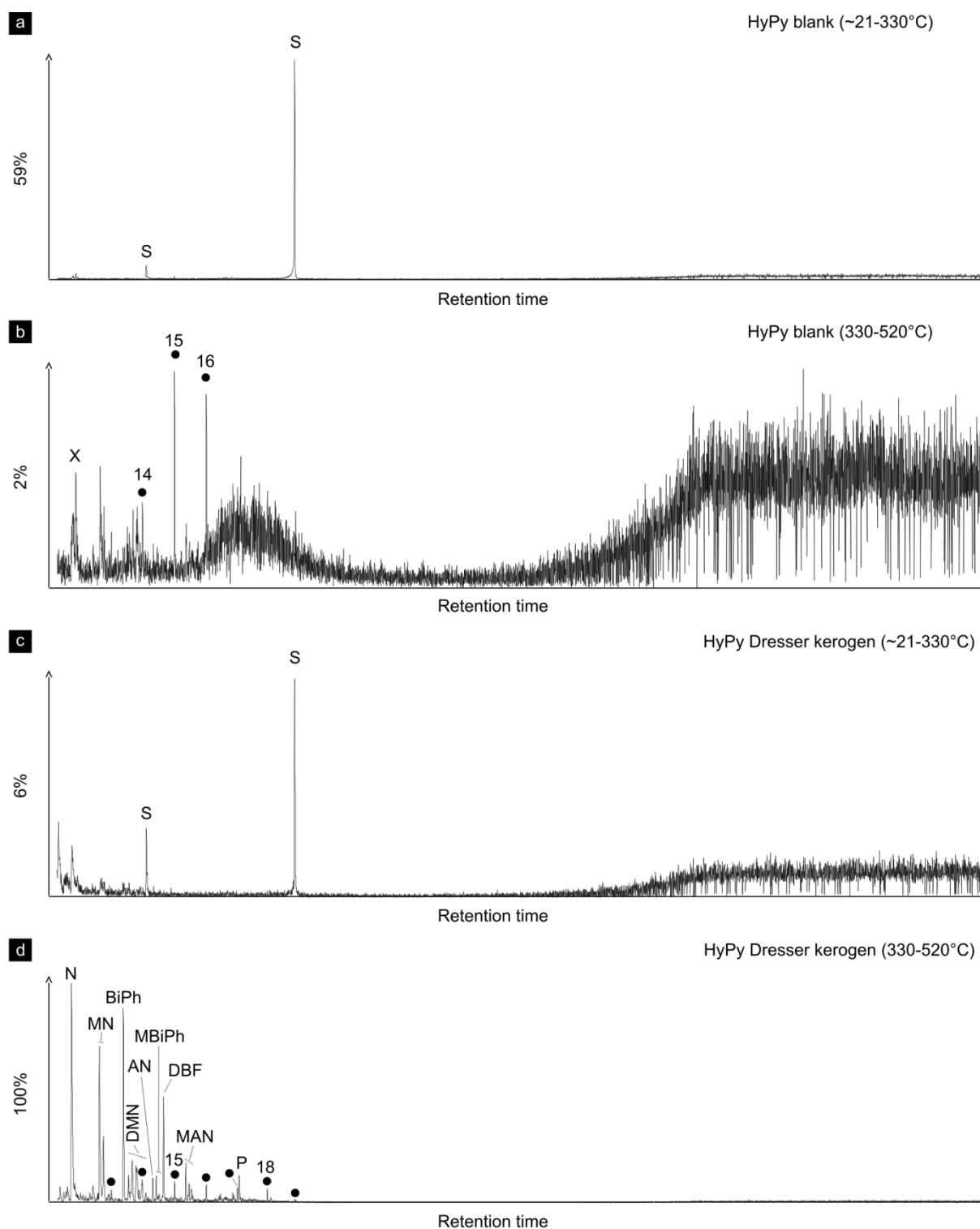


Fig. B4: Ion chromatograms selective for aromatic hydrocarbons (m/z 128, 142, 154, 156, 168, 178). Low temperature (**a**) and high temperature (**b**) HyPy products of analytical blank (combusted sea sand) obtained prior to HyPy of the Dresser kerogen. Low temperature (**c**) and high temperature (**d**) HyPy products of the Dresser kerogen. Note that high temperature HyPy of the Dresser kerogen yielded a variety of aromatic hydrocarbons, which are orders of magnitudes lower or absent in all other pyrolysates. Black dots: *n*-alkanes (numbers refer to carbon chain-lengths); N: naphthalene; MN: methylnaphthalenes; BiPh: 1,1'-biphenyl; DMN: dimethylnaphthalenes; AN: acenaphthene; MBIph: methylbiphenyls; DBF: dibenzofuran; MAN: methylacenaphthenes; P: phenanthrene; crosses: siloxanes (GC column or septum bleeding); S: elemental sulphur (likely derived from the sulfidic catalyst). Note: Percentage values given on the vertical axes of chromatograms (**a-c**) relate peak intensities to chromatogram (**d**) (HyPy Dresser kerogen, 330–520 °C).

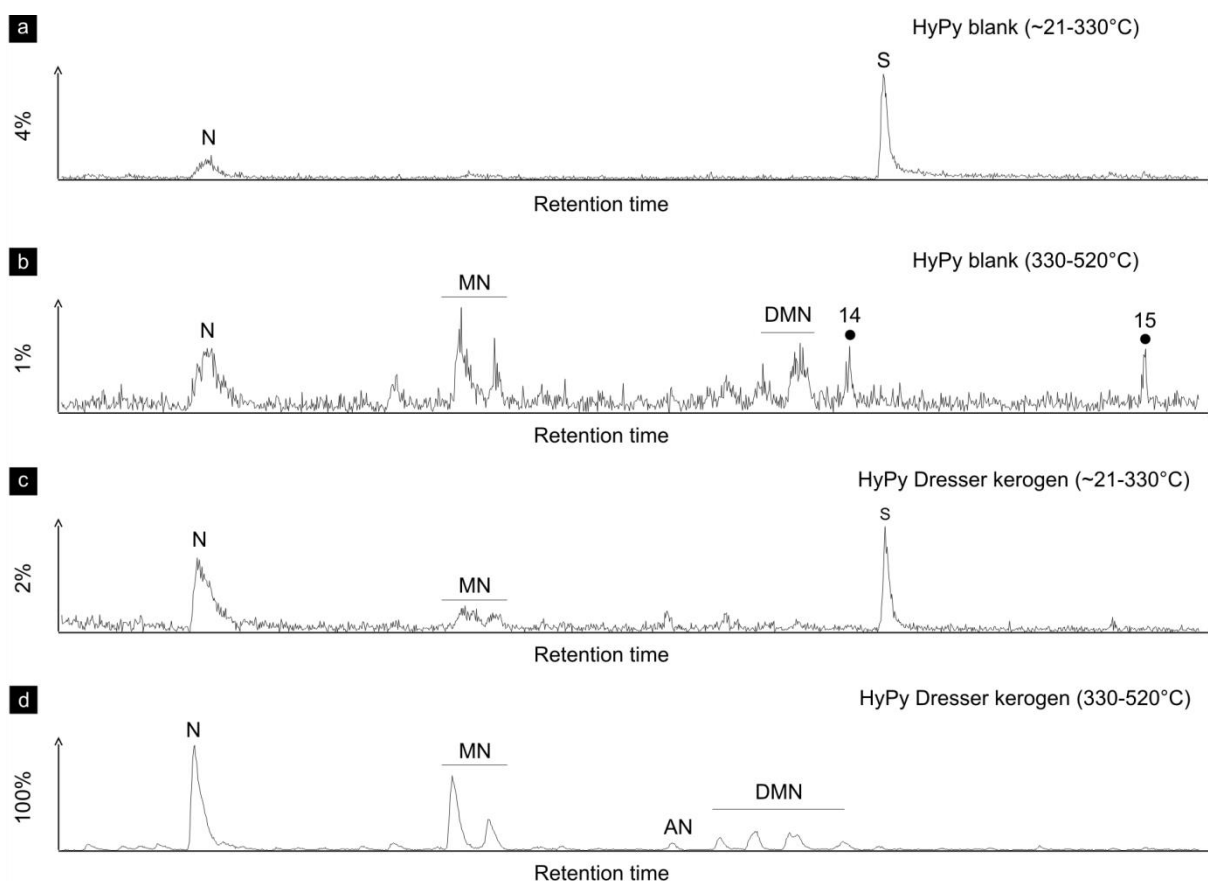


Fig. B5: Partial ion chromatograms selective for (dimethyl-, methyl-)naphthalenes (m/z 128, 142, 156). Low temperature (a) and high temperature (b) HyPy products of the analytical blank (combusted sea sand) obtained prior to HyPy of the Dresser kerogen. Low temperature (c) and high temperature (d) HyPy products of the Dresser kerogen. High temperature HyPy of the Dresser kerogen yielded naphthalene (N), methylnaphthalenes (MN), dimethylnaphthalenes (DMN) and acenaphthene (AN), which are orders of magnitudes lower or absent in all other pyrolysates. Black dots: n -alkanes (numbers refer to carbon chain-lengths); S: elemental sulphur (likely derived from the sulfidic catalyst). Note: Percentage values given on the vertical axes of chromatograms (a–c) relate peak intensities to chromatogram (d) (HyPy Dresser kerogen, 330–520 °C).

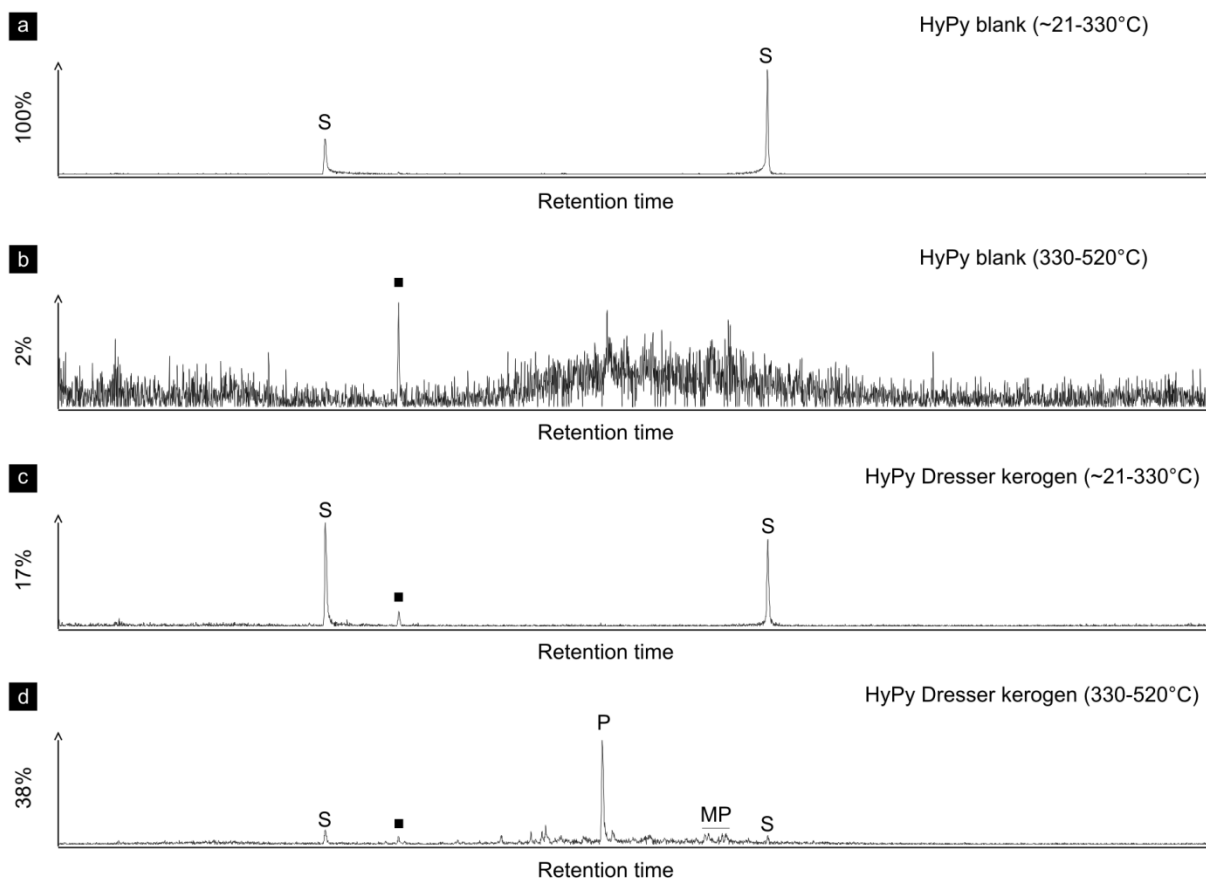


Fig. B6: Partial ion chromatograms selective for (methyl-)phenanthrenes (m/z 178, 192). Low temperature (a) and high temperature (b) HyPy products of the analytical blank (combusted sea sand) obtained prior to HyPy of the Dresser kerogen. Low temperature (c) and high temperature (d) HyPy products of the Dresser kerogen. Phenanthrene (P) and traces of methylphenanthrenes (MP) were only present in the high temperature HyPy pyrolysate of the Dresser kerogen. Squares: phenols; S: elemental sulphur (likely derived from the sulfidic catalyst). Note: Percentage values given on the vertical axes of chromatograms (b–d) relate peak intensities to chromatogram (a) (HyPy blank, ~21–330 °C).

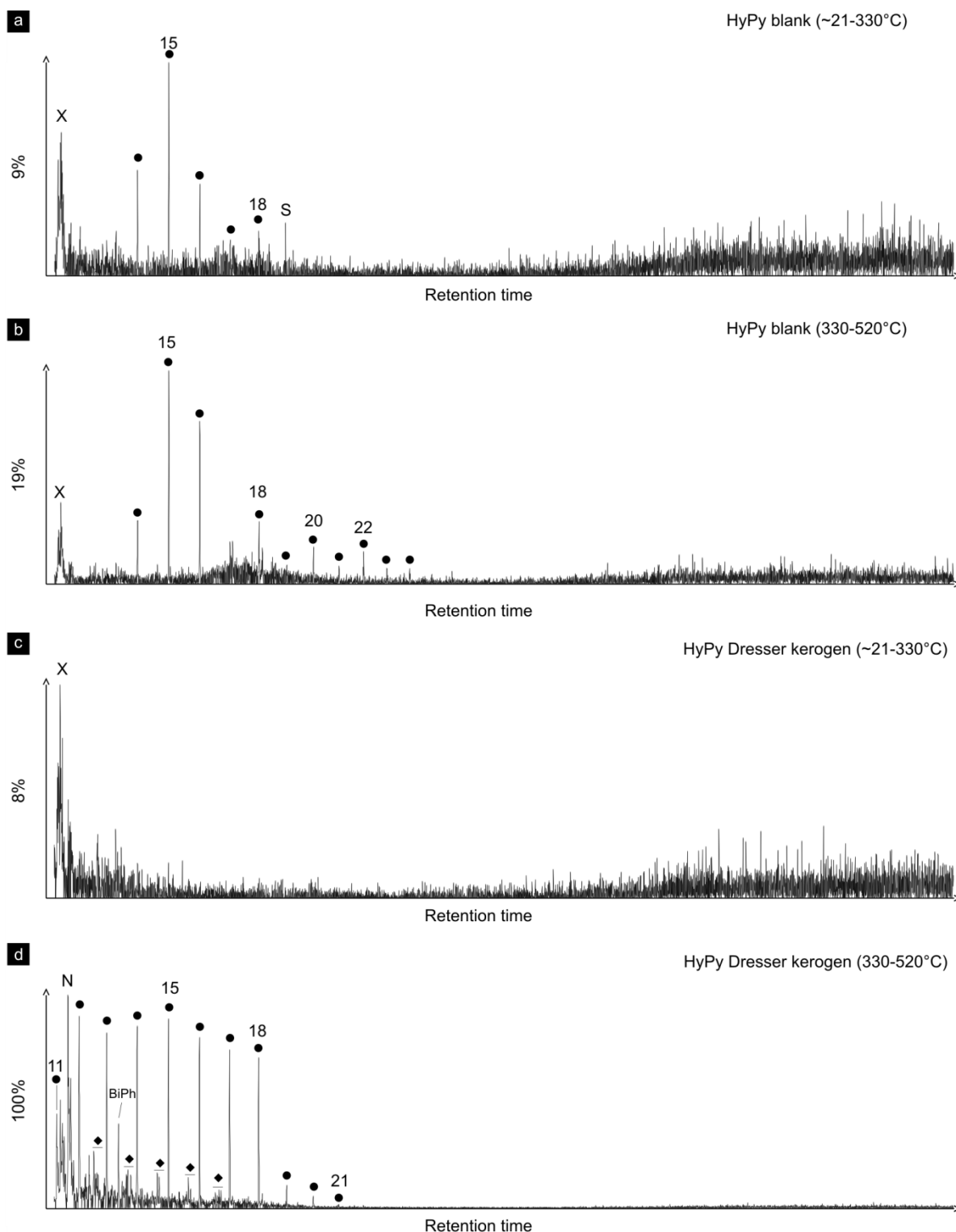


Fig. B7: Ion chromatograms selective for branched alkanes with quaternary carbon centres (BAQCs; m/z 127). Low temperature (a) and high temperature (b) HyPy products of the analytical blank (combusted sea sand) obtained prior to HyPy of the Dresser kerogen. Low temperature (c) and high temperature (d) HyPy products of the Dresser kerogen. Compounds detected in (a–c) represent background contamination and/or artefacts. Note the absence of BAQCs in all pyrolysates. Black dots: *n*-alkanes (numbers refer to carbon chain-lengths); diamonds: monomethylalkanes; N: naphthalene; BiPh: 1,1'-biphenyl; crosses: siloxanes (GC column or septum bleeding); S: elemental sulphur (likely derived from the sulfidic catalyst). Note: Percentage values given on the vertical axes of chromatograms (a–c) relate peak intensities to chromatogram (d) (HyPy Dresser kerogen, 330–520 °C).

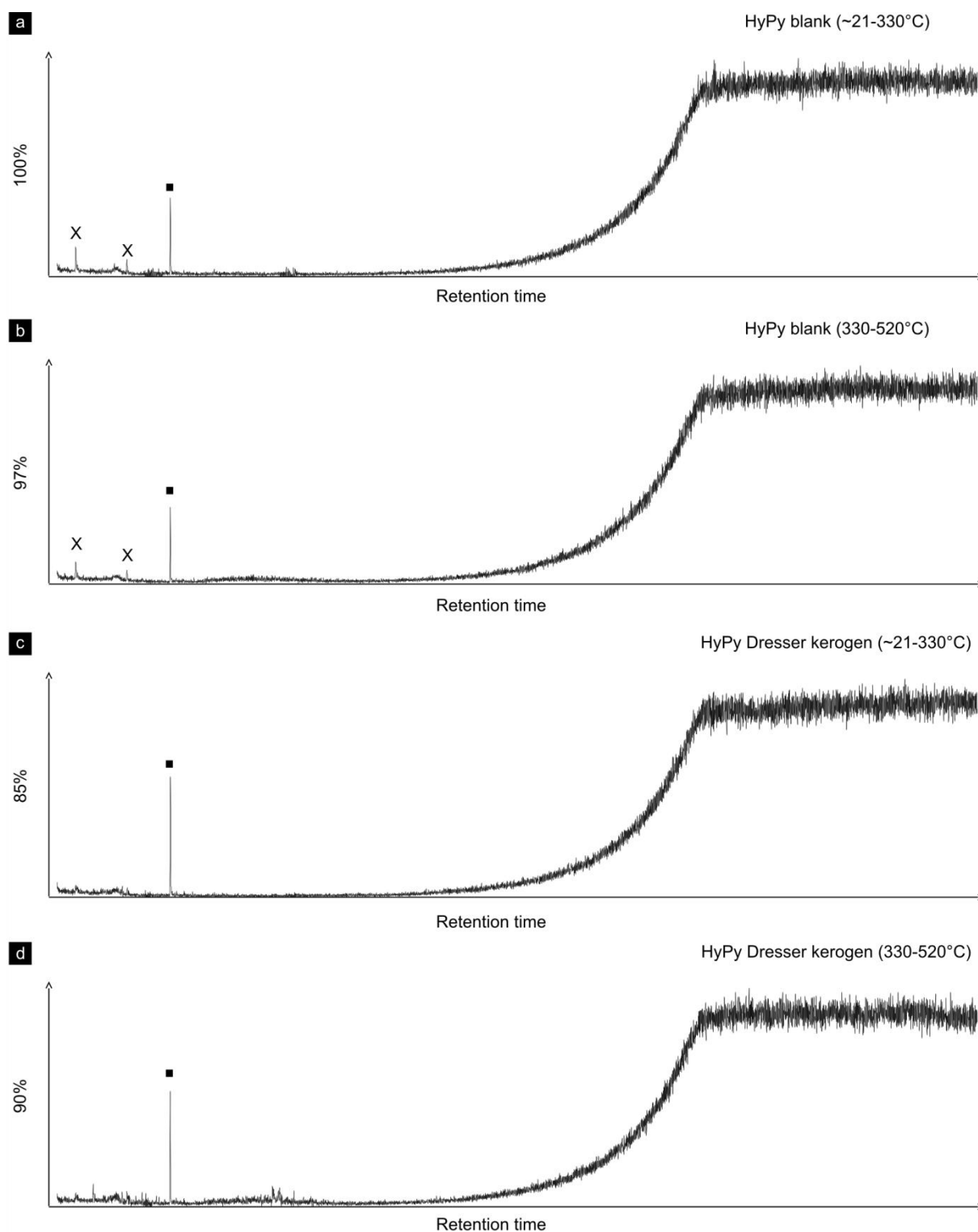


Fig. B8: Ion chromatograms selective for hopanes (m/z 191). Low temperature (a) and high temperature (b) HyPy products of the analytical blank (combusted sea sand) obtained prior to HyPy of the Dresser kerogen. Low temperature (c) and high temperature (d) HyPy products of the Dresser kerogen. All compounds in (a–d) represent background contamination and/or artefacts. Note the absence of hopanes in all pyrolysates. Crosses: siloxanes (GC column or septum bleeding); squares: phenols. Note: Percentage values given on the vertical axes of chromatograms (c–d) relate peak intensities to chromatogram (a) (HyPy blank, ~21–330 °C).

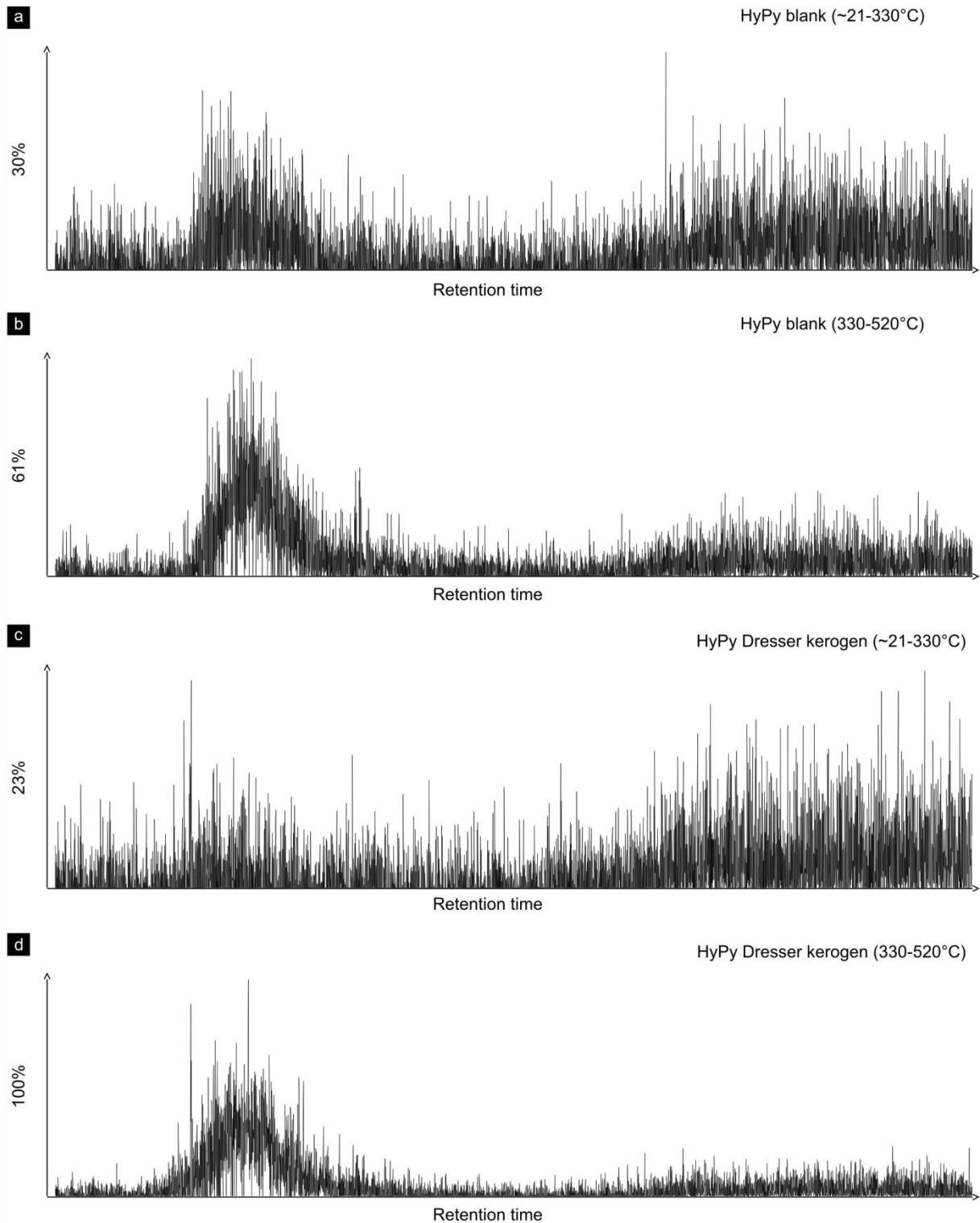


Fig. B9: Ion chromatograms selective for steranes (m/z 217). Low temperature (**a**) and high temperature (**b**) HyPy chromatograms of the analytical blank (combusted sea sand) obtained prior to HyPy of the Dresser kerogen. Low temperature (**c**) and high temperature (**d**) HyPy products of the Dresser kerogen. Note the absence of steranes in all chromatograms. Note: Percentage values given on the vertical axes of chromatograms (**a**–**c**) relate peak intensities to chromatogram (**d**) (HyPy Dresser kerogen, 330–520 °C).

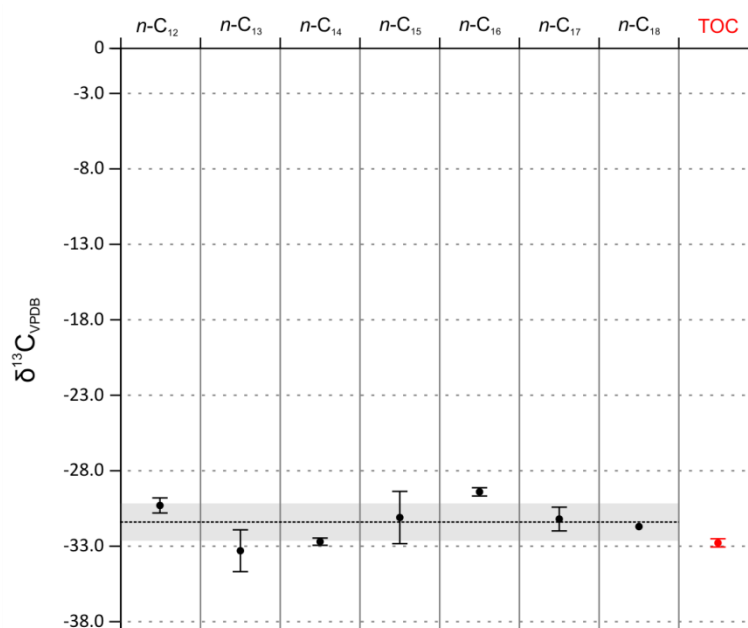


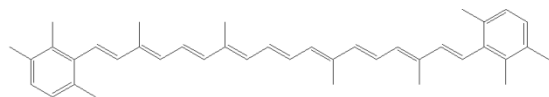
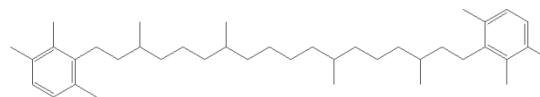
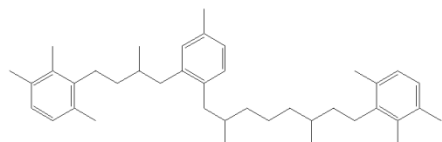
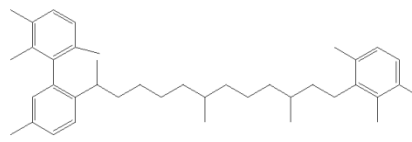
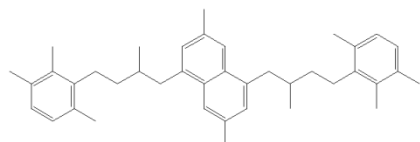
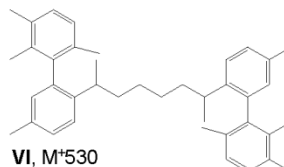
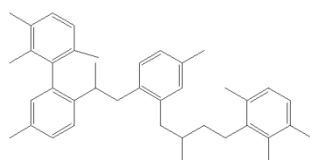
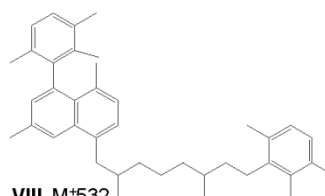
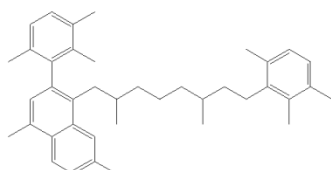
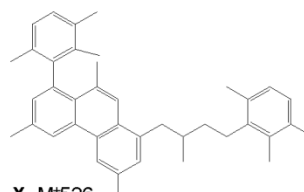
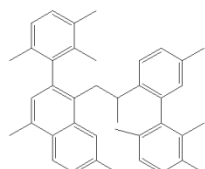
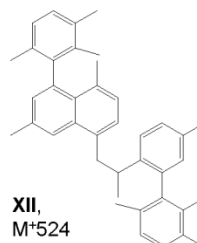
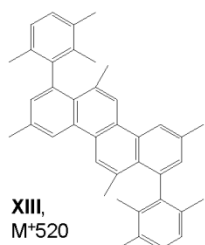
Fig. B10: Stable carbon isotope values ($\delta^{13}\text{C}$) of n -alkanes released upon high temperature HyPy and the total organic carbon (TOC). The isotopic similarity indicates that the n -alkanes (black dots) were generated from the kerogen (TOC, red dot). Vertical lines: Standard deviations of $\delta^{13}\text{C}$ values; dotted horizontal line: mean $\delta^{13}\text{C}$ value of n -alkanes (-31.4 ‰); shaded area: standard deviation of mean $\delta^{13}\text{C}$ value of n -alkanes (± 1.2 ‰).

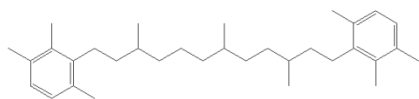
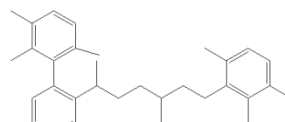
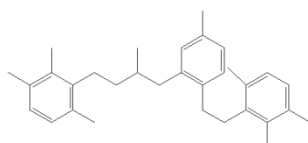
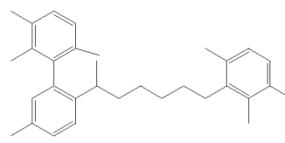
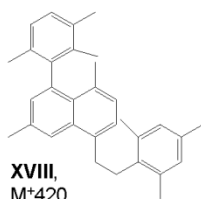
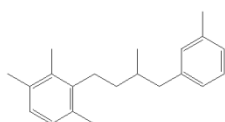
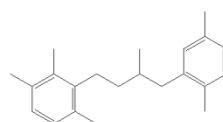
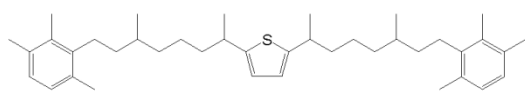
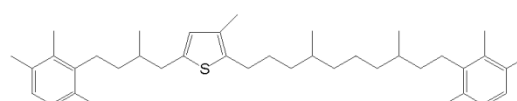
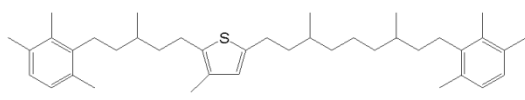
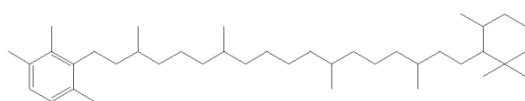
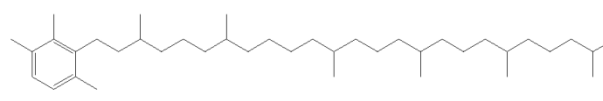
Appendix C

Supplementary information for chapter 4:

The taphonomic fate of isorenieratene in Lower Jurassic shales—controlled by iron?

Manuel Reinhardt, Jan-Peter Duda, Martin Blumenberg, Christian Ostertag-Henning, Joachim Reitner, Christine Heim, & Volker Thiel

Isorenieratene and C₄₀ derivatives with up to three additional aromatic rings**I, M*528****II, M*546****III, M*538****IV, M*538****V, M*532****VI, M*530****VII, M*530****VIII, M*532****IX, M*532****X, M*526****XI, M*524****XII, M*524***Fully aromatized C₄₀ isorenieratene derivative***XIII, M*520****Fig. C1:** Molecular structures of isorenieratene (**I**) and diverse derivatives.

C₃₃ isorenieratene derivatives with up to one additional aromatic ring**XIV**, M⁺448**XV**, M⁺440*C₃₂ isorenieratene derivatives with either one or two additional aromatic rings***XVI**, M⁺426**XVII**, M⁺426**XVIII**,
M⁺420**XIX**, M⁺420*Short-chain isorenieratene derivatives with either one or three additional aromatic rings***XX**, M⁺280**XXI**, M⁺294**XXII**,
M⁺338*Sulfurized isorenieratene derivatives***XXIII**, M⁺572**XXIV**, M⁺572**XXV**, M⁺572*β-Isorenieratane and chlorobactane***XXVI**, M⁺552**XXVII**, M⁺554**Fig. C1** continued.

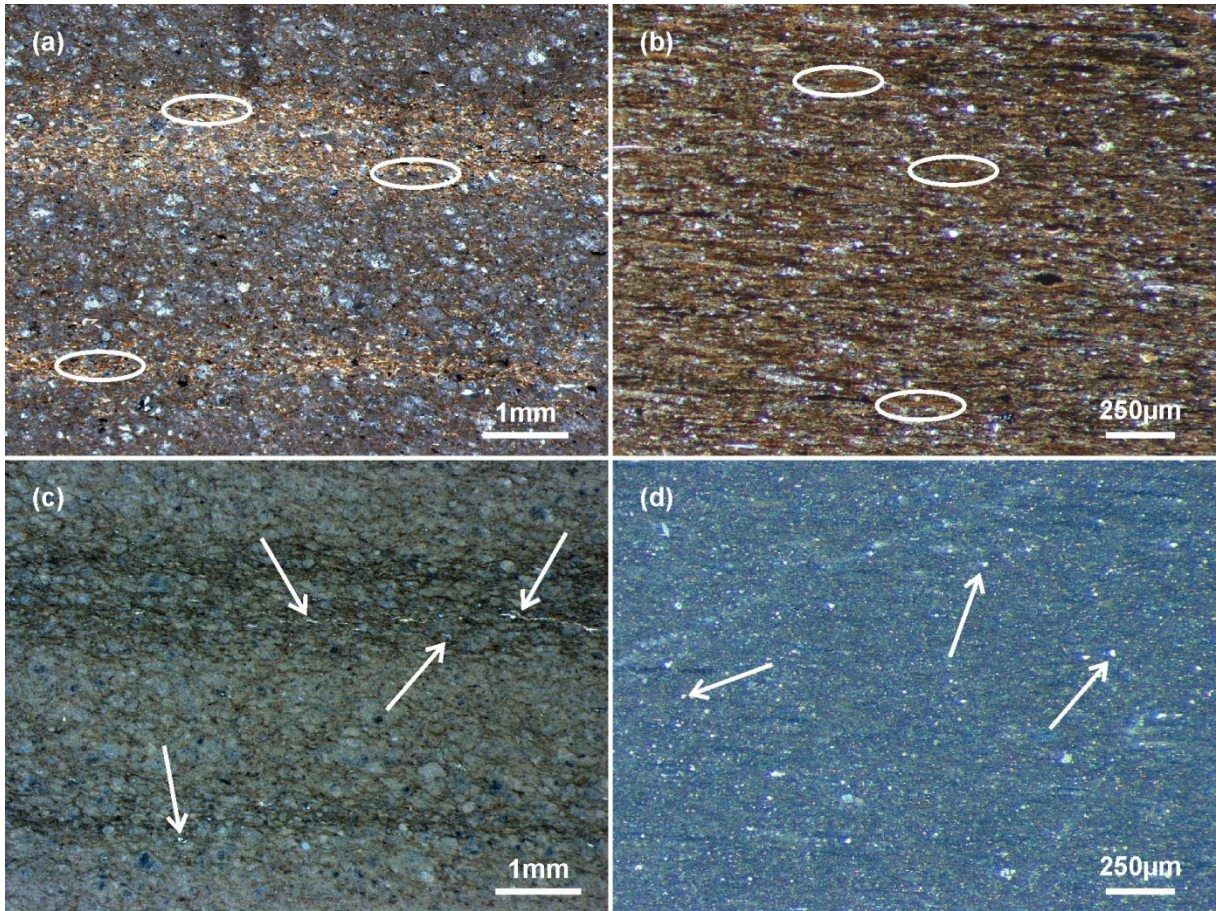


Fig. C2: Microscopic thin section images from Bäch-1385 (a, c) and Ohm-1387 (b, d) under transmitted (a, b) and reflected light (c, d) illustrating the microfacies. Organic matter is indicated by ovals, pyrite by arrows.

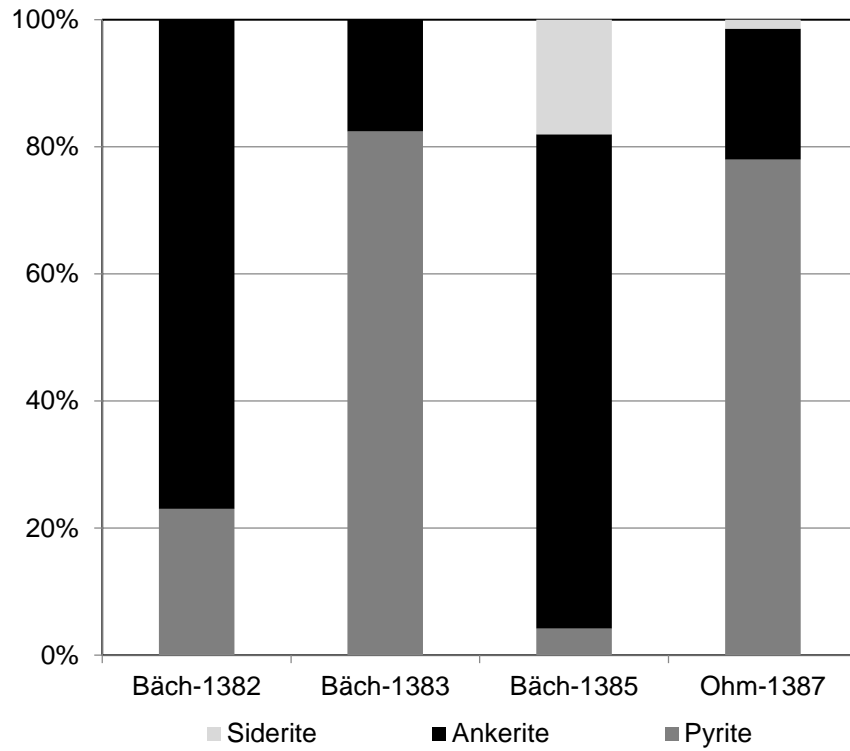


Fig. C3: Relative proportions of iron minerals (pyrite = FeS_2 ; ankerite = $\text{Ca}(\text{Mg,Fe,Mn})(\text{CO}_3)_2$; siderite = FeCO_3) in the analyzed samples from Bächental (Bäch-1382, Bäch-1383, Bäch-1384) and Ohmden (Ohm-1387).

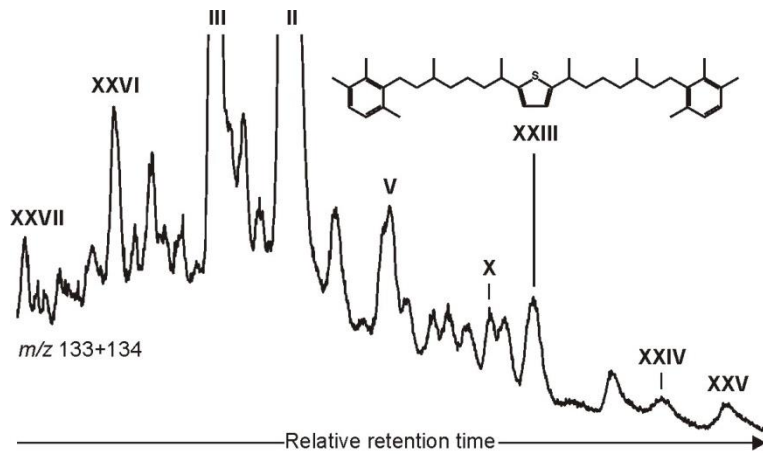


Fig. C4: Partial ion chromatogram (m/z 133+134) of the aromatic hydrocarbons (F2) in the bitumen from Bäch-1383. Please note the low amounts of sulfurized isorenieratene derivatives (**XXIII** to **XXV**) as compared to isorenieratane (**II**). **III**, **V** and **X** = C_{40} isorenieratene derivatives with up to three additional aromatic rings; **XXVI** = β -isorenieratane; **XXVII** = chlorobactane. **II** and **III** are cut at approximately 15 and 25% peak height, respectively.

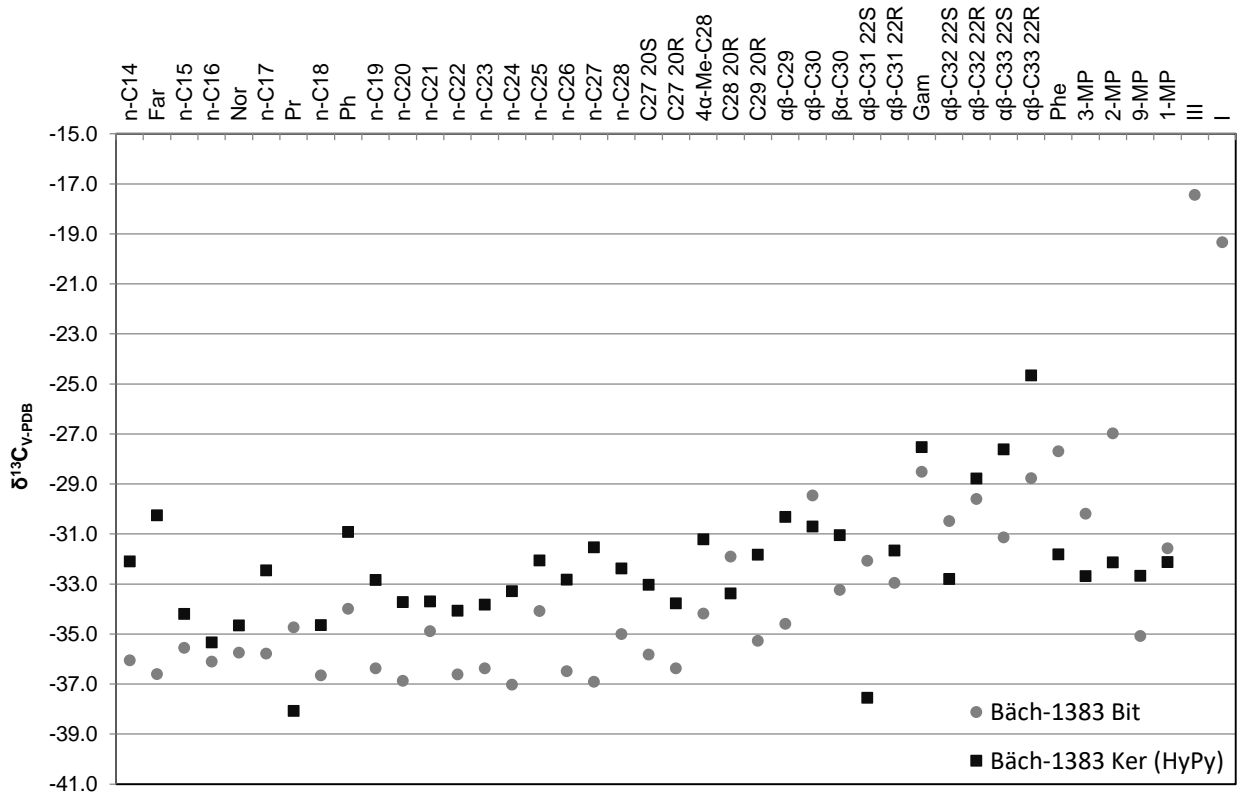


Fig. C5: Compound specific stable carbon isotopes ($\delta^{13}\text{C}$) from Bäch-1383. Grey dots = bitumen, black squares = kerogen. For explanations of compound abbreviations see main text (chapter 4, 4.3.2) plus Figs. 4.3 and 4.4.

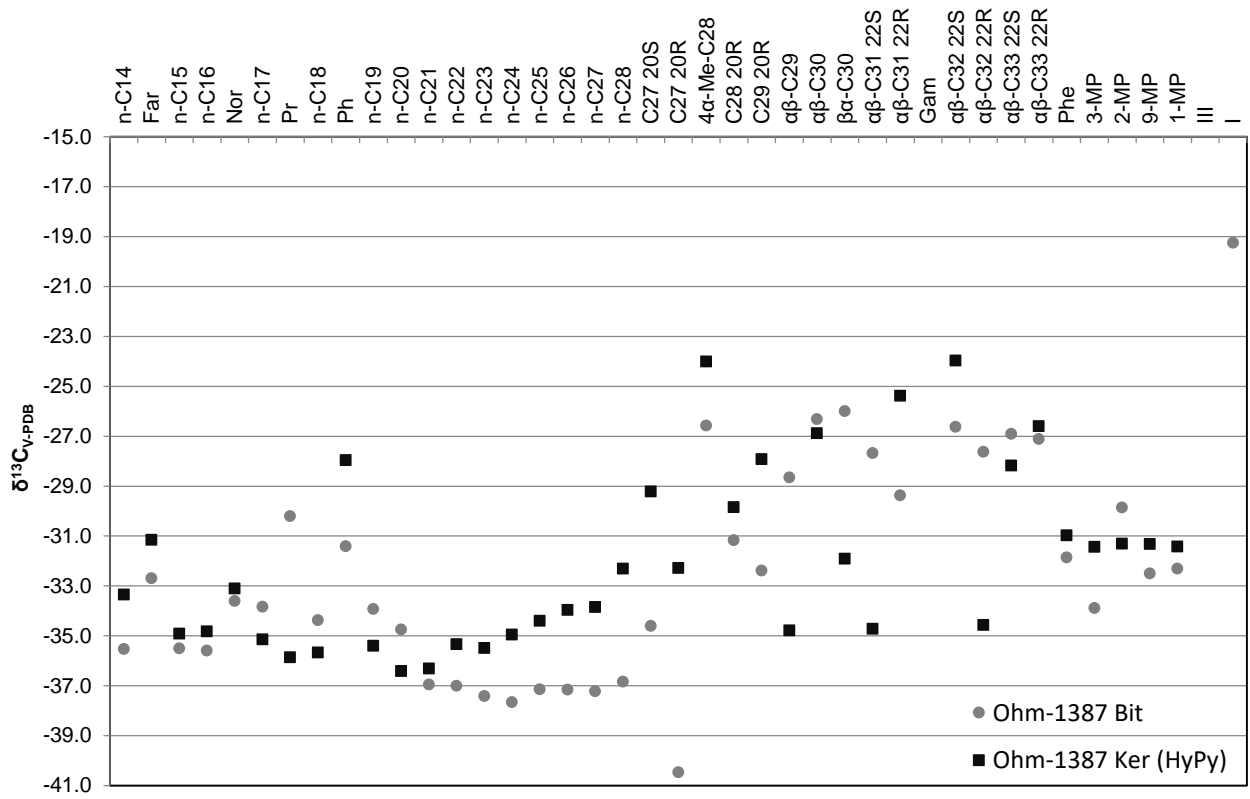


Fig. C6: Compound specific stable carbon isotopes ($\delta^{13}C$) from Ohm-1387. Grey dots = bitumen, black squares = kerogen. For explanations of compound abbreviations see main text (chapter 4, 4.3.2) plus Figs. 4.3 and 4.4.

Tab. C1: Ratios of selected compound concentrations in bitumen (Bit) vs. kerogen (Ker)

Sample	<i>n</i> -C ₁₇	17β,21α(H)-C ₂₉ ^a	4α-Me-5α(H)-C ₂₈ ^b	isorenieratane
	Bit/Ker	Bit/Ker	Bit/Ker	Bit/Ker
Bäch-1382	0.8	0.8	0.5	Bit only
Bäch-1383	0.3	0.7	1.0	28.2
Bäch-1385	0.8	2.4	0.6	Bit only
Bäch-1387	0.2	0.1	0.1	Bit only

^a17β,21α(H)-30-norhopane (normoretane)^b4α-methyl-5α(H)-sterane.

Tab. C2: Compound specific stable carbon isotopes ($\delta^{13}\text{C}$) from bitumens (Bit) and kerogens (Ker)

Sample	Bäch-1382				Bäch-1383			
	Bit		Ker (HyPy)		Bit		Ker (HyPy)	
	Mean	\pm	Mean	\pm	Mean	\pm	Mean	\pm
<i>n</i> -C ₁₄	-36.4	0.1	-34.0	0.3	-36.1	0.1	-32.1	0.3
Far	-34.7	0.1	-28.9	0.1	-36.6	0.1	-30.3	0.2
<i>n</i> -C ₁₅	-36.4	0.2	-34.8	0.2	-35.5	0.0	-34.2	0.1
<i>n</i> -C ₁₆	-36.1	0.3	-34.8	0.4	-36.1	0.2	-35.3	0.6
Nor	-35.7	0.1	-33.7	0.1	-35.7	0.2	-34.7	0.2
<i>n</i> -C ₁₇	-35.9	0.6	-34.6	0.5	-35.8	0.3	-32.5	0.1
Pr	-34.8	0.1	-28.8	0.0	-34.7	0.2	-38.1	0.3
<i>n</i> -C ₁₈	-36.3	0.2	-35.2	0.4	-36.6	0.4	-34.7	0.3
Ph	-34.2	0.2	-30.1	0.5	-34.0	0.5	-30.9	0.8
<i>n</i> -C ₁₉	-36.0	0.5	-34.3	0.0	-36.4	0.3	-32.8	0.8
<i>n</i> -C ₂₀	-35.7	0.3	-34.3	0.0	-36.9	0.4	-33.7	0.4
<i>n</i> -C ₂₁	-36.3	0.0	-34.2	0.2	-34.9	0.2	-33.7	0.0
<i>n</i> -C ₂₂	-35.7	0.0	-33.8	0.5	-36.6	0.3	-34.1	0.3
<i>n</i> -C ₂₃	-35.8	0.5	-32.4	0.2	-36.4	0.0	-33.8	0.0
<i>n</i> -C ₂₄	-35.2	0.2	-31.6	0.0	-37.0	0.2	-33.3	0.0
<i>n</i> -C ₂₅	-33.5	0.2	-31.4	0.2	-34.1	0.2	-32.1	0.5
<i>n</i> -C ₂₆	-35.0	0.5	-31.9	0.0	-36.5	0.3	-32.8	0.0
<i>n</i> -C ₂₇	-34.4	0.4	-31.2	0.4	-36.9	0.0	-31.5	0.3
<i>n</i> -C ₂₈	-34.3	0.5	-31.1	0.1	-35.0	0.3	-32.4	0.4
C ₂₇ 20S	-33.4	0.0	-	-	-35.8	0.2	-33.0	0.1
C ₂₇ 20R	-34.7	0.0	-37.4	0.1	-36.4	0.0	-33.8	0.0
4 α -Me-C ₂₈	-32.8	0.1	-31.7	0.0	-34.2	0.0	-31.2	0.7
C ₂₈ 20R	-32.9	0.0	-31.5	0.4	-31.9	0.6	-33.4	0.0
C ₂₉ 20R	-33.2	0.1	-30.3	0.2	-35.3	0.4	-31.8	0.5
$\alpha\beta$ -C ₂₉	-33.7	0.2	-35.8	0.2	-34.6	0.2	-30.3	0.0
$\alpha\beta$ -C ₃₀	-31.9	0.1	-33.0	0.0	-29.5	0.5	-30.7	0.1
$\beta\alpha$ -C ₃₀	-29.9	0.1	-27.1	0.1	-33.2	0.4	-31.0	0.1
$\alpha\beta$ -C ₃₁ 22S	-34.4	0.0	-31.5	0.4	-32.1	0.1	-37.5	0.1
$\alpha\beta$ -C ₃₁ 22R	-34.7	0.8	-31.8	0.0	-33.0	0.1	-31.7	0.1
Gam	-	-	-	-	-28.5	0.0	-27.5	0.2
$\alpha\beta$ -C ₃₂ 22S	-34.6	0.4	-30.2	0.7	-30.5	0.5	-32.8	0.4
$\alpha\beta$ -C ₃₂ 22R	-32.6	0.6	-32.2	0.8	-29.6	0.5	-28.8	0.2
$\alpha\beta$ -C ₃₃ 22S	-32.2	0.1	-27.8	0.4	-31.1	0.3	-27.6	0.3
$\alpha\beta$ -C ₃₃ 22R	-34.9	0.1	-27.7	0.5	-28.8	0.1	-24.7	0.3
Phe	-32.2	0.4	-29.5	0.1	-27.7	0.6	-31.8	0.0
3-MP	-32.1	0.6	-32.1	0.0	-30.2	0.0	-32.7	0.1
2-MP	-31.4	0.7	-31.8	0.0	-27.0	0.2	-32.1	0.0
9-MP	-31.5	0.0	-32.5	0.0	-35.1	0.1	-32.7	0.0
1-MP	-32.4	0.0	-32.2	0.0	-31.6	0.1	-32.1	0.1
III	-20.3	0.8	-	-	-17.4	0.3	-	-
I	-18.5	0.7	-	-	-19.3	0.5	-	-

For explanations of compound abbreviations see main text (chapter 4, 4.3.2) plus Figs. 4.3 and 4.4. Hyphen (-) = determination of $\delta^{13}\text{C}$ not possible.

Tab. C2 continued

Sample	Bäch-1385				Ohm-1387			
	Bit		Ker (HyPy)		Bit		Ker (HyPy)	
	Mean	±	Mean	±	Mean	±	Mean	±
<i>n</i> -C ₁₄	-35.9	0.5	-34.7	0.3	-35.5	0.1	-33.3	0.0
Far	-34.5	0.2	-	-	-32.7	0.1	-31.2	0.2
<i>n</i> -C ₁₅	-34.5	0.2	-33.7	0.0	-35.5	0.1	-34.9	0.1
<i>n</i> -C ₁₆	-36.0	0.2	-35.0	0.3	-35.6	0.2	-34.8	0.1
Nor	-36.4	0.2	-33.5	0.7	-33.6	0.7	-33.1	0.2
<i>n</i> -C ₁₇	-26.1	0.2	-35.5	0.3	-33.8	0.1	-35.1	0.2
Pr	-35.5	0.1	-33.2	0.5	-30.2	0.2	-35.9	0.1
<i>n</i> -C ₁₈	-36.5	0.0	-35.2	0.6	-34.4	0.1	-35.7	0.5
Ph	-34.2	0.1	-31.5	0.2	-31.4	0.2	-28.0	0.4
<i>n</i> -C ₁₉	-35.9	0.2	-34.0	0.0	-33.9	0.0	-35.4	0.2
<i>n</i> -C ₂₀	-36.9	0.4	-33.7	0.2	-34.7	0.6	-36.4	0.4
<i>n</i> -C ₂₁	-37.0	0.2	-33.5	0.2	-37.0	0.3	-36.3	0.8
<i>n</i> -C ₂₂	-37.2	0.1	-34.2	0.3	-37.0	0.5	-35.3	0.1
<i>n</i> -C ₂₃	-37.2	0.1	-33.9	0.2	-37.4	0.1	-35.5	0.4
<i>n</i> -C ₂₄	-36.3	0.3	-33.1	0.0	-37.6	0.2	-34.9	0.0
<i>n</i> -C ₂₅	-33.0	0.5	-32.7	0.3	-37.1	0.5	-34.4	0.1
<i>n</i> -C ₂₆	-34.2	0.5	-33.2	0.1	-37.1	0.1	-34.0	0.5
<i>n</i> -C ₂₇	-35.7	0.3	-33.3	0.4	-37.2	0.2	-33.8	0.5
<i>n</i> -C ₂₈	-34.1	0.2	-31.0	0.3	-36.8	0.1	-32.3	0.2
C ₂₇ 20S	-38.3	0.3	-31.7	0.0	-34.6	0.2	-29.2	0.5
C ₂₇ 20R	-31.5	0.0	-30.9	0.7	-40.5	0.1	-32.3	0.2
4α-Me-C ₂₈	-38.3	0.2	-32.9	0.1	-26.6	0.4	-24.0	0.6
C ₂₈ 20R	-32.3	0.1	-36.6	0.7	-31.2	0.0	-29.8	0.0
C ₂₉ 20R	-31.6	0.5	-29.1	0.1	-32.4	0.0	-27.9	0.1
αβ-C ₂₉	-34.4	0.1	-36.9	0.1	-28.7	0.5	-34.8	0.2
αβ-C ₃₀	-32.2	0.2	-31.7	0.0	-26.3	0.7	-26.9	0.4
βα-C ₃₀	-26.0	0.1	-31.2	0.1	-26.0	0.0	-31.9	0.2
αβ-C ₃₁ 22S	-33.6	0.1	-32.5	0.6	-27.7	0.5	-34.7	1.5
αβ-C ₃₁ 22R	-33.7	0.1	-36.6	0.1	-29.4	0.5	-25.4	0.0
Gam	-26.5	0.8	-	-	-	-	-	-
αβ-C ₃₂ 22S	-	-	-33.4	0.0	-26.6	0.7	-24.0	0.3
αβ-C ₃₂ 22R	-35.9	0.4	-37.0	0.3	-27.6	0.1	-34.6	0.3
αβ-C ₃₃ 22S	-28.4	0.1	-28.0	0.2	-26.9	0.3	-28.2	0.4
αβ-C ₃₃ 22R	-35.3	0.7	-31.7	0.1	-27.1	0.0	-26.6	0.1
Phe	-32.7	0.1	-31.3	0.1	-31.9	0.1	-31.0	0.4
3-MP	-32.4	0.1	-33.2	0.1	-33.9	0.2	-31.4	0.0
2-MP	-32.4	0.1	-32.7	0.0	-29.9	0.5	-31.3	0.0
9-MP	-32.5	0.1	-33.3	0.0	-32.5	0.5	-31.3	0.0
1-MP	-32.2	0.9	-30.7	0.3	-32.3	0.4	-31.4	0.0
III	-20.1	0.4	-	-	-	-	-	-
I	-19.8	0.5	-	-	-19.2	0.0	-	-

For explanations of compound abbreviations see main text (chapter 4, 4.3.2) plus Figs. 4.3 and 4.4. Hyphen (-) = determination of δ¹³C not possible.

Appendix D

Supplementary information for chapter 5:

Testing MOMA flight-like pyrolysis GC–MS on analog samples from Earth (iron-rich shale and opaline chert)—implications for MOMA pyrolysis during the ExoMars 2020 rover mission

Manuel Reinhardt, Walter Goetz, & Volker Thiel

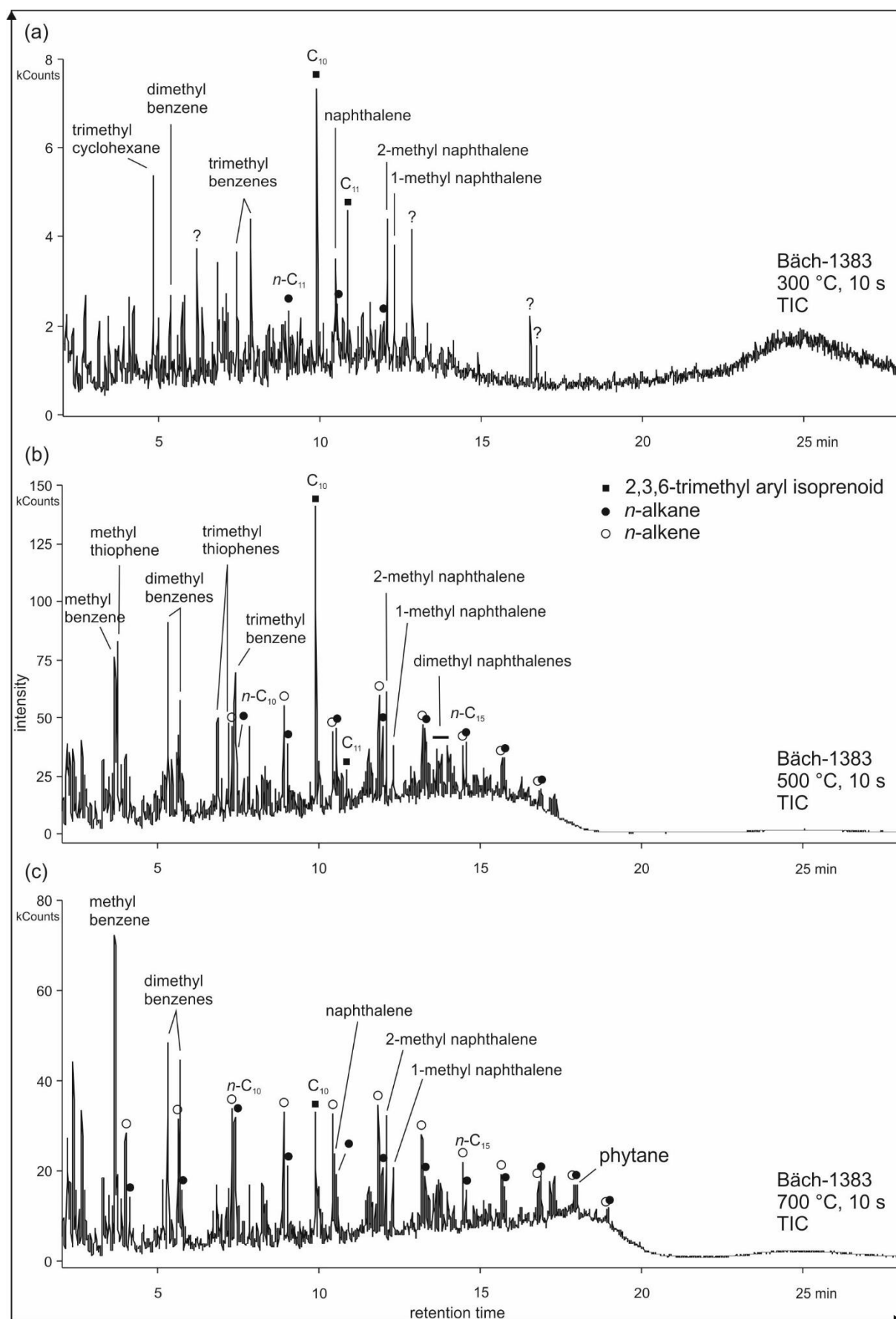


Fig. D1: Total ion chromatograms (TICs) from stepwise pyrolysis (300 °C, 500 °C, 700 °C, held for 10 s, respectively; a–c) of Bäch-1383. Mono- and polyaromatic hydrocarbons (including aryl isoprenoids; squares)

appear in all temperature steps with lowest abundances at 300 °C. *n*-Alkane/*n*-alkene doublets (filled and open circles, respectively) dominate the 500 °C and 700 °C pyrolysates.

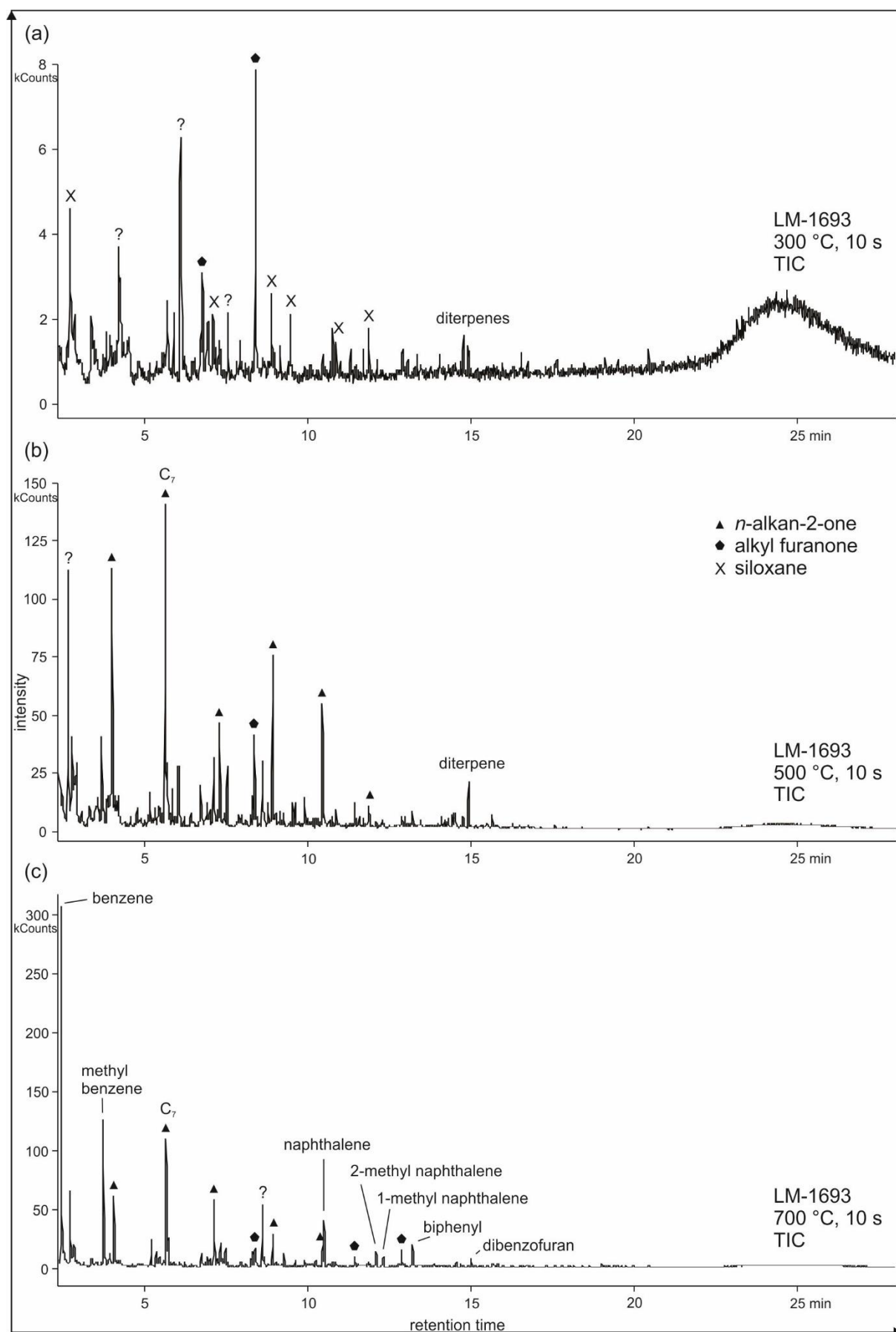


Fig. D2: Total ion chromatograms (TICs) from stepwise pyrolysis (300 °C, 500 °C, 700 °C, held for 10 s, respectively; a–c) of LM-1693. Alkyl furanones (pentagons) are present in all temperature steps. *n*-Alkan-2-ones

(triangles) are abundant at 500 °C and 700 °C, while mono- and polyaromatic hydrocarbons only appear at 700 °C. 'X' denotes siloxane contaminants.

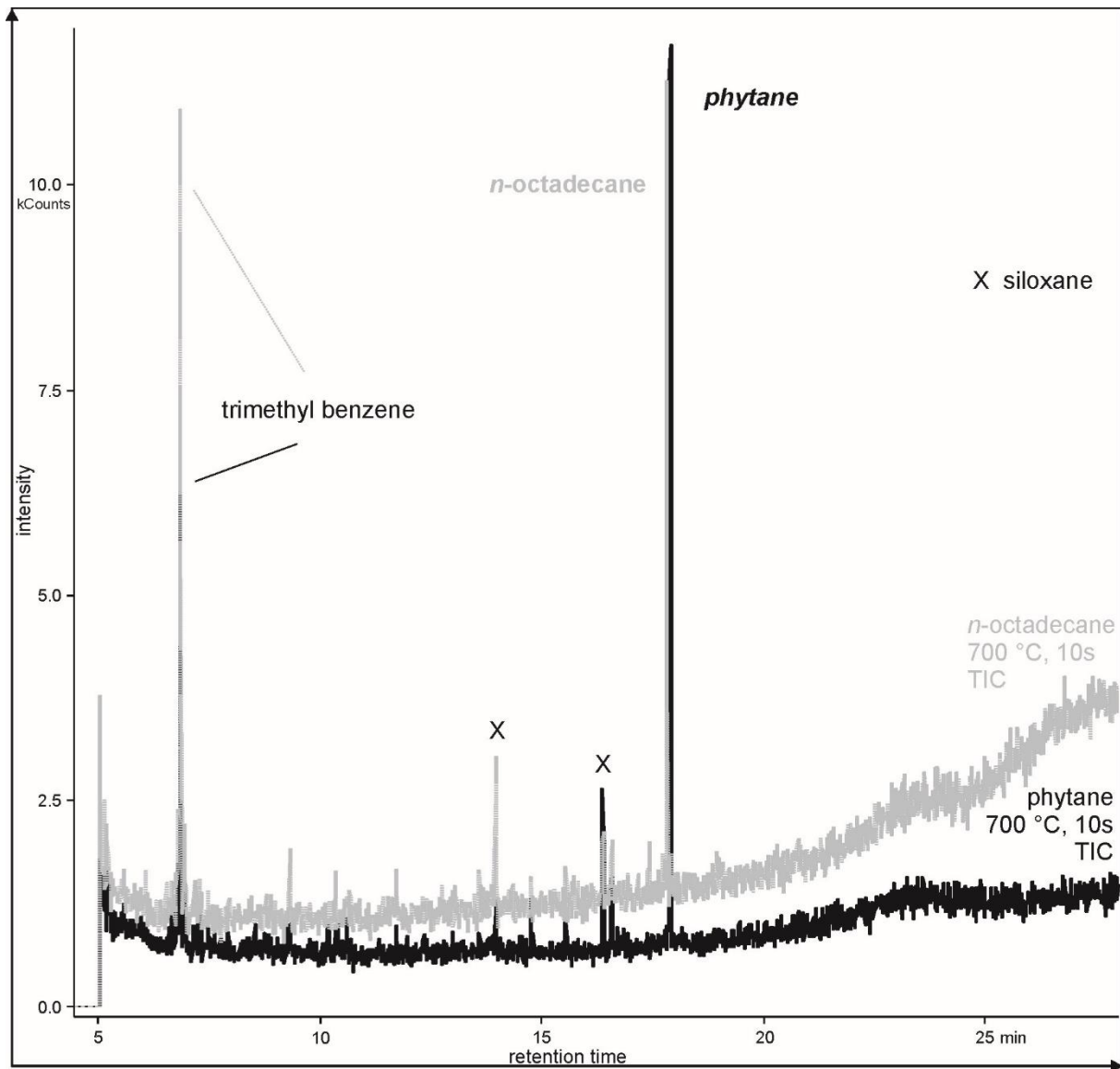


Fig. D3: Total ion chromatograms (TICs) from single step pyrolysis (700 °C, held for 10 s) of *n*-octadecane (100 ng; grey curve) and phytane (100 ng; black curve). Both hydrocarbons are not destroyed during heating at 700 °C and show similar abundances. Trimethyl benzene and siloxanes ('X') are contaminants from the FAS-trap and GC-column.

Curriculum Vitae

Manuel Reinhardt

Date of birth: 19.05.1990

Place of birth: Coburg

Education

- 2016–present **PhD Geosciences** (Max Planck Institute for Solar System Research Göttingen, Georg-August-University Göttingen)
Thesis title: “*Assessing the formation and preservation of organic signatures in extreme environments in the context of the ExoMars 2020 rover mission*”
Supervisors: Prof. Dr. V. Thiel, Dr. Walter Goetz
- 2012–2015 **MSc Geosciences** (Georg-August-University Göttingen)
Overall grade: 1.1 (very good)
Thesis title: “*Biomarkers in bitumens and kerogens from Lower Jurassic oil shales in the Northern Calcareous Alps (Bächental)*“
Supervisors: Prof. Dr. V. Thiel, Prof. Dr. J. Reitner
- 2009–2012 **BSc Geosciences** (Georg-August-University Göttingen)
Overall grade: 1.6 (good)
Thesis title: “*Gradually oscillating: The transgression of the Jurassic Sea exemplified by the clay pit of Ebersdorf b. Coburg*” (written in German)
Supervisors: PD Dr. F. Wiese, Prof. Dr. G. Arp
- 2009 **Abitur** (Gymnasium Ernestinum Coburg)
Overall grade: 1.8 (good)

Volunteering

- 2016–2017 **Student representative** (International Max Planck Research School for Solar System Science, MPS Göttingen)

Keynote presentations

- Reinhardt, M., Thiel, V., Duda, J.-P., Goetz, W., & Reitner, J. (2017). Lake Magadi cherts (southern Kenya Rift Valley) – a modern taphonomic analog for habitats on the early Earth. 4th International Conference of Geobiology, Wuhan, China

Further conference contributions

(own presentations only)

Oral presentations:

Reinhardt, M., Goetz, W., & Thiel, V. (2018). Deciphering organic signatures preserved in hydrothermal cherts from Lake Magadi, Kenya – results from conventional techniques and MOMA-like pyrolysis. MOMA Science Meeting 2, Nice, France

Reinhardt, M., Duda, J.-P., Blumenberg, M., Ostertag-Henning, C., Reitner, J., Heim, C., & Thiel, V. (2018). Tracing photic zone euxinia through time—implications from organic biomarker taphonomy. GeoBonn2018, Bonn, Germany

Reinhardt, M., Duda, J.-P., Reitner, J., & Thiel, V. (2017). Lipid biomarkers in Pleistocene cherts from Lake Magadi, Kenya – microbial signals and hydrothermal influence. GeoBremen2017, Bremen, Germany

Reinhardt, M., Thiel, V., Duda, J.-P., Goetz, W., & Reitner, J. (2017). The Pleistocene Lake Magadi cherts – a modern taphonomic analog for habitats on the early Earth and beyond?. Rocks & Stars II, Göttingen, Germany

Poster presentations:

Reinhardt, M., Duda, J.-P., Blumenberg, M., Reitner, J., Ostertag-Henning, C., & Thiel, V. (2017). Kerogen-bound isorenieratene derivatives in Lower Jurassic oil shales (Bächental, Tyrol, Austria) – a case study. 28th International Meeting on Organic Geochemistry, Florence, Italy

Publications

([‡] = corresponding author)

Reinhardt, M.[‡], Goetz, W., Duda, J.-P., Heim, C., Reitner, J., & Thiel, V. (2019). Organic signatures in Pleistocene cherts from Lake Magadi (Kenya), analogs for early Earth hydrothermal deposits. *Biogeosciences Discussions*, accepted with minor revisions for publication in *Biogeosciences*. <https://doi.org/10.5194/bg-2018-513>

Reinhardt, M.[‡], Duda, J.-P., Blumenberg, M., Ostertag-Henning, C., Reitner, J., Heim, C., & Thiel, V. (2018). The taphonomic fate of isorenieratene in Lower Jurassic shales—controlled by iron?. *Geobiology*, *16*, 237–251. <https://doi.org/10.1111/gbi.12284>

Duda, J.-P.[‡], Thiel, V., Bauersachs, T., Mißbach, H., Reinhardt, M., Schäfer, N., Van Kranendonk, M. J., & Reitner, J. (2018). Ideas and perspectives: hydrothermally driven redistribution and sequestration of early Archean biomass – the “hydrothermal pump hypothesis”. *Biogeosciences*, *15*, 1535–1548. <https://doi.org/10.5194/bg-15-1535-2018>